https://ntrs.nasa.gov/search.jsp?R=19650020184 2020-03-17T01:54:39+00:00Z

GPO PRICE $ _____

CFSTI PRICE(S) $ _____

Hard copy (HC) 5.00

Microfiche (MF) 1.00

ff 653 July 65

NASA CR-54325
4148-6013-SU-000

# PROGRAM OF ANALYTICAL AND EXPERIMENTAL STUDY OF POROUS METAL IONIZERS

by

A. Y. Cho, D. F. Hall, and H. Shelton

N65-29785

FACILITY FORM 602

(ACCESSION NUMBER) 163 (PAGES) CR 54325 (NASA CR OR TMX OR AD NUMBER)

(THRU) 1 (CODE) 09 (CATEGORY)

prepared for

NATIONAL AERONAUTICS AND SPACE ADMINISTRATION

CONTRACT NAS 3-5254

TRW SYSTEMS

NOTICE

This report was prepared as an account of Government sponsored work. Neither the United States, nor the National Aeronautics and Space Administration (NASA), nor any person acting on behalf of NASA:

A.) Makes any warranty or representation, expressed or implied, with respect to the accuracy, completeness, or usefulness of the information contained in this report, or that the use of any information, apparatus, method, or process disclosed in this report may not infringe privately owned rights; or

B.) Assumes any liabilities with respect to the use of, or for damages resulting from the use of any information, apparatus, method or process disclosed in this report.

As used above, "person acting on behalf of NASA" includes any employee or contractor of NASA, or employee of such contractor, to the extent that such employee or contractor of NASA, or employee of such contractor prepares, disseminates, or provides access to, any information pursuant to his employment with such contractor.

CASE FILE COPY

Requests for copies of this report should be referred to:

National Aeronautics and Space Administration
Office of Scientific and Technical Information
Attention: AFSS-A
Washington, D.C. 20546

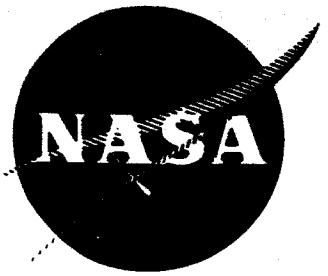

NASA CR-54325
4148-6013-SU-000

# PROGRAM OF ANALYTICAL AND EXPERIMENTAL STUDY OF POROUS METAL IONIZERS

by

A. Y. Cho, D. F. Hall, and H. Shelton

prepared for
NATIONAL AERONAUTICS AND SPACE ADMINISTRATION
CONTRACT NAS 3-5254

TRW SYSTEMS

NOTICE

This report was prepared as an account of Government sponsored work. Neither the United States, nor the National Aeronautics and Space Administration (NASA), nor any person acting on behalf of NASA:

A.) Makes any warranty or representation, expressed or implied, with respect to the accuracy, completeness, or usefulness of the information contained in this report, or that the use of any information, apparatus, method, or process disclosed in this report may not infringe privately owned rights; or

B.) Assumes any liabilities with respect to the use of, or for damages resulting from the use of any information, apparatus, method or process disclosed in this report.

As used above, "person acting on behalf of NASA" includes any employee or contractor of NASA, or employee of such contractor, to the extent that such employee or contractor of NASA, or employee of such contractor prepares, disseminates, or provides access to, any information pursuant to his employment with such contractor.

Requests for copies of this report should be referred to:

National Aeronautics and Space Administration
Office of Scientific and Technical Information
Attention: AFSS-A
Washington, D.C. 20546

NASA CR-54325
TRW 4148-6013-SU-000

SUMMARY REPORT

# PROGRAM OF ANALYTICAL AND EXPERIMENTAL STUDY OF POROUS METAL IONIZERS

by

A. Cho, D. F. Hall, and H. Shelton

Prepared for:

NATIONAL AERONAUTICS AND SPACE ADMINISTRATION

15 July 1965

CONTRACT No. NAS3-5254

Technical Management
NASA Lewis Research Center
Cleveland, Ohio
Spacecraft Technology Division

PHYSICAL ELECTRONICS LABORATORY
Physical Research Division
TRW Systems
One Space Park
Redondo Beach, California

# PROGRAM OF ANALYTICAL AND EXPERIMENTAL STUDY OF POROUS METAL IONIZERS

by

A. Cho, D. F. Hall and H. Shelton

## ABSTRACT

29785

23 different porous tungsten materials were tested to determine their cesium ion emitting characteristics at a j+ up to 25 ma/cm$^2$. Improved performance with a low neutral fraction and low critical temperature at high j+ was noted as the manufacturers increased the surface pore density by use of small, graded, spherical W powder. Effects on porous W of carbiding, O, Cr, Be, Ta, Ti and Zr were studied. Evaporative lifetimes of Cu, Cr, Be, Ni, Fe, and Ti on W vs. temperature, coverage, and oxygenation are presented.

author

TABLE OF CONTENTS


| | Page |
|---|---|
| SUMMARY | 1 |
| EVAPORATIVE LIFETIME EXPERIMENT | 2 |
| INTRODUCTION | 2 |
| BASIC THEORY | 2 |
| THEORY OF EXPERIMENT | 5 |
| DESCRIPTION OF APPARATUS | 9 |
| COMPARISON OF EVAPORATED LIFETIME OF MATERIALS FROM SELF AND FROM CLEAN TUNGSTEN | 22 |
| DATA: | |
| Copper | 23 |
| Chromium | 25 |
| Beryllium | 28 |
| Nickel | 32 |
| Iron | 36 |
| Titanium | 36 |
| Zirconium | 39 |
| Summary of Lifetimes Expressed as Heats of Evaporation | 40 |
| PROGRAM TO TEST POROUS TUNGSTEN PELLETS | 41 |
| INTRODUCTION | 41 |
| DESCRIPTION OF APPARATUS | 42 |
| Vacuum | 42 |
| Pellet Size | 42 |
| "Ω"-Field Accelerator | 43 |
| Feedtube and Plenum | 45 |
| Braze | 45 |
| Heater and Thermocouple | 46 |
| Mounting, Filament Current Leads, and Differential Pumping | 48 |
| Cesium Oven and Seal to the Baseplate | 48 |
| Accelerator | 50 |
| Neutral Detector | 51 |
| Surface Sintering and Etching | 52 |
| Permeability Measurements | 55 |
| Precautions Against Contaminants | 56 |
| Method of Taking Data | 56 |
| Results | 57 |
| Summary of Test Results | 60 |

TABLE OF CONTENTS


| | | Page |
|---|---|---|
| REFERENCES | | 63 |
| APPENDIX I. | Monthly Report No. 8 detailing surface sintering and effect of chromium. | |
| APPENDIX II. | Data sheets on tests. | |
| APPENDIX III. | Engineering sheets on test results. | |
| DISTRIBUTION LIST | | |

## LIST OF ILLUSTRATIONS


| FIGURE NO. | DESCRIPTION | PAGE NO. |
|---|---|---|
| 1 | Waveforms of re-evaporated material from hot tungsten vs time during opening and closing of atomic beam shutter. | 7 |
| 2 | Schematic of experiment to measure binding energy of assorted metals to tungsten. | 10 |
| 3 | Photograph of experiment to measure evaporative lifetimes of various metals from tungsten. | 11 |
| 4 | Photograph showing details such as oven, shutter and ionizing filament of lifetime experiment. | 12 |
| 5 | Schematic showing position of solid tungsten test strip relative to atomic beam and ionizing region. | 15 |
| 6 | Sketch showing oven construction. Oven is designed to allow stable, continuous high-temperature evaporation of a wide variety of materials. | 18 |
| 7 | Typical picture from which copper evaporative lifetime data was taken. | 21 |
| 8 | Evaporative lifetime of copper from polycrystalline solid tungsten. | 24 |
| 9 | Chromium lifetime versus temperature of polycrystalline tungsten with varying coverages. | 26 |
| 10 | Scope traces of chromium evolution from the interior of tungsten upon flashing. | 27 |
| 11 | Picture showing diffused chromium flashed off after varying times of exposure. | 29 |
| 12 | Plot of amount of diffused chromium versus the square root of the exposure time. | 30 |
| 13 | Evaporative lifetime of beryllium versus temperature of tungsten. | 31 |
| 14 | Schematic sketch of the observed nonunity sticking probabilify, s, versus approximate coverage. | 33 |
| 15 | Cesium neutral fraction versus temperature of porous tungsten on which beryllium is deposited. | 34 |

## LIST OF ILLUSTRATIONS


| FIGURE NO. | DESCRIPTION | PAGE NO. |
|---|---|---|
| 16 | Nickel evaporative lifetime versus tungsten temperature. | 35 |
| 17 | Evaporative lifetime of iron versus temperature of tungsten from which it was re-evaporated. | 37 |
| 18 | Approximate evaporative lifetime of titanium versus temperature of tungsten from which it was re-evaporated. | 38 |
| 19 | Computer results for the "Ω" field geometry. | 44 |
| 20 | Photomicrograph of braze of porous tungsten to plenum chamber. Large grain material is molybdenum plenum chamber, dark area is void. | 47 |
| 21 | Schematic of experiment to test porous tungsten pellets. | 49 |
| 22 | Photograph of experiment to test porous tungsten pellets. | 53 |
| 23 | View of experiment under lower plane. | 54 |
| 24 | Closeup photograph of the "Ω"-field accelerator. | 55 |

# PROGRAM OF ANALYTICAL AND EXPERIMENTAL STUDY OF POROUS METAL IONIZERS

by A. Cho, D. F. Hall, and H. Shelton

## SUMMARY

The first part of this report gives the evaporative lifetimes of copper, chromium, beryllium, nickel, iron, and titanium on solid tungsten as functions of temperature, coverage, and cleanliness. These lifetimes were determined for use in predicting the suitability of the materials tested for the accelerator electrode. The experiments demonstrated that copper is acceptable as an accelerator material, nickel and iron are possibly acceptable, beryllium and chromium should probably be avoided because of their interactions with oxygen, and titanium and zirconium are strictly to be avoided.

In a second set of experiments 23 porous tungsten materials that were fabricated by different manufacturers and had varying parameters were tested to determine their cesium-ion-emitting properties, particularly with respect to neutral fraction and critical temperature at ion current densities up to 25 $ma/cm^2$. Most clean porous tungsten manufactured of fine-graded spherical powder yielded a neutral fraction of about 1 to 2 percent at about $1450^{\circ}K$ and a current density of 20 $ma/cm^2$. Substantially fewer neutrals were observed from oxygenated surfaces. The best results from tests made without oxygen were obtained with carbided high-pore-count material, which yielded a 1/2 percent neutral fraction at $1440^{\circ}K$ and 20 $ma/cm^2$ current density. Results of this second series of tests are presented in two ways - on data sheets showing the neutral fraction versus temperature and current density for each test, and on engineering test sheets that include permeability and critical temperature measurements.

# EVAPORATIVE LIFETIME EXPERIMENT

## INTRODUCTION

It is common practice in developing ion engines using cesium contact ionization to use an accelerator made from copper, since this material, if it is evaporated or sputtered onto the porous tungsten, simply re-evaporates and in no way affects the ionization of the cesium. However, copper has a few disadvantages — it melts at low temperature, it gets soft and sometimes sags, and its sputtering yield, weight, expansion coefficient, and possibly other properties may not be optimum. It therefore seens desirable either to strengthen the copper with additives or replace it with some better material. Such a material must be compatible with porous tungsten, complete compatibility dictating that the material must re-evaporate and that the equilibrium amount present on the porous tungsten surface will not adversely alter the ion-emission characteristics of the system.

This experiment was therefore conducted to measure the residence time before re-evaporation of some of the materials considered for use in accelerators. From the residence time, the equilibrium coverage of a material can easily be calculated.

## BASIC THEORY

The evaporative (or adsorption) lifetime $\tau$ of a material on a substrate is defined throughout this report as

$$\tau = \sigma/\Gamma_{ev} , \qquad (1)$$

where $\sigma$ is the surface coverage of the material in particles/cm$^2$ and $\Gamma_{ev}$ is the evaporative particle current density (or flux) in particles/cm$^2$/sec. At equilibrium the arrival rate of atoms $\Gamma_{ar}$ is equal to $\Gamma_{ev}$, so that

$$\sigma_{eq} = \Gamma_{ar} \tau \ , \qquad (2)$$

where $\sigma_{eq}$ is the equilibrium surface coverage of the material. Therefore, a measurement of $\tau$ at a particular arrival rate allows a direct calculation of the equilibrium coverage for this value of $\Gamma_{ar}$.

The surface coverage is often specified as a fraction of a monolayer or $\theta$, one monolayer being defined as the coverage when the most readily available sites on the surface are completely occupied. I. Langmuir[1] found this coverage for cesium adions on a tungsten surface to be $3.6 \times 10^{14}$ particles/cm$^2$ -- one for every four tungsten atoms. Throughout this report a monolayer is considered to be about $1.5 \times 10^{15}$ particles per cm$^2$, which is close to the average tungsten density on all the crystal faces. For adsorbed cesium, which affects the work function and the evaporation energy of adjacent cesium adions more than any other material, the change of work function $\Delta\phi$ is $10 \times \theta$. If the tolerable $\Delta\phi$ is 0.1 volt, then the maximum tolerable coverage is 0.01, or 1 percent of a monolayer. Therefore, since cesium is the most active material known, no material on tungsten is objectionable in amounts of less than 1 percent of a monolayer, or $1.5 \times 10^{13}$ particles/cm$^2$.

To estimate the maximum evaporation lifetime of a material for it to be of interest as an accelerator material, consider a porous tungsten ionizer to be operating at 25 ma/cm$^2$ and back sputtering from the accelerator to be 1 percent. In this case the arrival rate of foreign atoms from the accelerator would be approximately $1.5 \times 10^{15}$ (one monolayer) per second. From Eq. (2) and the upper-bound surface coverage quoted above, the maximum lifetime of interest would be approximately 10 ms. If the lifetime of a material that causes an adverse work-function change with $\theta = 0.01$ were greater than 10 ms at the operation temperature of tungsten, a larger neutral fraction

would result and the temperature would have to be raised to improve results.

In addition to being a function of temperature, lifetime is also sometimes a function of coverage. This is particularly true if adsorption affects the work function. Conversely, when a wide range of lifetimes is observed as a function of coverage, it can be confidently expected[2] that the material will have a large effect on the work function and hence on cesium neutrals (and possibly critical temperature) when the tungsten is used as an ion emitter. With such materials a low coverage is required, so again attention is directed to finding the lifetime at low coverages ($\theta \lesssim 0.05$). These lifetimes are designated $\tau(\theta = 0)$.

Fortunately, in this experiment lifetimes are measured directly in seconds and are not affected by calibration constants; consequently great confidence can usually be placed on the values obtained. (A less desirable approach would be to measure adsorption energy, which then must be used in a formula with assumed constants to obtain a derived lifetime.)

Lifetime can be analytically expressed as a function of the reciprocal temperature by

$$\tau = \tau_o \left[ \exp (e/kT) E_{ev} \right] , \qquad (3)$$

where $E_{ev}$ is the heat of evaporation (or adsorption) in volts, T is the absolute temperature in degrees Kelvin, k is Boltzman's constant and equals $1.38 \times 10^{-16}$ ergs/$^{o}$K, and $\tau_o$ is interpreted as the period of thermal vibration ($1/\tau_o \cong \nu$, where $h\nu \cong kT$, hence $\tau_o \cong h/kT \cong 3 \times 10^{-14}$ sec. at 1500$^{o}$K). Although the constants $\tau_o$ and $E_{ev}$ are tabulated for the materials tested, primary attention in reading the test results should be directed to the actual plot of $\tau$ versus temperature.

## THEORY OF EXPERIMENT

In this experiment lifetimes were determined from the transient behavior of atoms as they re-evaporated from a hot tungsten ribbon when an atomic beam was started or stopped by a mechanical shutter. The theory of the experiment is given in the following paragraphs.

If lifetime is a constant independent of the coverages involved (which is true at low coverages) and the sticking probability is 1.0, then

$$\frac{d\sigma}{dt} = \Gamma_{ar} - \frac{\sigma}{\tau} \tag{4}$$

which upon integration becomes

$$\sigma = \sigma_{eq} \left[ 1 - \exp\ (-\ t/\tau) \right] \tag{5}$$

for $\sigma = 0$ at $t = 0$. This equation shows that when a shutter is opened to allow a constant stream of atoms to impinge on clean tungsten, the coverage builds up and approaches equilibrium coverage in an exponential manner, the time constant being equal to the lifetime. Since the re-evaporation flux is $\sigma/\tau$ and $\tau$ is a constant, the re-evaporation flux also increases exponentially as it approaches the arrival rate. It is this re-evaporation flux that is measured in this experiment.

Upon complete or partial closing of the shutter, the re-evaporation and coverage again exponentially approach their new equilibrium values (zero if the shutter is completely closed). The time constant can be determined from the time required for 63 percent of the change to occur or from the intercept of the initial slope of re-evaporation flux with the equilibrium value. The latter method has been used because the value obtained is not affected if the lifetime changes with coverage. This method yields the "low-coverage" lifetime, $\tau_{(\theta = 0)}$, provided the tungsten has been cleaned of any previous deposition.

Determining $\tau$ is more difficult for larger coverages of materials where the lifetime varies with the coverage since in such cases the transient response is more complicated. When the effect is a small perturbation, the over-all departure from exponential is very slight, but the difference is most noticeable in the initial slopes obtained upon opening and closing of the shutter. As the change of lifetime with coverage increases the curve becomes more complicated, usually displaying inflection points and small initial slopes followed by much larger slopes. These phenomena are illustrated in Figure 1.

The distance y in Figure 1(d) is proportional to the rate at which material is adhering to the tungsten. (Since the equilibrium re-evaporation rate is equal to the arrival rate, y is the difference between what is going on and what is coming off.) Therefore

$$\sigma = k \int y dt,$$

where k is the calibration constant determined by $\Gamma_{ar} = ky(0)$. At any given time $t_o$

$$\sigma = k \int_0^{t_o} y dt \quad \text{and}$$

$$\Gamma_{ev} = k \left[ y(0) - y(t_o) \right],$$

hence

$$\tau \left[ \sigma(t_o) \right] = \frac{\sigma}{\Gamma_{ev}}$$

$$= \frac{k \int_0^{t_o} y dt}{k \left[ y(0) - y(t_o) \right]} .$$

We see that the calibration constant cancels out and that again the lifetime is determined exactly, but the exact value of

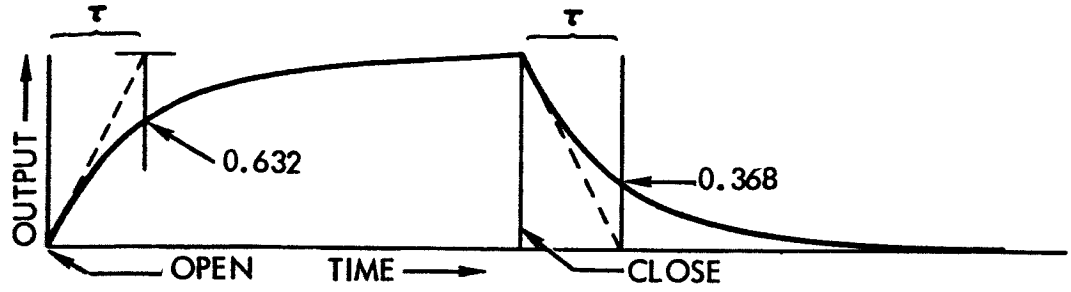


A LIFETIME CONSTANT

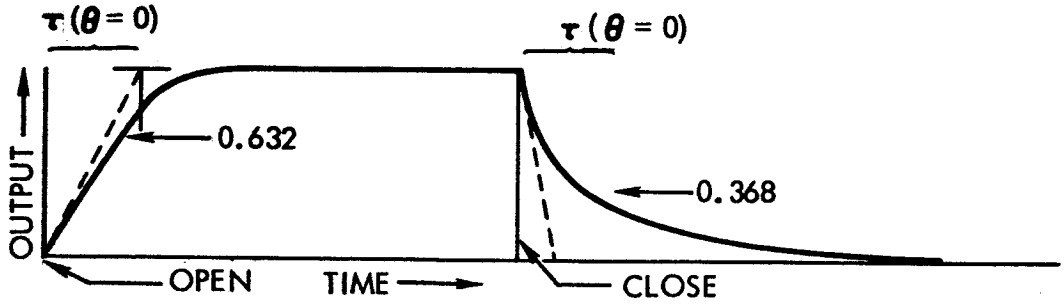


B. LIFETIME SLIGHTLY DECREASING WITH COVERAGE

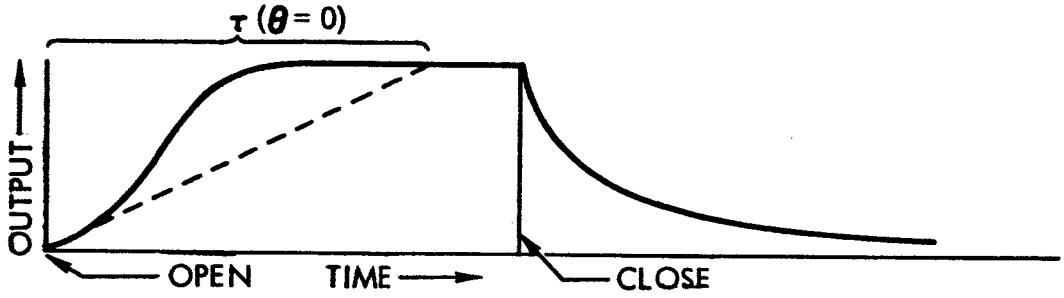


C. LIFETIME STRONGLY DEPENDENT ON COVERAGE

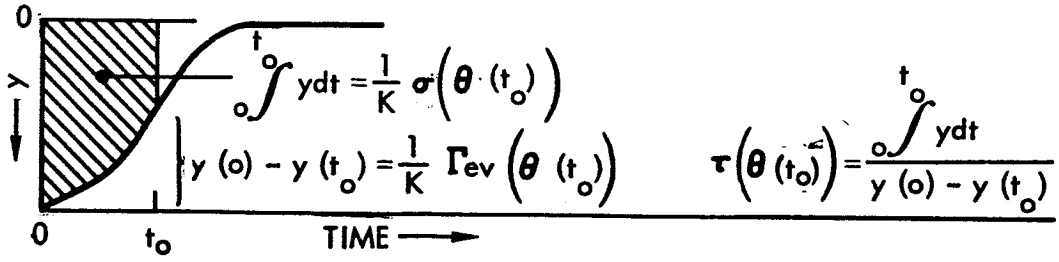


D. ILLUSTRATION OF ANALYSIS TO DETERMINE $\tau(\theta)$

Figure 1. Waveforms of re-evaporated material from hot tungsten versus time during opening and closing the atomic beam shutter.

$\sigma$ to which this lifetime is to be ascribed is dependent on the accuracy of calibration, which is the most difficult and uncertain aspect of the experiment.

Note that it is not difficult to find the exact functional relationship between the lifetime and the fractional value of some critical coverage. This coverage (the integral in above equations) might be the limit that is obtained before accumulation of the bulk material, or the coverage where a near discontinuity in lifetime occurs. When such a critical coverage has been observed, we have tended to call it a monolayer and have ascribed to it a surface density of $1.5 \times 10^{15}$ particles/cm$^2$. Measurement of the value of an observed critical coverage requires an absolute determination of the calibration constant, k. In theory this can be done by using previously determined values of vapor pressure. We have found, however, that for most materials the published vapor pressure data cannot be trusted. It is not known whether this is due to the presence of vacuum or alloying contaminants in the original experiments, temperature uncertainties, improper measurements of weight loss, improper assumptions of sticking probabilities, theoretical extrapolations, or other causes.

Calibration involves determining scope gain, electron multiplier gain, ion-to-electron efficiency, spectrometer transmission, gathering efficiency at the entrance of the spectrometer, the bombarding electron current, voltage, and focusing, ionization efficiency, the thermal velocity of the re-evaporated atoms, and the angular distribution and distance of evaporated atoms from the tungsten ribbon. Most of these factors can be held constant from one experiment to another or set to a reference value by, say, calibration with a known gas pressure. However, the ionization efficiency and the ion-to-electron efficiency cannot be calculated with any certainty. It is felt that the guess of $\theta = 1$ for $\sigma = 1.5 \times 10^{15}$/cm$^2$ is more accurate than the value obtained following the most painstaking calibrations when vapor pressure data are uncertain.

## DESCRIPTION OF APPARATUS

The experimental apparatus is shown schematically in Figure 2, and photographs of it are shown as Figures 3 and 4. The heart of the experiment is an electric quadrupole mass spectrometer, commonly called a "massenfilter" as designated in papers by its inventor, Professor W. Paul of Germany. Four 6-inch-long, centerless ground stainless steel rods 0.232 inch in diameter are mounted with 0.200 inch between opposite rods. These opposite rods are connected together, and a variable-amplitude, 4.5-mc voltage of magnitudes up to 1200 volts peak to peak is fed between adjacent pairs. A d-c voltage proportional to the a-c voltage is fed in series with the a-c to narrow the range of charge-to-mass ratios that can pass through the rods. As the proportion of d-c voltage is increased, the resolution increases until beyond a certain point no particles pass through. With the fraction of d-c (rectified from the a-c) fixed to give high resolution ( > 100), the a-c voltage is varied to tune to different atomic mass units. Small numbers like those of $H_2O$ (18), and $N_2$+CO (28) require a small voltage, whereas higher numbers for materials such as Cr (52), Fe (56), Ni (58), and Cu (63) require higher voltage. In addition, the frequency had to be lowered in testing zirconium (90).

At one end of the rods a pencil beam of electrons is directed toward the entrance of the mass spectrometer. Ions created in the electron beam are funneled into the spectrometer as the electrons are stalled.

Ions of the proper charge-to-mass ratio that exit from the rods are accelerated through a grid onto a tungsten plate at -2000 volts. Secondary electrons from the impact are multiplied in a novel electron multiplier,* which is the vertical box

* Bendix Model 306 Magnetic Electron Multiplier.

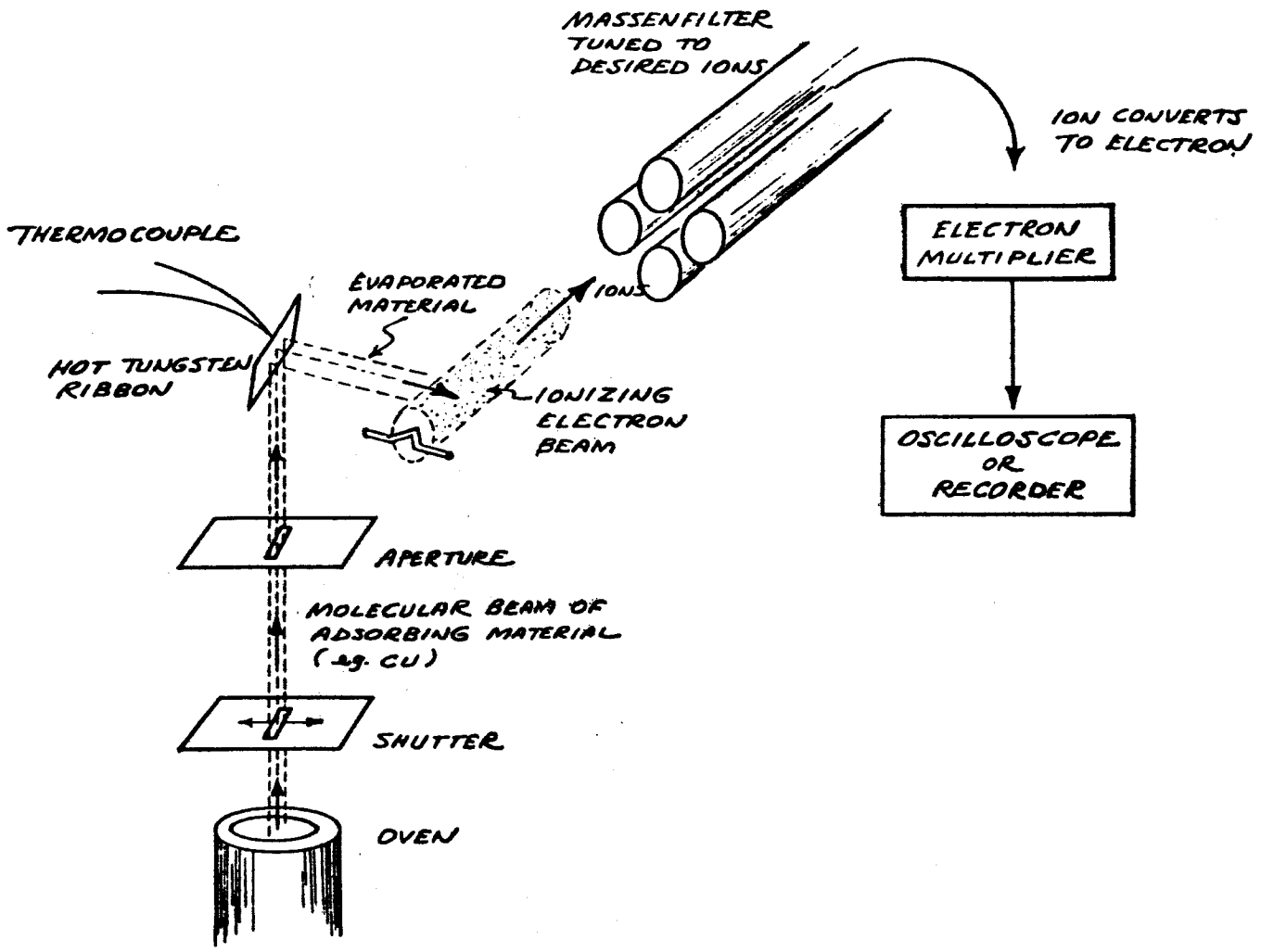


**Figure 2.** Schematic of experiment to measure the binding energy of assorted metals to tungsten.

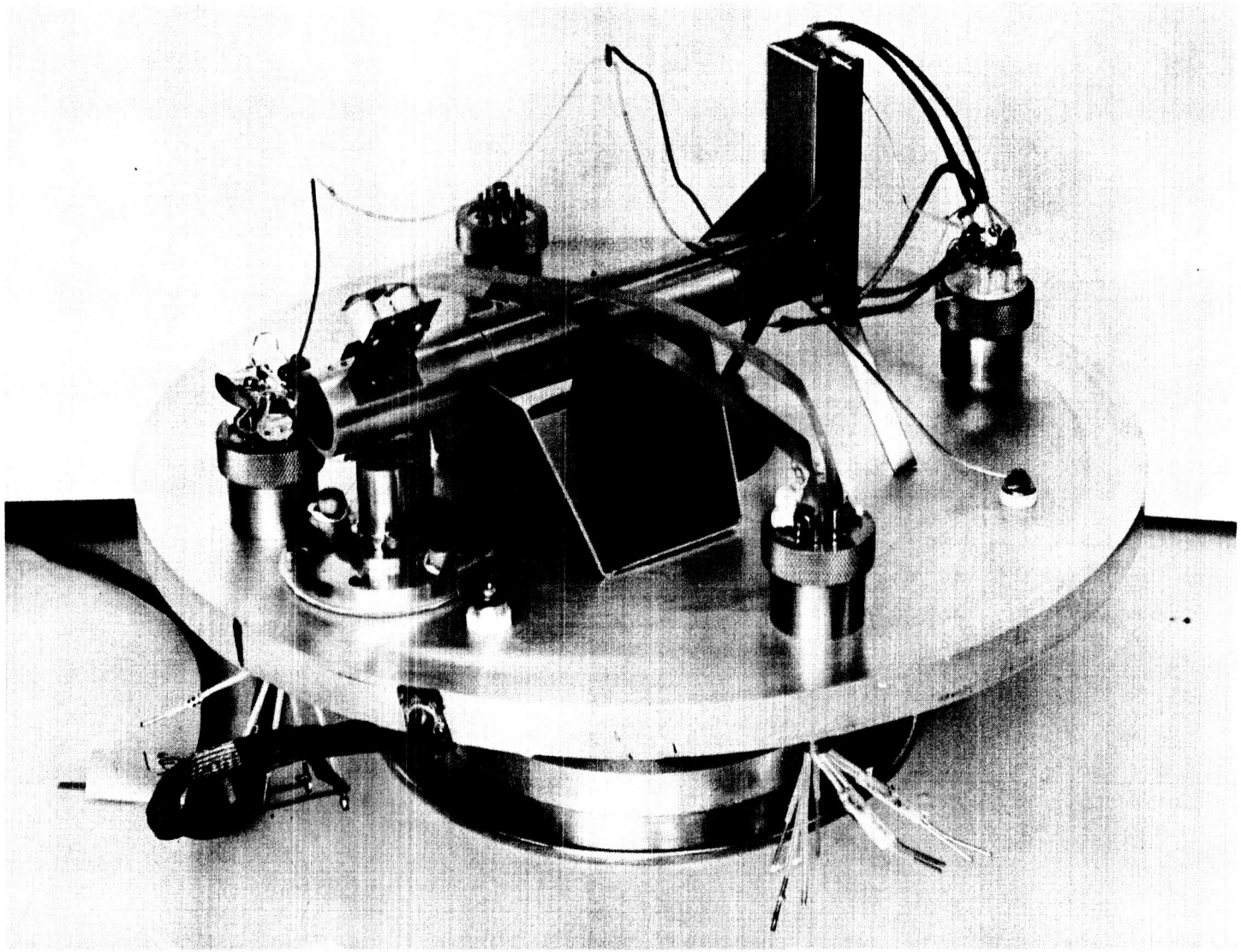

Figure 3. Photograph of experiment to measure evaporative lifetimes of various metals from tungsten. Long tube contains "Massenfilter". Electron multiplier is on right.

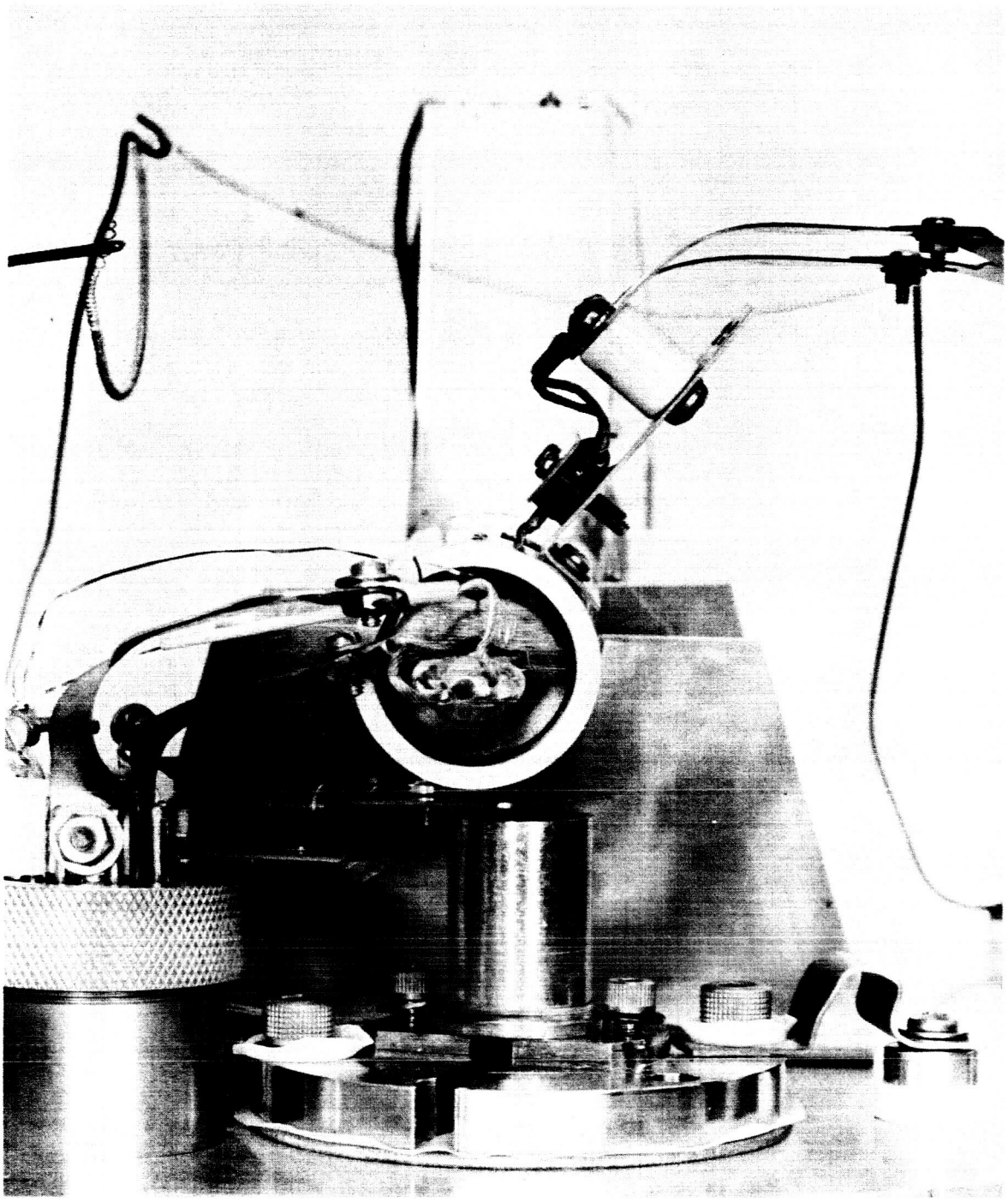

**Figure 4.** Photograph showing details such as oven, shutter, and ionizing filament of lifetime experiment.

to the right in Figure 3. This multiplier works with cycloidal electron trajectories in a crossed electric and magnetic field. Two resistive films coated on glass (about 150 megohms) about 3/16 inch apart have 1500 volts along their length. One which is attached to the ion target and on which multiplication occurs, has a voltage running from about -2000 to -500 volts; the other is 500 volts positive with respect to the first at all points along an approximate 2-inch length, with voltages running from -1500 volts to 0. The collector at 0 volts protrudes between these two plates at the end of the electron path. A simple resistive divider supplies all these voltages from a single regulated supply, which is varied to vary the gain of the multiplier.

The multiplier has proved very successful. It is quite stable in a variety of atmospheres, although chlorine in the system seems to ruin the gain. Also, the insulating materials used in its construction and the curie points of the magnet limit bakeout. One unit was destroyed because the pressure became too high and a discharge occurred between the plates, sputtering off the coating.

The collector goes directly to the scope (input resistance 1 megohm) on the 1-mv scale, and the equipment is adjusted so that $10^{-9}$ amps out of the multiplier gives a 1-cm deflection on the scope. The gain of the multiplier (capable of over $10^{6}$) is used at approximately $10^{4}$, so that if the ion-to-electron efficiency is 10 percent an ion current of $10^{-12}$ amps gives $10^{-13}$ amps of secondary electrons, which are multiplied to $10^{-9}$ amps and produce 1 mv across $10^{6}$ ohms to give a 1-cm deflection on the scope.

The part of the system described thus far is sensitive to background gases and makes a good gas analyzer.

To continue with the description of the total test system used in determining lifetimes, a test specimen of tungsten in the form of a ribbon 0.001 inch thick, 0.10 inch wide, and 0.45 inch long is mounted at 45 degrees to the direction of an atomic beam of material whose lifetime on tungsten is to be measured (see Figure 5). Scattered (or re-evaporated, or desorbed) atoms are thus deflected so that they traverse the pencil ionizing beam of electrons directed toward the spectrometer. The test setup is carefully arranged so that the ribbon is as close to the ionizing region as is possible with perfect shielding to ensure that none of the primary atomic beam can reach the ionizing region. Scattered atoms enter the ionizing can through a rectangular aperture cut in its side.

In order to ensure uniform coverage and no end effects, the tungsten strip is sharply bent at 0.45 inch so that the length beyond this point is shadowed from the atomic beam. About 1/16 inch beyond the bend the ribbon is carefully spot welded to 0.020-inch-diameter tantalum wire. Tantalum was chosen for ease of spot-welding and because it would heat to the same temperature as the tungsten, thus avoiding end-cooling and temperature distribution along the tungsten length.

The original plan was to monitor the temperature of the tungsten with a fine-wire thermocouple spot-welded to the back of the ribbon; however, the difficulty of spot-welding such small wires of refractory metals dissuaded us from this scheme. The method adopted for measuring the temperature was to use a pyrometer looking normally through clean glass (out of the path of evaporated material) onto the rear of the tungsten strip, which is seen at an oblique angle. The back of the ribbon remains pure tungsten during all of the experiment so that the correction for the spectral emissivity of solid tungsten is valid. It is felt that the temperature is accurate to within $\pm 10^{o}$K.

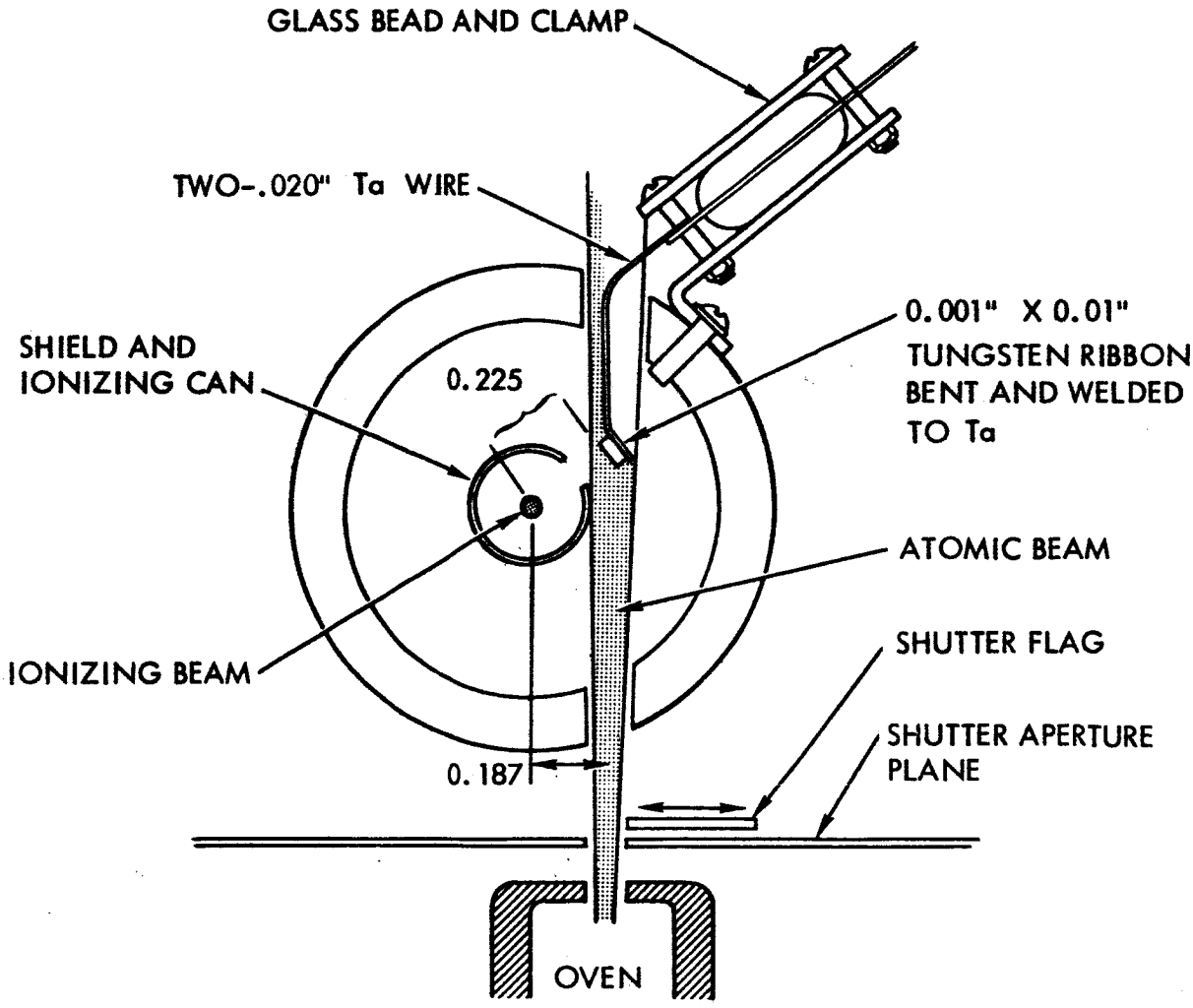


Figure 5. Schematic showing position of solid tungsten test strip relative to atomic beam and ionizing region.

The ribbon is heated with direct current, as the magnetic field modulates the spectrometer sensitivity and heating by a-c would produce fluctuation of the output. The electron source for the spectrometer is also heated with direct current to prevent 60 and 120 cps modulation of the output. The heating current for the oven can also be bothersome if the leads are not dressed properly.

In order to prevent an electrostatic-field deflection of the ionizing electron beam, the ribbon is set at the same potential as the ionizing can. This arrangement also prevents the acceleration of electrons into the ionizing region if the tungsten strip is at electron emission temperature. These two electrodes are usually set at +150 volts.

It is of interest to estimate the density of particles at the ionizing region for any evaporation rate. Let us consider a material that has a vapor pressure p at a temperature T. When a surface of this material is in equilibrium with its vapor pressure, the density of atoms everywhere outside the surface is p/kT. The density at the ionizing beam would be this same p/kT if it were surrounded by a complete cylinder emitting atoms at this pressure. However, the 0.10-inch width of tungsten at a radius of about 0.225 inch results in only $0.1/2\pi \times 0.225$, or about 1/15 of a complete cylinder. Dilution also occurs in the axial direction because the ribbon is not infinitely long. It is estimated that this causes a further factor of 2 dilution. Therefore the density in the ionizing region, and hence the probability of ionization, is down by a factor of 30 from the equilibrium density that would be predicted from the vapor pressure. Also, the temperature of measurement is about $1500^{\circ}K$, rather than the $300^{\circ}K$ associated with conventional gases, so one suffers another factor of 5. These calculations suggest that a material evaporating off the ribbon at $1500^{\circ}K$ with a vapor pressure of $1 \times 10^{-6}$ torr will populate the ionizing region to the same

extent as $7 \times 10^{-9}$ torr of a noble-like gas rebounding from all the walls at room temperature. This discussion has been included mainly to illustrate the need for keeping the ribbon close to the ionizing beam and to indicate the high level of sensitivity needed even when they are as close as possible.

A sketch of the oven is shown in Figure 6. The oven was designed to achieve sustained, stable high temperatures without causing the overheating and outgassing of adjacent parts. Another design objective was to make the container massive enough that it would not readily be destroyed by alloying. These objectives were for the most part achieved. The oven has successfully evaporated titanium requiring a temperature in excess of $2000^{\circ}K$.

Molybdenum was chosen for the sample holder because of its machinability. For those materials that alloy rapidly at evaporation temperature (nickel, for instance), a tungsten insert is used. The needs for stability of temperature despite the presence or absence of evaporants and for a massive container distated that the container be radiatively heated, rather than heated directly by passing current through it. To heat the holder, about 100 amps of 60-cps current are passed through a 0.001-inch tantalum filament surrounding the holder, through the holder itself, and through a thin stem designed to generate heat rather than cool. Heat is thus conducted into the molybdenum holder from both ends and is radiated from the tantalum ribbon.

A copper can in which a heat shield of 0.0005-inch tantalum sheet is wound intercepts most of the stray radiated power and conducts it into the massive base plate via a thin sheet of teflon that serves as a thermal conductor. This seemingly incongruent usage of a normally insulating material illustrates a principle used extensively in these experiments: that is, if a poor thermal conductor is thin enough and has enough area, it can provide very efficient cooling. Teflon was chosen because

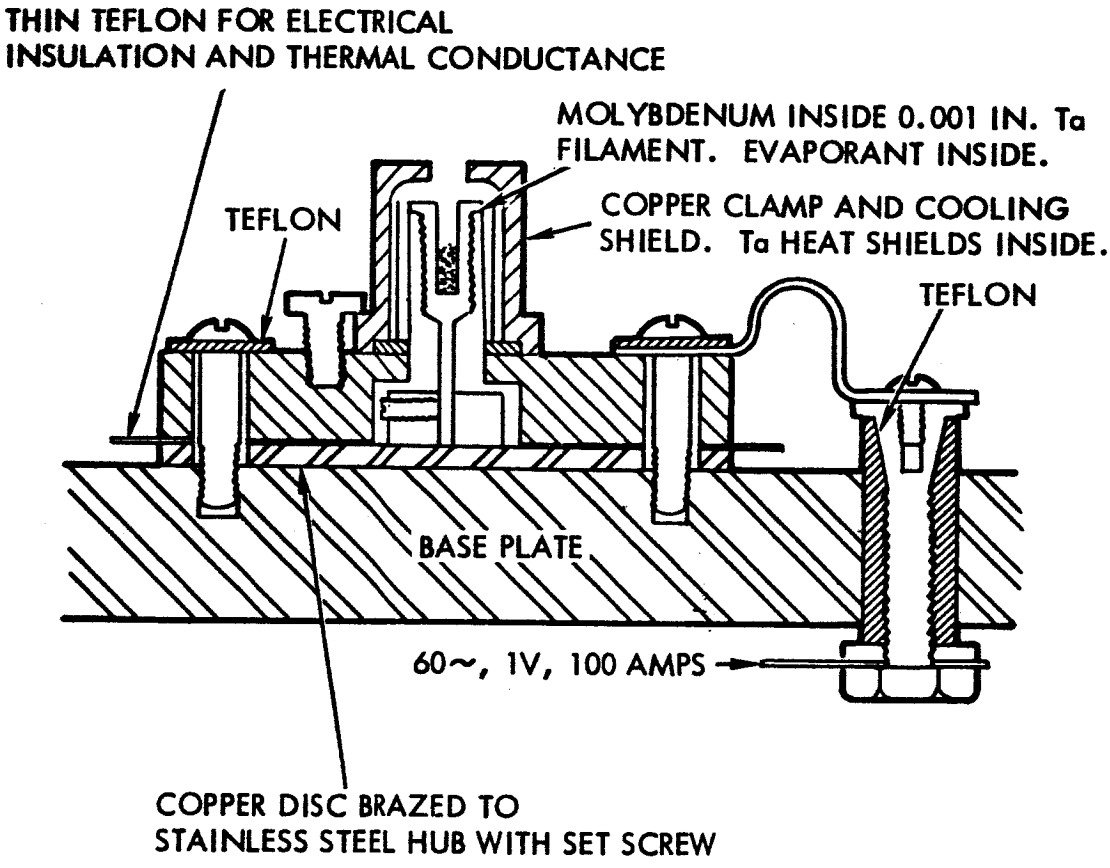


Figure 6. Sketch showing oven construction. Oven is designed to allow stable, continuous high-temperature evaporation of a wide variety of materials.

of its tendency to flow and thus make good surface contact. It also provides excellent electrical insulation. Alternative schemes would use massive current-carrying leads to conduct the heat away. The temperature rise with such designs could be excessive and injurious to seals and other parts. If we calculate the temperature rise across 5-mil teflon used in the oven at 100 watts of power through 40 $cm^2$,

$$100 = \frac{0.03 \times 40 \times \Delta T}{0.0127} \quad ,$$

$$\Delta T = 1^{\circ}C \ .$$

If this power had to be conducted 2 inches along a copper bar 1/8 x 1/4 inch in cross section,

$$100 = 4 \times 1/32 \times \frac{6.45 \times \Delta T}{2 \times 2.54} \quad ,$$

$$\Delta T = 630^{\circ}C!$$

The shutter consists of an aperture above the oven across which a flag of thin metal can be driven impulsively to close or open it. The "hammer" that drives the flag to one of its extremes is a solenoid-actuated slug. A charged capacitor is discharged across one of two solenoids to actuate the shutter, one solenoid opening it and the other closing it. The shutter usually opens or closes completely in less than 5 ms. For comparison, the minimum lifetime measured was about 30 ms.

The method of data-taking has been to let an electrical pickup from the solenoid voltage trigger the sweep of the scope on which the output is displayed. A polaroid picture is then taken of the scope face, the lens being opened just prior to the initiation of the shutter action (and hence the trace).

Examples of the single-trace photos obtained are presented in Figure 7.

An additional mode of data-taking was required to measure low-coverage lifetimes at low temperatures. The method used was to determine the coverage by abruptly flashing the ribbon to a high temperature and measuring the integrated current, which is proportional to the coverage. Synthesized curves of the form shown in Figure 1(a) were obtained by flashing at different accumulation times measured from opening of the shutter or previous flashing and plotting the data obtained. These measurements were made at very low arrival rates -- below the instrument sensitivity for measuring steady state -- and a constant uncertainty when taking data in this mode is that the arrival rate of oxygen might be sufficient to alter the surface during the long time required for equilibrium coverage to be established.

The experiment was performed on a Veeco oil-diffusion pumped vacuum system in a bell jar sealed with a Viton gasket. Other gaskets in the system were Viton O-rings and teflon lead-through insulators, as illustrated in Figure 6. Dow-Corning 704 oil was used, and the system was continuously trapped with liquid nitrogen. To improve trapping efficiency, an additional baffle was added to the trap.

A light bake was performed by operating a large radiative filament inside the bell jar. The oxygen and water partial pressure was reduced to the point that the sample tungsten ribbon would remain unoxygenated for minutes after flashing.

Hydrocarbon vapors were objectionable unless much effort was expended to reduce their pressure to very low values. In this case they were objectionable not because they might form carbides (at these low pressures, any cracked carbon could easily diffuse into the tungsten or over long periods react with oxygen), but because they presented a background in the spectro-

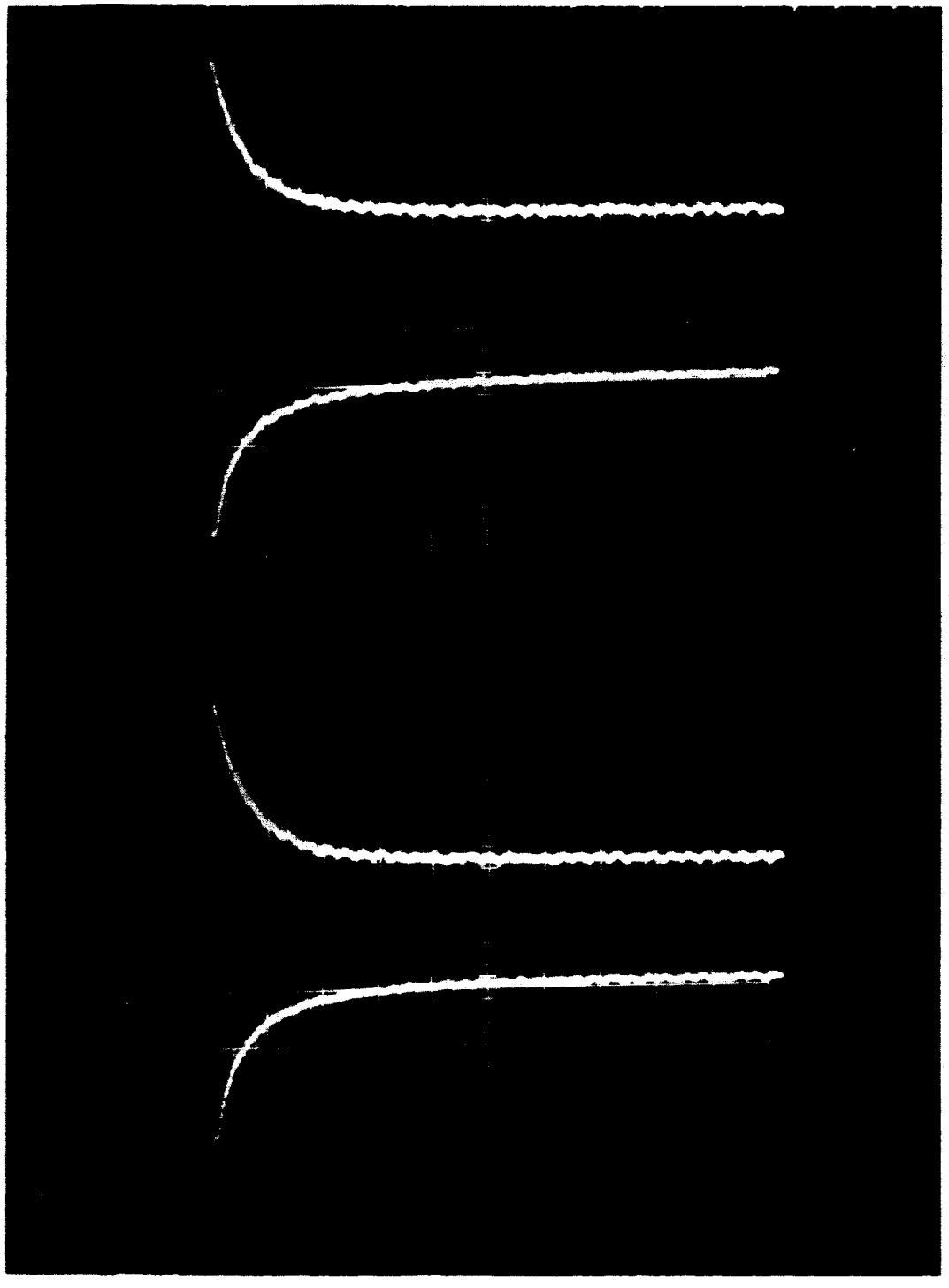

Figure 7. Typical picture from which copper evaporative lifetime data was taken. 1400°K, 50 ms/div. Downward deflection is proportional to evaporated copper from a hot tungsten ribbon at times after opening or closing shutter.

meter that interfered with the small currents that were being measured. Some materials fortunately fell between hydrocarbon groups, but others fell among the hydrocarbon groups, with the result that a hydrocarbon peak or the "skirt" of an adjacent strong hydrocarbon peak would often represent more current than we were measuring.

## COMPARISON OF EVAPORATED LIFETIME OF MATERIALS FROM SELF AND FROM CLEAN TUNGSTEN

It is instructive to convert a vapor pressure into a "self" lifetime, $\tau = \sigma/\Gamma_{ev}$, where $\sigma = n^{2/3}$, n being the volume density of atoms in the solid and equal to $\rho/m$. For copper

$$n = (8.9/63 \times 1.67 \times 10^{-24}) = 83 \times 10^{21} . \quad n^{2/3} = 1.9 \times 10^{15}/cm^2 .$$

For $10^{-6}$ torr at approximately $1150^{\circ}K$, $\Gamma = \dfrac{P}{\sqrt{2\pi mkT}}$

$$\Gamma_{ev} = \frac{\frac{10^{-6} \times 10^{6}}{760}}{\sqrt{6.28 \times 63 \times 1.67 \times 10^{-24} \times 1.38 \times 10^{-16} \times 1150}} \cong 1.3 \times 10^{14}/cm^2 \text{ sec.}$$

Therefore the self lifetime is $1.9 \times 10^{15}/1.3 \times 10^{14}$, or approximately 14 seconds.

We say, then that the lifetime of copper from copper is 14 seconds when its vapor pressure is $10^{-6}$ torr (at $1150^{\circ}$ K, from Honig RCA[3]). This value compares with its lifetime of 30 seconds from clean tungsten at the same temperature.

These parameters are tabulated in Table I for various materials tested in this program.

TABLE I

| Material | Density ($gr/cm^3$) | M amu | $\sigma=n^{2/3}$ no./$cm^2$ | T* for $10^{-6}$ torr ($^\circ K$) | $\Gamma_{ev}$ at T* (no./$cm^2$ sec.) | $\tau_{self}$ (sec) | $\tau_W(\theta=0)$ (sec) |
|---|---|---|---|---|---|---|---|
| Air | | 29 | $10^{15}$ | 300 | $3.77\times10^{14}$ | | 2.65 |
| Tungsten | 19.3 | 184 | $1.6\times10^{15}$ | 2670 | $5\times10^{13}$ | 32 | |
| Copper | 8.9 | 63.6 | $1.9\times10^{15}$ | 1150 | $1.3\times10^{14}$ | 15 | 30 |
| Chromium | 7.2 | 52 | $1.9\times10^{15}$ | 1255 | $1.38\times10^{14}$ | 14 | 2000 |
| Beryllium | 1.85 | 9 | $2.48\times10^{15}$ | 1100 | $3.53\times10^{14}$ | 7 | 3000 |
| Nickel | 8.9 | 58.7 | $2\times10^{15}$ | 1340 | $1.25\times10^{14}$ | 16 | 50 |
| Iron | 7.8 | 55.8 | $1.9\times10^{15}$ | 1295 | $1.31\times10^{14}$ | 14.5 | 200 |
| Titanium | 4.5 | 47.9 | $1.47\times10^{15}$ | 1500 | $1.31\times10^{14}$ | 11 | $2\times10^{6}$** |
| Zirconium | 6.44 | 91.2 | $1.21\times10^{15}$ | 2000 | $8.2\times10^{13}$ | 15 | $>> 10^{6}$** |

*Vapor pressure from Honig RCA[3].

**Estimated

Air and tungsten are included on the list only for comparison. Particular attention should be paid to the difference between the last two columns, first of which gives the lifetime of a material from itself and is the value approached at high coverages on tungsten, while the last gives our data for low coverages on tungsten. A wide difference indicates a strong dependence of both lifetime and work function on coverage. Titanium and zirconium are extremes in this respect. Copper is the most attractive material on the list because of the low temperature at which its vapor pressure is $10^{-6}$ torr and the similar lifetimes of copper from copper and copper from tungsten, with the associated small work function effect.

DATA

Copper

Copper was the easiest material to test. It vaporized easily from the oven and had negligible dependence on coverage, so that the waveforms were almost perfectly exponential. Its lifetime versus reciprocal temperature is shown in Figure 8. As shown

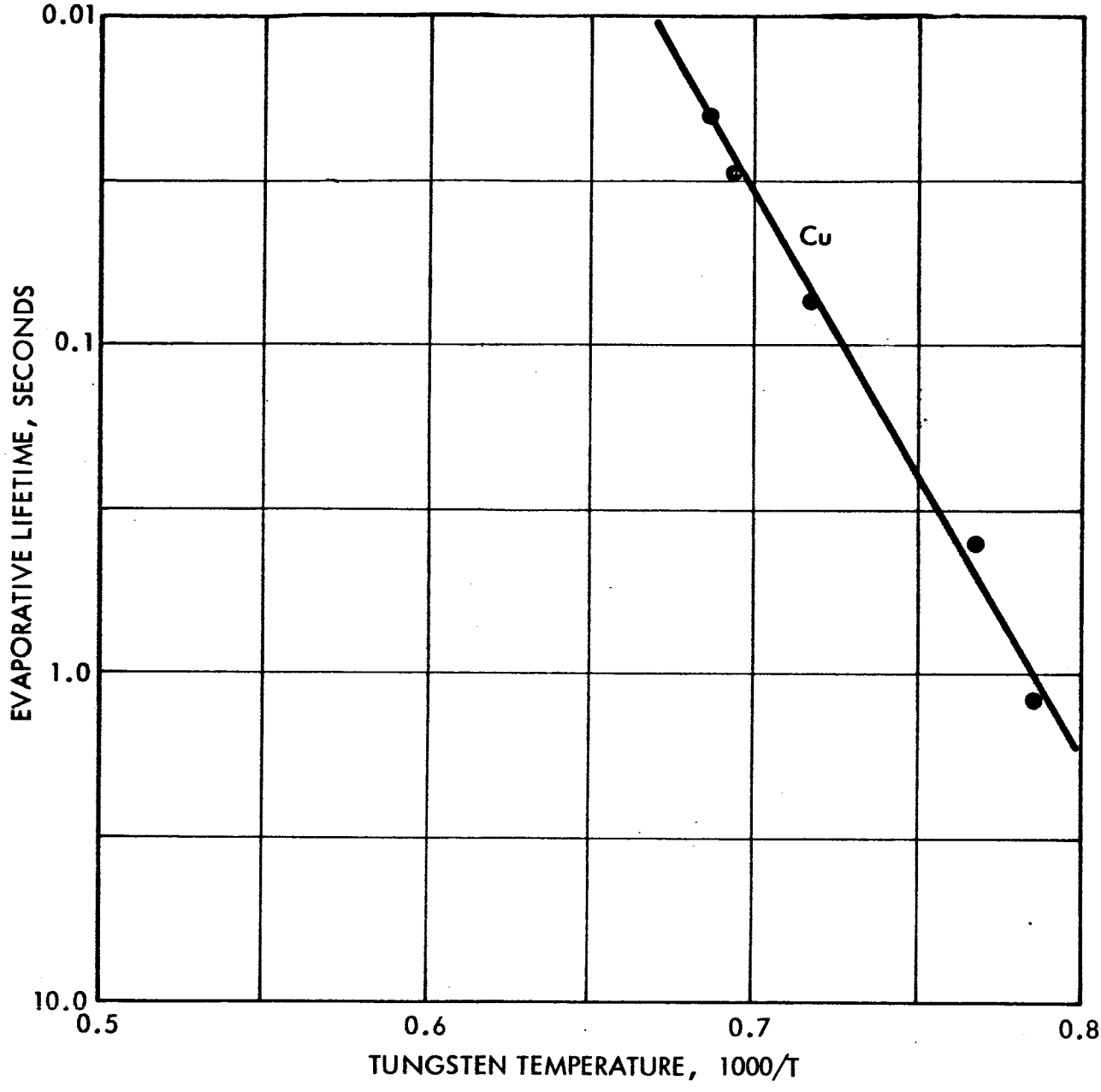


**Figure 8.** Evaporative lifetime of copper from polycrystalline solid tungsten.

in Table I this lifetime is only twice the lifetime of copper from itself, a fact that indicates that even a high coverage of copper on a surface would not alter the work function ($\phi = 4.5$).

The use of copper in ion engines for many years indicates its compatibility. A confirmatory experiment in which copper was placed in the ion beam immediately above the accelerator showed that the neutral fraction and critical temperature were the same before and after exposure.

Chromium

The adsorption of chromium on tungsten is much more complicated than that of copper. The lifetime of chromium is dependent on coverage, and in addition, chromium diffuses into tungsten. Oxygen on the surface decreases the lifetime, but the effect is small.

A distinguishing feature of chromium is that its lifetime (shown in Figure 9) changes abruptly at one coverage, which is called a monolayer ($\theta = 1$). We do not have an accurate knowledge of what density this coverage represents; we say it is about $1.5 \times 10^{15}$ atoms per square centimeter. The maximum coverage before bulk chromium is formed is 1.3 monolayers. The 0.8 and 1.1 monolayer lines are sketched in the figure to indicate the more rapid variation of lifetime for coverages greater than a monolayer.

Of the materials tested, only chromium demonstrated unmistakable and measurable diffusion. We cannot distinguish between bulk and grain boundary diffusion, which are both into the bulk of the material. The evidence of this diffusion is shown in Figure 10. It can be seen in Figures 10(a) and 10(b) that the amount of chromium that comes out of and off the tungsten when its temperature is flashed increases with the time of exposure. The structure is due to the temperature increase

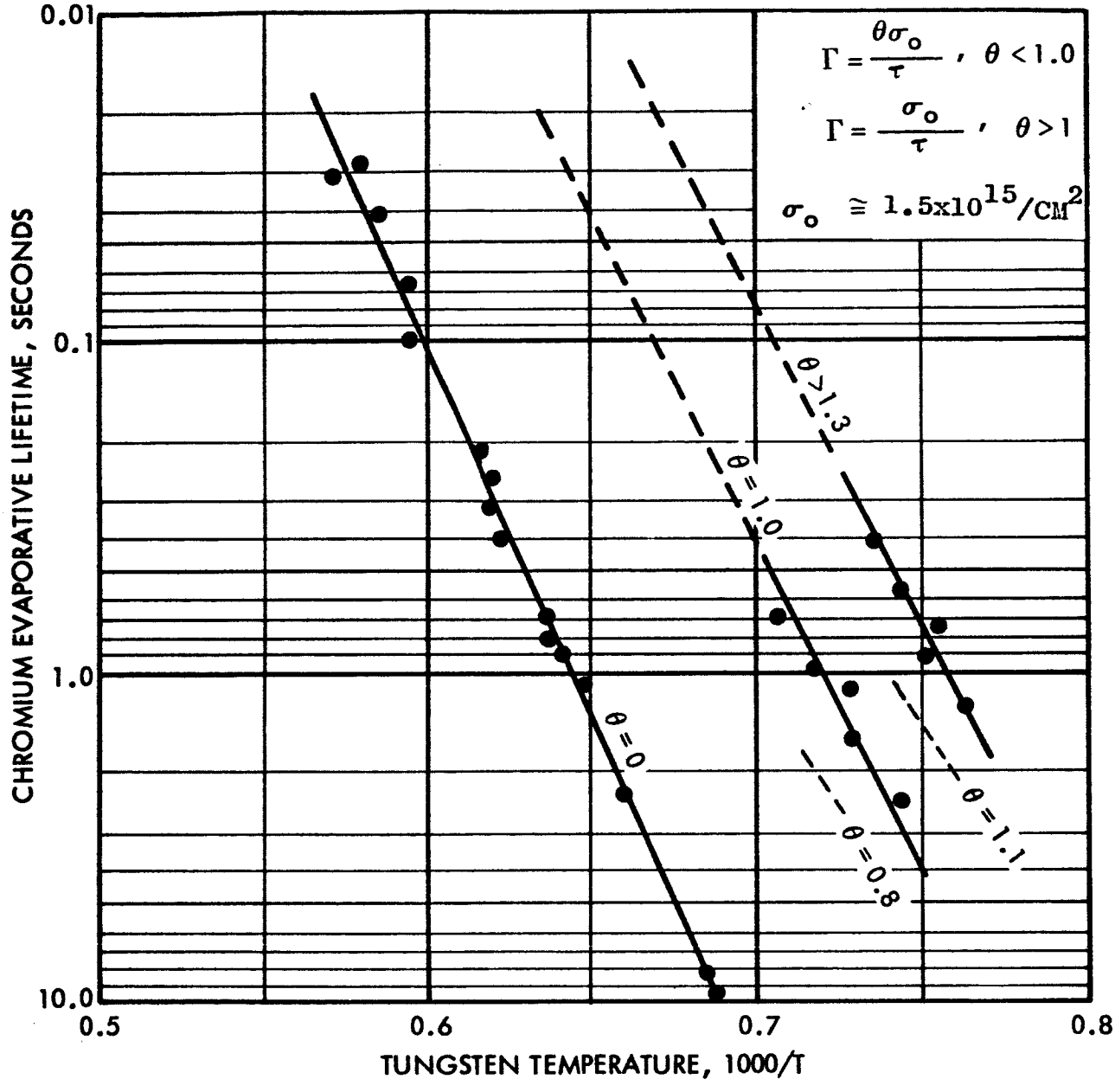


Figure 9. Chromium lifetime versus temperature of polycrystalline tungsten with varying coverages.

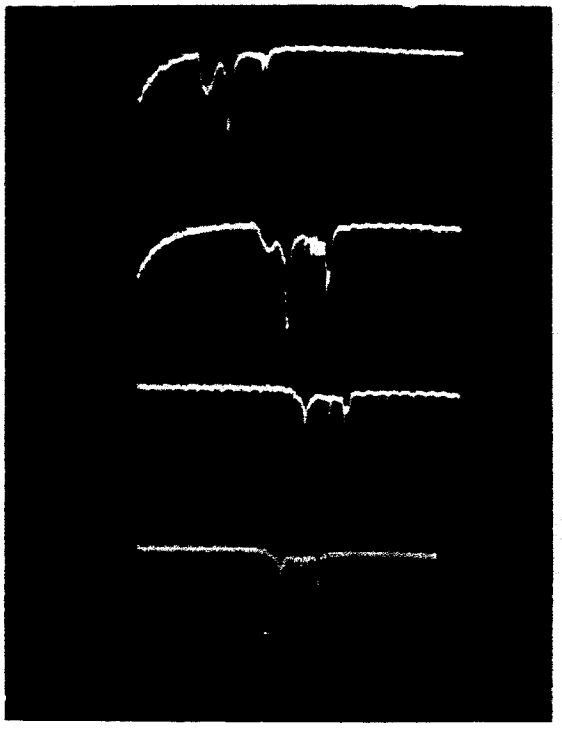

(a) Exposure 10 sec. flash after 0.2 sec.

(b) Exposure 20 sec. flash after 0.4 sec.

(c) Exposure 10 sec. flash after 10 sec.

(d) Exposure 10 sec. flash after 20 sec.

Figure 10. Scope traces of chromium evolution from the interior of tungsten upon flashing for various exposure times and periods of delay between oven shutter closure and flashing. Downward deflection represents evolution; horizontal portion of trace represents approximately zero evolution. Temperature of tungsten 1615°K. Horizontal scale: 100 ms/div.

during the flash and shows differing degrees of ease of re-emission. In Figure 11 these flashed currents integrated by a capacitor across the input of the scope are shown for different accumulation times, all of which are beyond the time required for equilibruim adsorption coverage. In Figure 12 we can see that the plot of accumulated chromium against the square root of the time is linear, which is indicative of a diffusion process.

When chromium is applied to an operating porous tungsten ionizer, the results are very apparent; under most conditions the critical temperature is higher, and the neutral fraction is low, possibly because of the tight oxygen-to-chromium bond. It is nearly impossible to rid the porous tungsten of the last remnants of chromium, which continue to cause these effects. In a pressure of oxygen the critical temperature changes -- the higher the oxygen pressure, the lower the critical temperature; if the oxygen is stopped, the critical temperature is at first extremely high. These effects are detailed in Monthly Report No. 8, which is included as Appendix I.

Beryllium

The lifetime of beryllium on tungsten presents a complicated picture. Not only is the lifetime strongly dependent on coverage, but it varies widely with the presence of oxygen. In addition, the sticking probability is not unity and varies with the degree of coverage and oxygenation. The story of beryllium lifetime is told in Figure 13. In this figure, the data for $\theta \cong 0$ is the most reliable, the higher coverage data having been obtained from analysis, as discussed previously and illustrated in Figure 1(d). The value $\theta \cong 1$ was taken as the maximum integral before bulk condensation began. The information on beryllium on oxygenated tungsten is only approximate because of the difficulty of measuring arising from the nonunity sticking coefficient. The lower dotted line is an estimate of this lifetime, which is about $10^4$ times longer than the lifetime from clean tungsten.

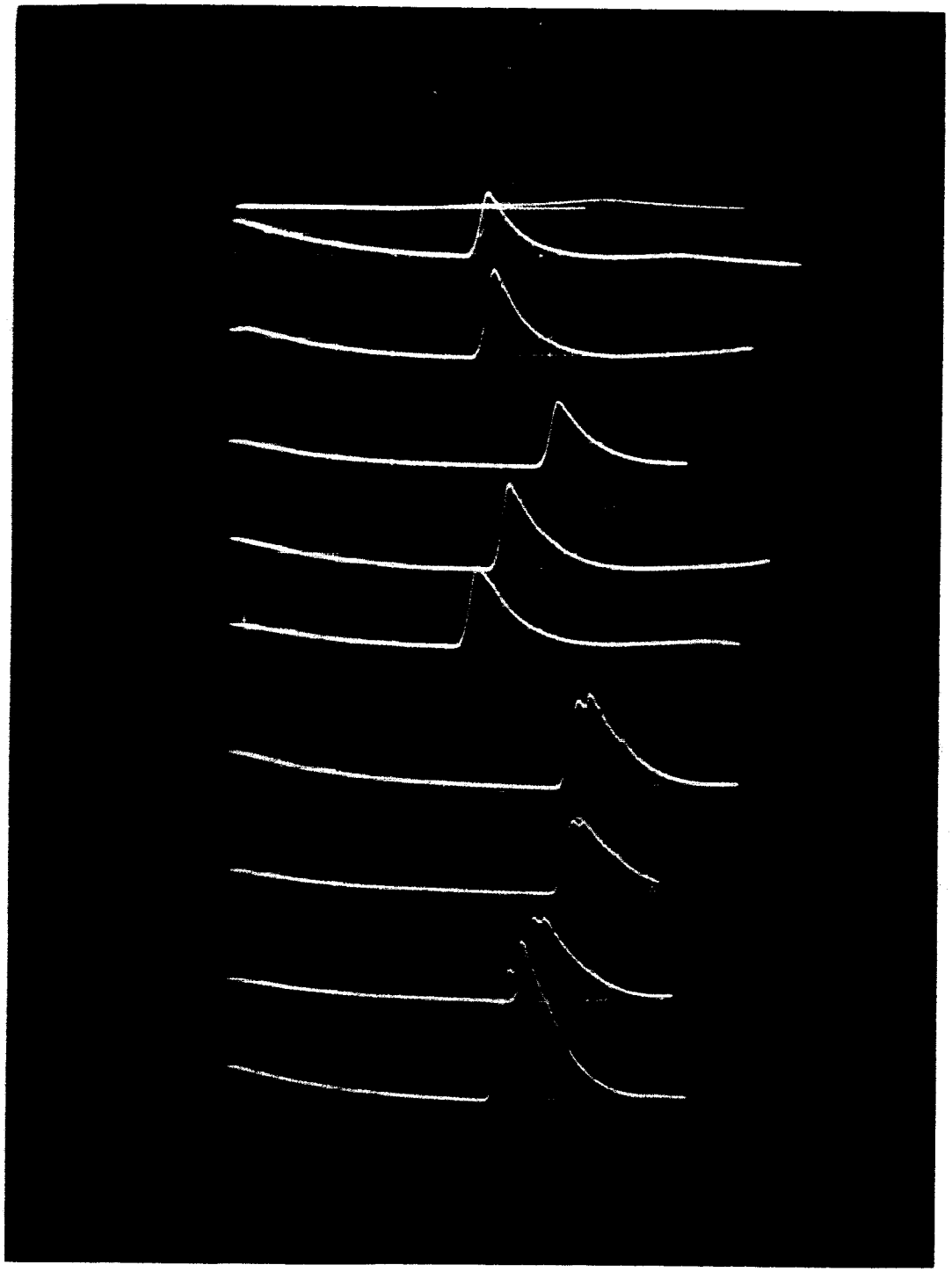

Figure 11. Picture showing diffused chromium flashed off after varying times of exposure. This picture differs from Figure 10 in that a capacitor smoothes the curves to allow easier geometrical integration. Accumulation times are 5, 10, 15, 20, 25, 30, 60, 90, and 120 seconds at 1515$^{o}$ K.

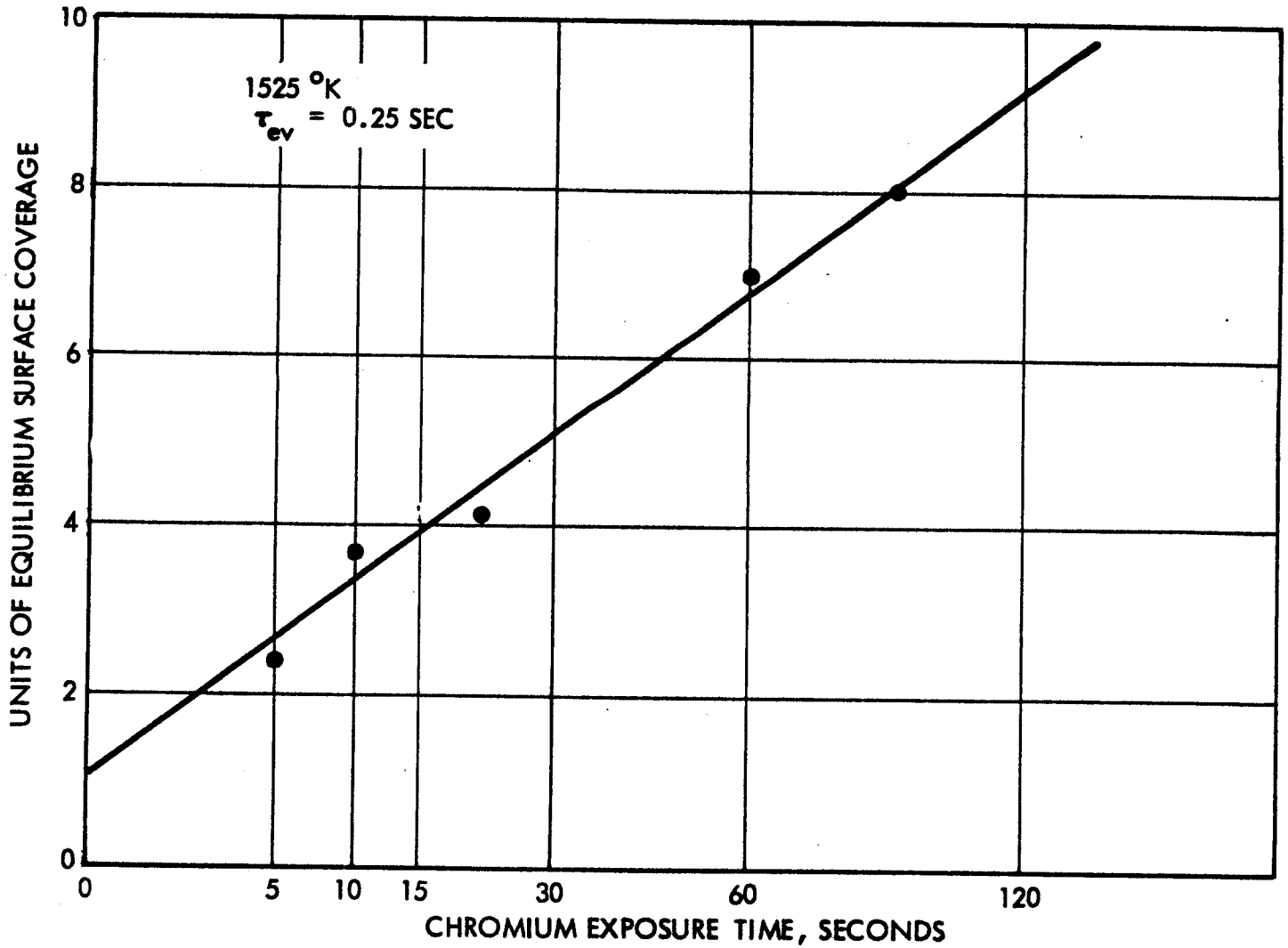


Figure 12. Plot of amount of diffused chromium versus the square root of the exposure time. The straight line confirms that diffusion laws are obeyed.

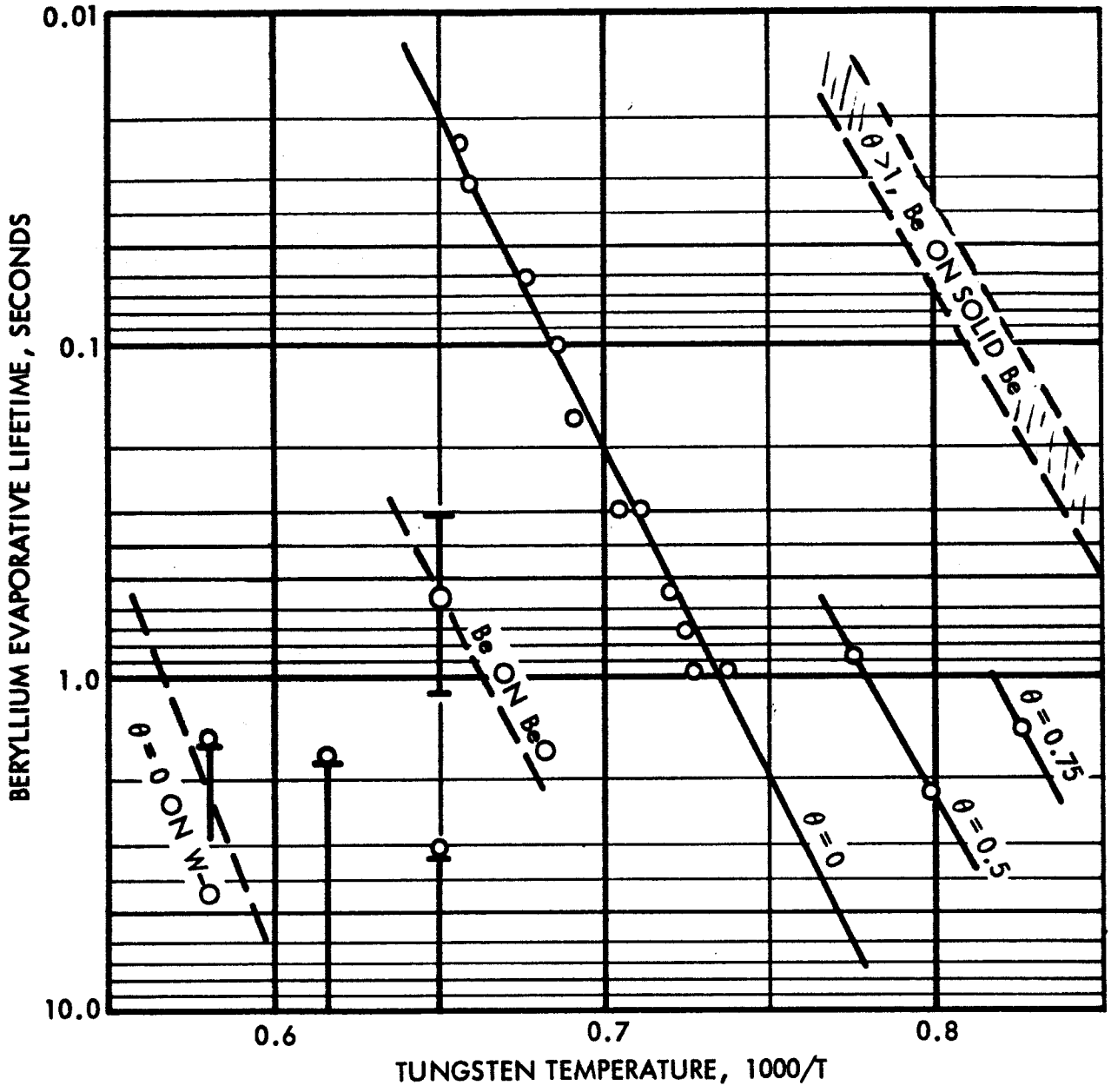


Figure 13. Evaporative lifetime of beryllium versus temperature of tungsten from which it evaporates for different degrees of coverage and cleanliness.

Sticking probabilities differing from unity -- sometimes approaching zero -- were observed at various times during data-taking, in contrast to the fact that no other material studied showed a detectable departure from unity. These observations for beryllium are sketched in Figure 14, where the curves shown are qualitative only, not quantitative. No detectable bulk diffusion could be observed.

When beryllium is sputtered onto an ion-emitting pellet, the results are similar to those with chromium -- the material is impossible to get rid of, and although small amounts are undetectable by themselves, when traces of oxygen are present the critical temperature is high. Continuous oxygen pressure lowers the critical temperature, as illustrated in Figure 15.

We have found this oxygen effect to be similar with chromium, beryllium, and tantalum and attribute it to the known affinity of these elements for oxygen. The conclusion is somewhat suspect, however, since some of our later pellet tests show this effect to some degree even when these materials purportedly are not present. We suspect that in these cases the use of tantalum as a heat shield while sintering, vacuum distilling, or brazing has contaminated the pellet.

## Nickel

The lifetime of nickel on tungsten is relatively simple, with only a small dependence on coverage. Strangely, the lifetime of nickel on oxygenated tungsten is shorter than on pure tungsten and increases with coverage, as shown in Figure 16.

Also remarkable, in the light of the known enhancement of sintering by nickel, was the complete lack of any evidence of diffusion of the nickel into the tungsten. These results tend to suggest there is no solubility of nickel in solid tungsten, and that the small limit of solubility that has been reported[4] might be adsorbed material in crystal boundaries. Such a conclusion makes the observed enhanced sintering of tungsten by nickel very confusing.

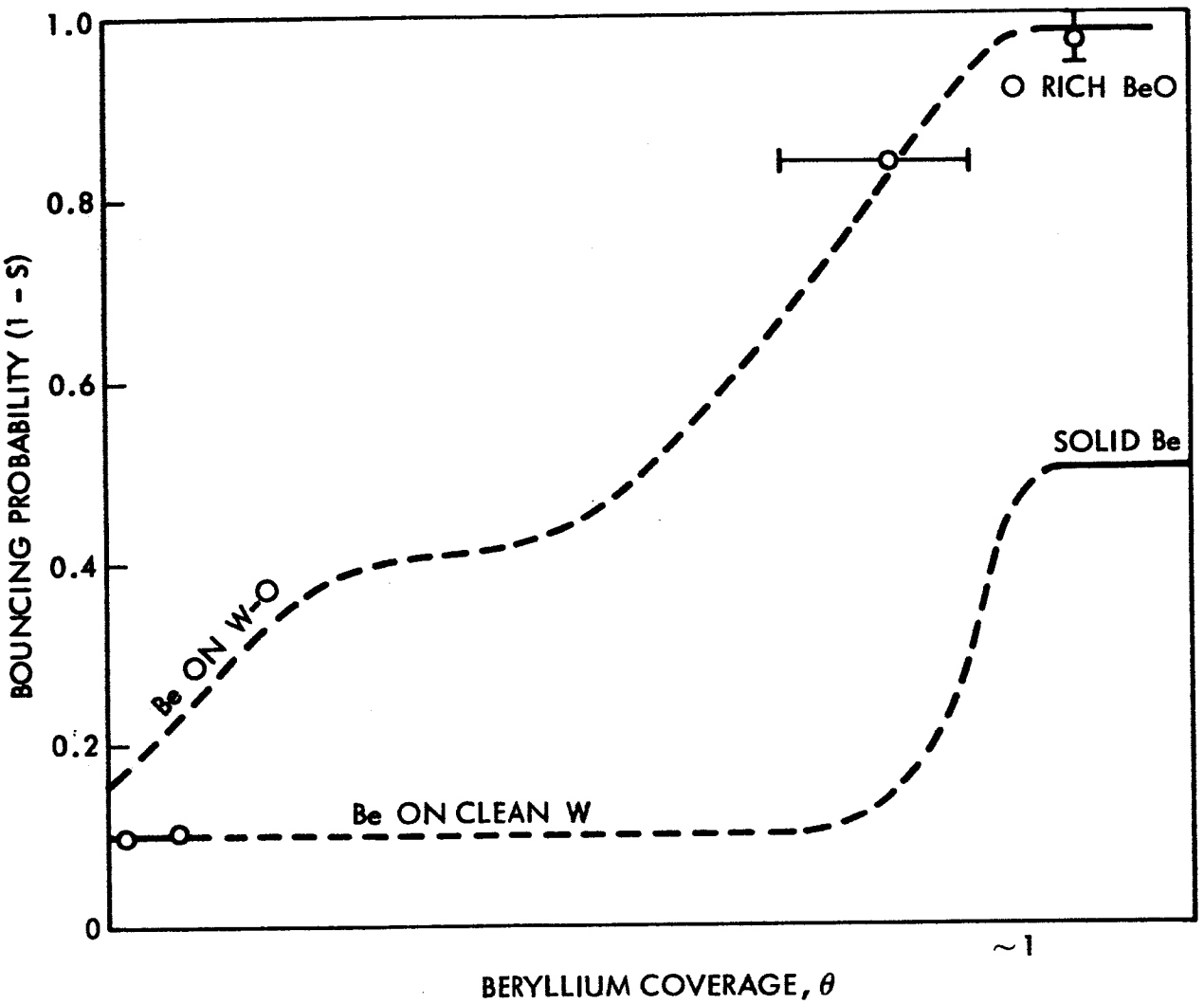


Figure 14. Schematic sketch of the observed nonunity sticking probability, s, versus approximate coverage.

1. ◇ CLEAN
2. ● SPUTTERING BERYLLIUM ON FOR TWO MINUTES
3. * AFTER STABILIZING AT 1600 °K FOR 10 MINUTES
4. □ 30 MINUTES LATER AND HEATED UP TO 1850 °K
5. ⌂ AFTER SPUTTER CLEANING AT LOW TEMP (1530 °K)
6. ○ WITH 5 X $10^{-6}$ TORR OXYGEN
7. ✕ OXYGEN OFF
8. △ AFTER SPUTTER CLEANING FOR 10 MINUTES
9. ■ WITH 5 X $10^{-6}$ TORR OXYGEN
10. ▼ SPUTTERING BERYLLIUM ON WITH OXYGEN, BUT DATA WAS TAKEN WITH $O_2$ OFF
11. ◇ WITH 5 X $10^{-6}$ TORR OXYGEN

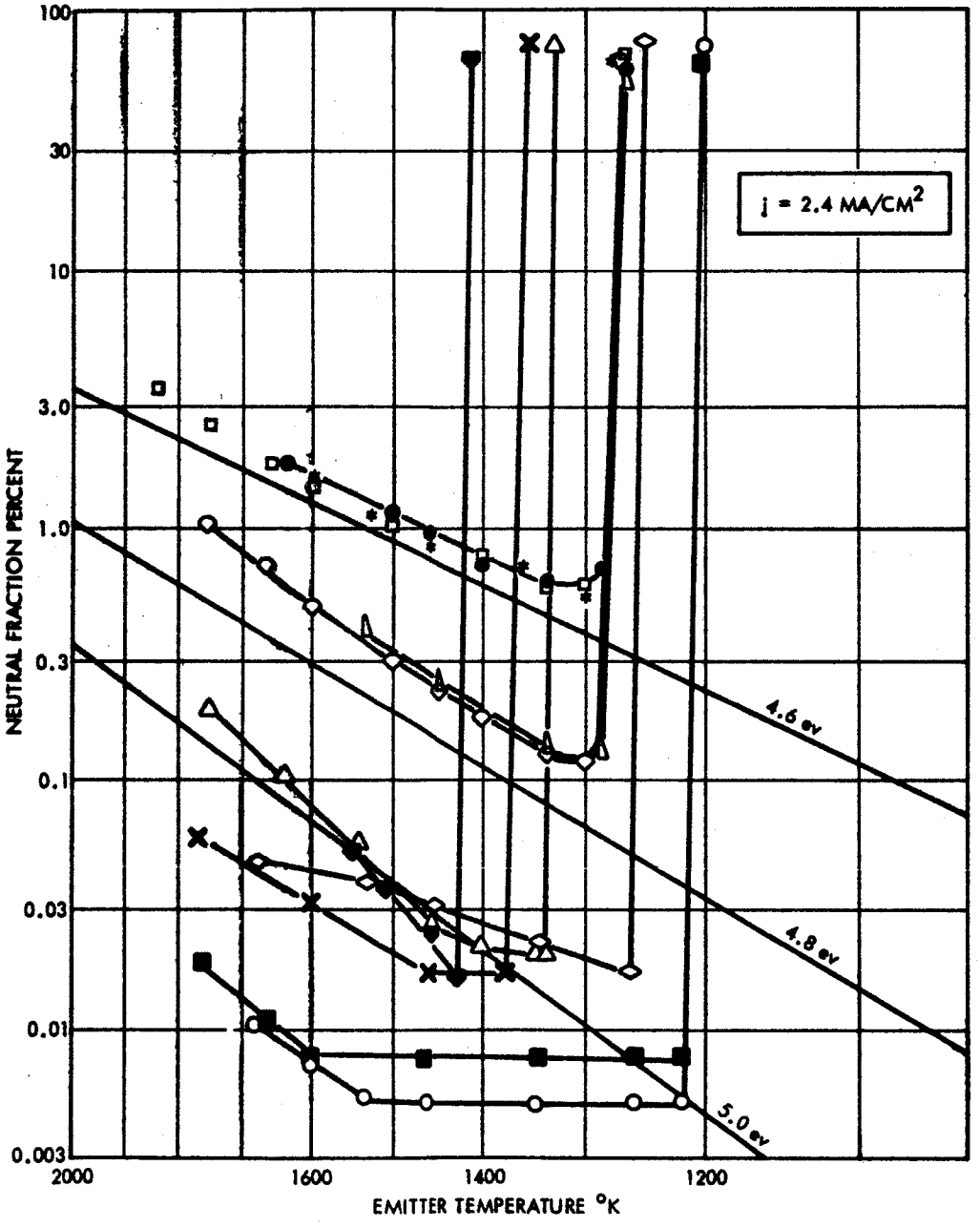


Figure 15. Cesium neutral fraction versus temperature of porous tungsten on which beryllium is deposited. Testing sequence reveals interesting interaction with oxygen.

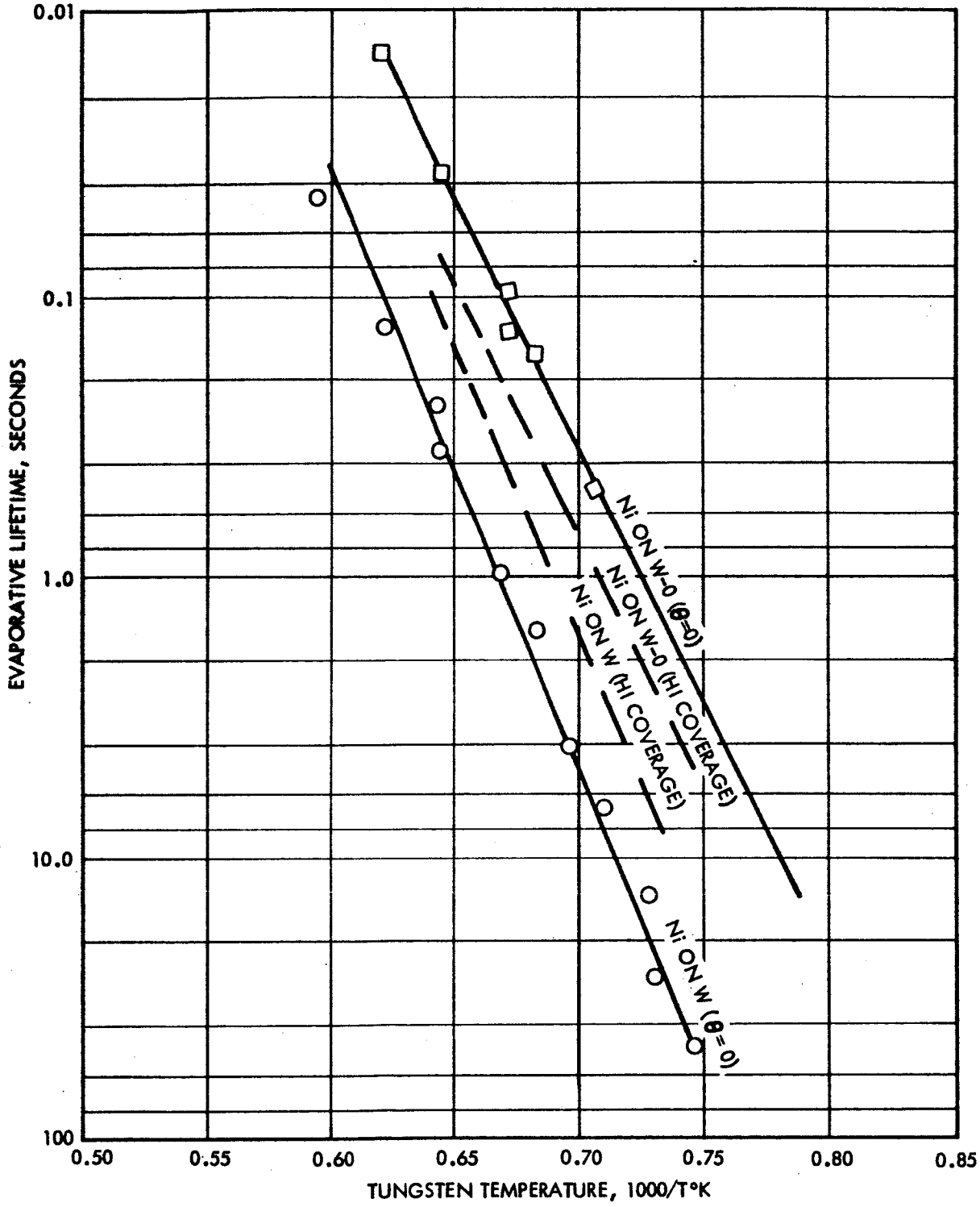


Figure 16. Nickel evaporative lifetime versus tungsten temperature.

It is suspected that if the coverage of nickel is kept below a monolayer, no sintering will be detected. This supposition is somewhat supported by an experiment in which we heated a carefully measured tungsten pellet above a chamber in which nickel was placed. No sintering ($< 0.3$ percent) was observed after 30 minutes of heating with a continuous bombardment of more than a monolayer per second; also, the surface remained open. (Later, when molten nickel-moly alloy ran into the porous tungsten, sintering was measurable.)

In further tests, when nickel was sputtered onto an operating ion emitter at a rate of about 1/2 monolayer per second for periods as long as 2 hours with the temperature ($1400^{\circ}K$) selected to produce more than a monolayer, no effect on neutrals, critical temperature, or transmittivity was detected. On the basis of these evidences, we see no objection to the use of nickel in the accelerator.

## Iron

Lifetime data for iron are presented in Figure 17. Iron resembled nickel in all qualitative aspects, having no effect on an ion-emitting pellet. These findings suggest the use of iron accelerator structures despite the long-standing worry about sintering. The fact that E.O.S. at one time used 2-atomic-percent iron in their infiltrant supports the evidence that sintering does not occur with small amounts of iron -- especially if incident only from the surface.

## Titanium

Titanium has a very long lifetime, especially at low coverages, and its measurement was very difficult. Approximate lifetimes are presented in Figure 18. Whereas the lifetime data obtained for most other materials (iron, chromium, nickel, and beryllium) are considered to be within about 20 percent for low coverages, the data for titanium might well be off by half a decade.

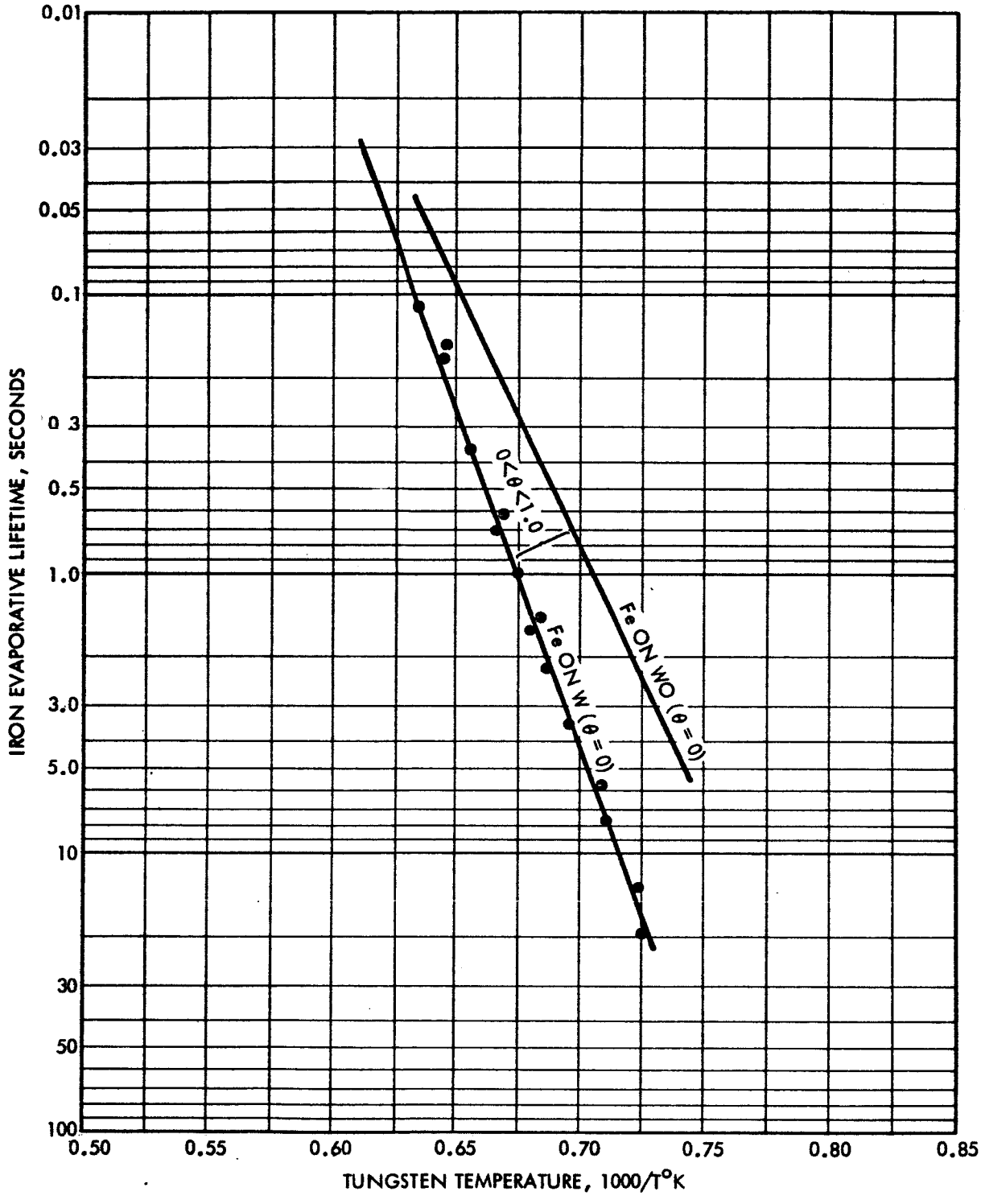


**Figure 17.** Evaporative lifetime of iron versus temperature of tungsten from which it was re-evaporated.

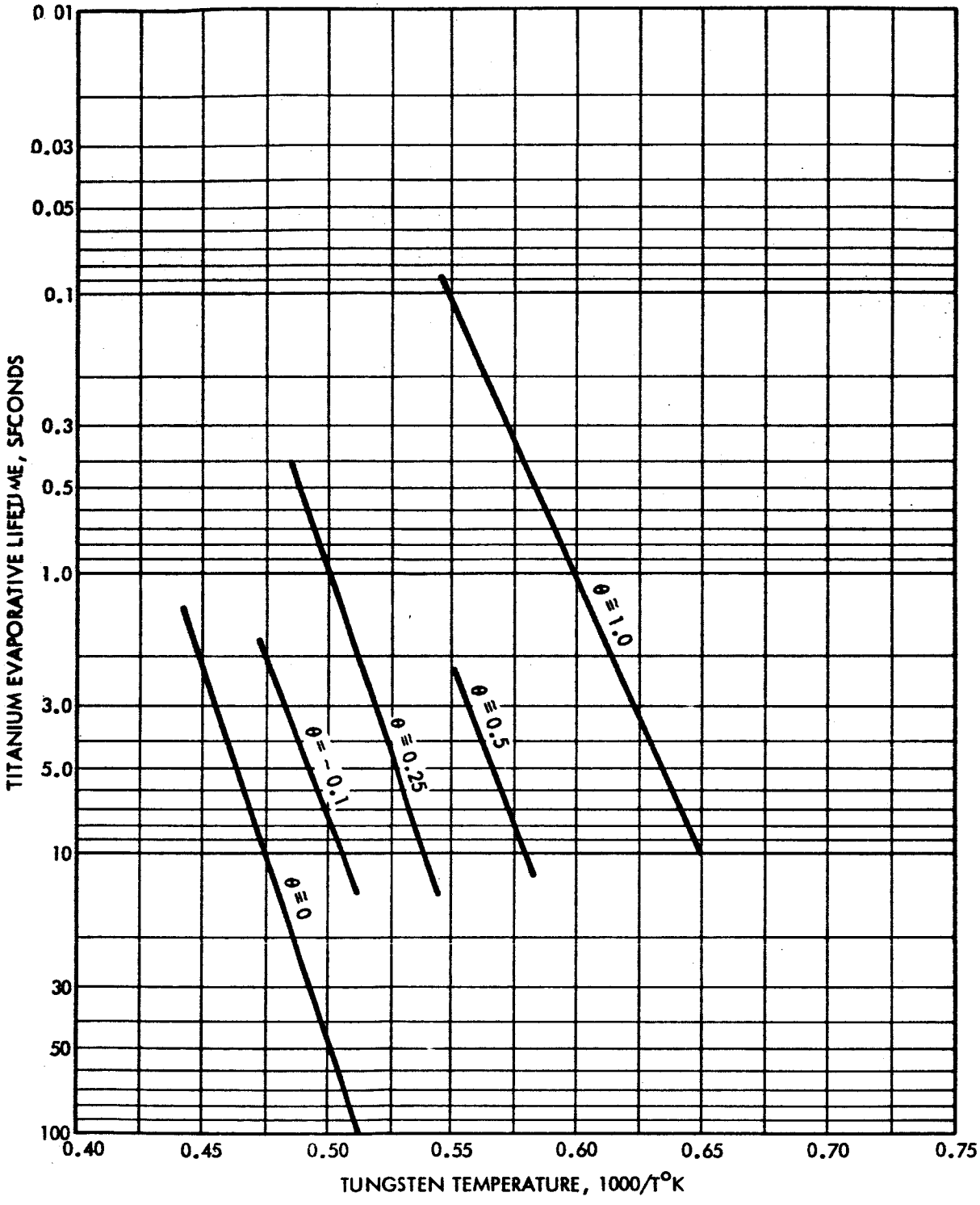


Figure 18. Approximate evaporative lifetime of titanium versus temperature of tungsten from which it was re-evaporated.

When titanium was sputtered onto an operating ion emitter, it was found to be a bad poison. High titanium coverages increased the neutrals to over 50 percent, and high-temperature operation diluted the titanium, probably allowing it to surface-migrate into the interior of the porous tungsten. Cleaning by sputtering would temporarily reduce the surface concentration of neutrals, but then more would diffuse to the surface. For example, after about 100 monolayers were placed on the surface, heating for about 20 minutes at 1600°K would reduce the neutrals to about 5 percent, sputtering would further reduce this to 1/2 percent, but upon further operation, the neutrals would again increase to a few percent.

Small amounts of titanium increase the neutrals but the critical temperature is slightly reduced. Interactions with oxygen were not studied. This was an oversight, and in light of the interesting oxygen effect that was observed on a zirconium poisoned surface, the investigation might have proved of interest.

Zirconium

Zirconium sputtered onto an operating ion emitter poisons it severely, reducing the ion current to about 25 percent and increasing the neutrals to 75 percent. After an hour of heating at 1600°K neutrals still measure over 50 percent and sputtering cleaning only temporarily helps. Remnant oxygen increases the work function and lowers the neutrals to a fraction of a percent; then when carbon removes the oxygen, the poisoning effects of zirconium are once more observed.

Difficulties were encountered in an experiment to measure the lifetime of zirconium on tungsten because of the nearly infinite lifetime of the material at low coverages and temperatures below 2000°K. Evidence of surface-migration, interaction with oxygen, and severe thermal emissivity change seems to indicate a characteristic of zirconium beyond its poisoning effect.

## Summary of Lifetimes Expressed as Heats of Evaporation

Table II lists $\tau_o$ and $E_{ev}$ in volts when the lifetime at low coverages is expressed at $\tau = \tau_o \exp (E_{ev}\, e/kT)$, (Eq. 3).

TABLE II

Lifetimes on Clean Tungsten

| Material | $\tau_o$ (sec) | $E_{ev}$ (volts) | $\tau$ at 1500°K (sec) |
|---|---|---|---|
| Copper | $4.7 \times 10^{-14}$ | 3.365 | 0.01 |
| Chromium | $5 \times 10^{-15}$ | 4.4 | 4 |
| Beryllium | $2 \times 10^{-15}$ | 3.965 | 0.04 |
| Nickel | $5.6 \times 10^{-15}$ | 4.22 | 1 |
| Iron | $1.4 \times 10^{-17}$ | 4.95 | 0.7 |
| Titanium | $\tau \sim 50$ sec. at 2000°K | | $\gtrsim 10^5$ |
| Zirconium | $\tau$ est. $> 10^6$ sec. at 2000°K | | $\sim \infty$ |

# PROGRAM TO TEST POROUS TUNGSTEN PELLETS

## INTRODUCTION

Space Technology Laboratories was asked to test a maximum of 24 porous tungsten pellets that would be supplied throughout the year by Lewis Laboratories. These pellets were to have their cesium neutral fractions measured as a function of current density up to 25 $ma/cm^2$, and as a function of temperature at 1, 10, and 20 $ma/cm^2$. These measurements were to be made both from clean tungsten in a high vacuum and from oxygenated tungsten in $5 \times 10^{-6}$ torr of oxygen. We had previously demonstrated that by using a hydrocarbon-free high vacuum and cleaning by sputtering, the clean surface condition could be achieved.

The results of testing a sample of porous tungsten may vary with the testing procedure and the equipment used. If the vacuum is poor the surface will be either oxygenated, resulting in continual tungsten removal, or carbided, causing the continual addition of carbon. If foreign materials are allowed to reach the sample surface, the test might be conducted on a completely altered surface. If high temperature and sputtering are not used, the results are likely not to represent tests on clean tungsten. If scattering apertures are in front of the emitter, the measured neutrals might not represent the actual neutral fraction emitted from the surface. In addition to the procedures and equipment used in testing, certainly the method used to prepare the surface of the sample is extremely important to test results, as any etching will open the surface pores and alter their geometry, and some types of etch will expose high-work-function crystal faces. The experimental apparatus and the procedures used in testing the sample pellets are described fully in the following pages.

## DESCRIPTION OF APPARATUS

### Vacuum

The experiment to test porous tungsten pellets was conducted in a pyrex bell jar sealed with a Viton A "L" gasket to a stainless steel baseplate that was mounted with bakable metal gaskets to a Welch Turbomolecular Pump. This pump has no diffusion pump oil or "head gate"; it consists of cascaded turbine blades rotating at 16,000 rpm, through which heavy organic molecules have no chance of diffusing. An oil backing pump is used, and the bearings are oil-lubricated. To break the vacuum system, air is let in and then the turbine is stopped. Oil vapors are barred from getting into the experimental region by the long path of air through which they must diffuse. This pump has a pumping speed of 140 liters/sec and an advertised ultimate vacuum of better than $1 \times 10^{-10}$ torr. It has worked very satisfactorily, and a mass spectrometer has shown it to be free of hydrocarbon vapors (except when the turbine pump has failed and the fore-pressure invaded the ball jar).

A large area of copper at liquid nitrogen temperature surrounds the experiment and eliminates water vapor, which is the dominant gas load of the system, and comes from the bell jar and from cesium compounds that are difficult to remove from previous operation.

### Pellet Size

The pellet configuration chosen for all our testing is a flat cylinder 0.156" (5/32 inch) in diameter and 0.020 inch thick. This size was originally chosen so that the pellets would fit on the end of 3/16 inch molybdenum tubing that we had been using in our feed system and had on hand. This size proved just about small enough to achieve the desired current densities with non gridded, single-aperture guns without using voltages that are excessively difficult to work with because of breakdown and X-rays and yet not so small that braze pene-

tration and geometrical variations due to thermal expansion would present a problem. The small size does not restrict availability or necessitate excessive machining. We call the effective area of this pellet 0.10 $cm^2$, partly to facilitate our conversion to current density and partly because 0.10 $cm^2$ is equal to the effective area of 0.141 inch of diameter, just 15 mils less than the actual diameter, which compensates for a small braze penetration and the shoulder on which the pellet sits.

"Ω"-Field Accelerator

An accelerator to the side and slightly behind the pellet mount has been used in this testing program. This arrangement has quite a few attractive features: no cesium is incident on the accelerator; no material from the accelerator can strike the porous tungsten pellet under test; no scattering structure exists to alter the interpretation of measured neutral fraction; and a hot ionizing surface can be placed above and close to the emitter to clean it by sputtering with cesium ions.

A computer program was run to prove out the intuitive design and to determine the trajectories and perveance. The computer results are shown in Figure 19 for a fully space-charge-limited beam. Note first that the emitter surface is surrounded by a lip to focus the ions inward against space-charge repulsive forces and to make the electric field and current density uniform across the emitter surface. The uniformity of current density can be judged by the constant distance from the emitter of the +3000 volt equipotential (-300 volts with respect to the emitter). Braze material occupies the region of field reduction near the edges. The example shown here has +3300 volts on the emitter and -6700 volts on the accelerator for a total acceleration voltage of 10 kv but exits the ions through a 1/2 inch aperture 1/4 inch above the emitter at zero volts (off the figure but

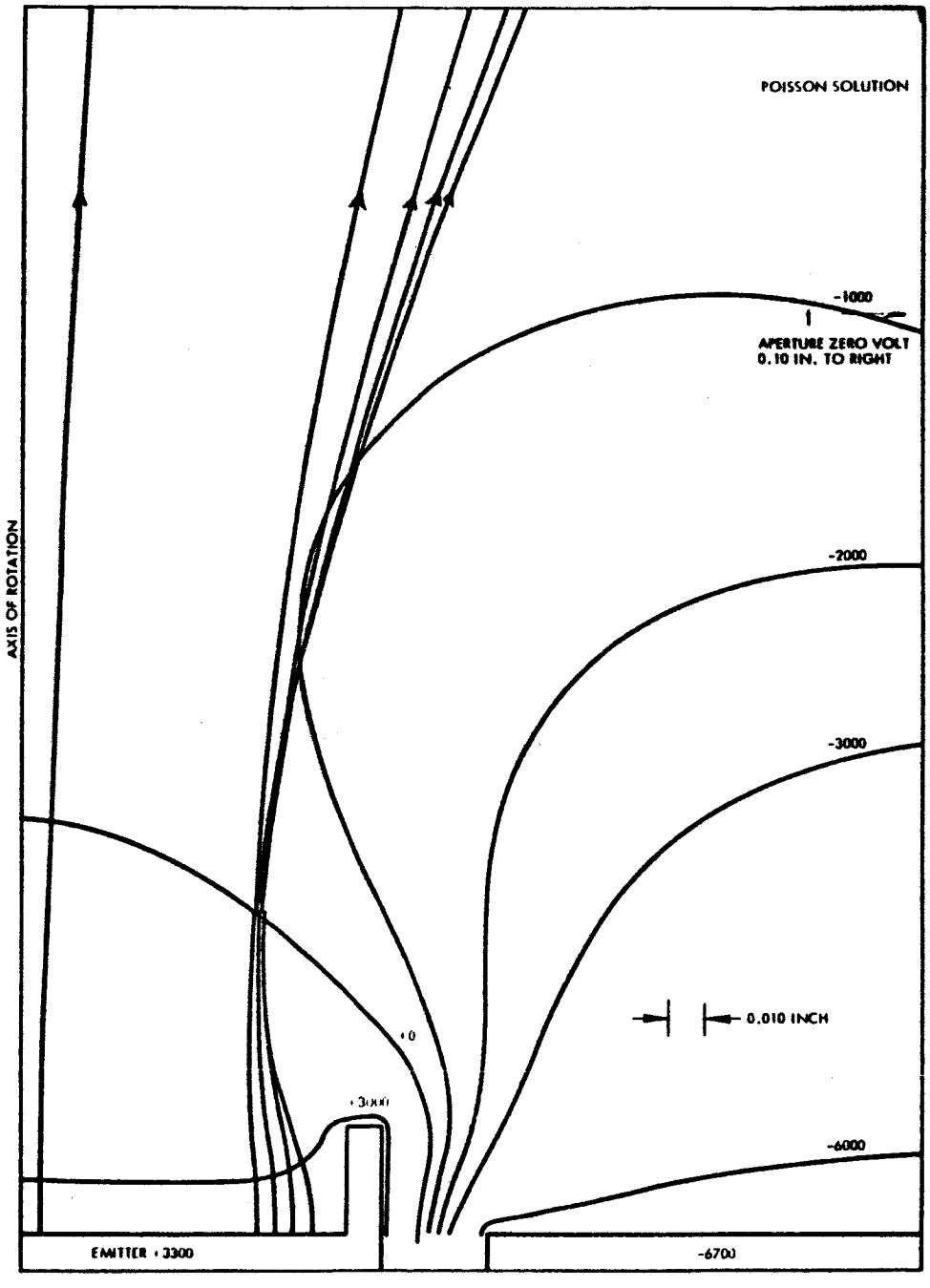


Figure 19. Computer results for the "Ω" field geometry: Space-charge-limited equipotentials and ion trajectories.

part of the computer problem). The computer predicted a current density of about 17 ma/cm$^2$. This figure can be confirmed by applying the planar space-charge law to the observed 300 volt equipotential at about 0.038 cm:

$$J = \frac{4.6 \times 10^{-9}(300)^{3/2}}{(0.038)^2} = 16.5 \text{ ma/cm}^2$$

In practice we operate the accelerator plate closer to top of the rim and so realize a higher perveance. Also, we use an accel-decel ratio nearer 2:1 that is, +5000 and -5000 volts -- and get less divergence and slightly higher perveance.

Feedtube and Plenum

Original plans were to braze the pellets into a holder that could be replaced simply, without brazing, by setting it on a fixed heater and feed system. Leakage was to be handled by properly designed differential pumping. The design was troubled by excessive leakage and had no chance of success when cesium pressures high enough to lift off the emitter holder were considered. The design settled upon utilizes a small molybdenum plenum assembly, used so that heat shielding would be unnecessary, joined to a 1/16 inch diameter molybdenum tube. (Designed to minimize heat loss, generate some heat, and, originally, fit a Swaglok-type fitting).

Braze

In a one-step operation, the emitter is rhodium-brazed into the plenum chamber and the plenum chamber is brazed onto the tube. Pure rhodium powder is mixed with turpentine to form a paste, which is placed in a groove around the emitter and at the joint between the plenum chamber and the tube. A minimum of the

paste is used in the latter joint because it gets hotter during the braze and the moly-rhodium alloying might seriously weaken the thin tube. The brazing is carried out by carefully observing the braze material while electron-bombarding it with about 50 ma of 2000-volt electrons from slightly below the plane of the emitter. At the first sign of rhodium melting (2240°K), the temperature is dropped. The braze is usually successful (see Figure 20, which is a photomicrograph of the cross section of a braze).

At times we get a trace of braze material on the top, although the burnishing from machining helps prevent this. During one test (No. 10) a loose-fitting pellet whose surface was eroded and porous had its lower side almost completely sealed. The probability of success is improved by having a close fit, burnishing the sides of the pellet, and keeping the porous tungsten colder (by radiation) than the molybdenum prior to the instant of braze. It is felt that the rhodium powder sinters together and withdraws from the porous tungsten, making creepage on top less likely. Penetration of the braze material into the porous tungsten is very slight.

Heater and Thermocouples

After brazing the permeability is checked and the surface is etched. (Both of these processes are described in later sections.) The next assembly process is to install the filament and thermocouple. This operation is performed with a spotwelder. A 0.001-inch-wall tantalum tube (with a spotwelded seam), 0.200-inch OD and about 1/2-inch long is spotwelded to the outside of the plenum tube below the rim. The other end is then spotwelded to a nickel bushing, which is kept from touching the feed tube by a ceramic tube. Next, 0.003-inch thermocouple wires (6 and 26 percent rhenium-tungsten) are sandwiched between a small bend in a 0.001-inch niobium tab and spotwelded to the side of the plenum chamber so that they protrude under the accelerator electrode.

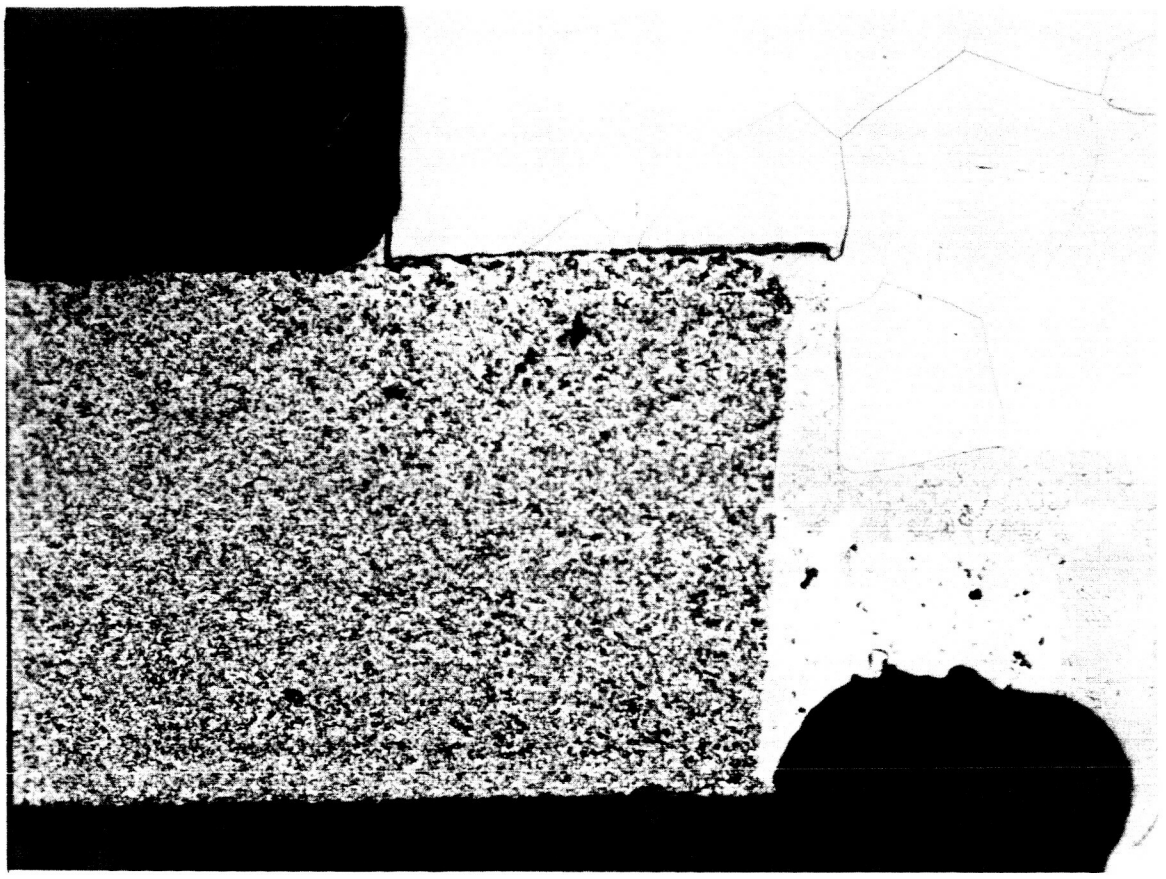

Figure 20. Photomicrograph of braze of porous tungsten to plenum chamber. Large grain material is molybdenum plenum chamber, dark area is void.

## Mounting, Filament Current Leads, and Differential Pumping

Figure 21 is a schematic sketch of the assembly of the experiment and can be referred to during the following discussion. The 2-inch long, 1/16-inch diameter molybdenum feed tube slides for about 1 inch into the thick-wall molybdenum tube and is secured with a set screw. Leakage is handled by cascade differential pumping of the cesium to an area where it is completely trapped. Also, as a further insurance against leakage, a small drop of aqueous solution of $C_sCl$ is placed in the tight-fitting joint. The nickel bushing to which the filament is spotwelded is held by stainless steel screws in a stainless steel clamp which is kept cool to minimize diffusion welding and galling of the screws by the copper strips leading from it. (Many laminated strips are used for flexibility.) The copper strips are joined to a block that is cooled across thin teflon to the water-cooled base. The current-carrying capacity of the heremetic seal is increased by having heat generated in itself, and heat conducted down the filament lead, go into the base and not develop a huge temperature drop across the seal.

## Cesium Oven and Seal to the Baseplate

The heavy molybdenum rod into which the 1/16-inch OD molybdenum feedtube is set-screwed was chosen for its high thermal conductivity and low thermal expansion. This tube is brazed to a stainless steel fitting that seals onto a flared 1/2-inch OD copper tubing about 4-inches long that forms the oven. The OFHC copper tube is sealed at its bottom end by pinching and melting the copper and is wrapped with nichrome wire coated with glass thread, which forms the heater for the oven. A glass ampoule of cesium is placed in the oven, and the flare seal is then tightened with two large wrenches. After the chamber is evacuated, the glass ampoule is broken by squeezing the copper, a thermometer is attached, and the whole oven is wrapped with glass wool for thermal insulation.

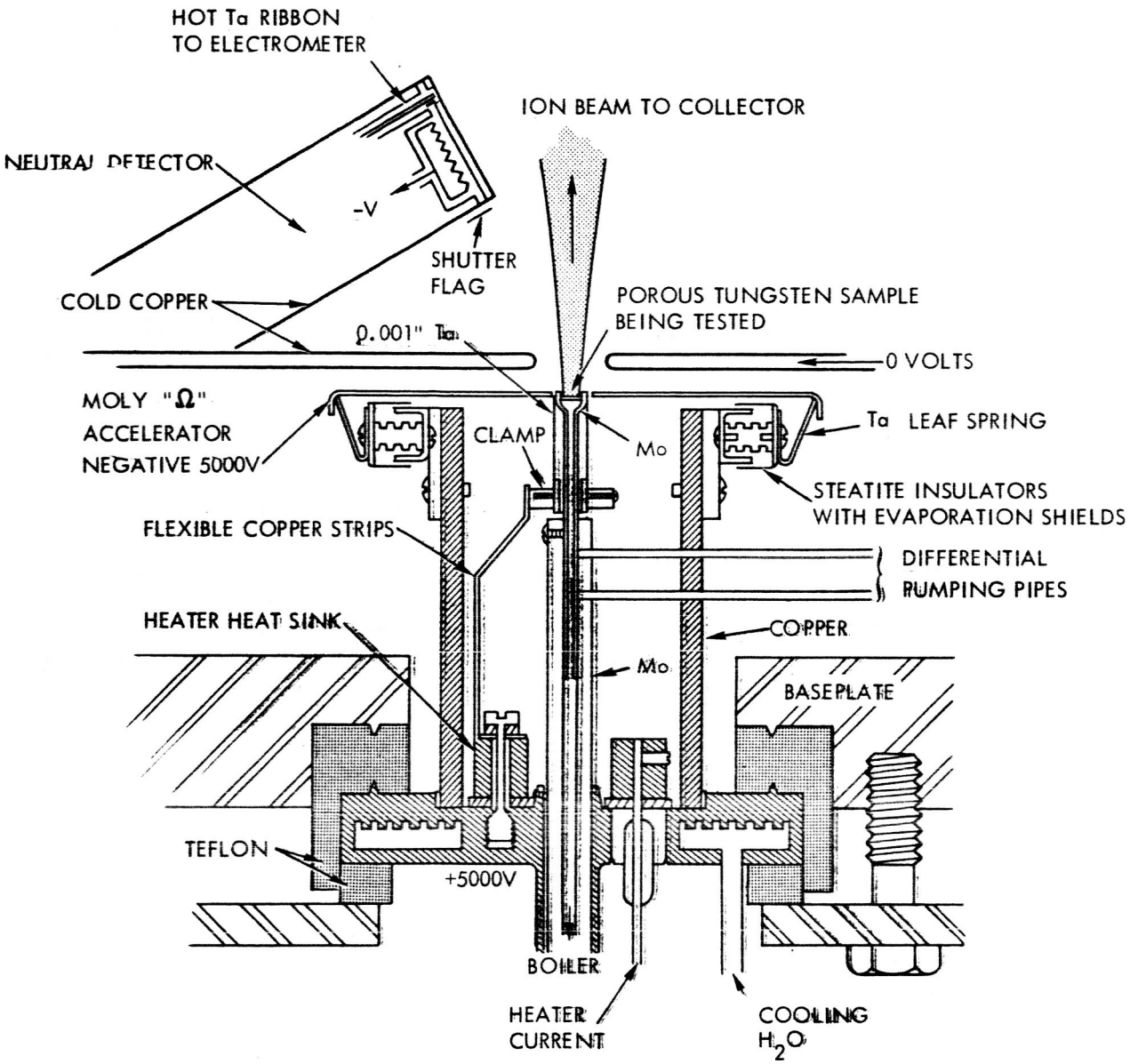


Figure 21. Schematic of experiment to test porous tungsten pellets.

This oven and seal assembly has successfully withstood temperatures over $400^{o}$ C at which level sufficient cesium pressure to achieve 25 $ma/cm^2$ ion current density is usually obtained unless pellet permeability is very low.

The whole emitter assembly is sealed with teflon between two stainless steel knife-edges and projects through the bottom of the baseplate. The teflon makes a good vacuum seal and provides adequate voltage insulation. On a copper jacket surrounding the emitter and filament are mounted the insulators that support the accelerator. The copper, which is attached to the water cooled base, shields and cools the insulators, and their mounts and evaporation shields. These insulators are standard 1/2-inch steatite standoff insulators with 6-32 threads but with grooves machined on their outside surfaces to inhibit sliding sparks.

## Accelerator

The original plan was to use an accelerator that could be heated to remove surface products that cause electron drain currents. It was found, however, that a simpler nonheated accelerator worked reasonably well. As a result we used the following design. Into a molybdenum strip about 0.040 inch thick and 1-inch wide is drilled a 0.250-inch diameter hole, the edges of which are rounded and electropolished. This stiff strip has sharply bent ends that clip onto leaf springs that were originally designed to support a ribbon that could be heated by passing current through it.

Some drain problems have been encountered after sputtering because cesium is deflected onto the accelerator and the low-work-function cesium compounds field-emit electrons.

The ions are exited through an aperture in a liquid-nitrogen-cooled copper plate toward a collector biased with +10 to +20 volts to recollect secondary electrons. No attempt is made to neutralize the beam, and it is suspected that there are trapped electrons in the ion beam.

The base of the emitter assembly (which carries voltages up to 10,000 volts) is cooled by the same water used for cooling the bearings of the turbomolecular pump but is electrically isolated by two glass drip columns.

Neutral Detector

Neutral cesium is detected at an angle of 30 degrees off the axis by a liquid-nitrogen-cooled, shuttered sensor. A hot tantalum ribbon is used to surface-ionize incoming neutral cesium and emit the resulting positive ions to surrounding negative electrodes. Positive ion current from the filament is monitored by a Hewlett Packard 425A Micro-Micro Ammeter.

The neutral detector is calibrated by correlating ion decreases with neutral increases. To determine the neutral fraction emitted off the surface by this method of detection and calibration, the assumption has to be made that the angular distribution is the same (presumably a cosine distribution) for both low and high neutral evaporation. This assumption might well be in error if the ions come from deep within the pores. The neutrals from these deep sites could only get to the neutral detector by scattering off outer rims of the pores that are free of cesium and they therefore would have a high probability of being converted into ions. Neutrals that can escape without this conversion to ions are emitted in a normal direction, hence it is very possible that the density of neutrals at normal incidence is significantly higher than at 30 degrees; however, the integral of this normal peak is still a small part of the whole neutral emission.

In defense of our measurements, it must be said that the correlation of ion change with neutral change is very good all the way from 5 to 100 percent neutral fraction. Also varying the electric field over a wide range which would be expected to change the distribution as the field reaches different distances into the pores, causes no change in the measured neutrals.

Photographs of the experiment to test porous tungsten pellets can be seen in Figures 22, 23, and 24.

In Figure 22 the copper container for liquid nitrogen, which is attached to both the lower plane containing the aperture and sensor and the upper insulated collector, is prominent. The shield, behind which is the nude ionization gage, is seen behind the lower plane. The ribbon that can be swung over the ionizer for sputtering cleansing can also be clearly seen. In Figures 23 and 24, the location of the emitter and accelerator can be seen in relationship to the baseplate, copper mounting shield, and the grounded aperture plane through which the ions pass.

## Surface Sintering and Etching

During the course of the testing poor test results were obtained on several occasions because surface sintering closed the majority of the pores. Good results were obtained after such surfaces were taken out of the system and chemically etched. Dramatic examples of this effect are the two tests made of E.O.S. E4 material and of material overheated to try to rid it of chromium. This latter case is chronicled in the monthly report included as Appendix I.

When it was confirmed that better results were obtained with etched surfaces we routinely etched the surface of all the later emitters before test. The benefits resulting from this process are many:

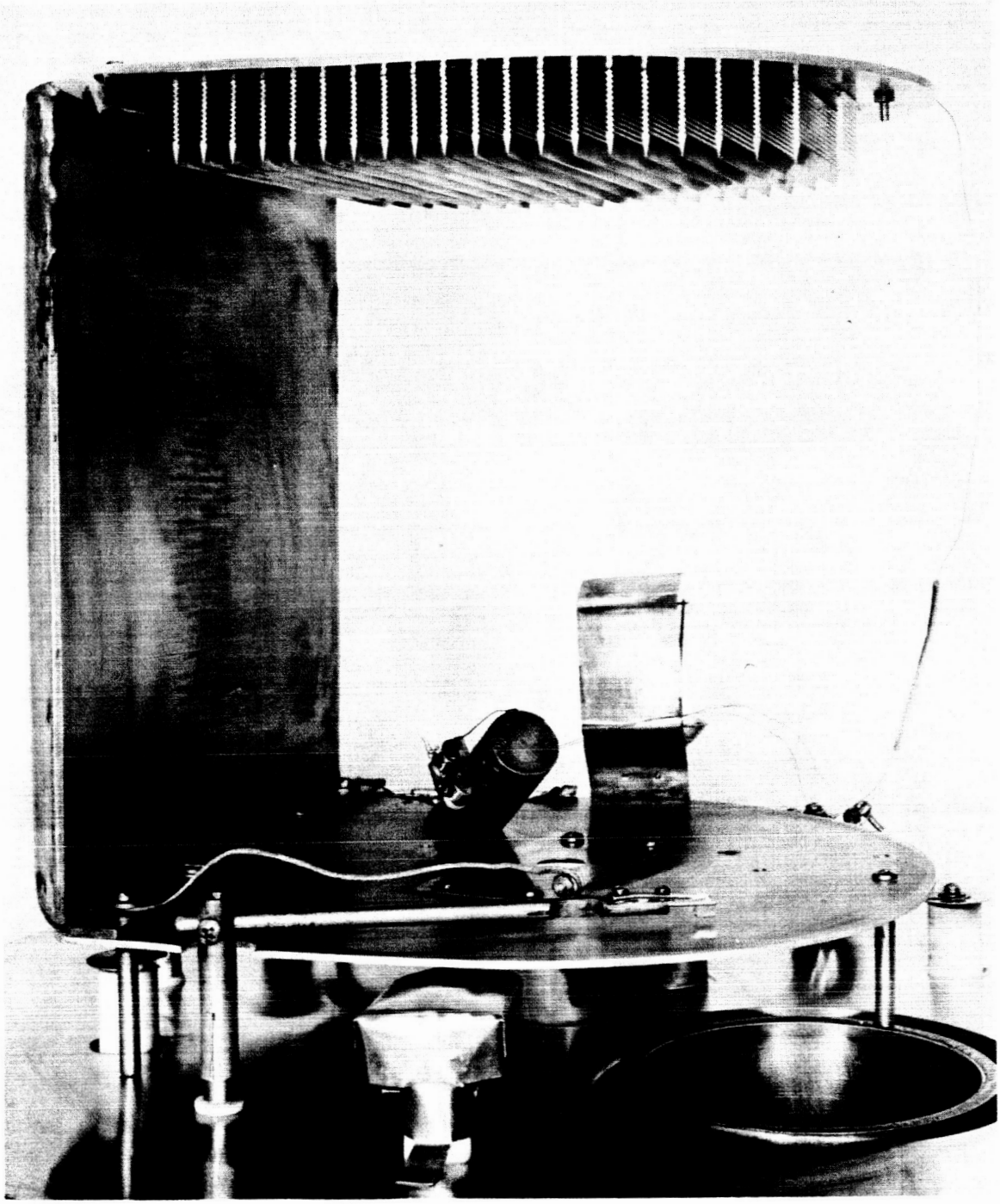

Figure 22. Photograph of experiment to test porous tungsten pellets. Large structure to left is liquid nitrogen container.

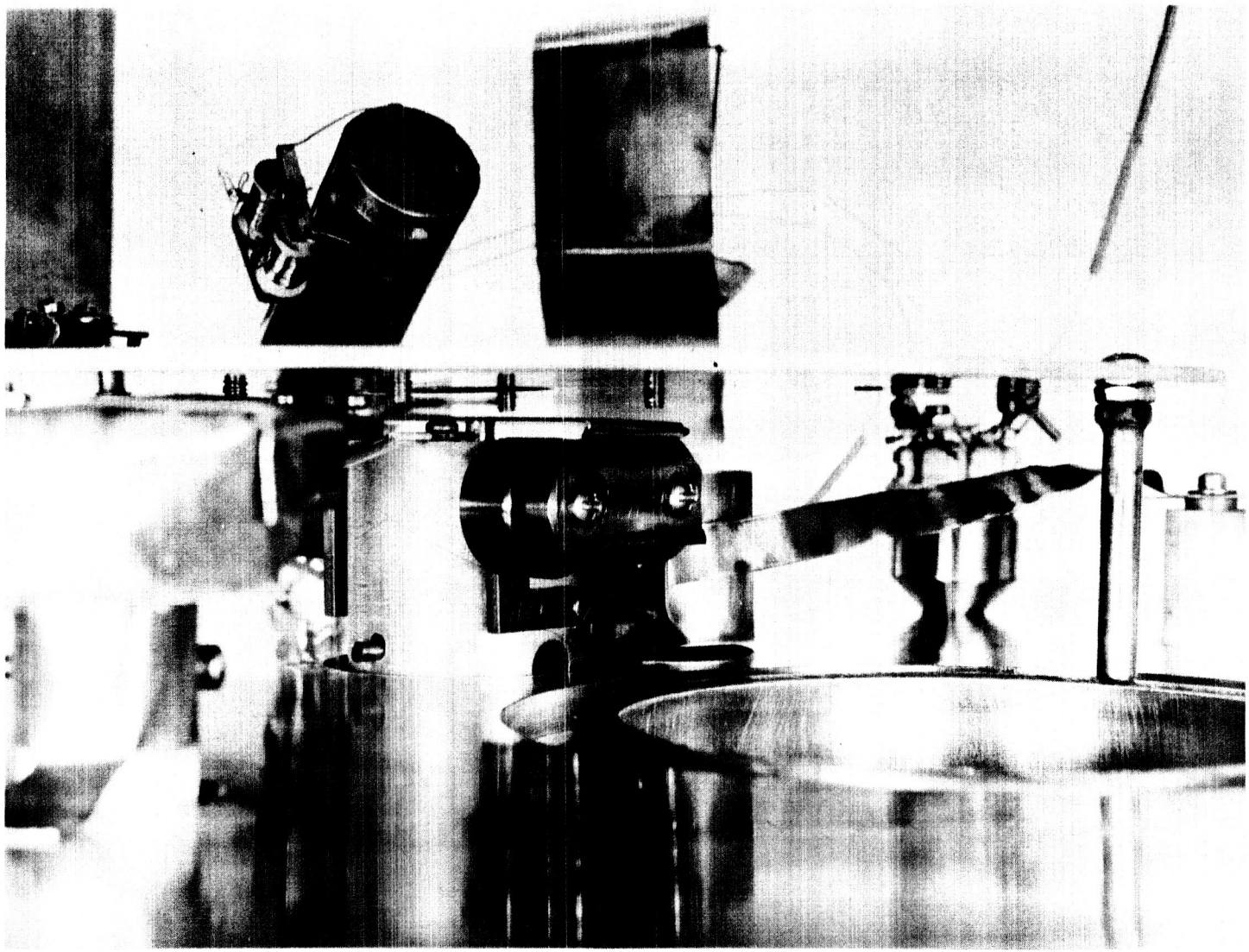

Figure 23. View of experiment under lower plane. Shutter on neutral detector is prominent on top.

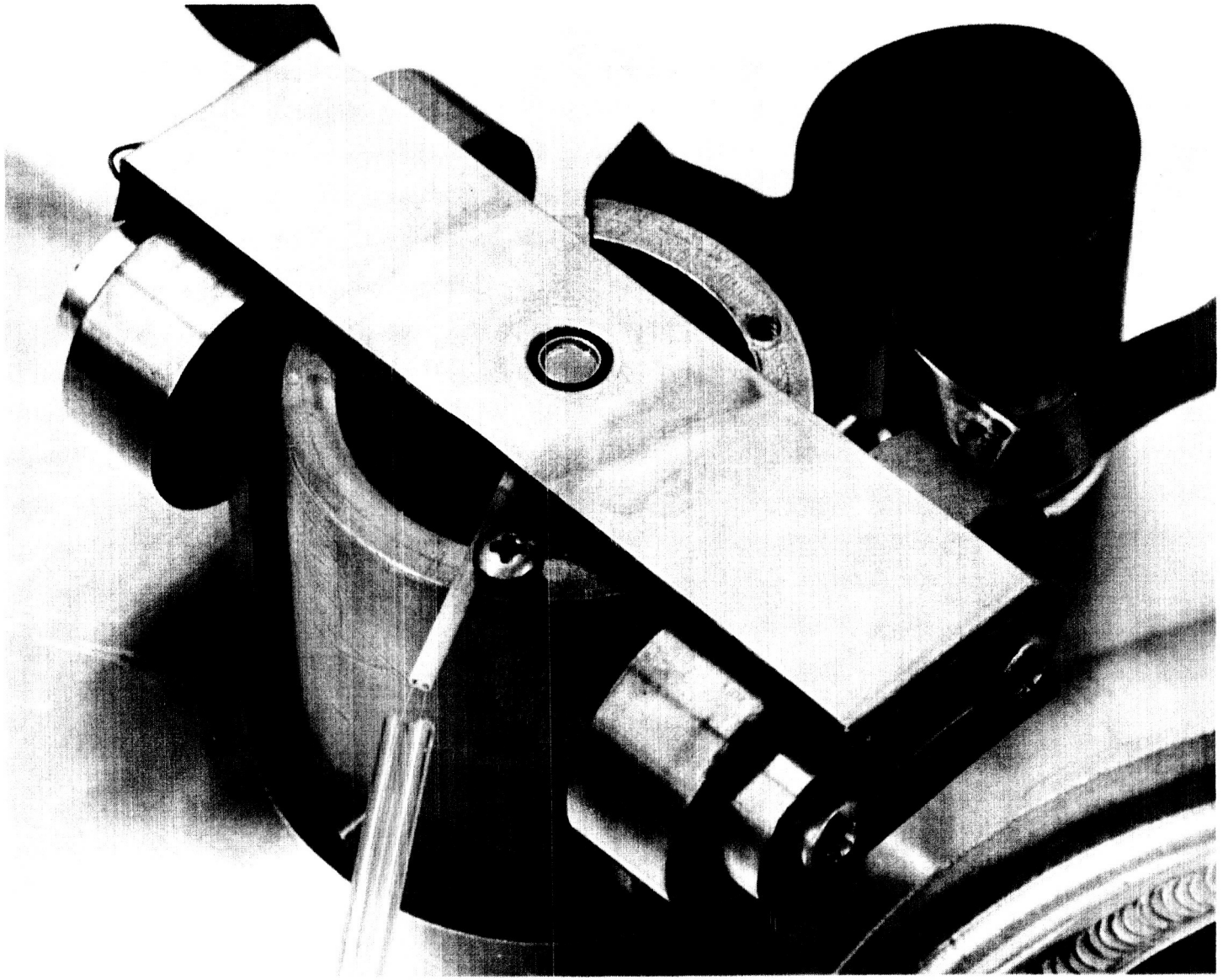

Figure 24. Close up photograph of "Ω"-field accelerator. Thermocouple wires can be seen.

(1) Surface sintering due to cold-working of the surface during machining is removed. (Burnishing of the surface during brazing is desired to retard creepage of braze material.)

(2) High-work-function facets of the tungsten crystals comprising each grain are probably exposed.

(3) Contaminants from the vacuum deposited on the surface during brazing and other handling are removed.

Anodic electroetching in sodium hydroxide has been used on the front surface. It is hoped that the electroetch does not make big holes preferentially bigger, as a more passive etch might. Such an etch is used on the rear by filling the plenum chamber with a mixture of sodium hydroxide and purex and immersing it in boiling distilled water for 2 minutes. The porous tungsten is then force-flushed with distilled water until the flush water no longer shows any basic reaction.

Permeability Measurements

The transmittivity of the pellet brazed into its plenum chamber and feedtube is measured before and after testing. This measurement is made by pumping 30 cc of air through the pellet to vacuum and measuring the time required for it to fall from 11 to 9 cm of octoil pressure. This low pressure is to assure Knudsen flow. The time constant of the plug is five times the measured time, $t_m$, and the time for 1 $cm^2$ (instead of 0.1 $cm^2$) would be one half the measured time. Since the leak rate of a hole of 1 $cm^2$ to vacuum is 11,600 cc/sec, the transmittivity is $\left[30/(1/2\ t_m)\right]/11{,}600$.

To give a value that is meaningful for the material and independent of the particular thickness we use (approximately 1/20 cm), we state a transmittivity thickness product which is

$\left[1/20 \times 30/(1/2\ t_m)\right]/11{,}600$, or $2.6 \times 10^{-4}/t_m$ cm. The measured time is often around 50 seconds, giving a transmittivity thickness product of about $5 \times 10^{-6}$ cm. Although it is felt that this dimensionless quality, which is applicable for any molecular weight and any temperature, is more meaningful than permeability, we will also give the conversion factor: $K\left[\text{grams/cm}^2\text{/sec/(torr/cm)}\right] = m \cdot (10^6/760)(2\pi mkT)^{-1/2} \times$ (transmittivity thickness product); this factor is $1/8 \times 10^{-2}$, so our average 50-second material has a permeability to air flow in the Knudsen regime of about $10^{-7}$ grams-cm$^{-1}$-sec$^{-1}$-torr$^{-1}$.

## Precautions Against Contaminants

The use of copper for the collector assures us that no contaminants are sputtered onto the pellet surface, and the use of the "Ω"-field geometry assures us that no foreign materials, such as tantalum oxide or molybdenum oxide, are evaporated onto the surface during oxygen exposure. The feed system has proven not to be a source of contaminants. Other possible sources of contamination are molybdenum used in the hot portions of the system and the stainless steel and glass ampoule used in the cooler portions.

## Method of Taking Data

When a pellet first produces ions the test outputs fluctuate rapidly. Usually about an hour's operation at 5 ma/cm$^2$ at about 1700°K will stabilize the surface to a slightly oxygenated condition with low neutrals and high critical temperature. If the pellet is not oxygenated at this time, it is exposed to $5 \times 10^{-6}$ torr of oxygen to remove carbon by conversion to carbon monoxide. However, enough oxygen is left from etching so usually this step is unnecessary.

Sputtering is initiated at high temperature (1850°K) until a stable condition is obtained and continues after sputtering is stopped through temperature cycles between 1850°K and critical temperature. This surface is the reproducible "clean" surface representative of the sample. The neutrals are higher and the critical temperatures lower than they were before sputtering.

After cleaning, data are taken at current densities from 1 ma/cm$^2$ to 25 ma/cm$^2$ at 1600°K, with pauses at 5 ma/cm$^2$, 10 ma/cm$^2$, and 20 ma/cm$^2$ to sputter and take neutral fraction versus temperature curves. Oxygen at 5 x 10$^{-6}$ torr is then admitted and the current density is decreased, with pauses at 20 ma/cm$^2$, 10 ma/cm$^2$, and 5 ma/cm$^2$ to take neutral fraction versus temperature curves. All too often the degree of oxygenation depends on the length of oxygen exposure and the past temperature history of the sample, as carbon impurity in diffusing from the bulk can rid the surface of oxygen as fast as it arrives.

## Results

The indexed data sheets for all the pellets tested are contained in Appendix II. If explanation of any points alluded to on these sheets is desired, further detail can be found in the monthly reports originally containing these sheets which are referenced at the beginning of the Appendix. Test sheets on each pellet tested are found in Appendix III. The conclusions that appear on the bottom of each of these sheets are included in this section as a summary, which follows the following general remarks.

A very marked advance in the quality of porous tungsten pellets for high ion current density has been made. The higher uniform pore-count that results from the use of fine-graded spherical powder does indeed product superior high-current-density operation. The more pores per area, the higher is the ion-current density showing the neutral fraction and

critical temperature of solid tungsten. The best material tested shows almost no variation (at well above the critical temperature) of neutrals from 1 to 5 ma/cm$^2$. The mark of a superior material is how little it deviates from solid tungsten at current densities above this level.

Some materials have an inherently poor pore count or suffer surface-sintering. Others simply are not tungsten. The tantalum-containing pellets generally have the characteristics of partial oxygenation and have higher critical temperatures.

Most of the data sheets include neutral fraction versus temperature curves at 5 ma/cm$^2$. It was found that this was an informative curve because it often was in the transition region where the characteristics were first deviating from that of solid tungsten. Also, it is a convenient current density with which to run comparative curves and do extended sputtering, since it is high enough that backgrouhd impregnation effects are not significant and yet not so high that severe high-voltage and drain-current problems are encountered. Generally the low-current-density data with oxygen present is emitted because the neutrals were below our limit of detection.

Some materials have a poor surface pore count because of the size distribution of the tungsten powder used in their manufacture. However, even the best material can show poor results due to surface closure. Surface preparation is extremely important in avoiding this difficulty. Also, it is important to understand the reasons for surface sintering. It seems probable that cold work from previous machining can leave the surface so disarranged that rapid surface sintering occurs, and it also seems evident that oxygen from the vacuum system can keep the surface open, but at the expense of volatizing $WO_3$. The

role of $WO_3$ as it diffuses from the interior to the surface is not known. Certainly if carbon from the vacuum system concentrates near the surface, the tungsten is deposited at the surface and CO is evolved. More work is needed on the subject of surface sintering.

Test No. 20 was made on high pore-count material that was carbided by cracking $C_2H_2$ and operating to high current densities. The material used was Hughes G2A. The results, which are presented in the data sheets in Appendix II, showed lower neutrals and critical temperatures for the carbided surface at all current densities. Special attention was directed to continuous operation in hydrocarbon vapor. If oxygen or water vapor exceeded the hydrocarbon vapor no effect was noticed (eventually the tungsten would be decarbonized), and $CH_4$ seemed to have no effect. However, a vapor pressure as low as $1 \times 10^{-6}$ torr (nitrogen equivalent) of $C_2H_2$ would raise the neutrals and critical temperature when the pellet was operated at a low temperature (e.g., close to critical temperature at low current densities). The higher the temperature, the greater was the tolerance for high vapor pressures. The desired carbide surface could be maintained in a $C_2H_2$ pressure of $3 \times 10^{-6}$ torr at $1450^{\circ}K$ but would deteriorate at $1410^{\circ}K$, presumably because pure carbon formed on the surface faster than it could surface-migrate away or diffuse through the carbide to the base tungsten. Operation at $1450^{\circ}K$ would restore the desired condition. At this temperature $4 \times 10^{-6}$ torr was required to alter the surface adversely. Again raising the temperature and lowering the pressure would cause the good surface to reappear.

When this surface was examined with X-rays, WC was identified. We had earlier been ascribing this good ion-emission characteristic to $W_2C$, but neither $W_2C$ or tungsten could be detected! If the cracking probability is markedly below one, the outer layers of the porous tungsten are permeated with hydrocarbon gas and the surface grains are carbided from the sides and back also. Cracking of carbon beyond the times when these grains are completely converted to WC would undoubtedly produce a poor ionizing surface.

Summary of Test Results

Test No. 1 - E.O.S. E6

Neutral fraction low 1-5 ma/$cm^2$ - increases rapidly above. Critical temperature high-increases rapidly above 10 ma/$cm^2$. Would probably been better results if sputtering and etching were used.

Test No. 2 - E.O.S. E-7A

Neutral fraction high and increasing with current density. Critical temperature high. Would probably have benefited from sputtering and etching. Surface crack terminated test.

Test No. 3 - E.O.S. E3

Brazed by E.O.S. Neutrals high. Probable contaminant or surface closure.

Test No. 4 - E.O.S. E4

Poor results due to surface sintering.

Test No. 5 - Phillip Mod E

Valid test on clean tungsten (by sputtering) but high neutrals because of poor pore count.

Test No. 6 - E.O.S. E3

Repeat test with etching and sputtering. Excellent results.

Test No. 7 - E.O.S. E4

Superior high-current-density performance (about 1/2 percent neutrals at 1450°K for 20 ma/cm$^2$).

Test No. 8 - Astromet 10-1

Performance improved after re-etching. However, results are very poor because of low, nonuniform pore count.

Test No. 9 - E.O.S. "1-10μ" (G1)

Shows steady increase of neutrals with current density. Good critical temperature. (2 percent neutrals at 1430°K for 20 ma/cm$^2$.)

Test No. 10 - Astromet 12-1

Low permeability because of braze penetration on reverse side. Test poor, but possibly invalid.

Test No. 11 - E.O.S. "1-10μ" (G1)

After elox machining. Critical temperatures at high current density higher and more sloppy after elox.

Test No. 12 - E.O.S. E-4 - 10 Ta

Knees more rounded at low current density. Good high current density performance (~ 2 percent neutrals at 1420°K for 20 ma/cm$^2$).

Test No. 13 - Hughes (G2a)

Neutrals low and indicate high pore count. Critical temperature unaccountably high.

Test No. 14 - E.O.S. Bar No. 5 (G3)

Neutrals and critical temperature continuously increase with current densities. Knees sharp and solid tungsten appearing. (About 2 percent neutrals at 1430°K for 20 ma/cm$^2$.)

Test No. 15 - E.O.S. 2% Ta

Critical temperature high - rounded knees. Work function high at low current density probably because of oxygen associated with tantalum. (2 percent neutrals at 1600°K at 20 ma/cm$^2$.)

Test No. 16 - E.O.S. 5% Ta

Critical temperatures and neutrals high (7 percent neutrals at 1600°K at 20 ma/cm$^2$).

Test No. 17 - E.O.S. 10% Ta

Same general characteristics of Ta series (15 - 17) - rounded drooping knees - oxygenated - high critical temperatures. (1-1/2 percent neutrals at 1600°K for 20 ma/cm$^2$.)

Test No. 18 - E.O.S. Bar 2 (G4)

Good high current density performance (1 percent neutrals at 1430°K at 20 ma/cm$^2$).

Test No. 19 - E.O.S. Bar 2 (G4)

After elox machining, surface carbided upon initial operation. (Low criticals and low neutrals.) After oxygen and sputtering results nearly identical with test Number 18.

Test No. 20 - Hughes G2a (Carbided-WC)

Generally lower critical temperature and neutrals (1/2 percent neutrals at 1430°K at 20 ma/cm$^2$).

Test No. 21 - Astromet 10-1 (Improved)

Excellent results below 10 ma/cm$^2$ (3 percent neutrals at 1420°K at 20 ma/cm$^2$).

Test No. 22 - Hughes G2B

Results very good up to 5 ma/cm$^2$. Couldn't exceed because of very low permeability.

Test No. 23 - STL (G5B)

Results very good up to 10 ma/cm$^2$ neutral fraction and critical temperature low. Effect of pore density abruptly seen at higher current densities.

## REFERENCES


1. J. B. Taylor and I. Langmuir, Phys. Rev. 44, 423, 1933
2. J. H. DeBoer "The Dynamical Character of Adsorption", (Oxford University Press London 1953).
3. R. E. Honig, RCA Rev. 18, 195, 1957.
4. F. H. Ellinger and W. P. Sykes, Trans. ASM 28, 619, 1940.

# APPENDIX I

## Monthly Report No. 8

# PROGRAM OF ANALYTICAL AND EXPERIMENTAL STUDY OF POROUS METAL IONIZERS

## TECHNICAL STATUS

During this reporting period the effect of chromium on hot tungsten has been extensively studied. The evaporative lifetime of chromium on polycrystalline tungsten has been found to be very dependent on coverage with about a two decade decrease in lifetime from clean tungsten to bulk chromium. When chromium is deposited on an operating cesium ion source, a situation similar to the results with beryllium occurs -- with traces of oxygen present the neutrals are low, but the critical temperature is very high while under a continuous supply of oxygen the critical temperature is greatly reduced. While trying to remove the chromium, a very difficult job, we caused surface sintering by high temperature heating. This surface sintering which severely degraded the high ion current density performance of the porous tungsten, was completely removed by surface electrolytic etching. A sample of porous tungsten designated "Block 5" manufactured by E.O.S. and to be tested in the large STL engine was also tested during this period.

### Chromium Lifetime

In the last monthly progress report tentative data on the lifetime of chromium on polycrystalline tungsten were given. It was recognized that the lifetimes presented were not for a constant coverage but varied from zero coverage at high temperature to about a monolayer at low temperature. This month the lifetimes at low coverage are presented along with the lifetimes for a monolayer coverage and from bulk chromium. These data are shown in Fig. 1. The low coverage data were extended to lower temperatures by increasing the spectrometer sensitivity and decreasing the arrival rates of chromium but still using the observations of accumulative and depopulation times as outlined in the last report. The data at very low temperatures and long

lifetimes were determined at very low arrival rates by timing the accumulated coverage as observed by flashing it off.

One monolayer was recognized by the abrupt decrease in lifetime as the coverage progressed beyond this value. Evaporation from bulk chromium had a fixed value for a given temperature independent of arrival rate and persisted at the same level after the arrival rate was stopped. Data for a single monolayer and for bulk chromium were only taken at the lower temperatures because higher arrival rates necessary to extend the data would deplete the oven inconveniently rapidly. The dotted lines extend the observed points to higher temperatures with the anticipated slopes. The positions of $\theta = 0.8$ and $\theta = 1.1$ are schematically indicated to show the greater change in lifetime per incremental change in coverage above $\theta = 1$ than below. The surface coverage corresponding to what is here called a monolayer were computed from Honig's (RCA Rev. 18 195-204 June 1957) vapor pressure data. The particle current from Honig, $\Gamma = P/\sqrt{2\pi mkT}$ was compared to our observed $\Gamma = \sigma_o/\tau$ . The monolayer coverage, $\sigma_o$ then is found to equal about $1 \times 10^{15}$ particles per square centimeter. This value is about what one would expect. The site density on the cubic face of tungsten is $1 \times 10^{15}/cm^2$.

Effect of Chromium on Tungsten Ion Emitting Properties

Chromium was introduced into a porous tungsten pellet both by painting a solution of chromium trioxide onto the porous surface and later by sputtering chromium onto the surface of a previously tested clean tungsten pellet. The test results of this pellet are shown in Figures 2 and 3. This material manufactured by E.O.S. from graded spherical tungsten is designated here as "Block No. 5" and was supplied by NASA Lewis for use in a large STL engine. The results are typical of clean, high pore count porous tungsten manufactured from graded spherical powder. The reasonable neutral fraction of three percent at 25 $ma/cm^2$ and its not too rapid increase with current density speaks well

for the material. The critical temperature at 21 ma/cm$^2$ is 1450$^o$ K which is only about 120$^o$ higher than Taylor and Langmuir predict for solid tungsten. Some of the pellets tested in this program have had critical temperatures about 200$^o$ K higher than solid while some have been only about 70$^o$ K higher. This material had before and after test, a knudsen gas transmittivity thickness product of 3 x 10$^{-6}$ cm.

The many curves of the remaining figures of the report tell the story of chromium on tungsten. They show the original high oxygenation with the very low neutrals and high critical temperature. They show the difficulty of removing the oxygen by prolonged heating and sputtering and how even when the neutrals increase by a hundred, the critical temperature remains high. They show the 150$^o$ K reduction in critical temperature by operating in oxygen. The severe degradation in high current density ion emitting properties due to surface sintering is chronicled with the subsequent restoration by surface sintering. Then as excess chromium is alternately sputtered on, oxygen added and then sputtered off, the effect of minute amounts of chromium on critical temperature is emphasized. At about 5 ma/cm$^2$, the Taylor Langmuir critical temperature is 1270$^o$ K; the clean porous tungsten critical temperature is 1300$^o$ K; the chromium impregnated porous tungsten operated in oxygen has a critical temperature of 1330$^o$ K; the chromium impregnated porous tungsten sputtered clean of most of the oxygen has a critical temperature of 1390$^o$ K; the chromium impregnated porous tungsten with difficult to remove amount of oxygen has a critical temperature of about 1490$^o$ K while just after oxygen exposure with ample chromium, the critical temperature may be as high as 1550$^o$ K.

In Figure 4, the story begins with Curve 1. The critical temperature is high and neutrals very low, indicating a high degree of oxygenation. Curve 2 and curve 3 shows this highly oxygenated surface operating at higher current densities. Curve

4 shows an attempt at removing the oxygen by sputtering. Much oxygen is removed resulting in an increase of neutrals by a factor of one hundred, but the critical temperature is still the same -- very high. Curve 5 and 6 shows the depressed critical temperature while operating in oxygen followed by the raising of critical temperature immediately following exposure to oxygen. Curve 7 shows the same oxygenated surface after over night operation and sputtering; the neutrals are still low and the critical temperature is still high. Prolonged high temperature was employed to hopefully remove the chromium. Instead as shown in curve 8, poor high ion current density operation reminescent of surface pore stoppage results. The curves in Figure 5 show this condition worsening upon further heating, shows the effect at different densities, and shows that oxygen fails to affect its usual improvement.

Figure 6 shqws the results after electrolytic etching was used to remove surface sintering. Also prolonged sputtering was employed to clean the surface. Small traces of chromium and oxygen seem to remain to lower the neutrals and raise the critical temperature. Evidence that chromium remains is that operation in oxygen lowers the critical temperature and sputtering more chromium onto this surface does not affect the surface.

These points and the differing critical temperature of this surface are illustrated in Figure 7. Curves 1, 2, and 3 show no effect when chromium is sputtered onto the surface previously cleaned by sputtering. Curve 4 shows the now familiar (with Be and Cr) lowering of critical temperature when operating in an oxygen pressure. Curve 5 also shows the familiar increase in critical temperature following operation in excess oxygen.

Figure 8 shows in a set of neutral fractures versus ion current density curves the history of this pellet. Note the characteristic "plugged pore" surface with its high neutrals and steep dependence on increasing current density. A comparison of curves 4 and 9 illustrate the complete restoration after etching.

Statement Complying With Reporting of New Technology Clause:

It has been noted that porous tungsten impregnated with BeO or CrO binds cesium very tightly and therefore in a cesium atmosphere makes a very good electron emitter. Such an improved emitter might have application in thermionic converters, cathodes in cesium bombardment engines, ion engine neutralizers and elsewhere.

Project Hours for October 1964

A graph showing a comparison of actual versus planned expenditures is attached. The names and hours worked by scientific personnel are as follows:

| | |
|---|---|
| A. Cho | 160 hours |
| H. Shelton | 144 hours |
| | 304 hours |
| Project Total Hours for October | 391.0 hours |
| Project Hours to 10-25 | 3,361.5 hours |
| Percentage of Total Manhours | 51.3% |

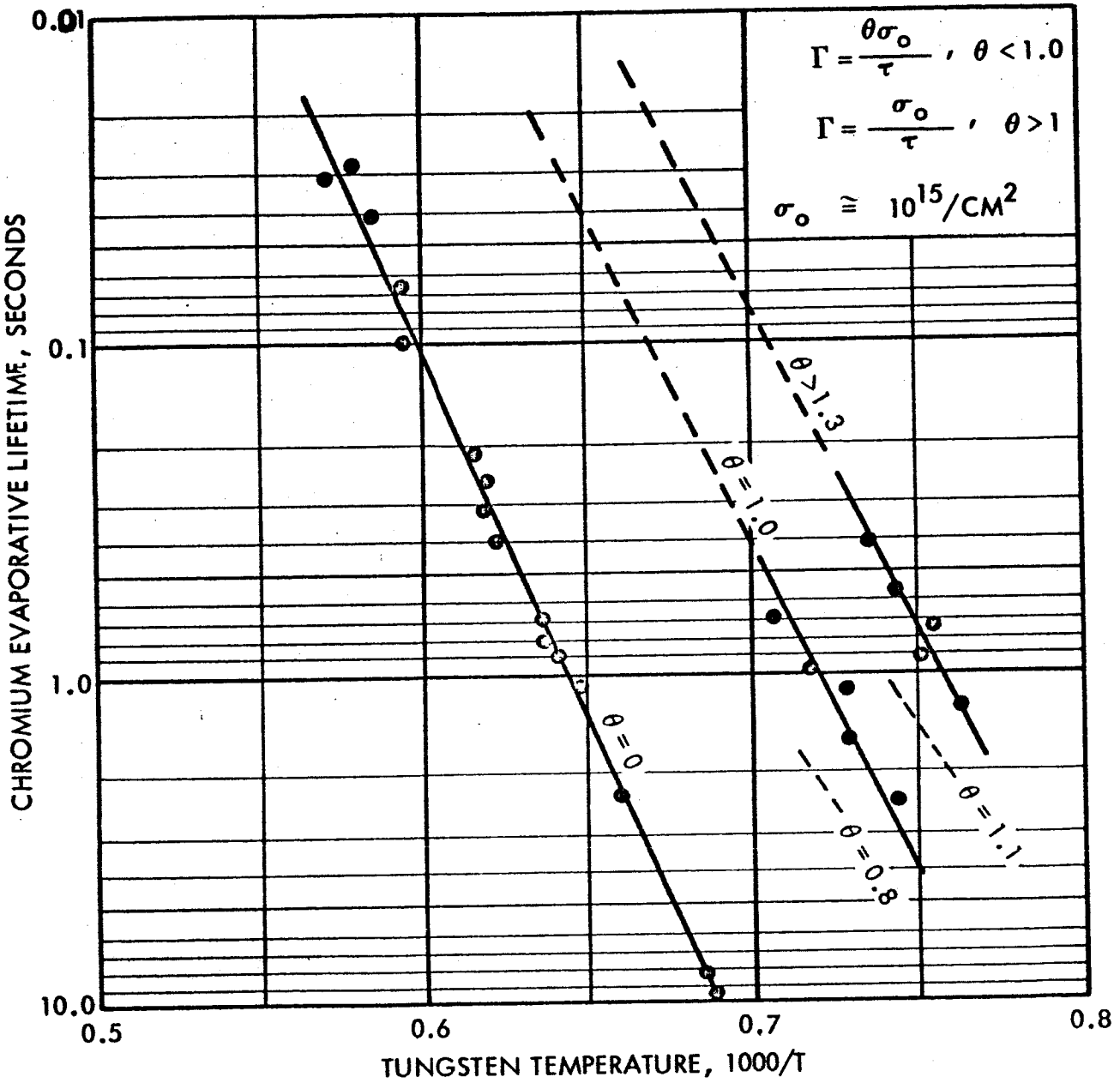


Figure 1. Chromium lifetime versus temperature of polycrystalline tungsten with varying coverages.

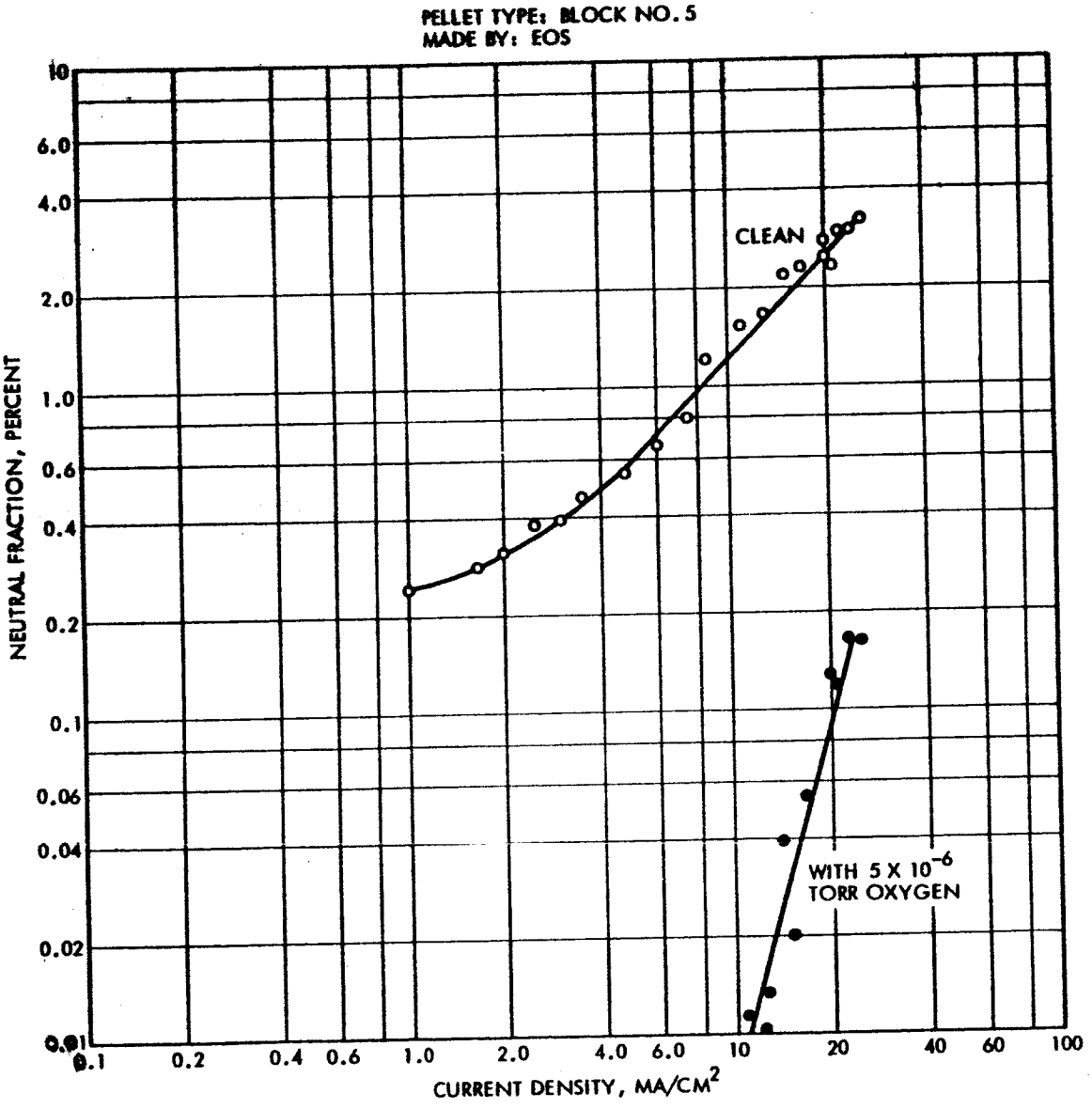


Figure 2. Cesium neutral fraction versus ion current density from porous tungsten manufactured by E.O.S. from graded spherical powder and designated "Block No. 5".

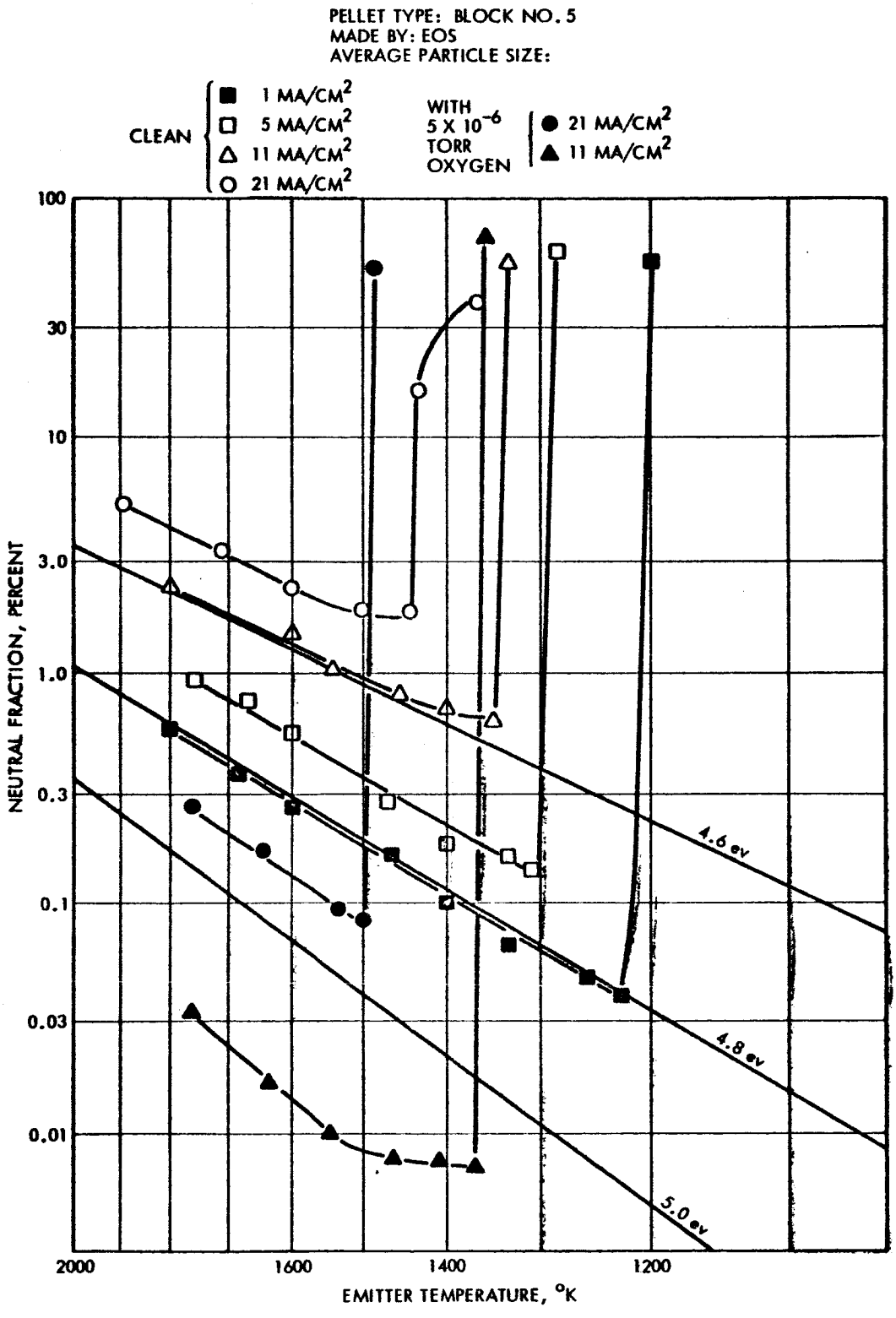


Figure 3. Cesium neutral fraction versus temperature of porous tungsten designated "Block No. 5".

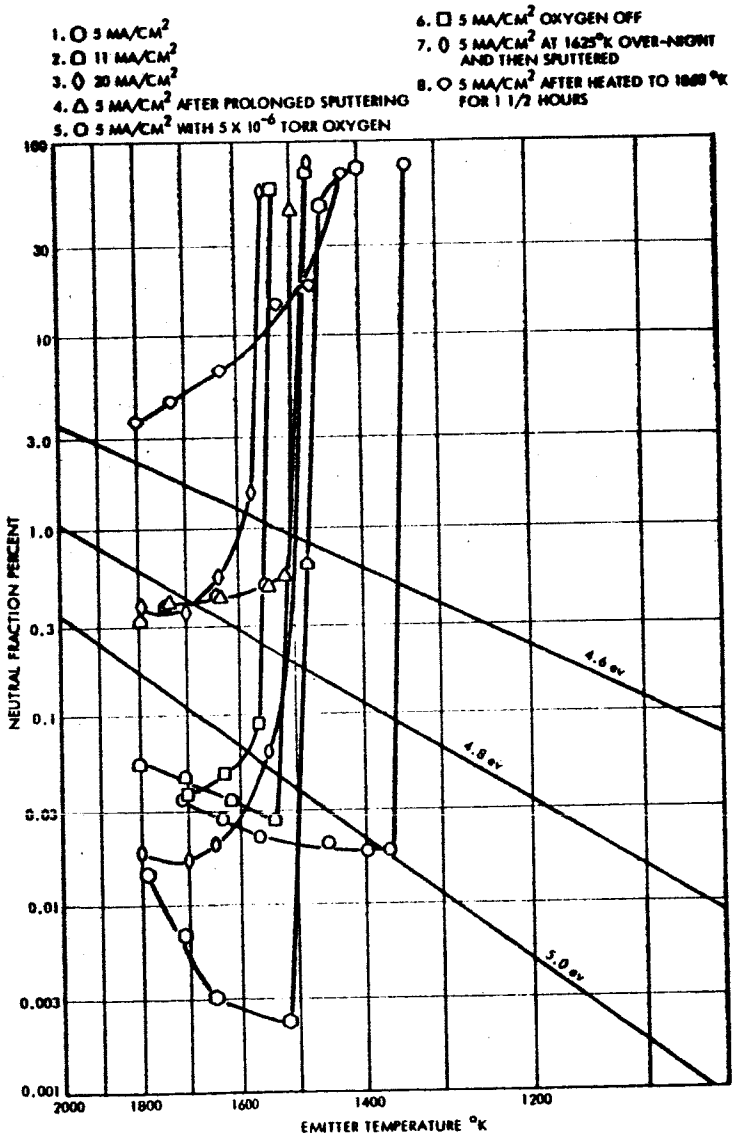


**Figure 4.** Cesium neutral fraction versus temperature of porous tungsten emitter impregnated with $CrO_3$ with differing surface treatments.

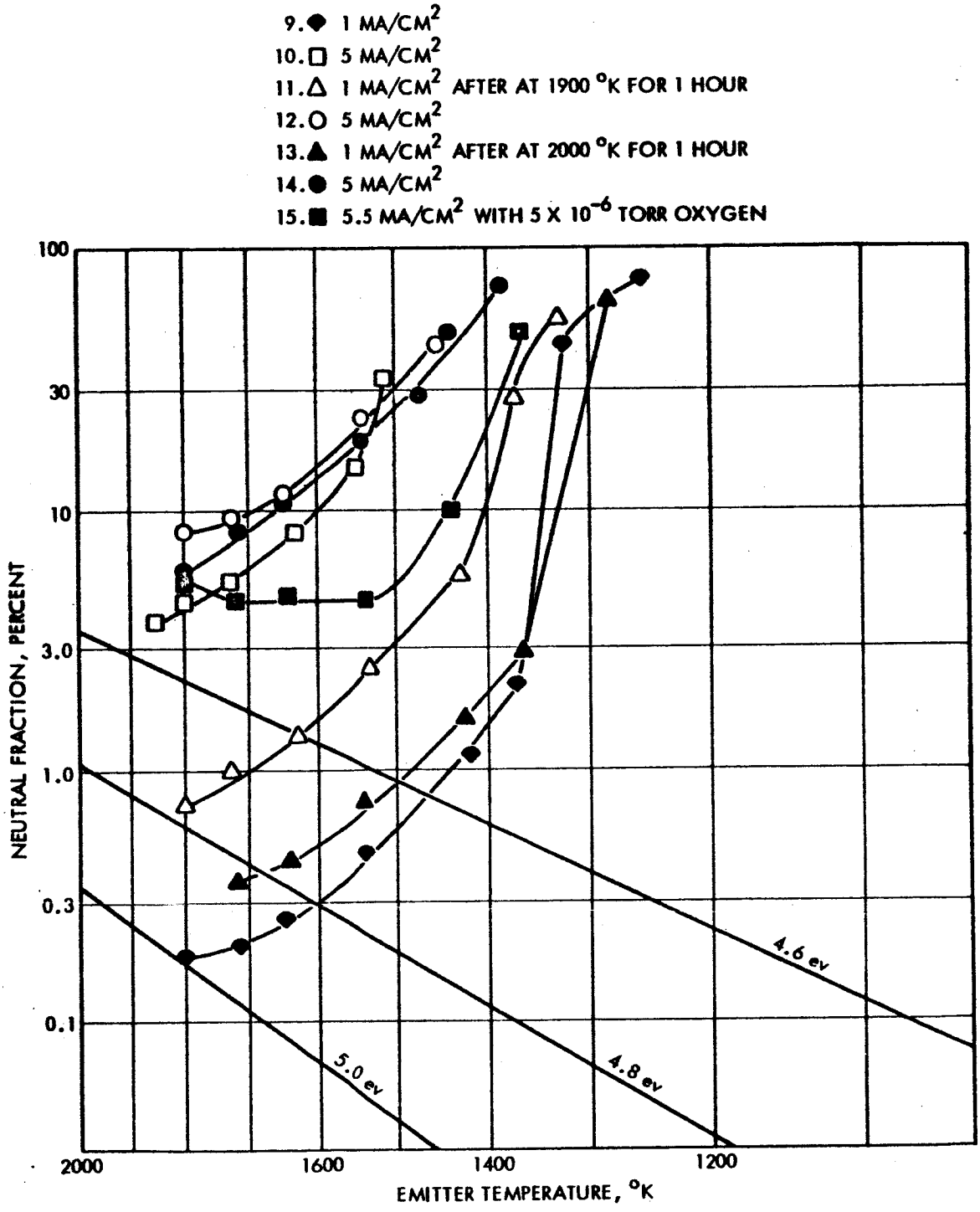


Figure 5. Cesium neutral fraction versus temperature of chromium impregnated porous tungsten showing surface sintering due to prolonged high temperature operation.

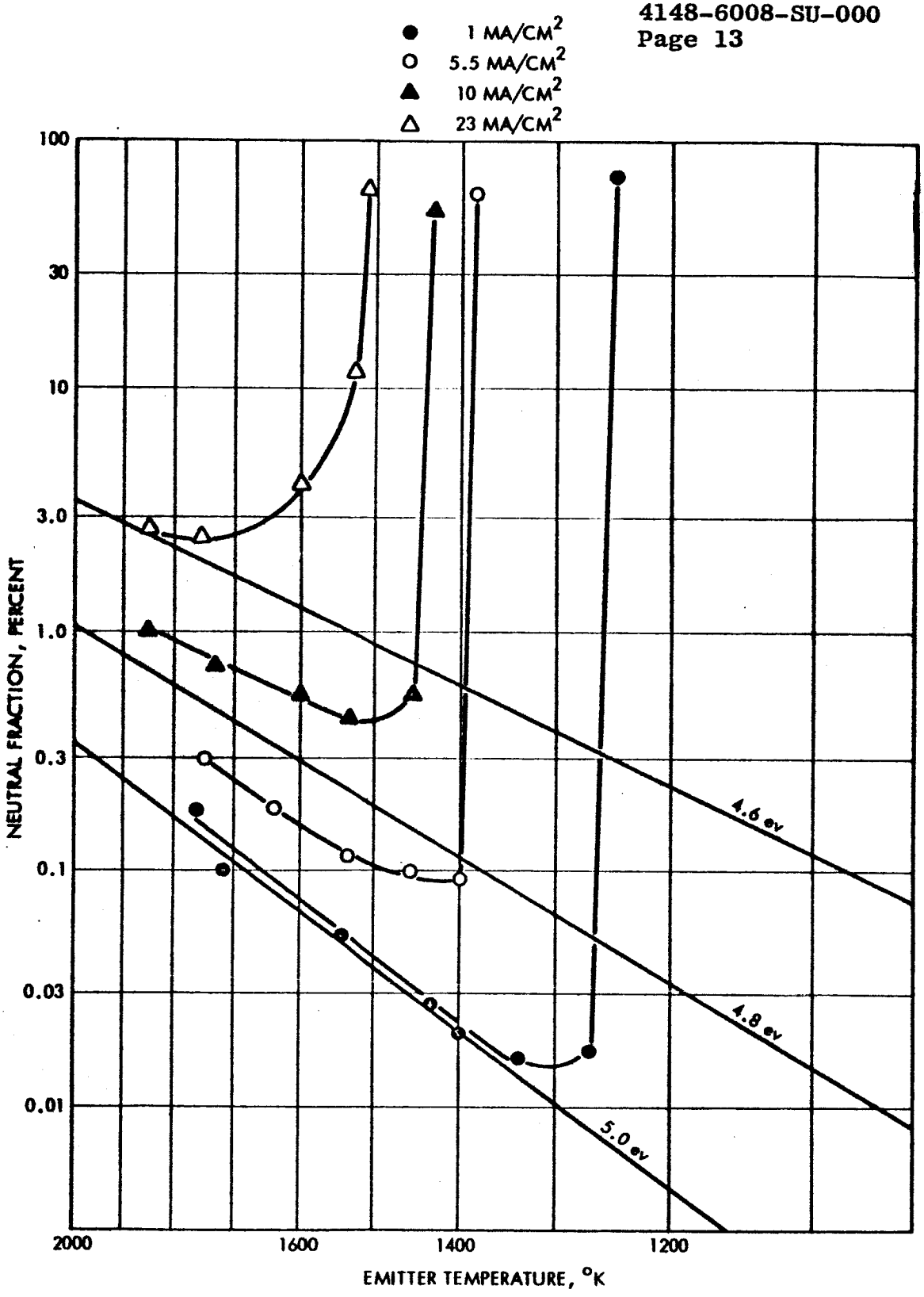


Figure 6. Cesium neutral fraction versus temperature of porous tungsten with traces of chromium but after etching to remove surface sintering and sputtering to remove most of the oxygen.

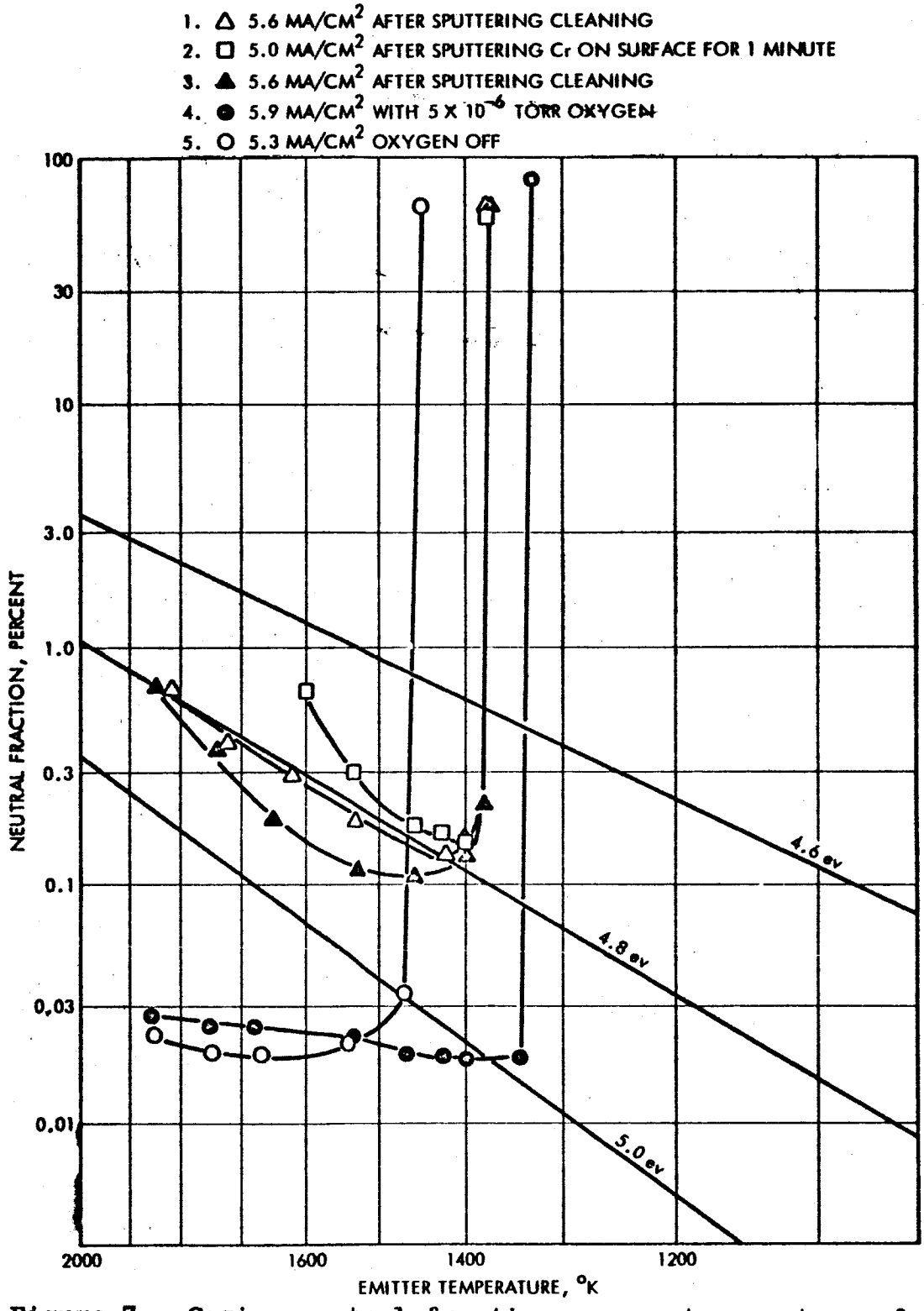


**Figure 7.** Cesium neutral fraction versus temperature of chromium impregnated porous tungsten with varying degrees of oxygenation.

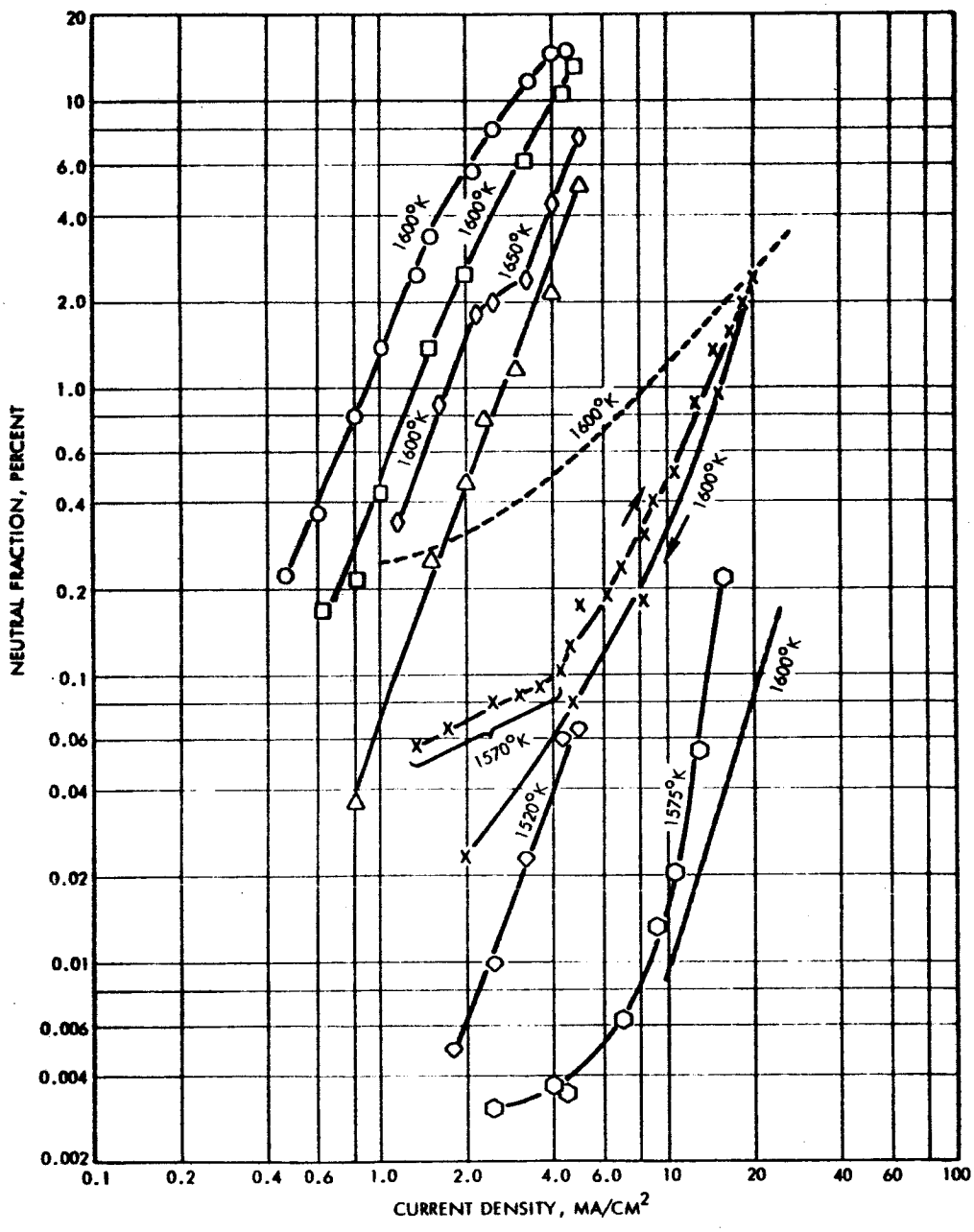


Figure 8. Cesium neutral fraction versus ion current density from porous tungsten when clean, oxygenated, impregnated with chromium, surface sintered, and later etched.

# APPENDIX II.

## DATA SHEETS

# APPENDIX II

## DATA SHEETS

Contents


| Test No. | | From Monthly Report No. | Page |
|---|---|---|---|
| 1 | EOS - E6 | 1 | II 3-4 |
| 2 | EOS - E7A | 3 | II 5-6 |
| 3 | EOS - E3 | 3 | II 7-8 |
| 4 | EOS - E4 | 3 | II 9-10 |
| 5 | Philips Mod E | 4 | II 11-12 |
| 6 | EOS - E3 | 4 | II 13-14 |
| 7 | EOS - E4 | 4 | II 15-16 |
| 8 | Astromet 10-1 | 5 | II 17-18 |
| 9 | EOS "1-10μ" (G1) | 5 | II 19-20 |
| 10 | Astromet 12-1 | 5 | II 21-22 |
| 11 | EOS "1-10μ" (G1) after elox | 6 | II 23-24 |
| 12 | EOS - E4 10% Ta | 7 | II 25-26 |
| 13 | Hughes G2A | 7 | II 27-28 |
| 14 | EOS Bar No. 5 (G3) | 8 | II 29-30 |
| 15 | EOS 2% Ta | 9 | II 31-32 |
| 16 | EOS 5% Ta | 9 | II 33-34 |
| 17 | EOS 10% Ta | 9 | II 35-36 |
| 18 | EOS Bar 2 (G4) | 10 | II 37-38 |
| 19 | EOS Bar 2 (G4) elox-carbide | 10 | II 39-40 |
| 19 | EOS Bar 2 (G4) clean | 10 | II 41 |
| 20 | Hughes G2A carbided | 11 | II 42 |
| 21 | Astromet (Improved) | 12 | II 43-44 |
| 22 | Hughes G2B | --- | II 45-46 |
| 23 | STL (SW10) (G5b) | --- | II 47-48 |

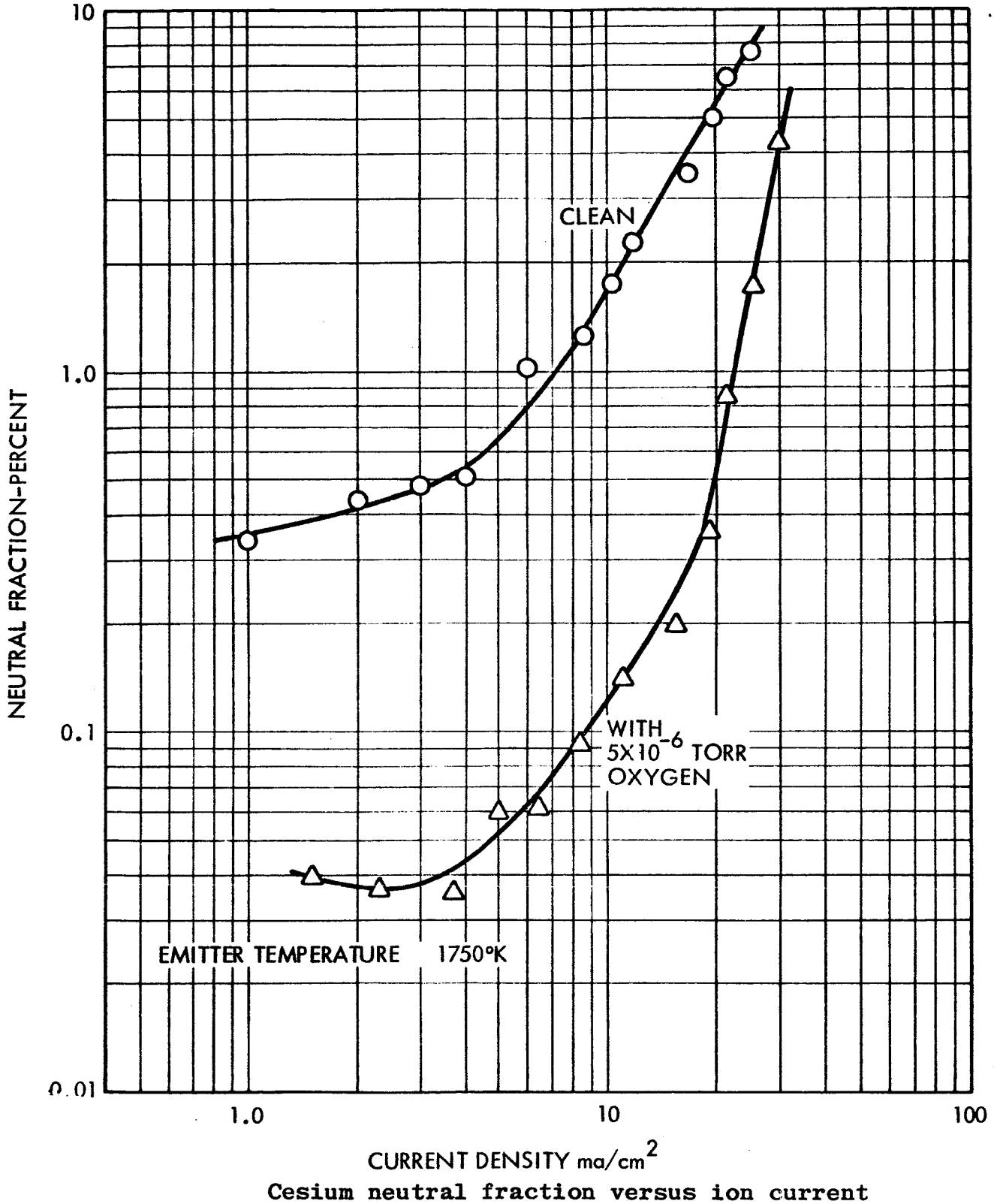


Cesium neutral fraction versus ion current density from E.O.S. - E6 porous tungsten

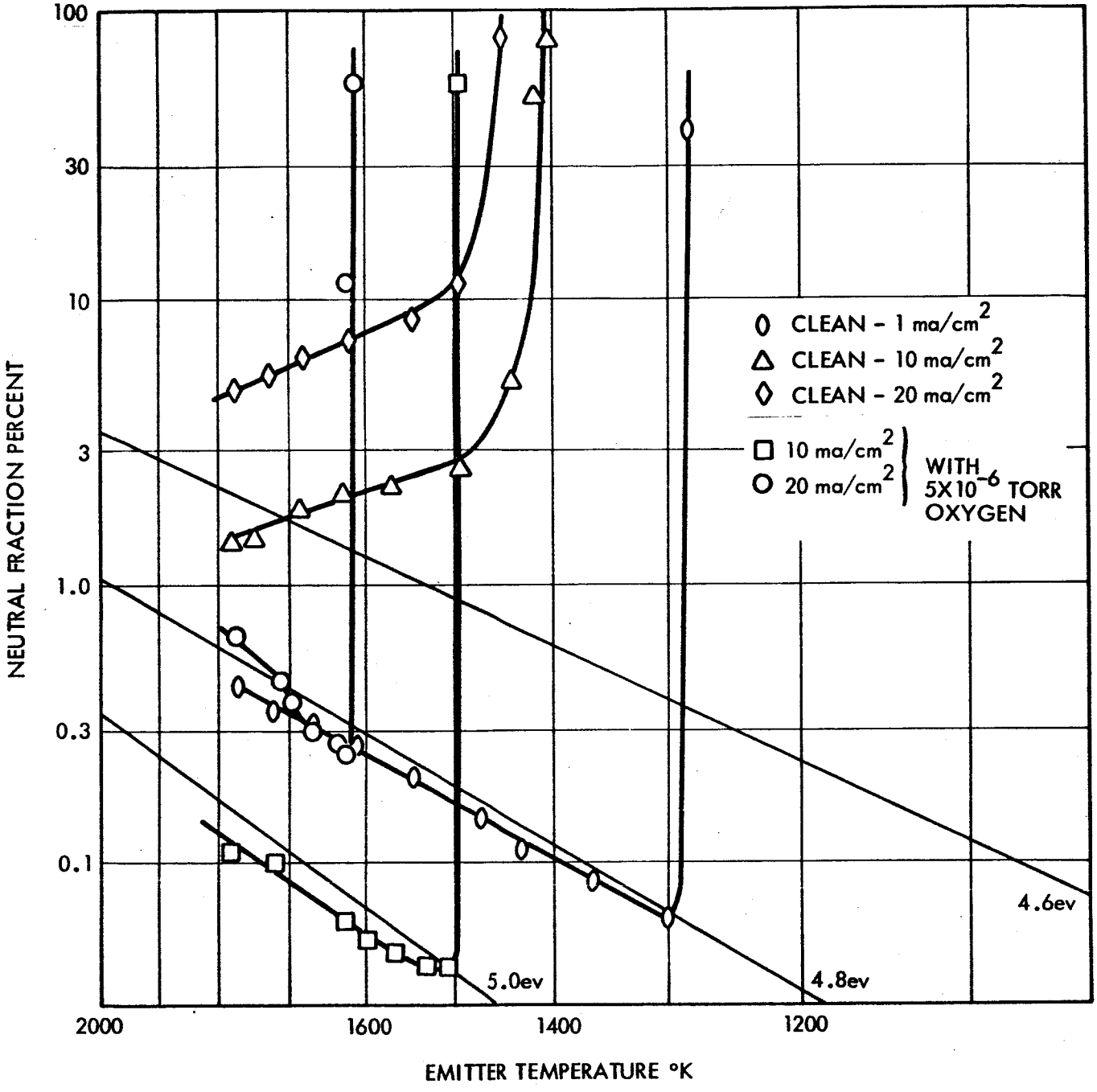


Cesium neutral fraction versus temperature of E.O.S. - E6 porous tungsten.

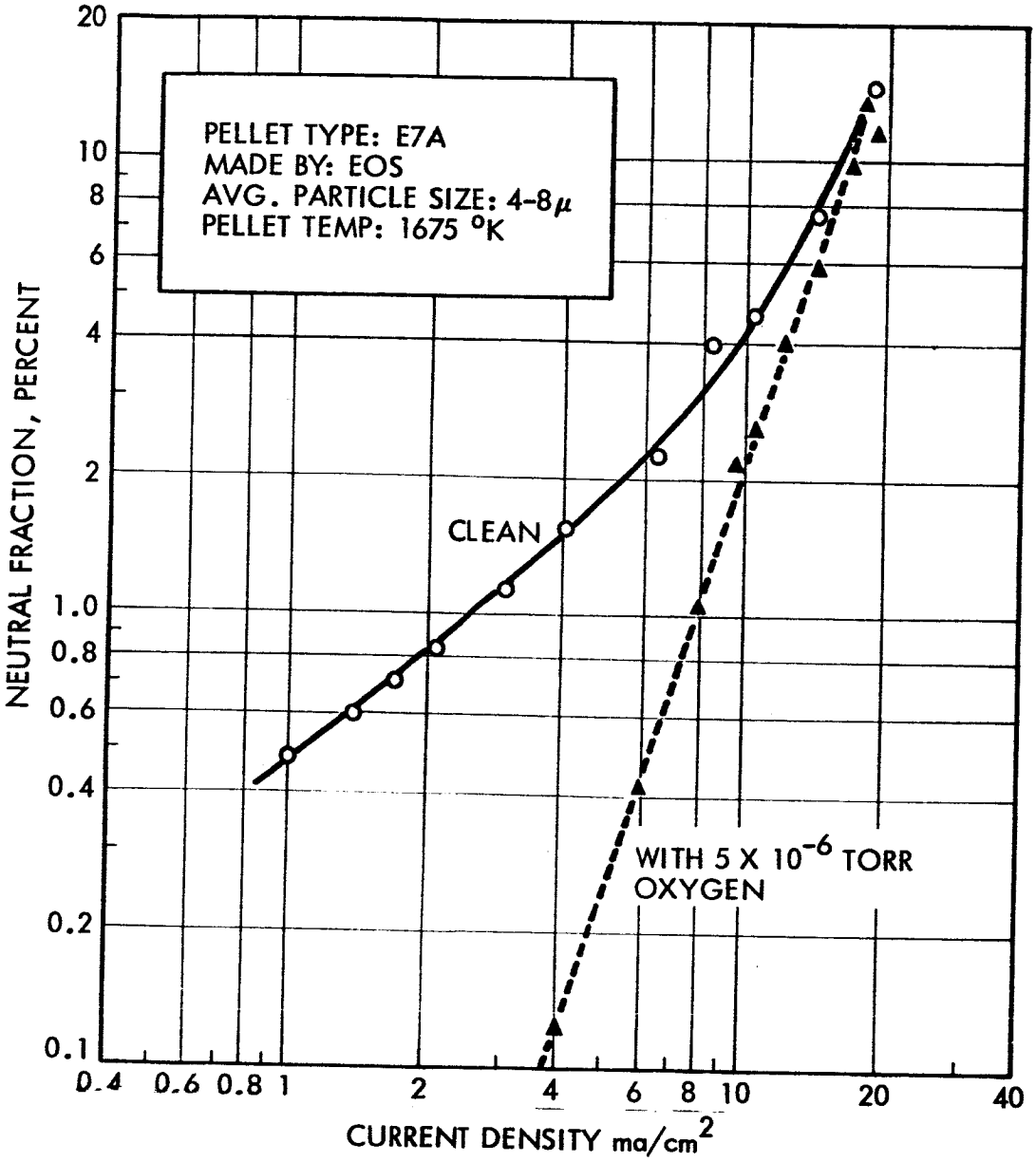


Cesium Neutral Fraction Versus Ion Current Density from E.O.S. E-7A Porous Tungsten.

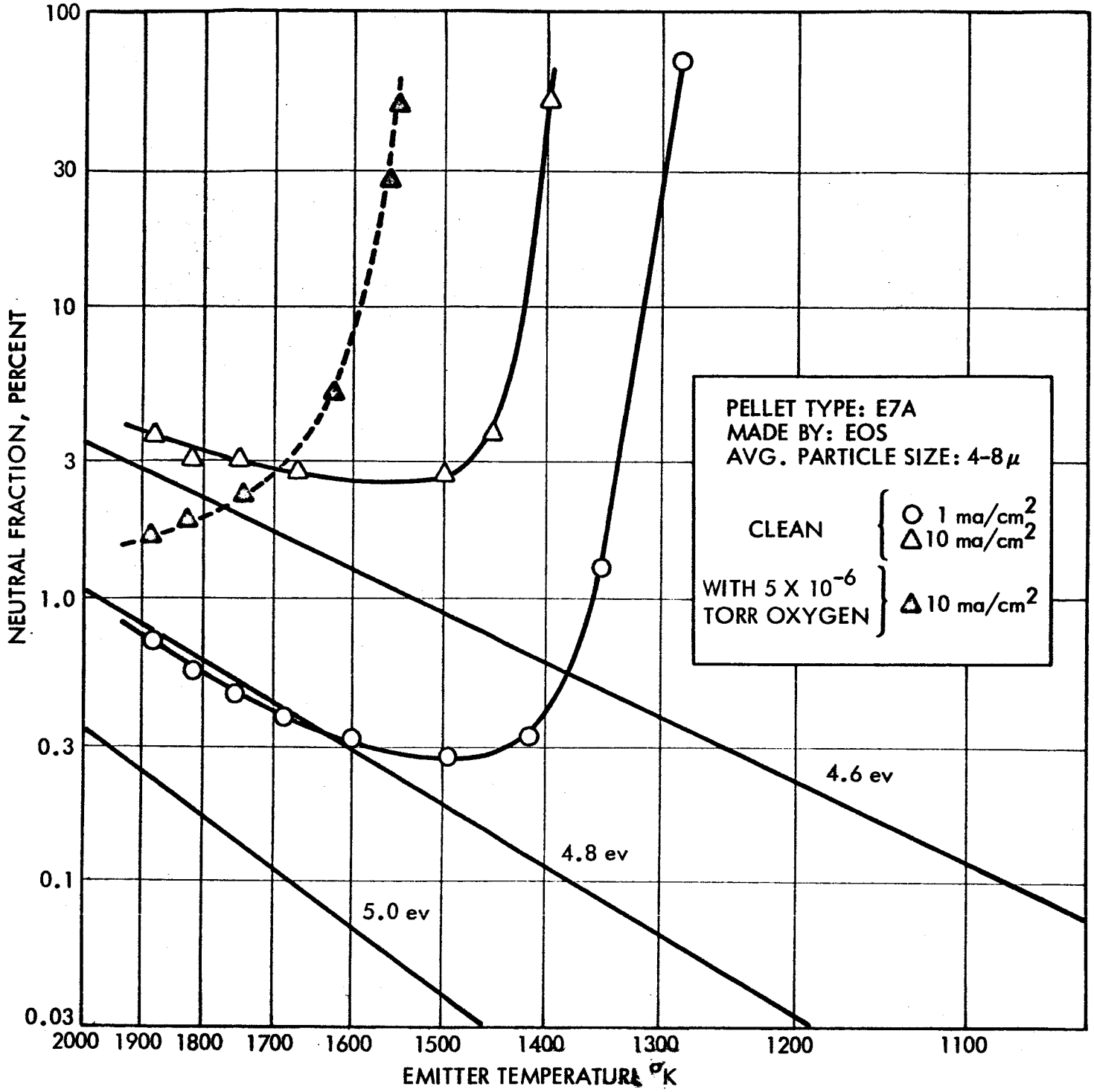


Cesium Neutral Fraction Versus Temperature of E.O.S. E-7A Porous Tungsten.

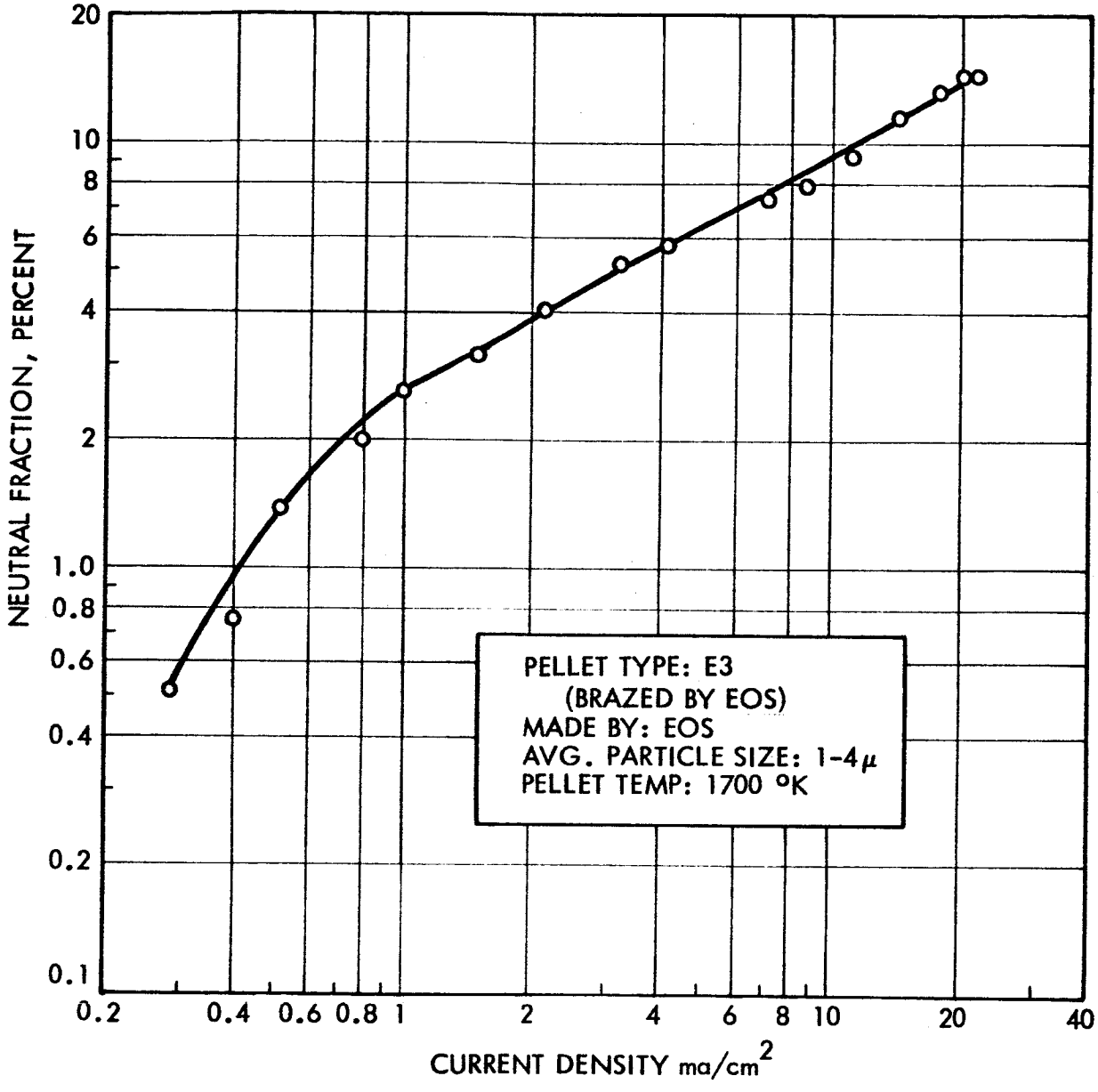


Cesium Neutral Fraction Versus Ion Current Density from E.O.S. E-3 Porous Tungsten.

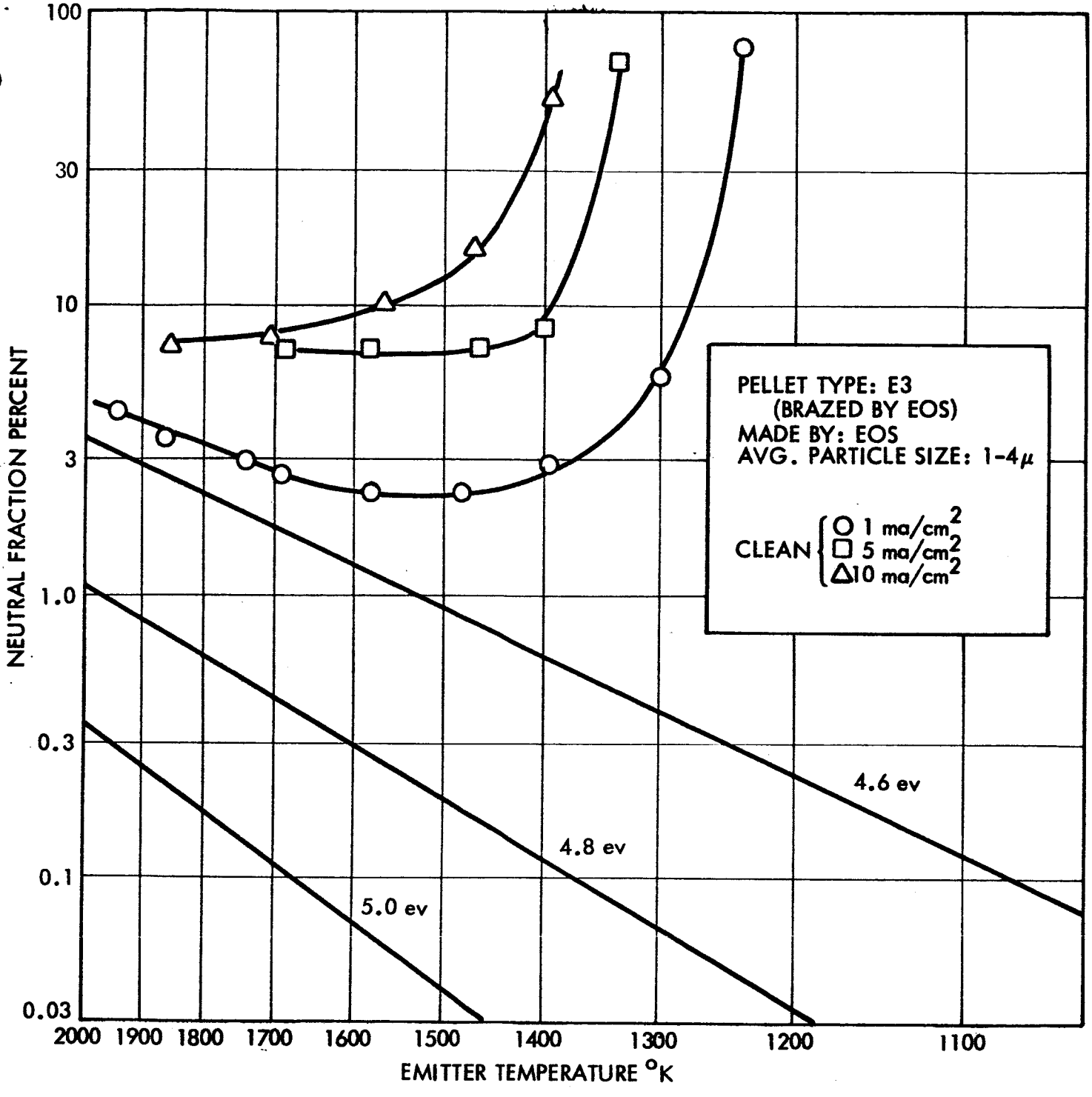


Cesium Neutral Fraction Versus Temperature of E.O.S. E-3 Porous Tungsten.

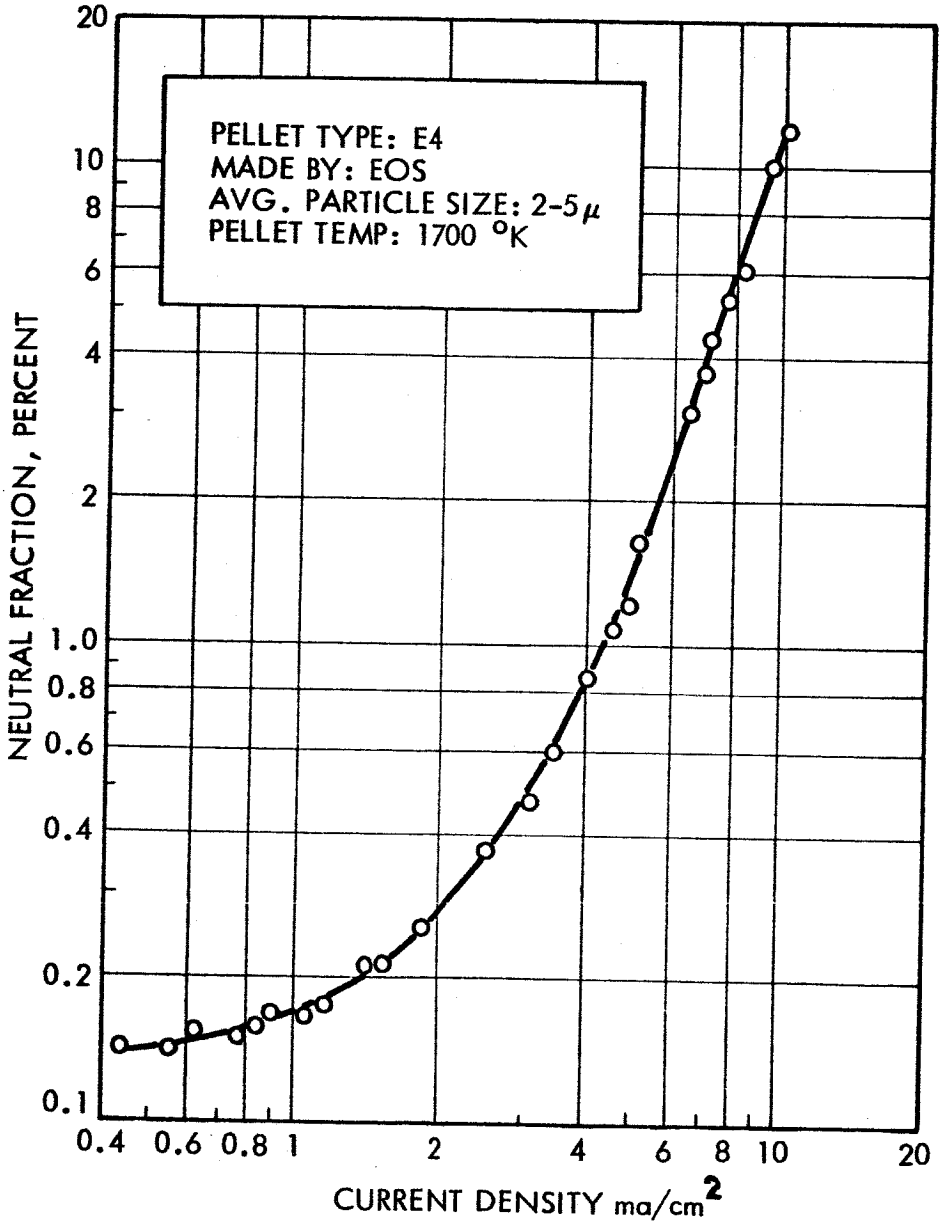


Cesium Neutral Fraction Versus Ion Current Density from E.O.S. E-4 Porous Tungsten.

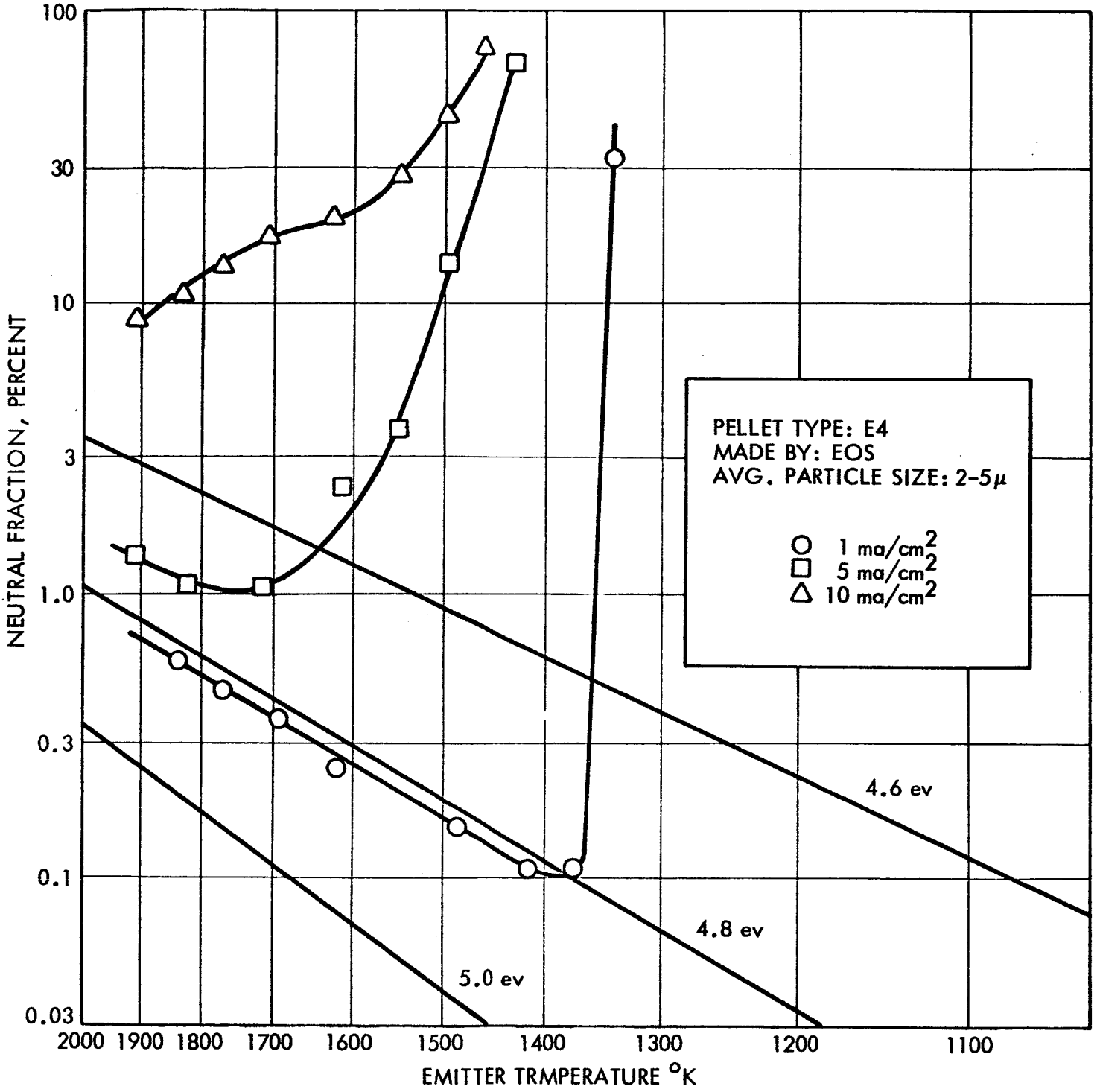


Cesium Neutral Fraction Versus Temperature of E.O.S. E-4 Porous Tungsten.

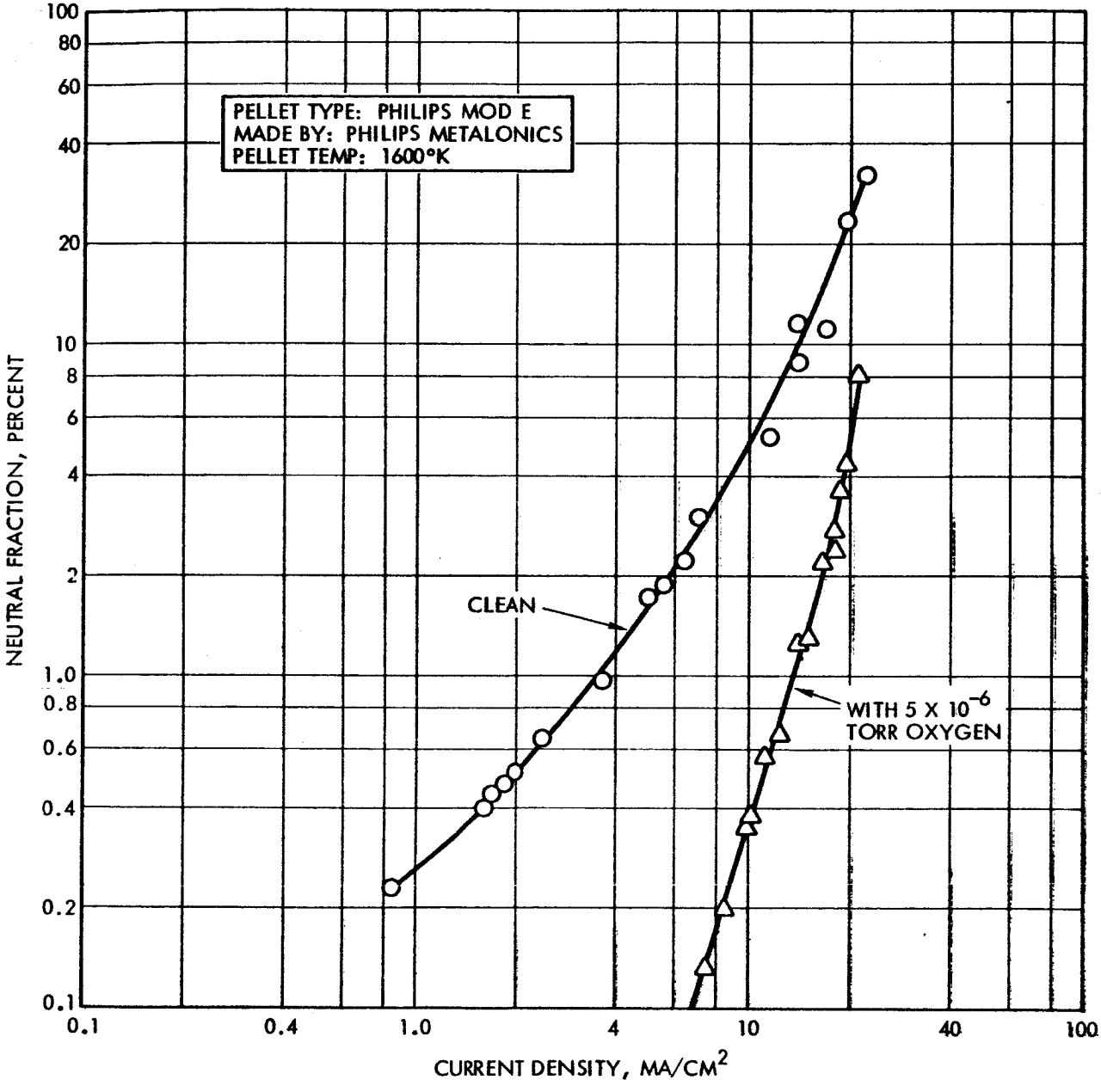


Cesium neutral fraction versus ion current density from Philips' Mod E porous tungsten.

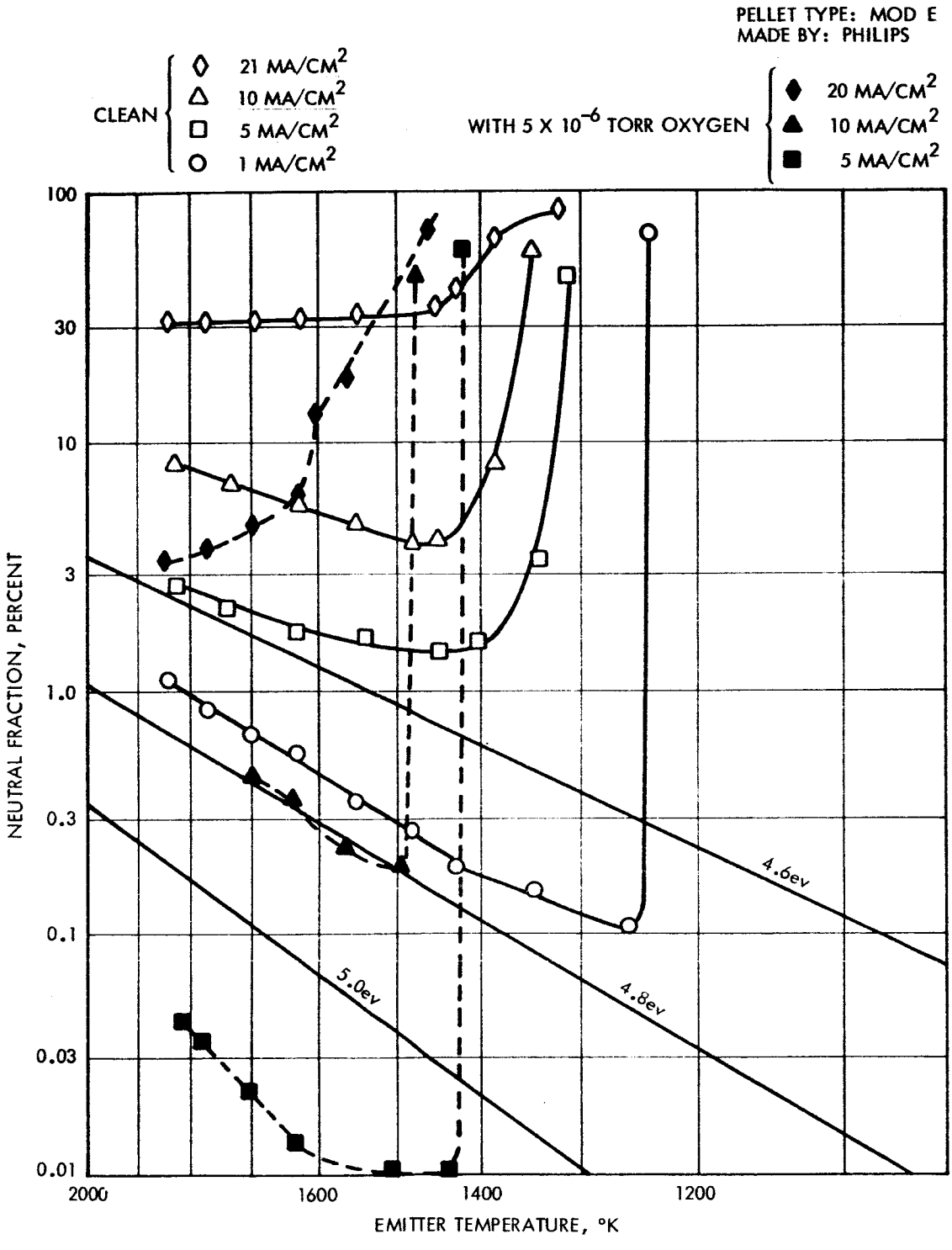


**Cesium neutral fraction versus temperature of Philips' Mod E porous tungsten.**

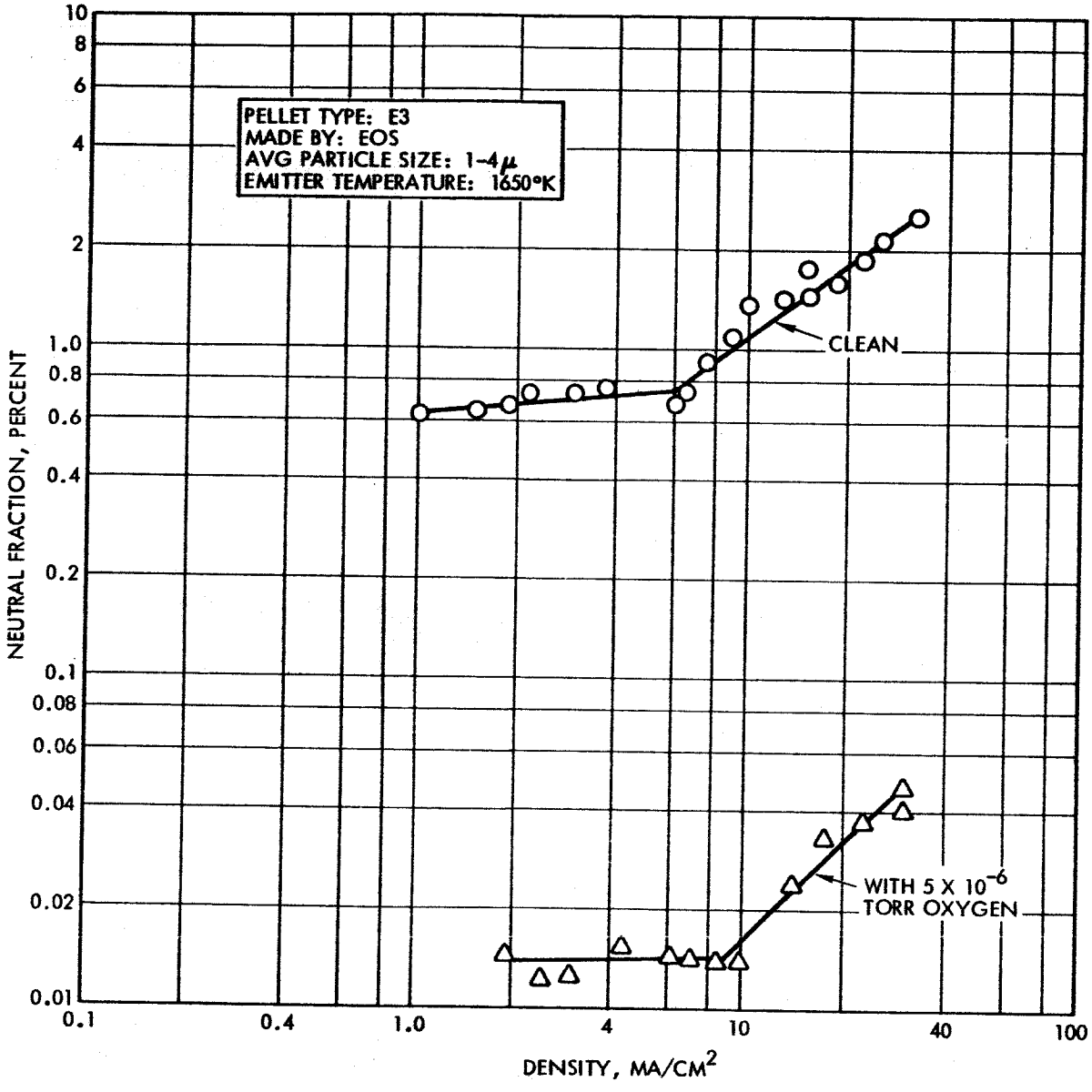


Cesium neutral fraction versus ion current density from E.O.S. E3 porous tungsten.

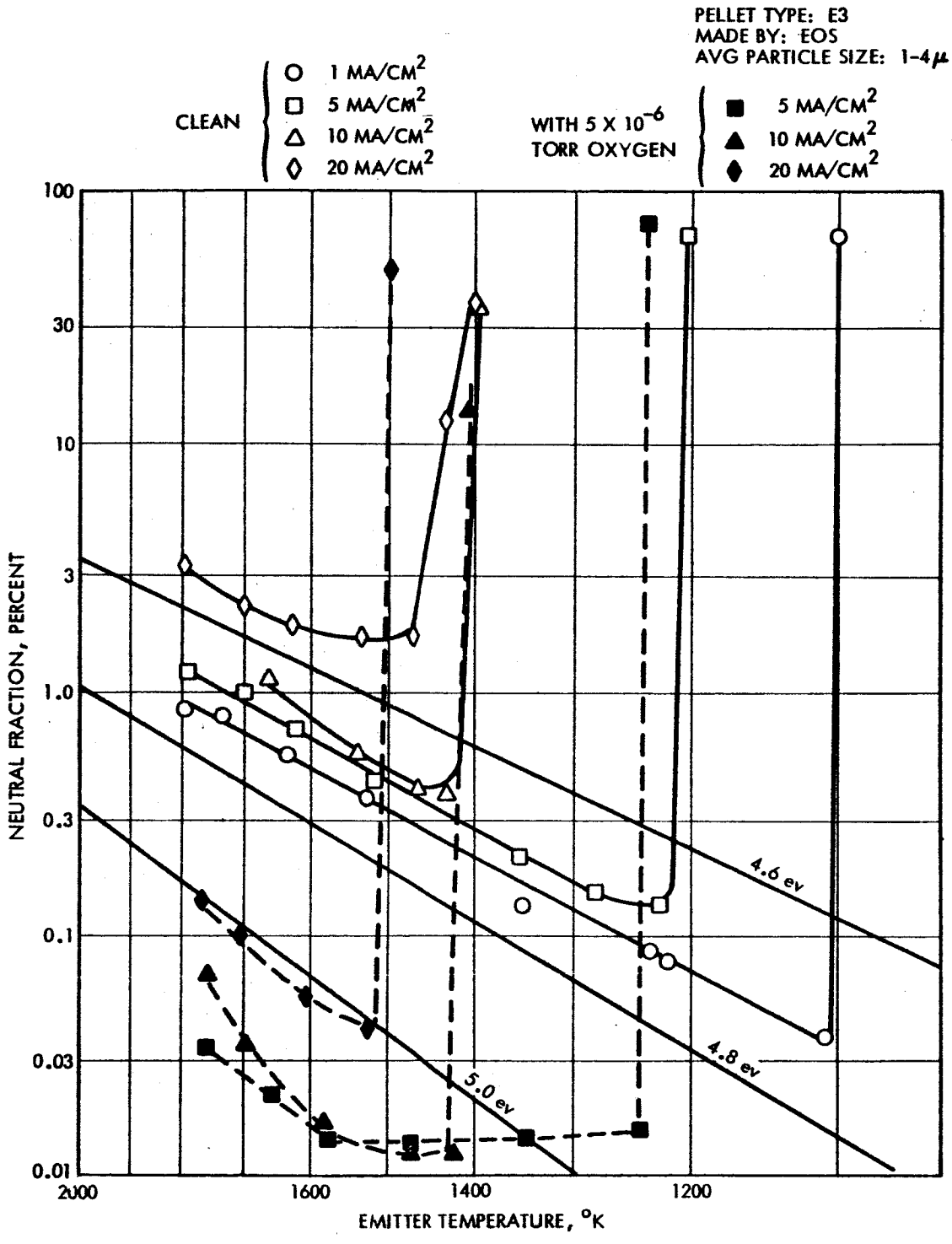


Cesium neutral fraction versus temperature of E.O.S. E3 porous tungsten.

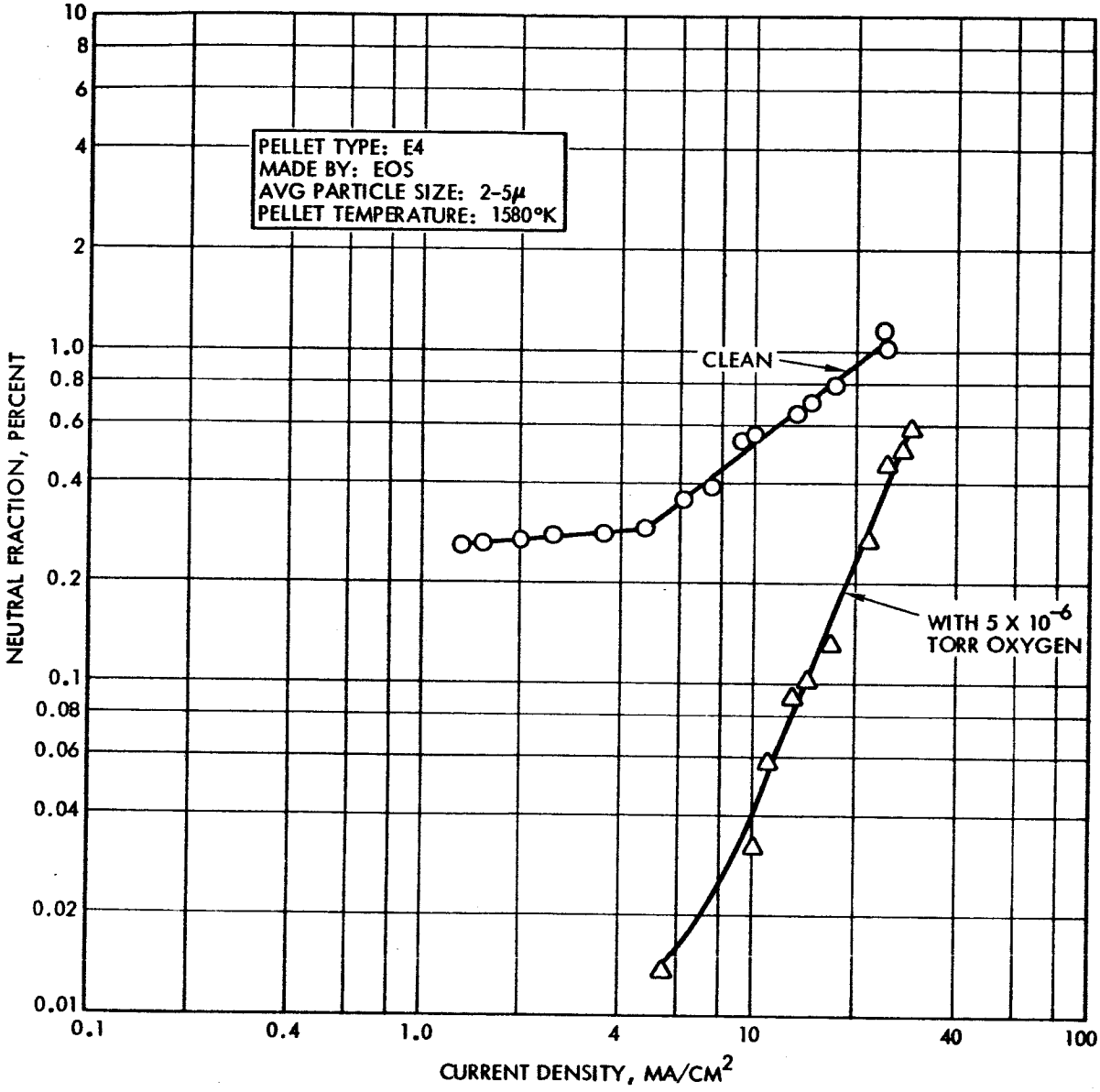


Cesium neutral fraction versus ion current density from E.O.S. E4 porous tungsten.

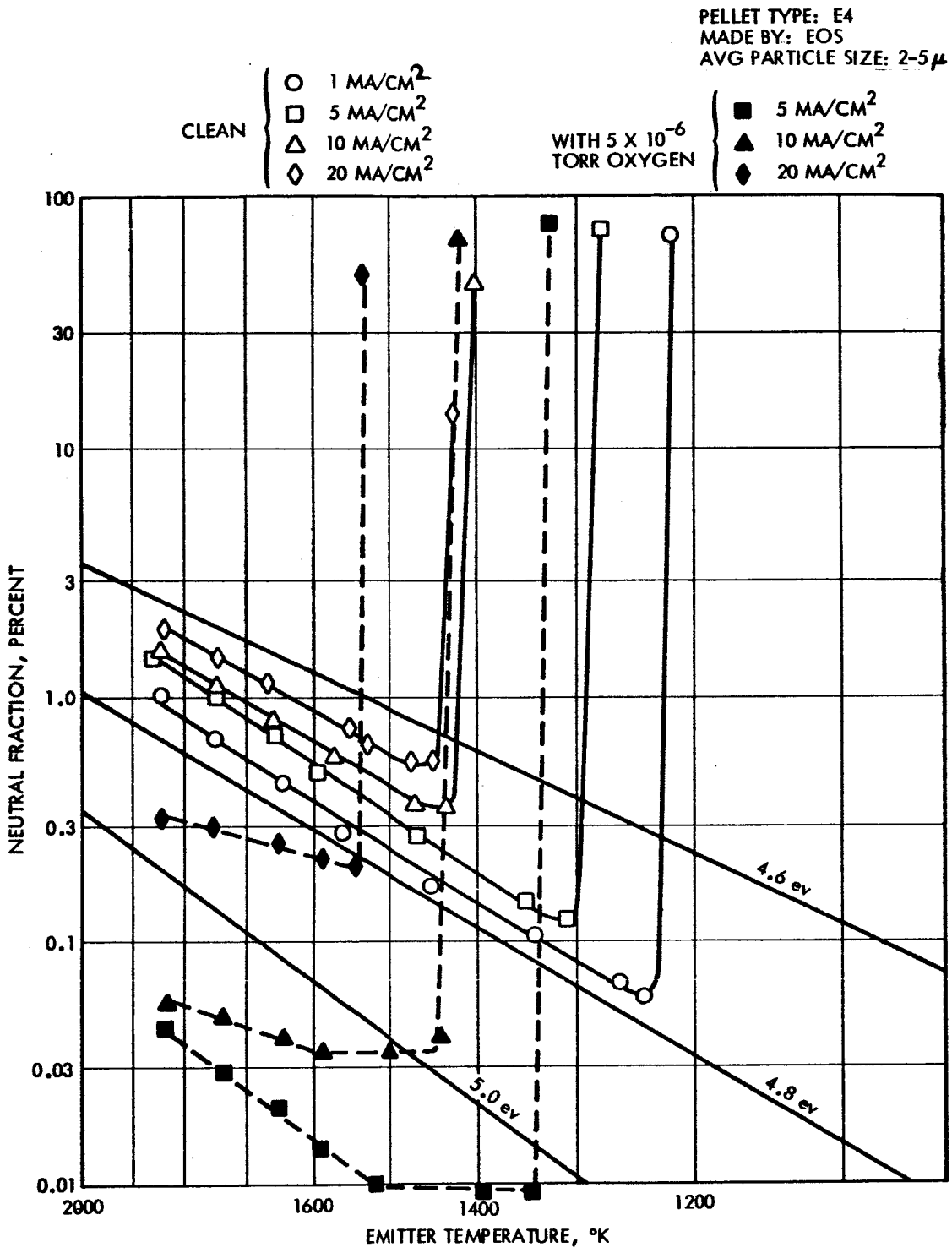


Cesium neutral fraction versus temperature of E.O.S. E4 porous tungsten.

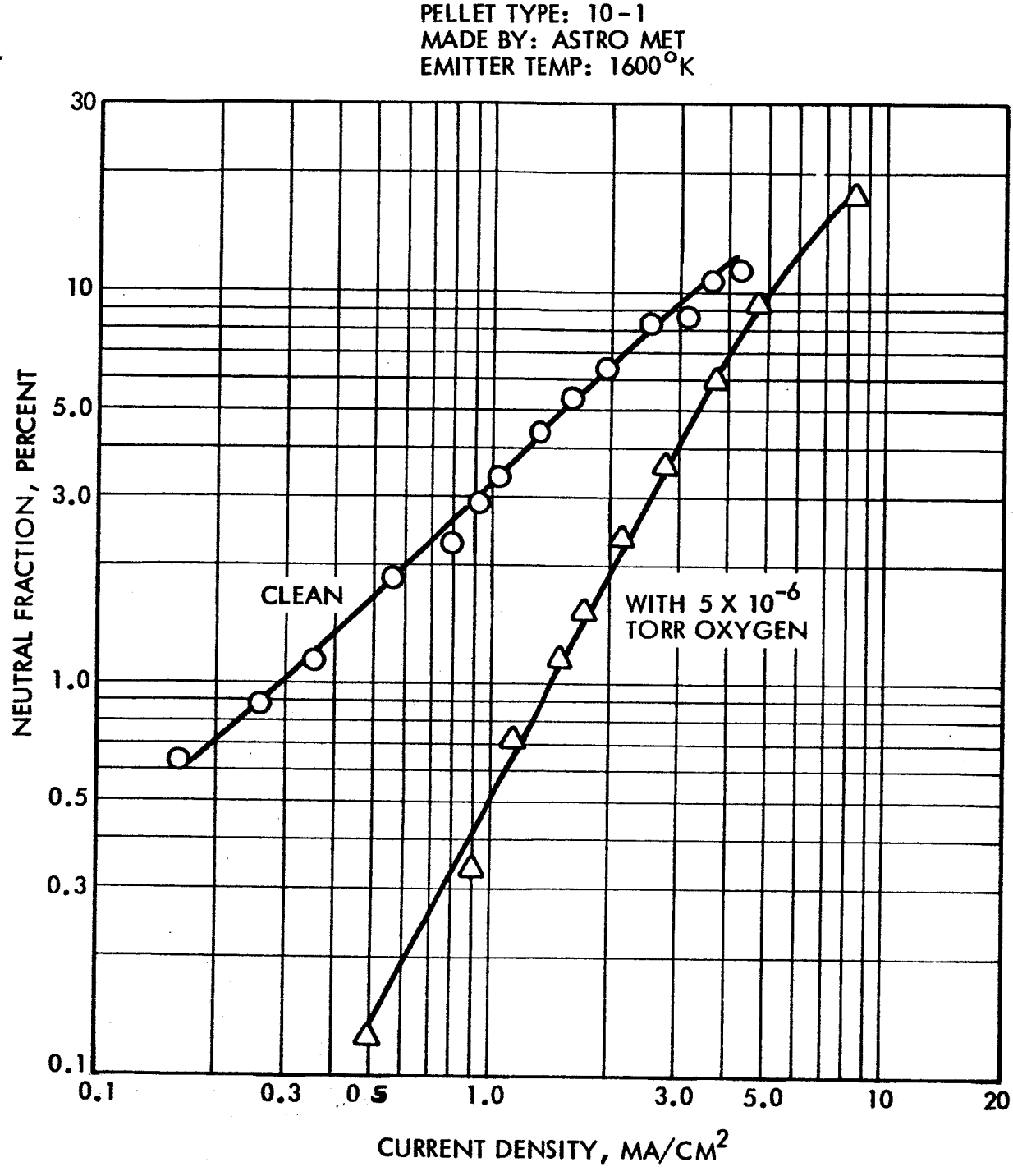


Improved cesium neutral fraction versus ion current density from Astromet 10-1 after etching.

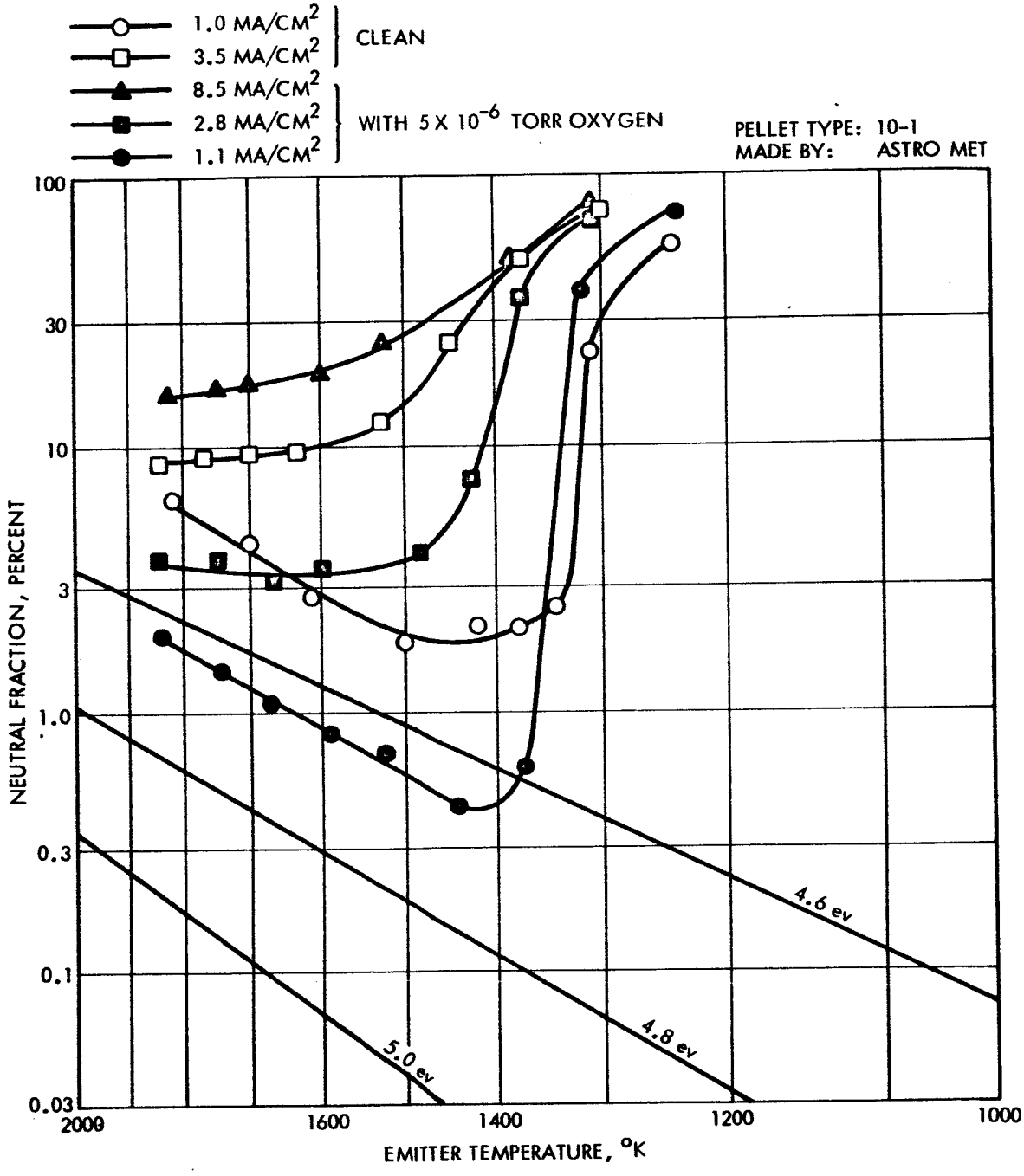


Cesium neutral fraction versus temperature of Astromet 10-1 porous tungsten.

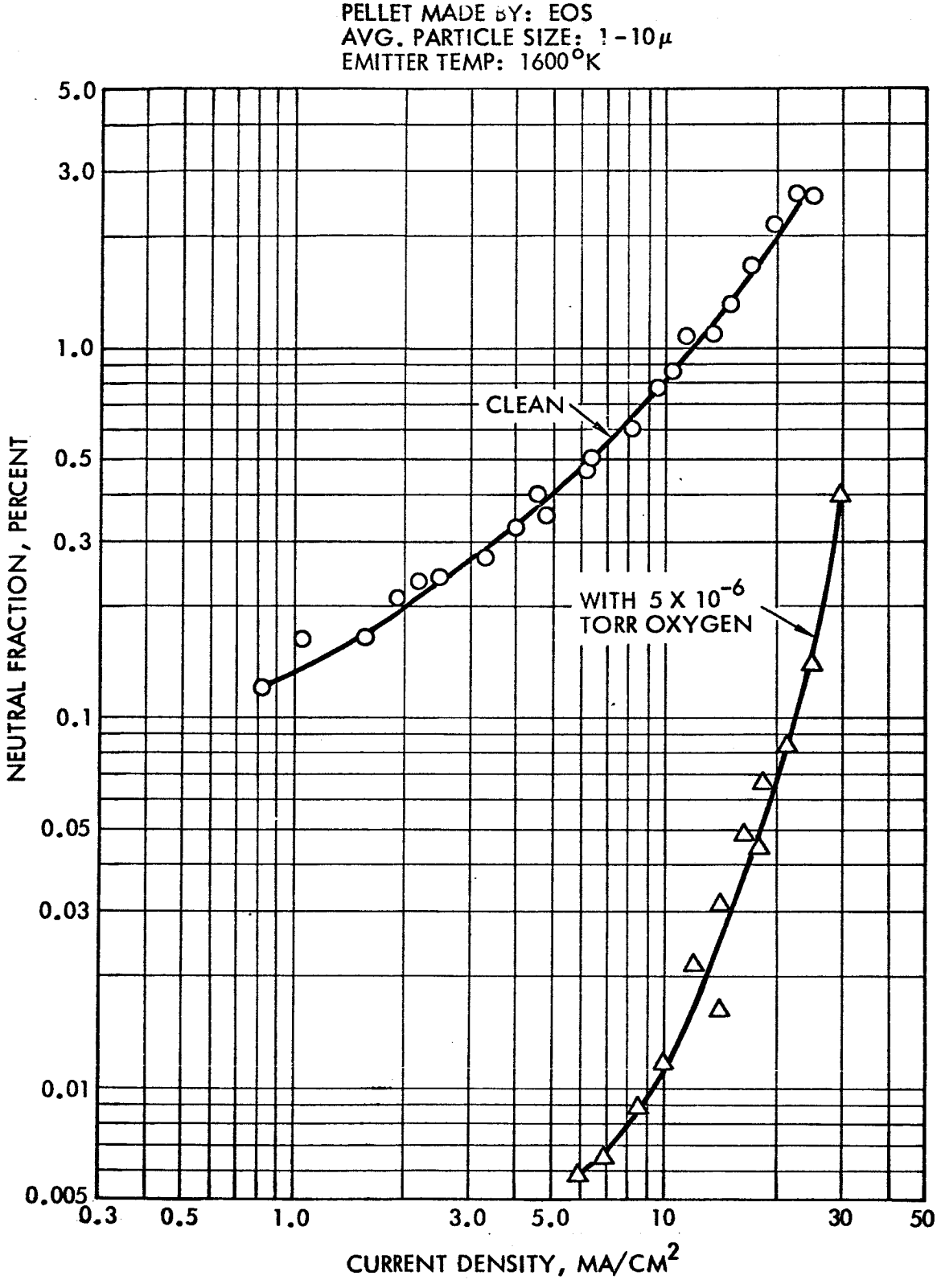


Cesium neutral fraction versus ion current density from porous tungsten manufactured by E.O.S. to be used in a large ion engine. (G1)

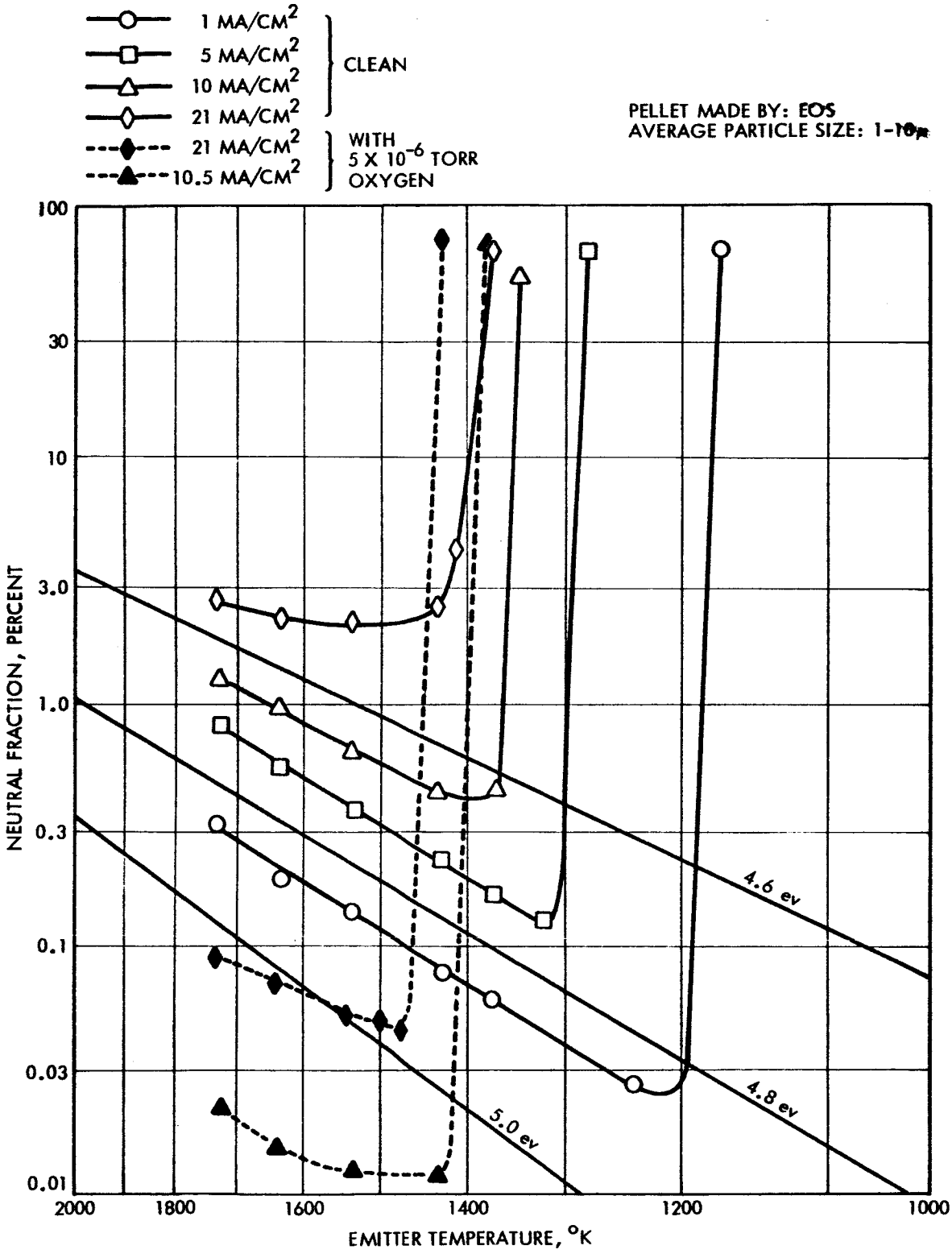


Cesium neutral fraction versus temperature of the E.O.S. tungsten. (G1)

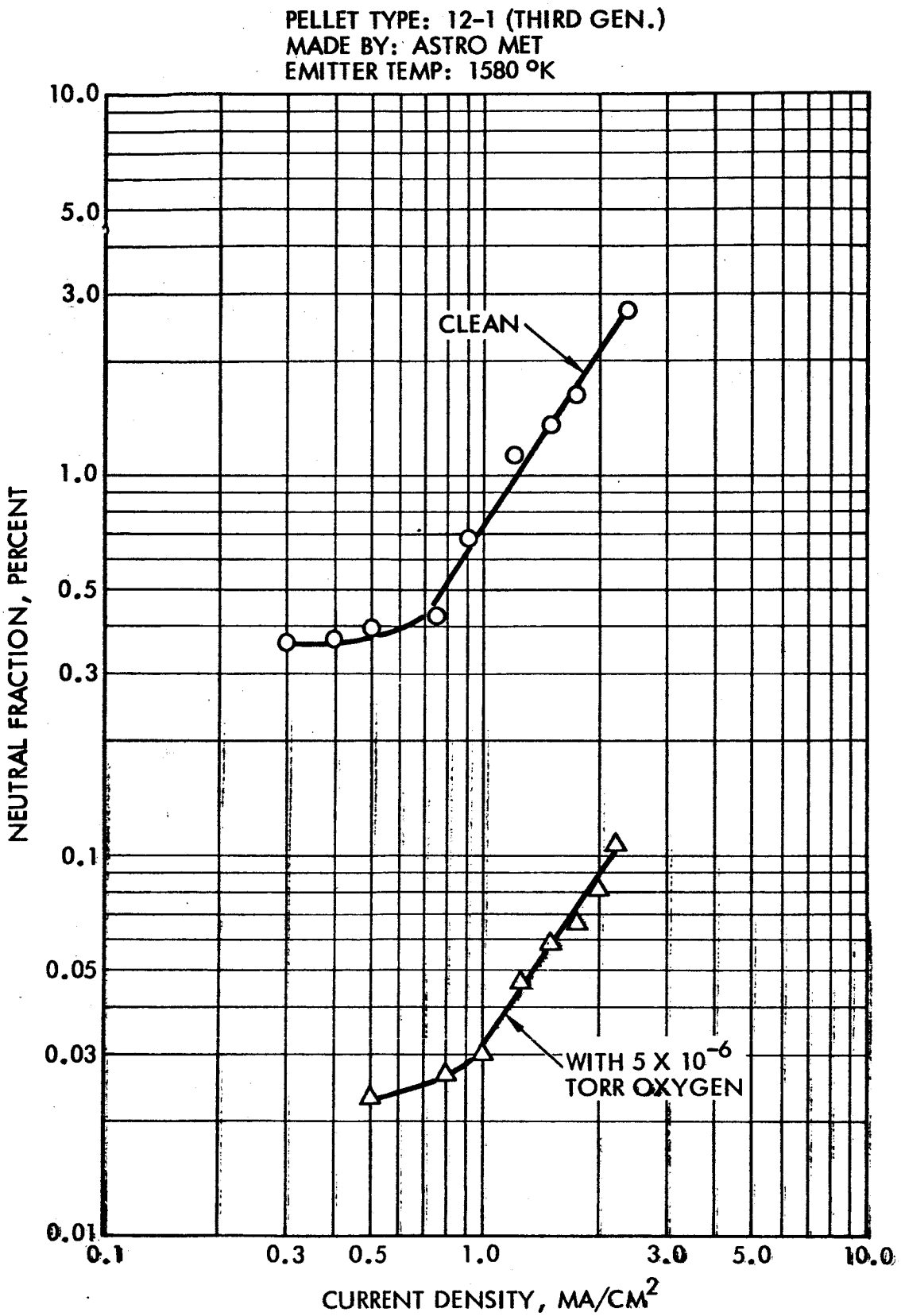


Cesium neutral fraction versus ion current density from Astromet 12-1 porous tungsten.

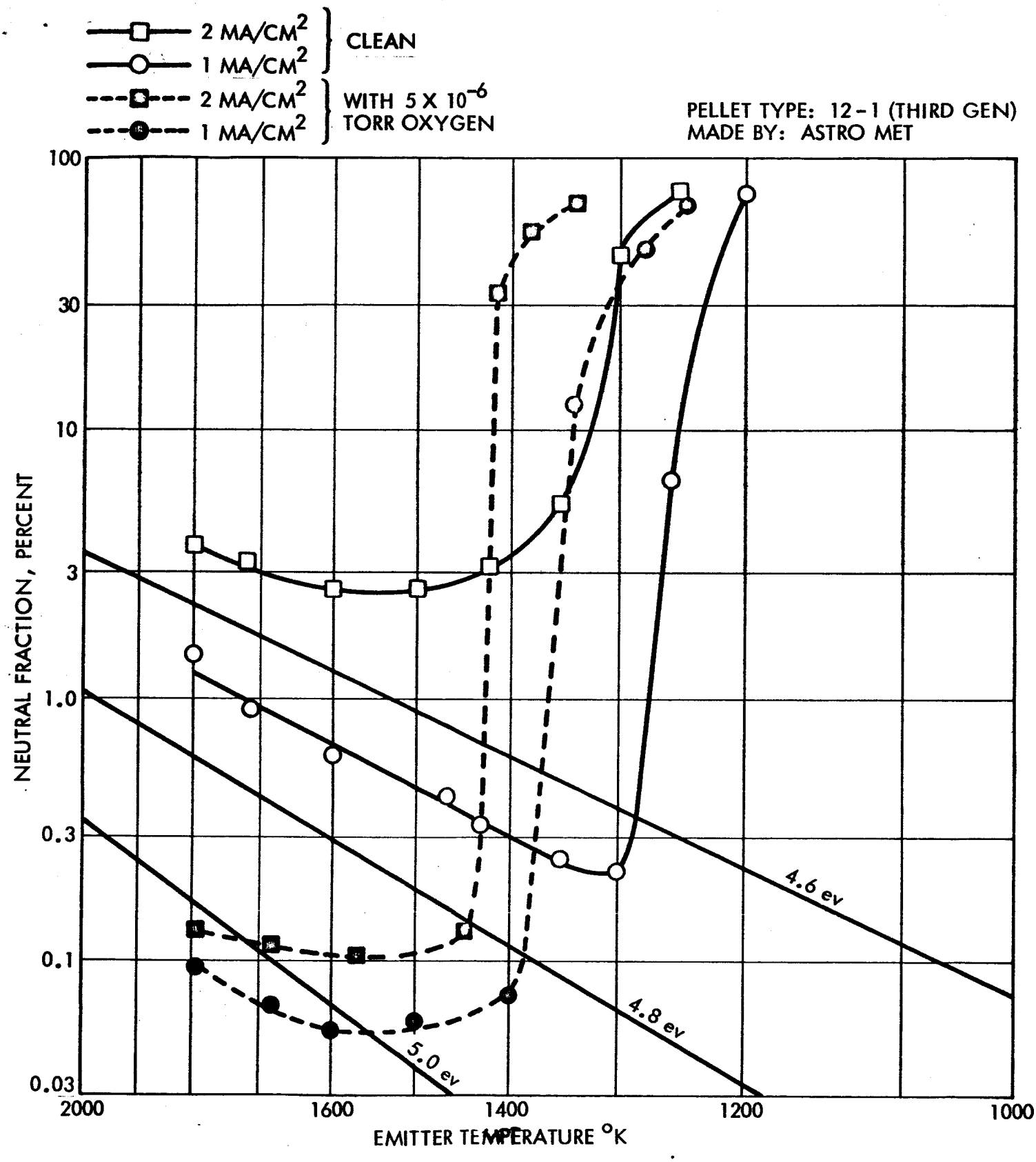


Cesium neutral fraction versus temperature of Astromet 12-1 porous tungsten.

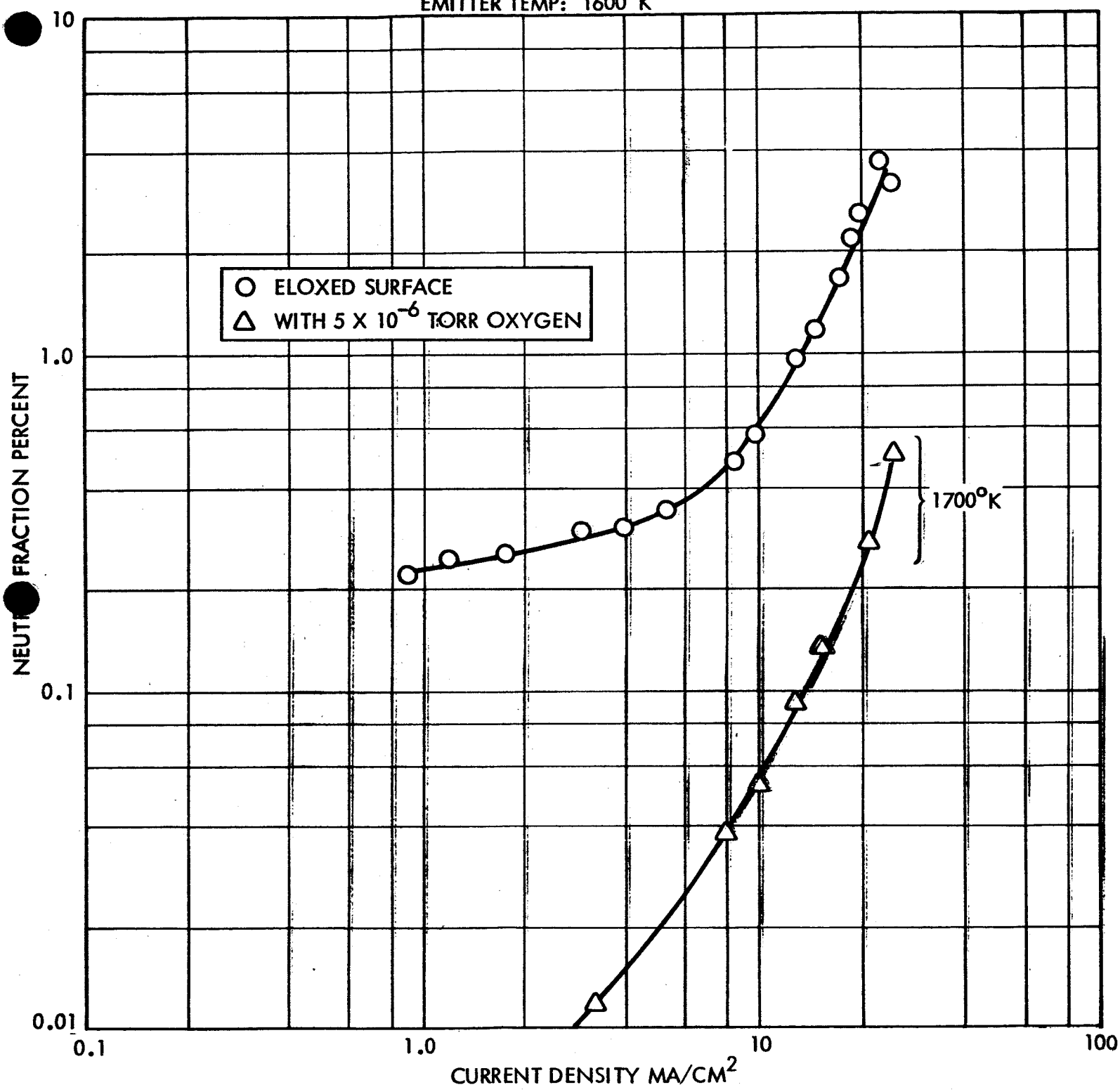


Cesium neutral fraction versus ion current density from "elox" machined E.O.S. engine material. (G1)

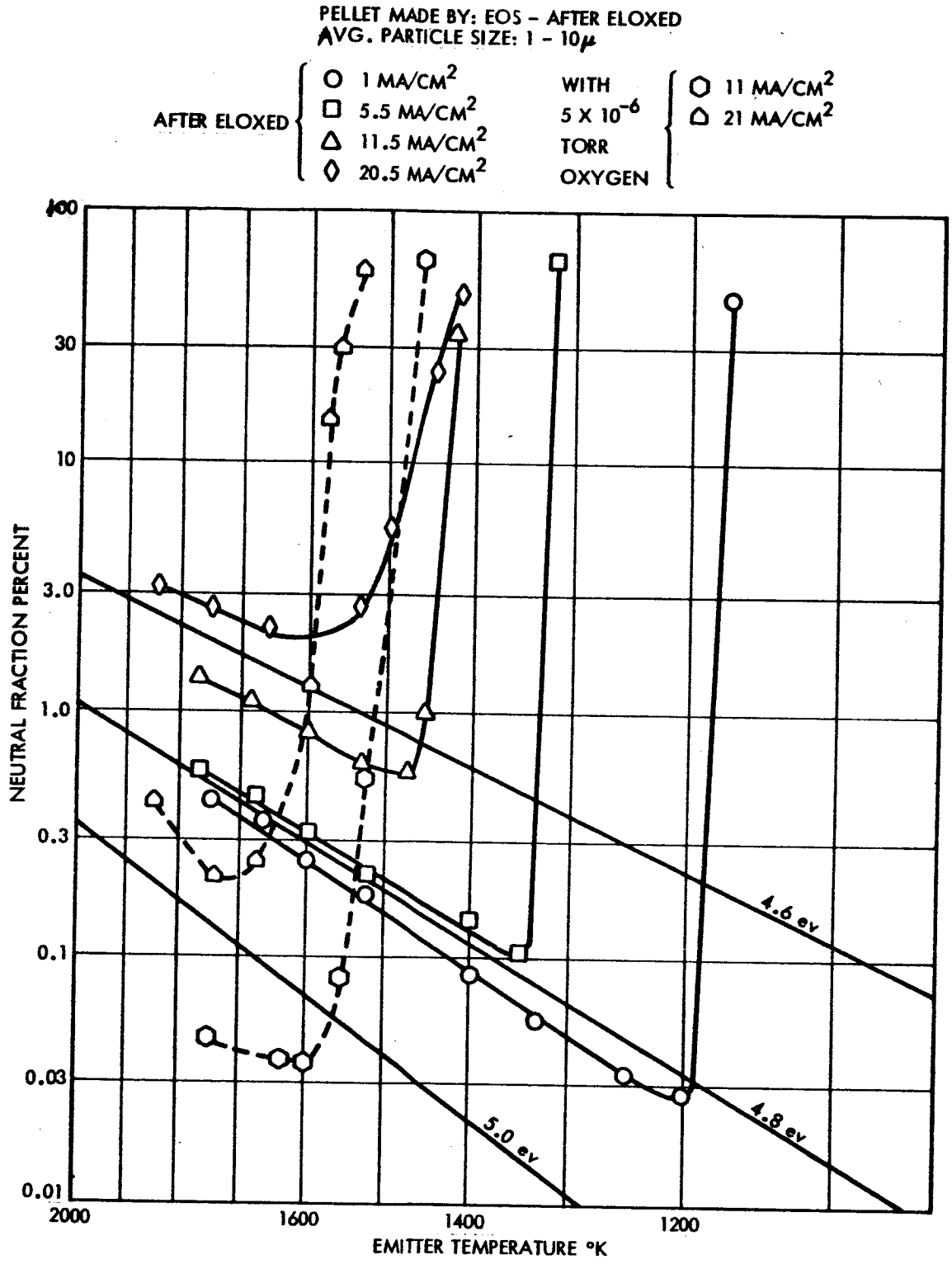


Cesium neutral fraction versus porous tungsten temperature. (G1)

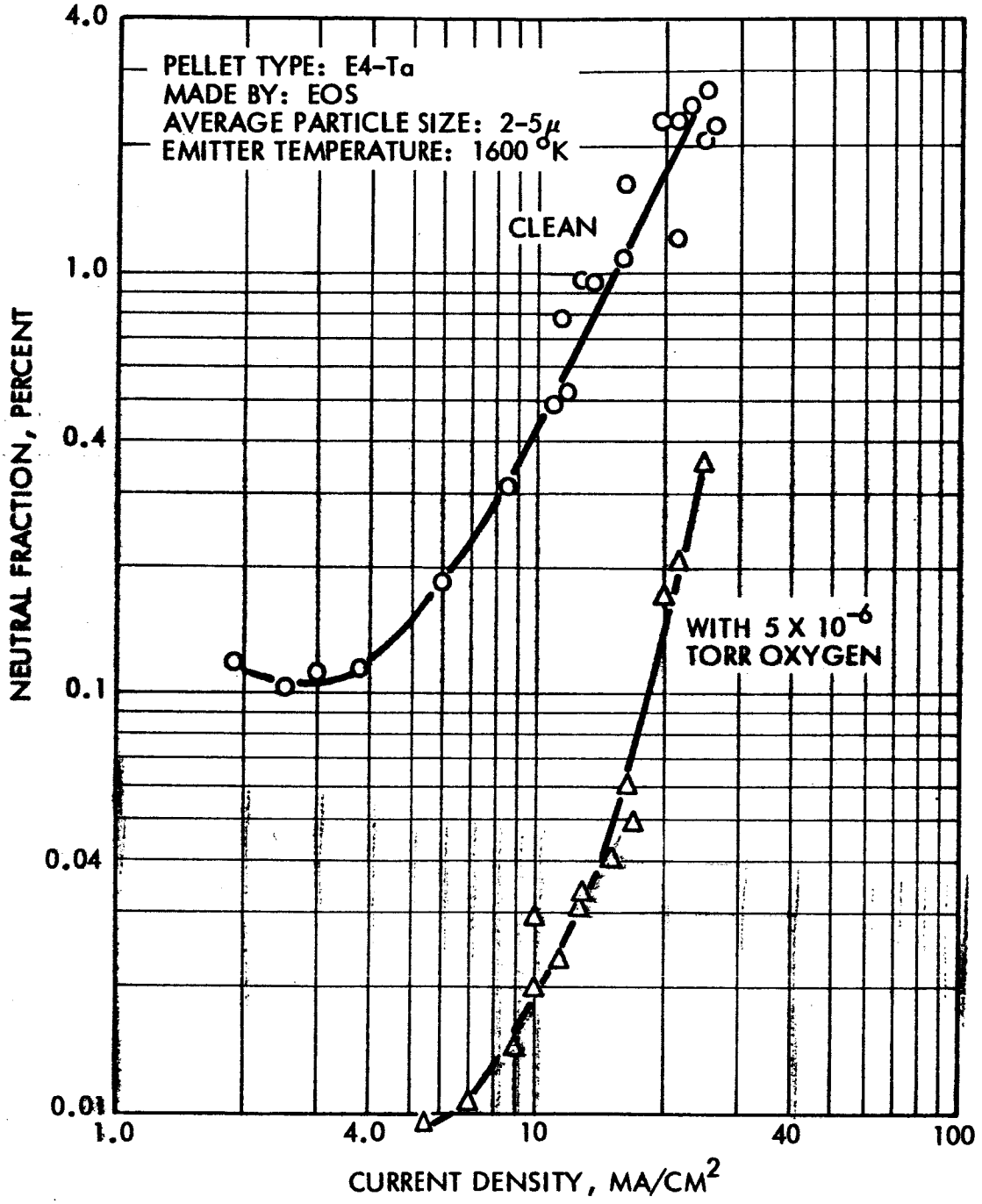


Cesium neutral fraction versus cesium ion current density from E.O.S. porous tungsten manufactured from a compact of graded spherical tungsten powder and tantalum powder. (E4-Ta)

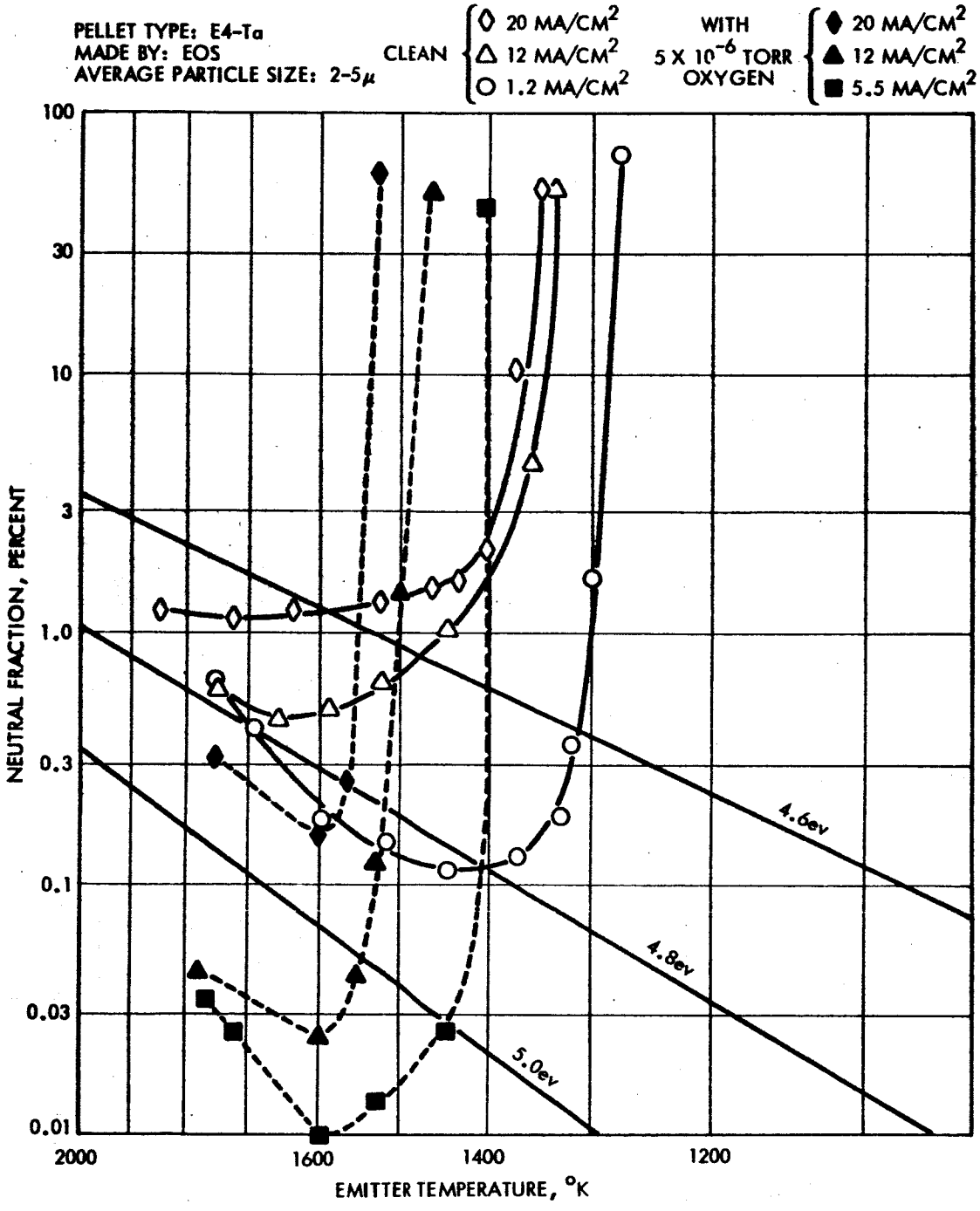


Cesium neutral fraction versus temperature of the E.O.S. E4-10A% Ta porous tungsten ion emitter.

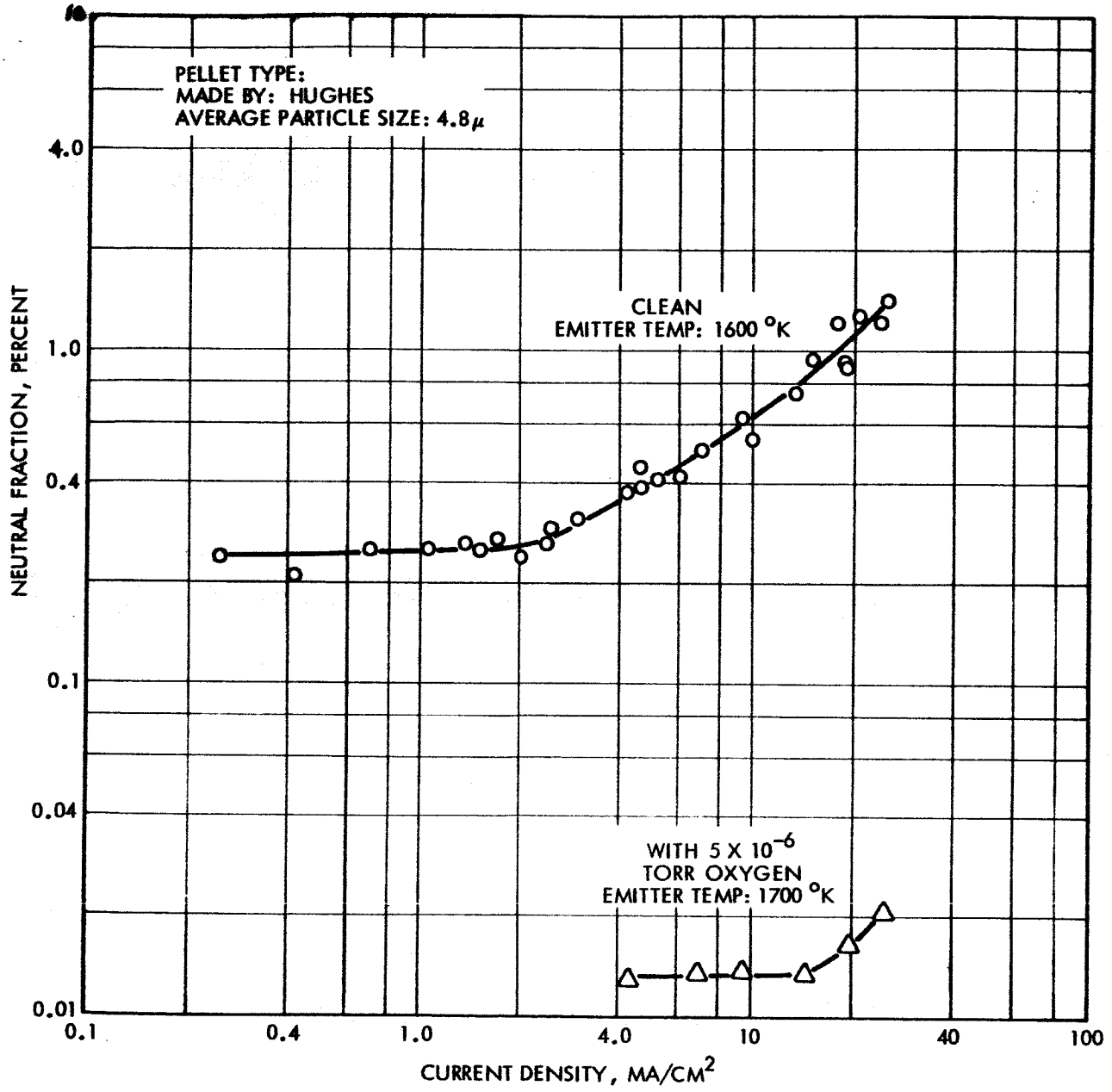


Cesium neutral fraction versus cesium ion current from porous tungsten manufactured by Hughes. (G2A)

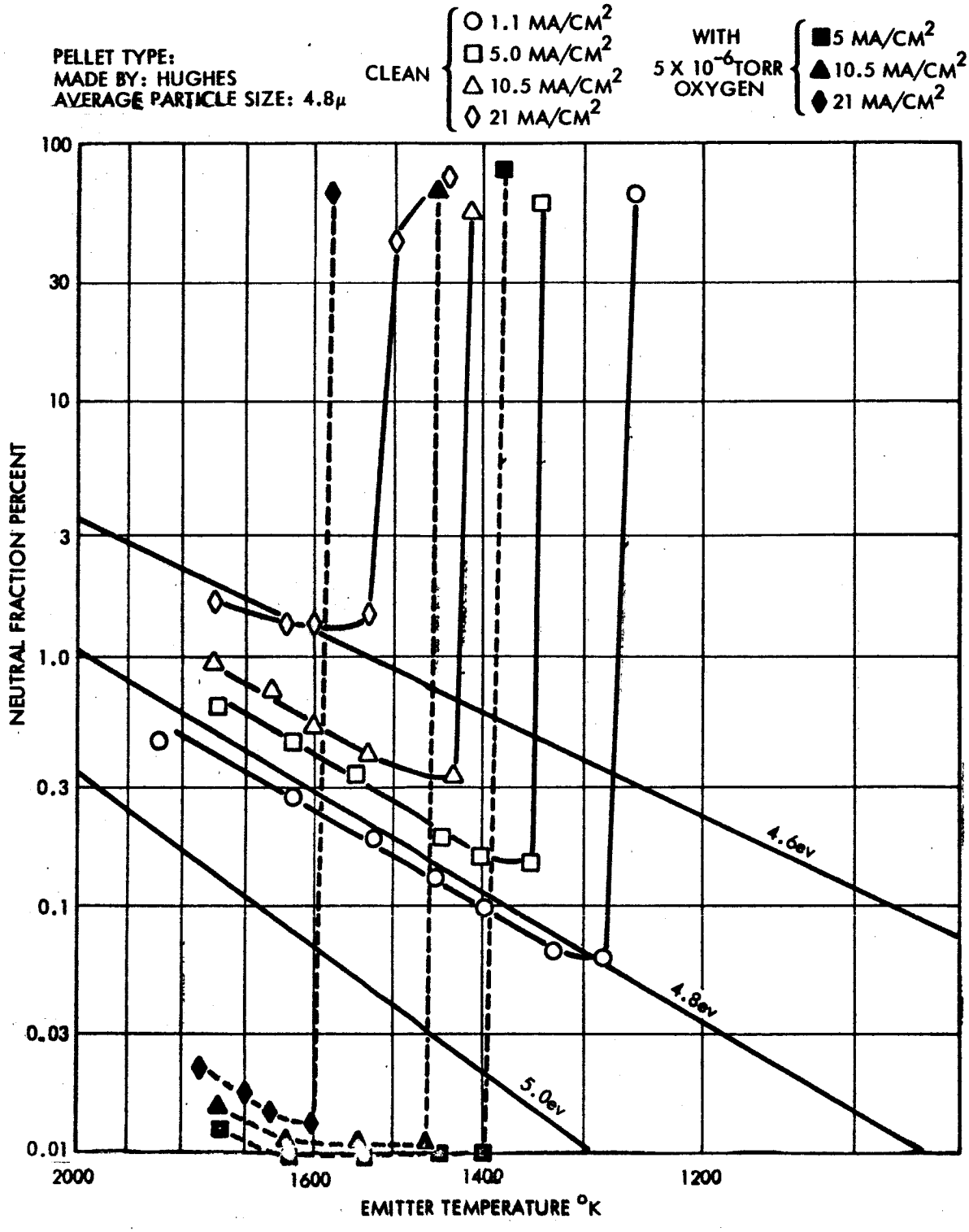


Cesium neutral fraction versus temperature of Hughes porous tungsten. (G2A)

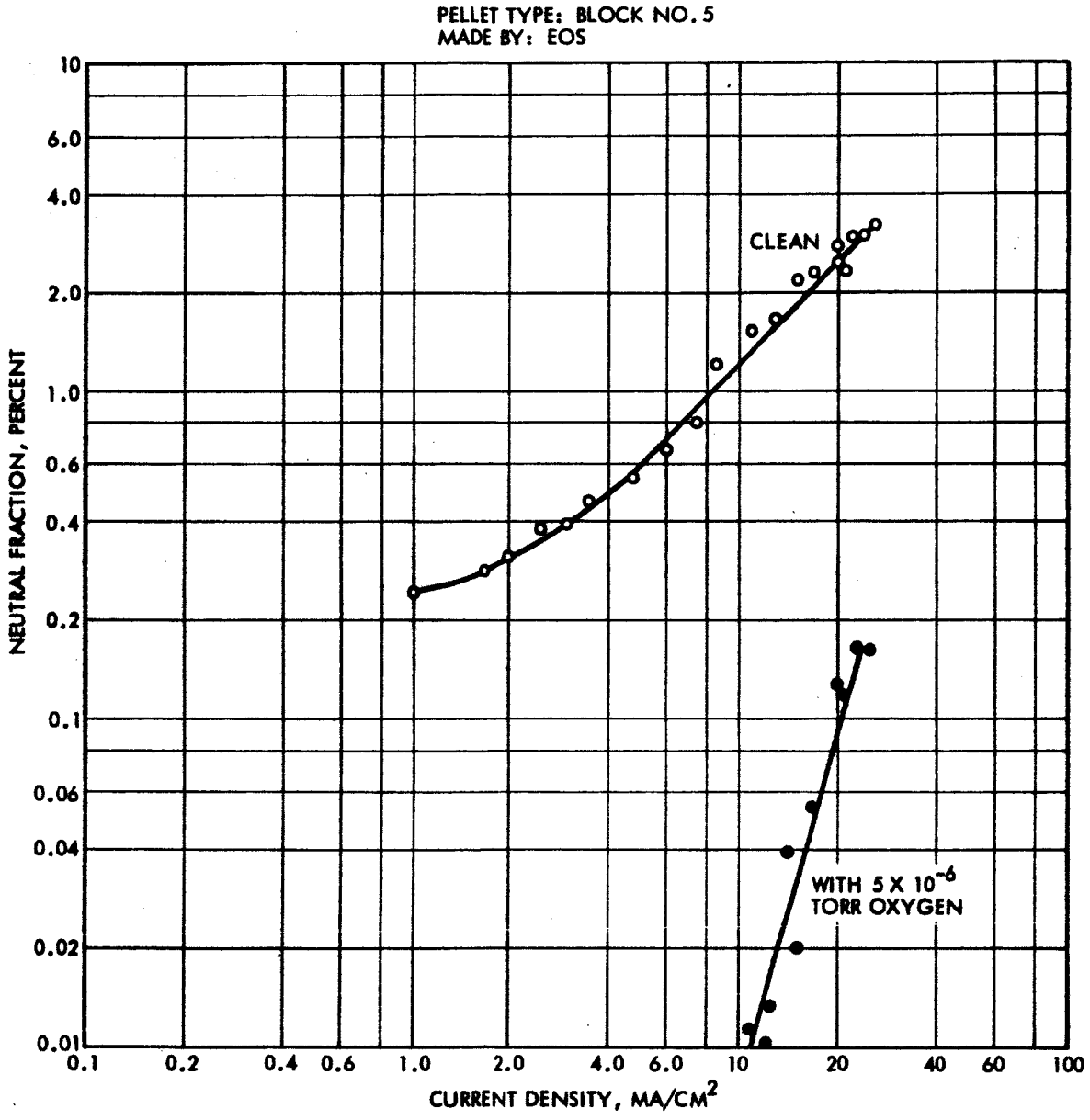


Cesium neutral fraction versus ion current density from porous tungsten manufactured by E.O.S. from graded spherical powder and designated "Block No. 5". (C3). Emitter temp: 1600°K.

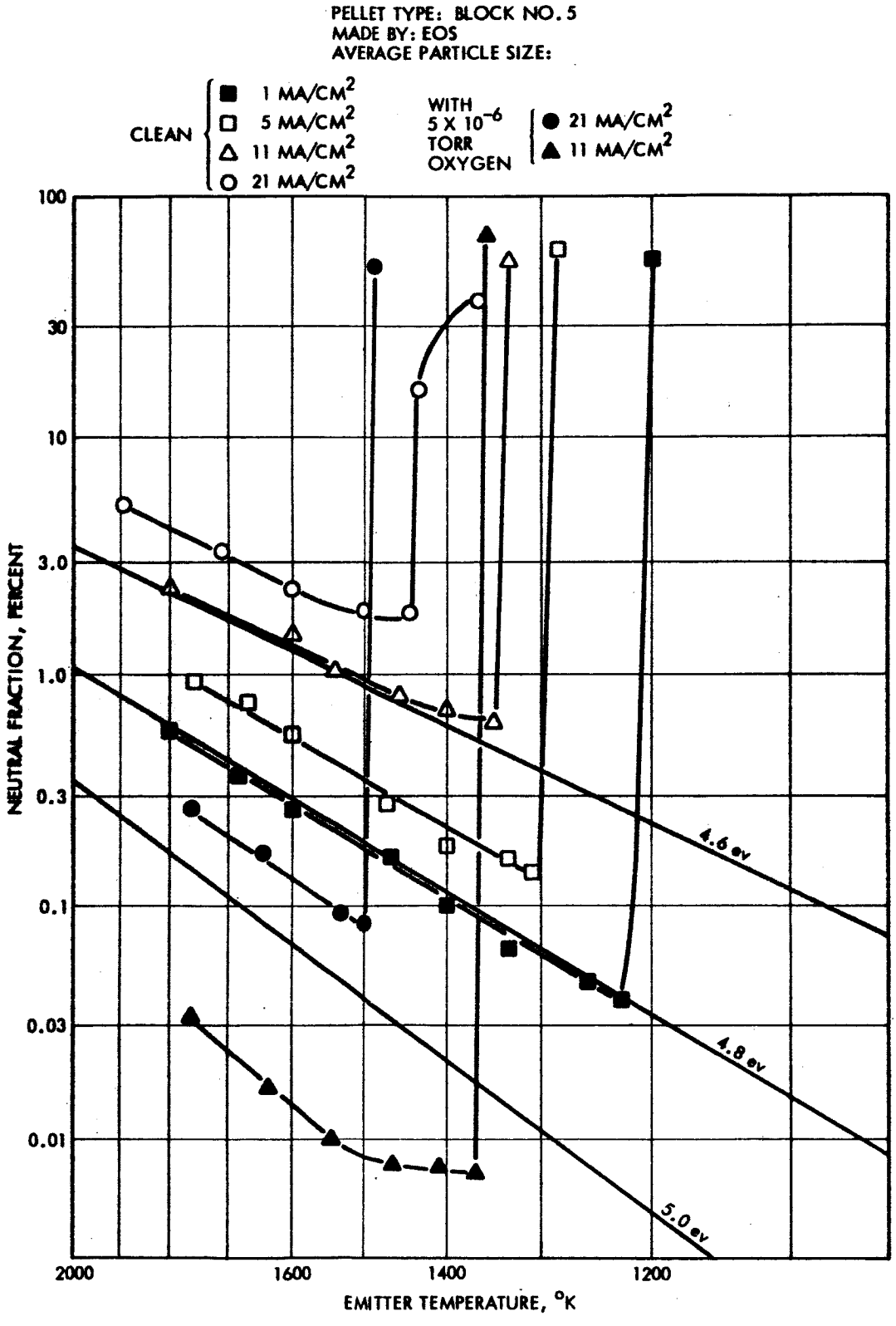


Cesium neutral fraction versus temperature of porous tungsten designated "Block No. 5". (G3)

PELLET TYPE: LB 2 Ta
MADE BY: EOS
PARTICLE SIZE: 1 - 3 μ Ta (2%)
1.7 - 5 μ W

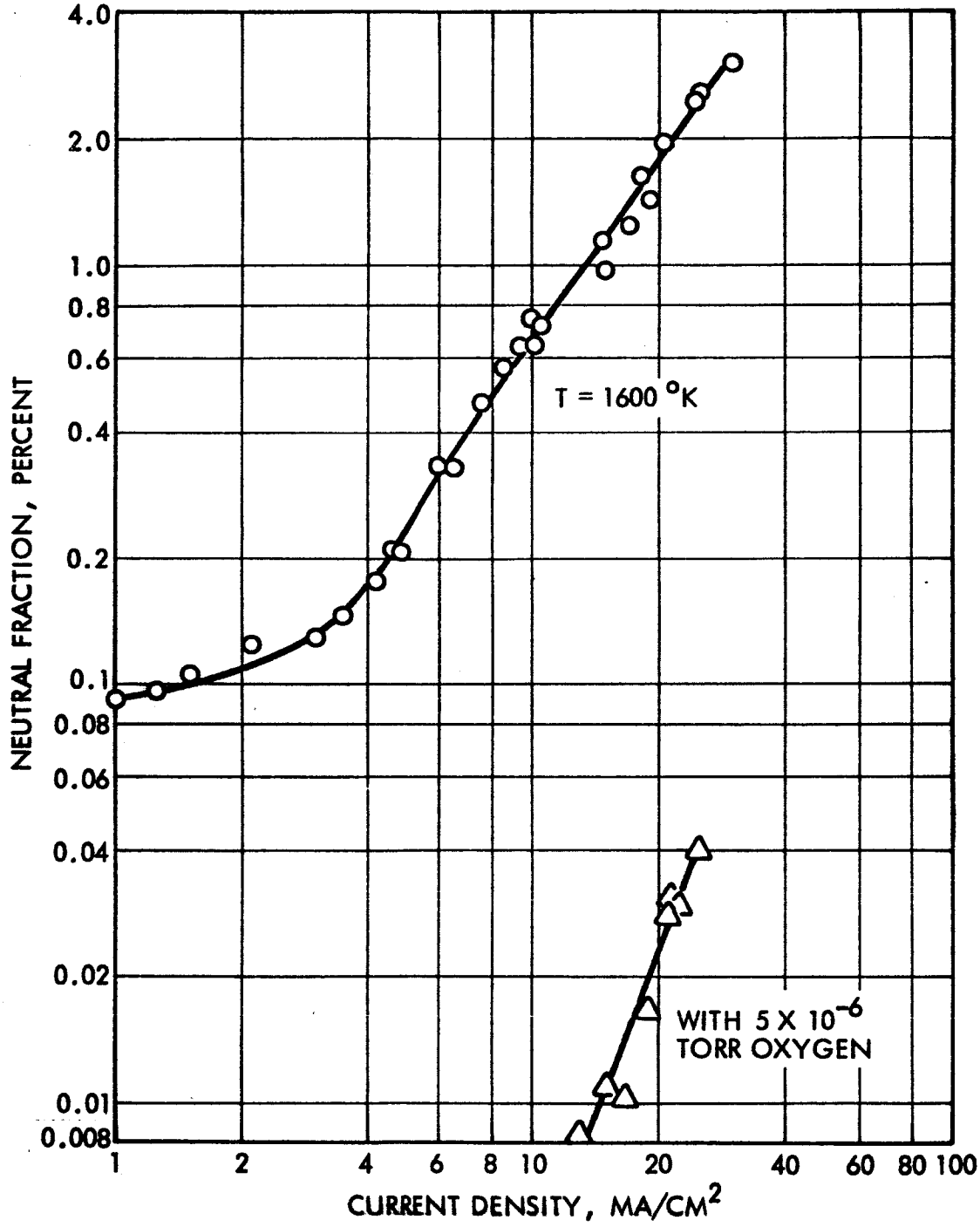


**Cesium neutral fraction versus ion current density from porous tungsten containing 2 atomic percent tantalum.**

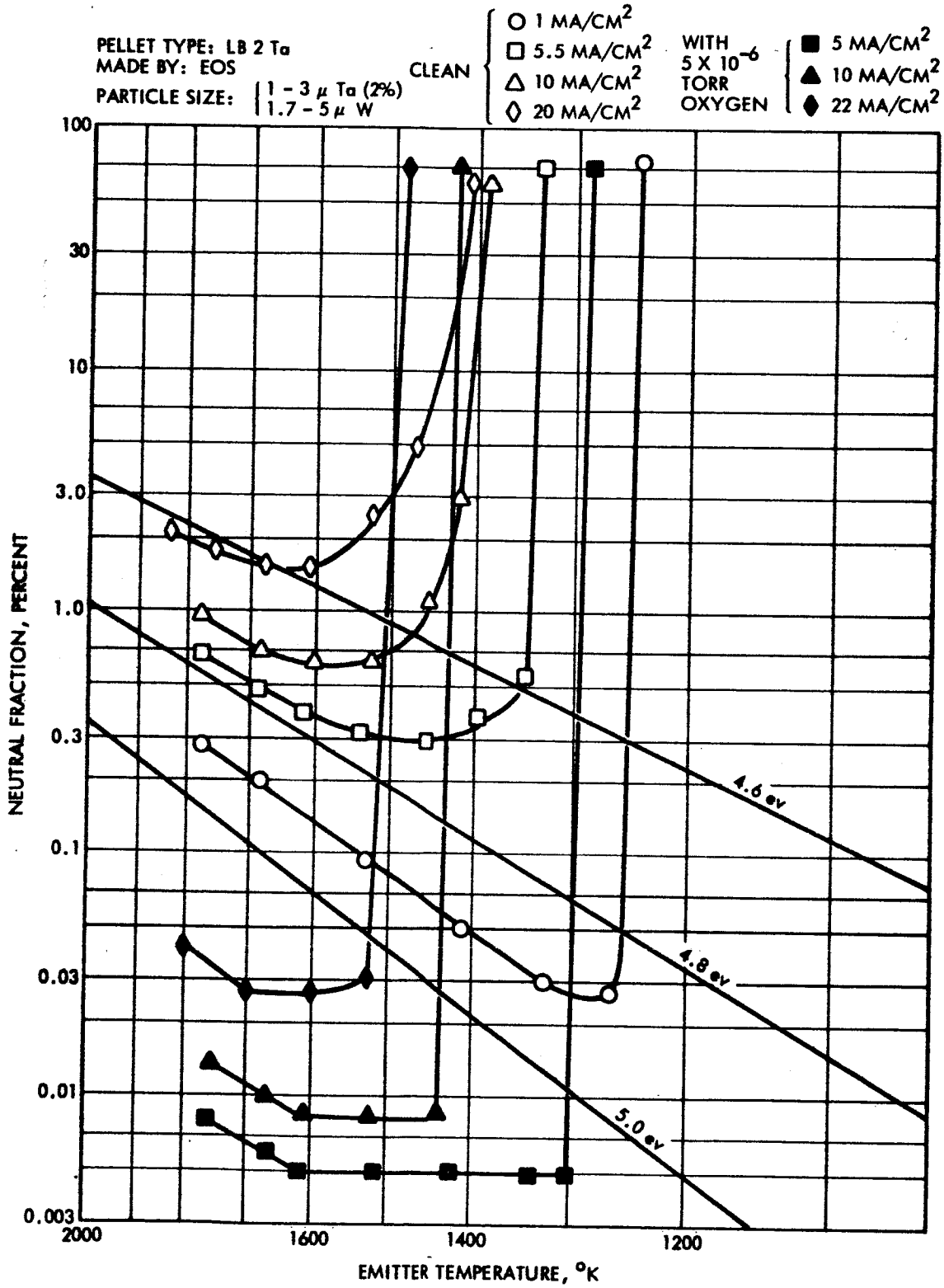


Cesium neutral fraction versus temperature of porous tungsten ionizer containing 2 atomic percent tantalum.

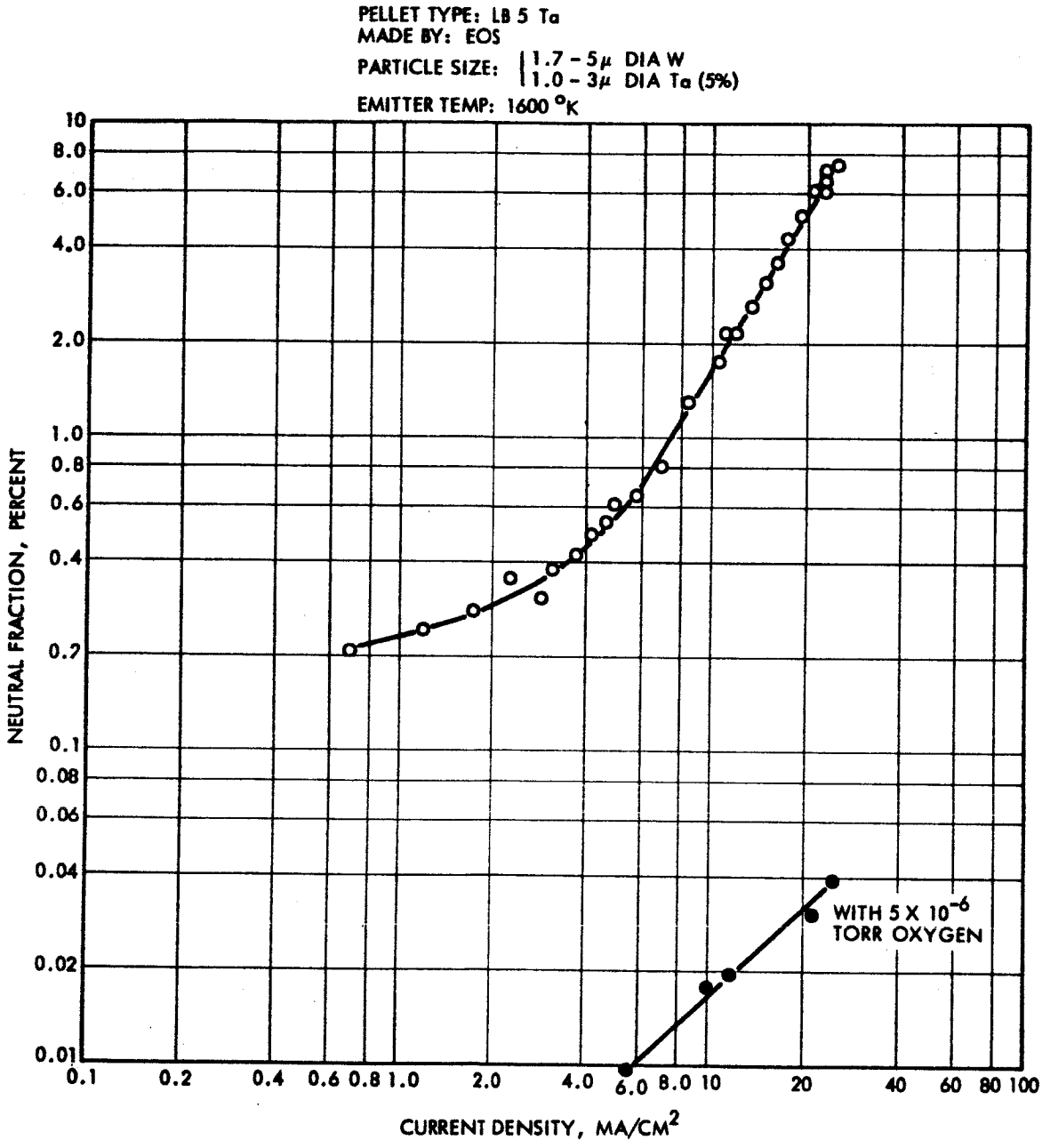


Cesium neutral fraction versus ion current density from porous tungsten containing 5 atomic percent tantalum.

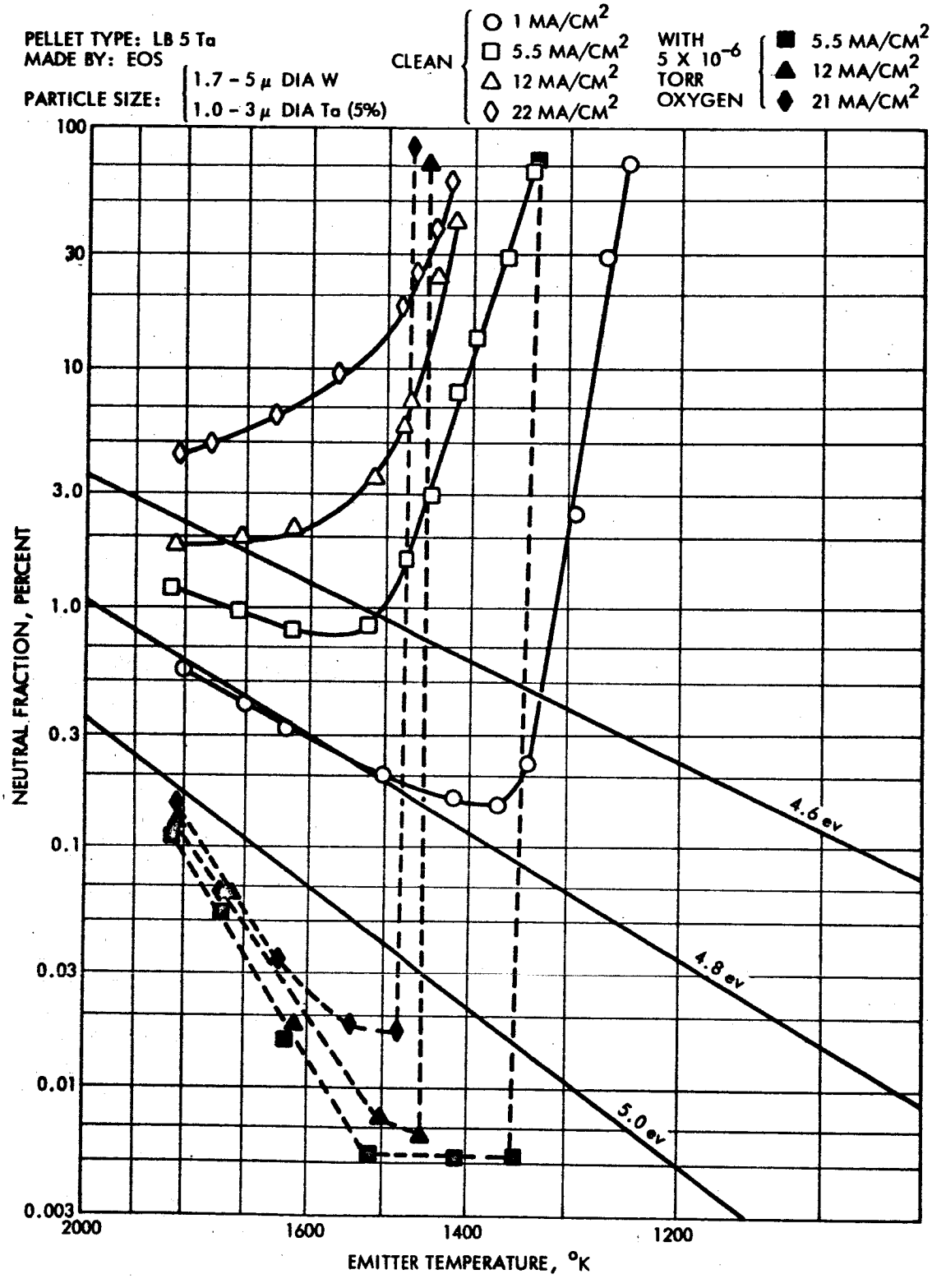


Cesium neutral fraction versus temperature of porous tungsten containing 5 atomic percent tantalum.

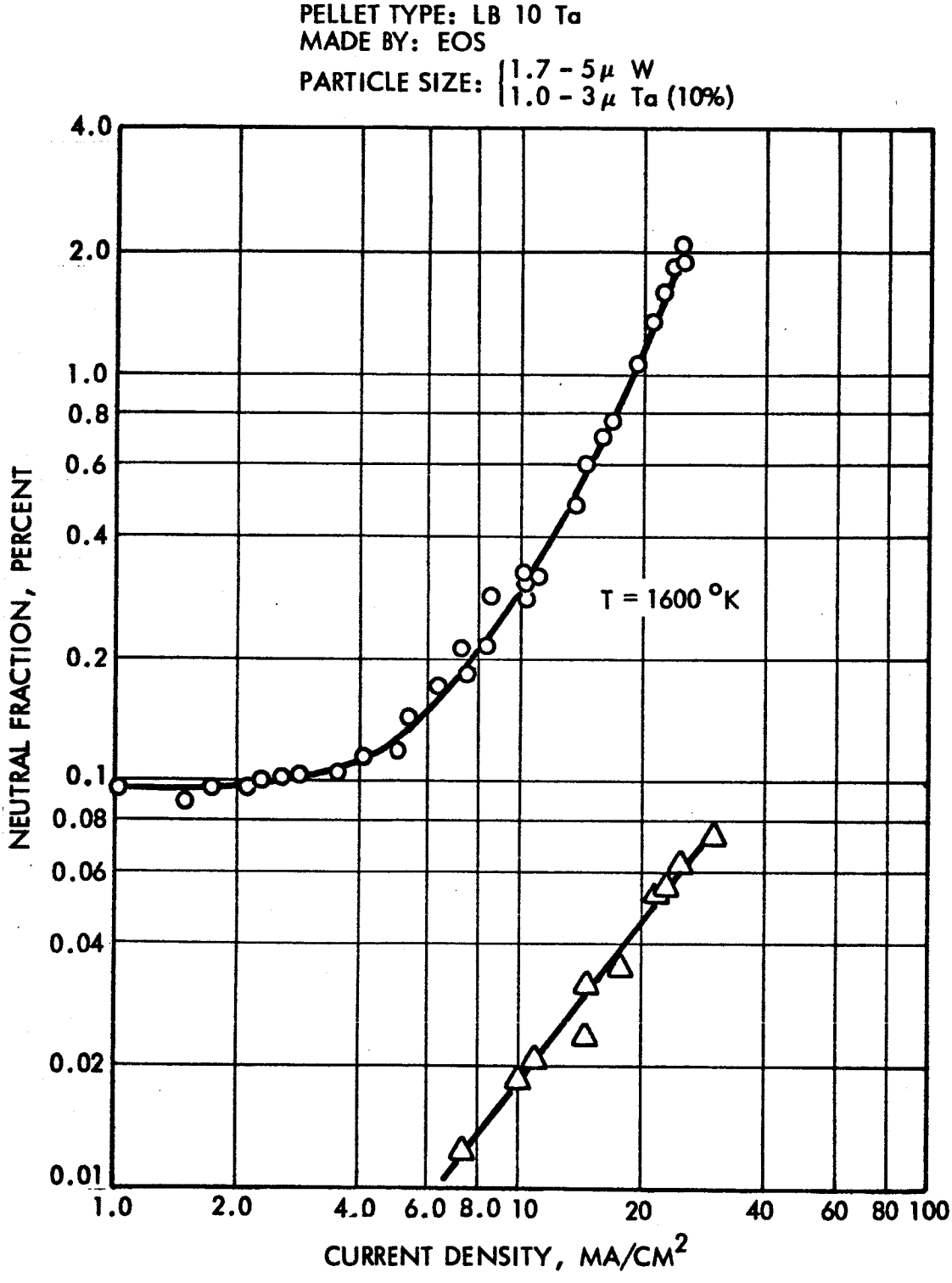


**Cesium neutral fraction versus ion current density from porous tungsten containing 10 atomic percent tantalum.**

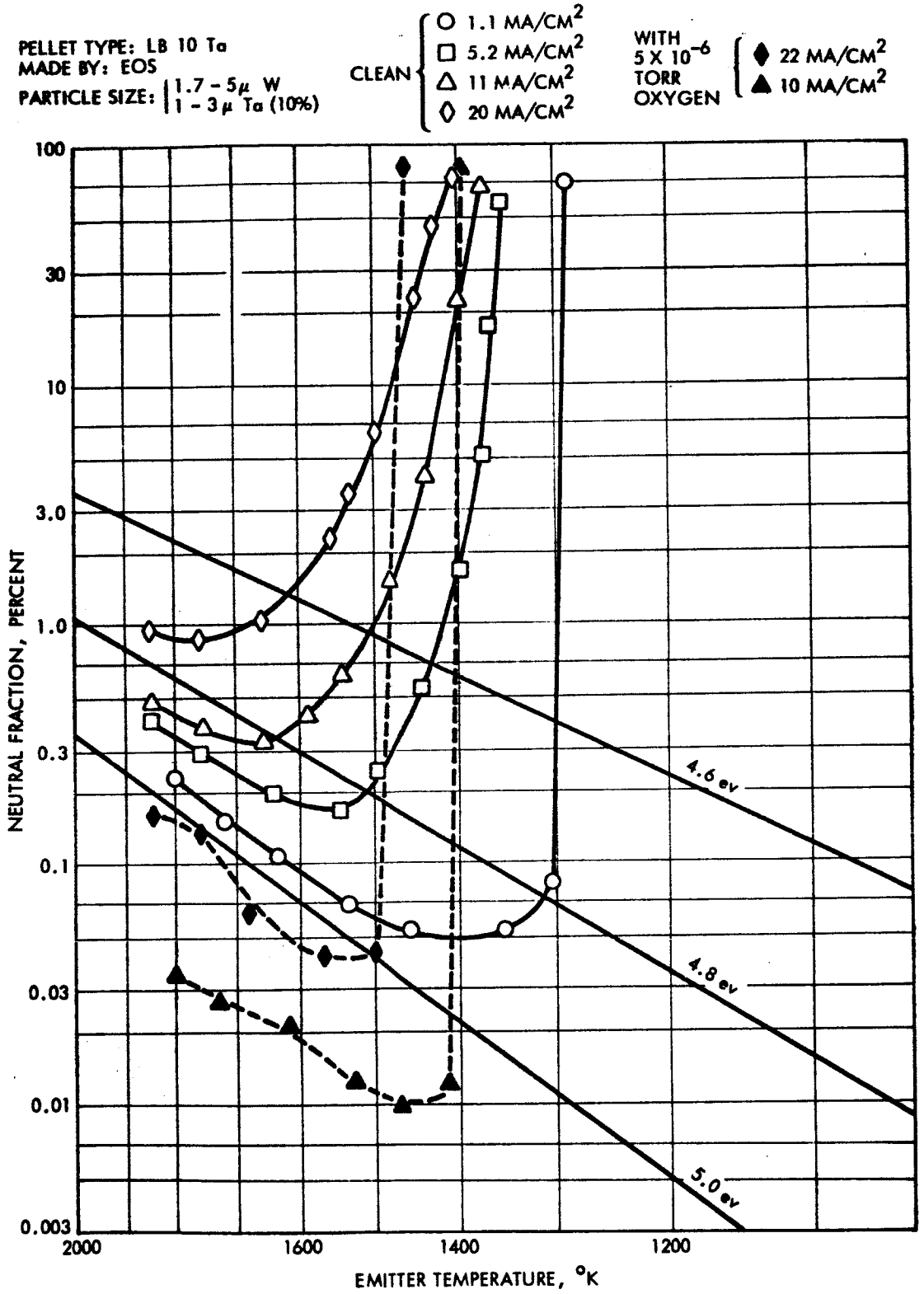


Cesium neutral fraction versus temperature of a porous tungsten ionizer containing 10 atomic percent tantalum.

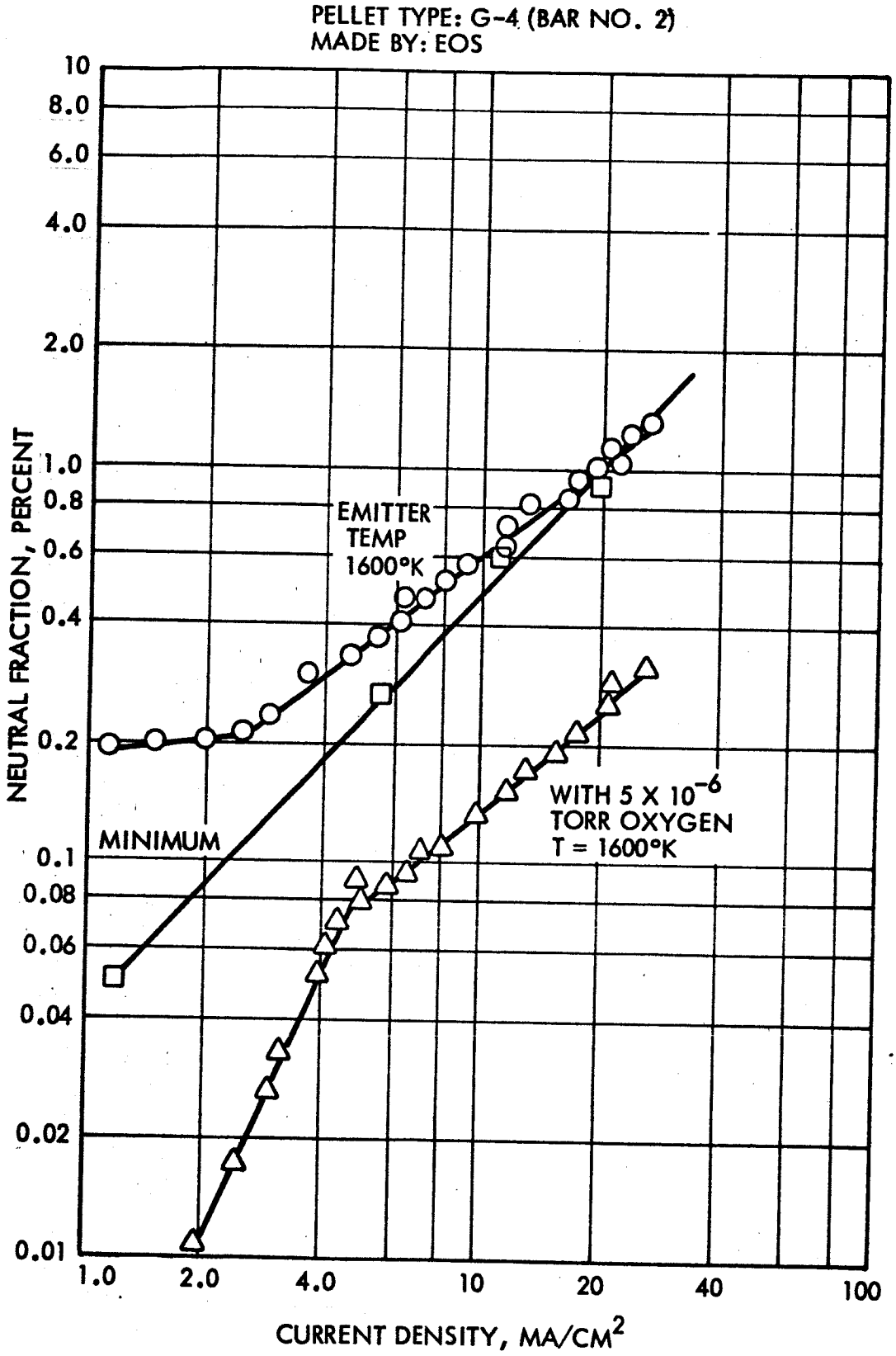


Cesium neutral fraction versus ion current density from porous tungsten before "elox" machining. (G4)

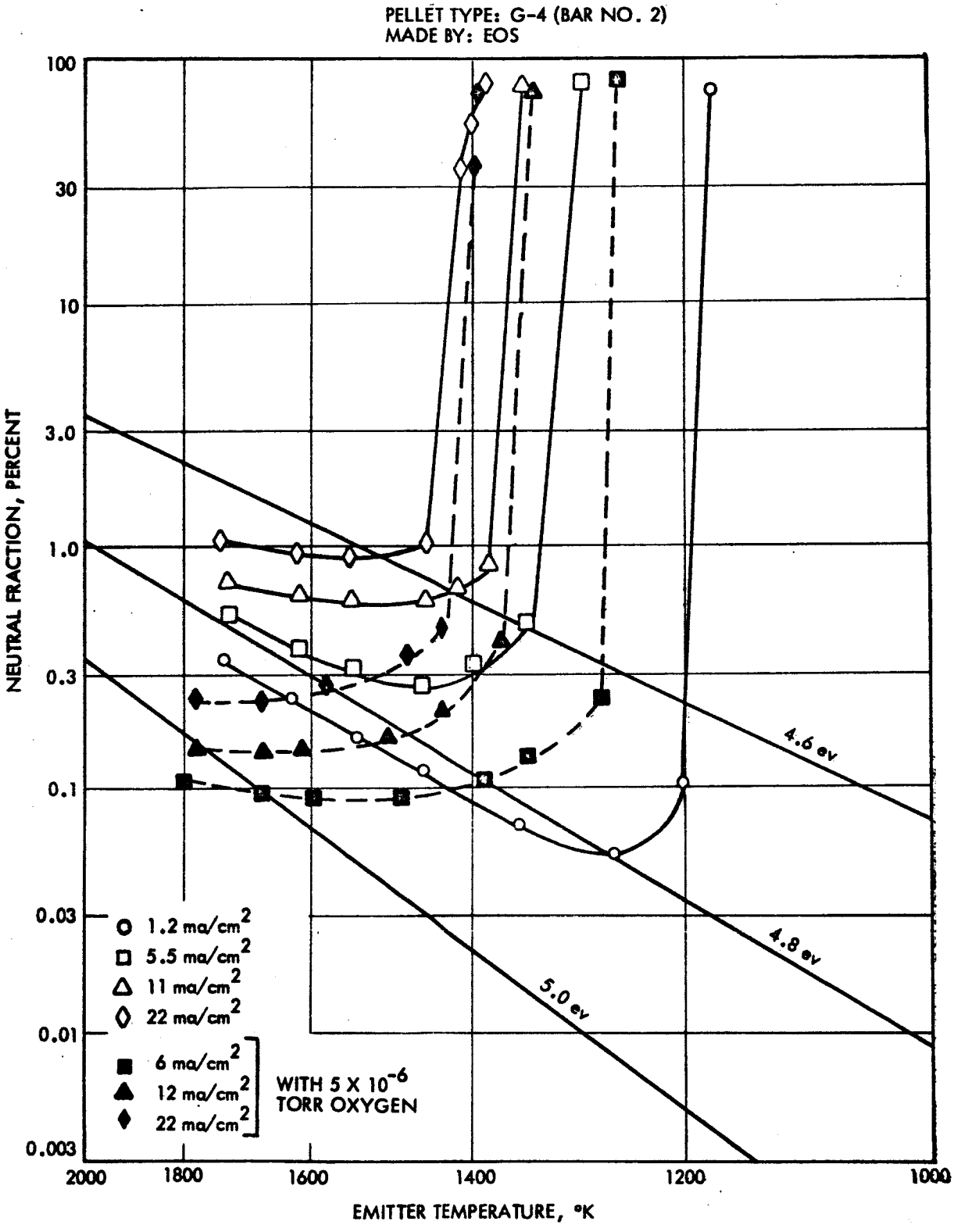


Cesium neutral fraction versus temperature of porous tungsten before "elox" machining. (G4)

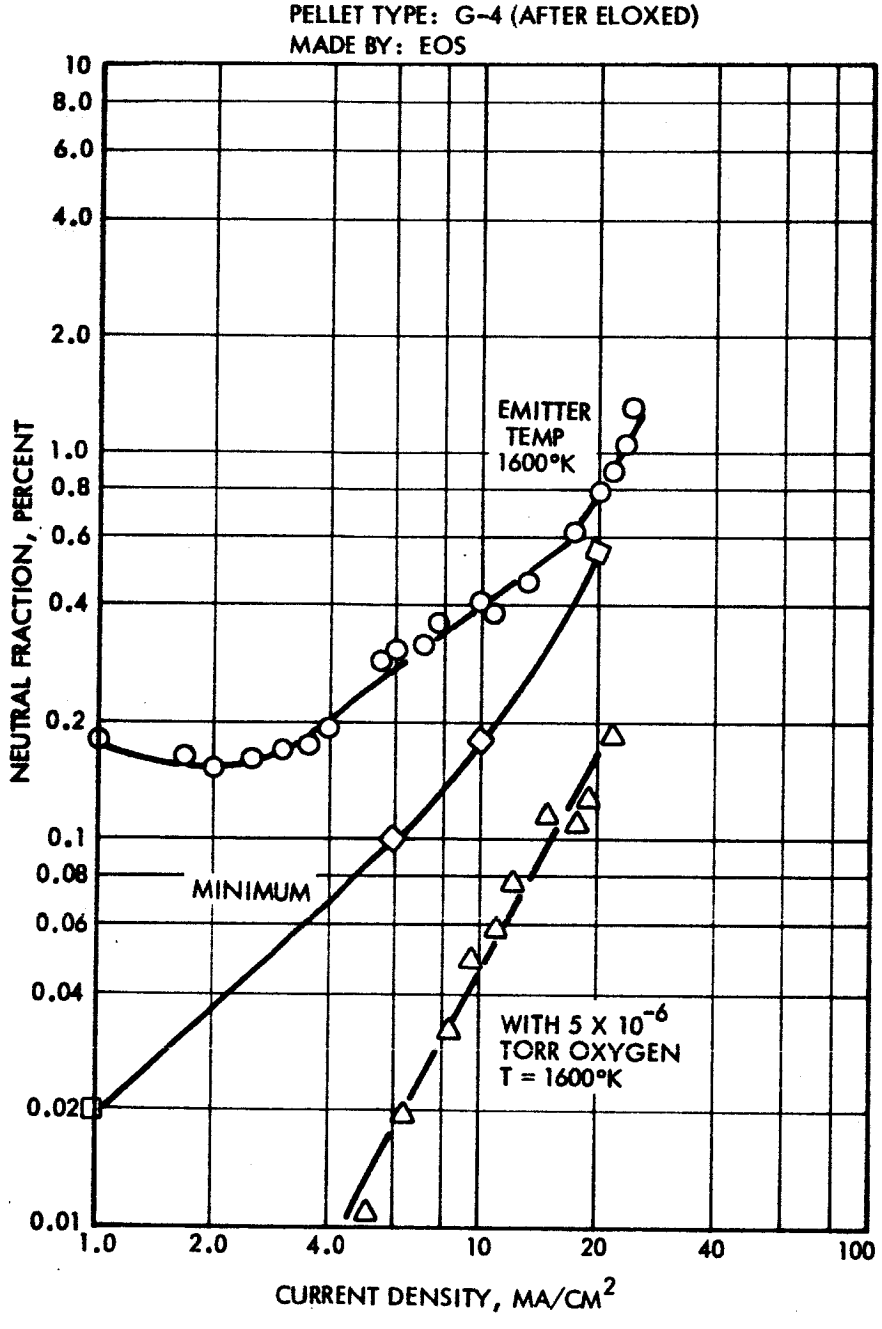


Cesium neutral fraction versus ion current density from porous tungsten after "elox" machining. (G4)

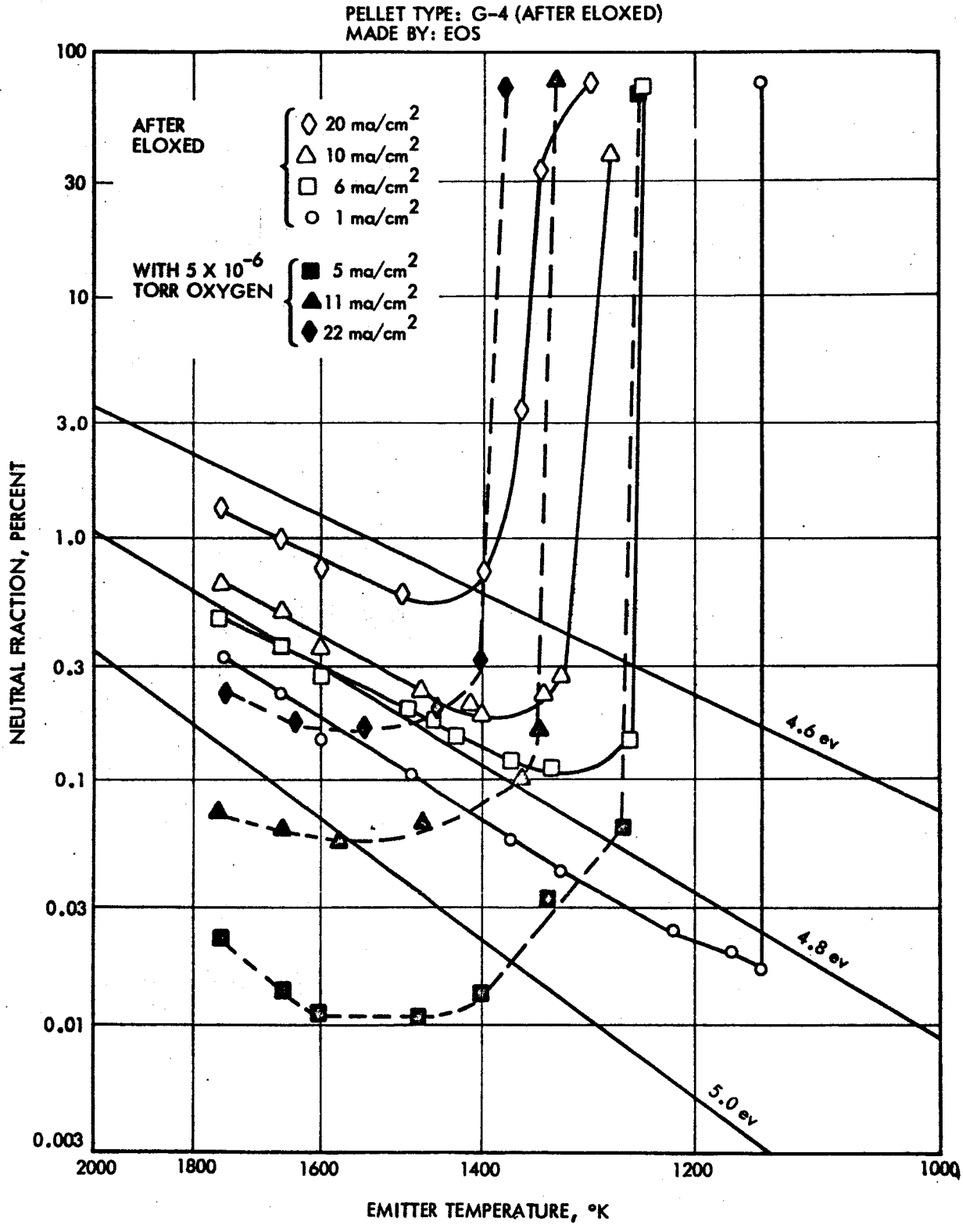


Cesium neutral fraction versus temperature of ion emitter after "elox" machining. (G4)

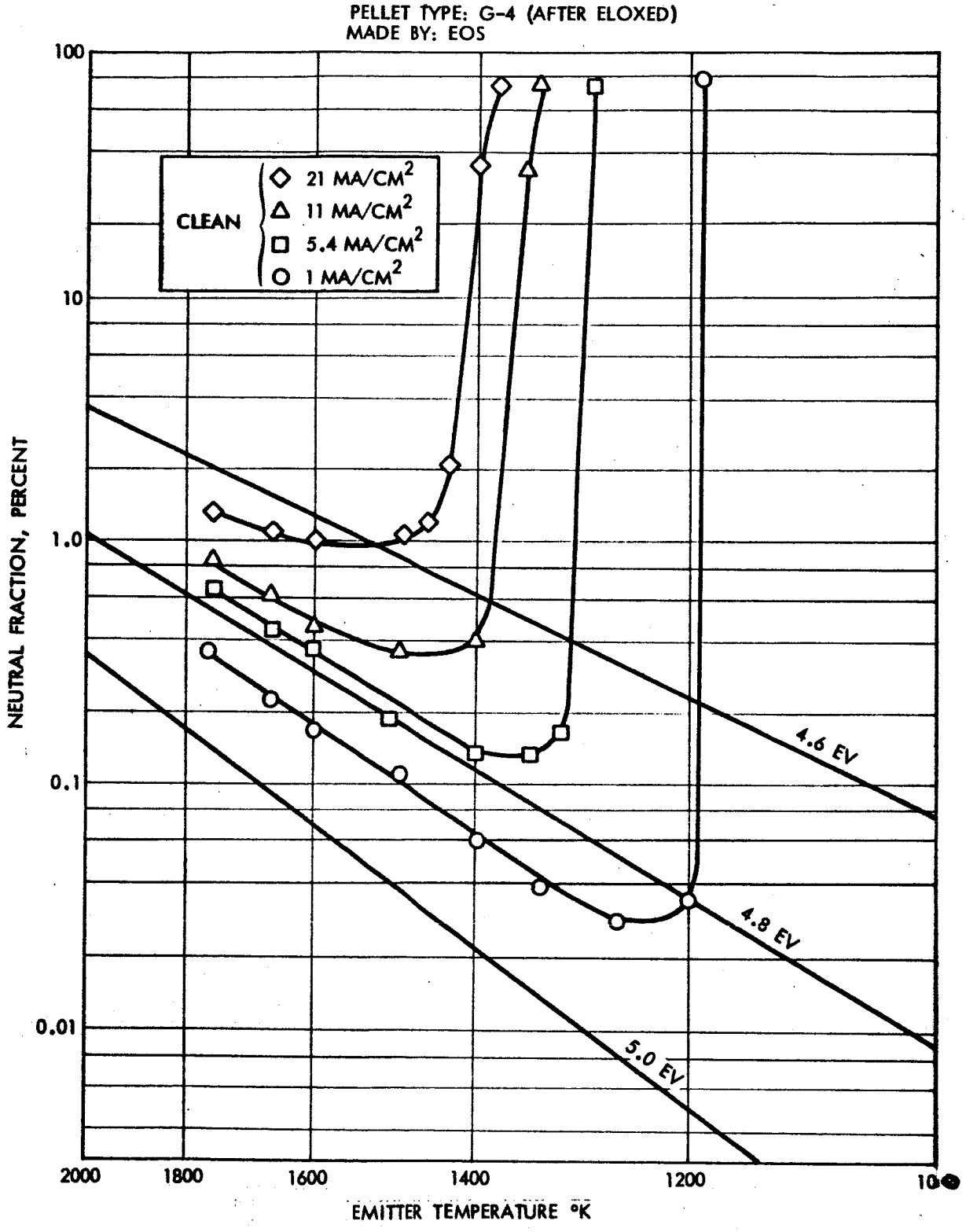


Cesium neutral fraction versus temperature of an ion emitter after "elox" machining. Surface has been cleaned of carbon by previous exposure to oxygen followed by sputtering. (G4)

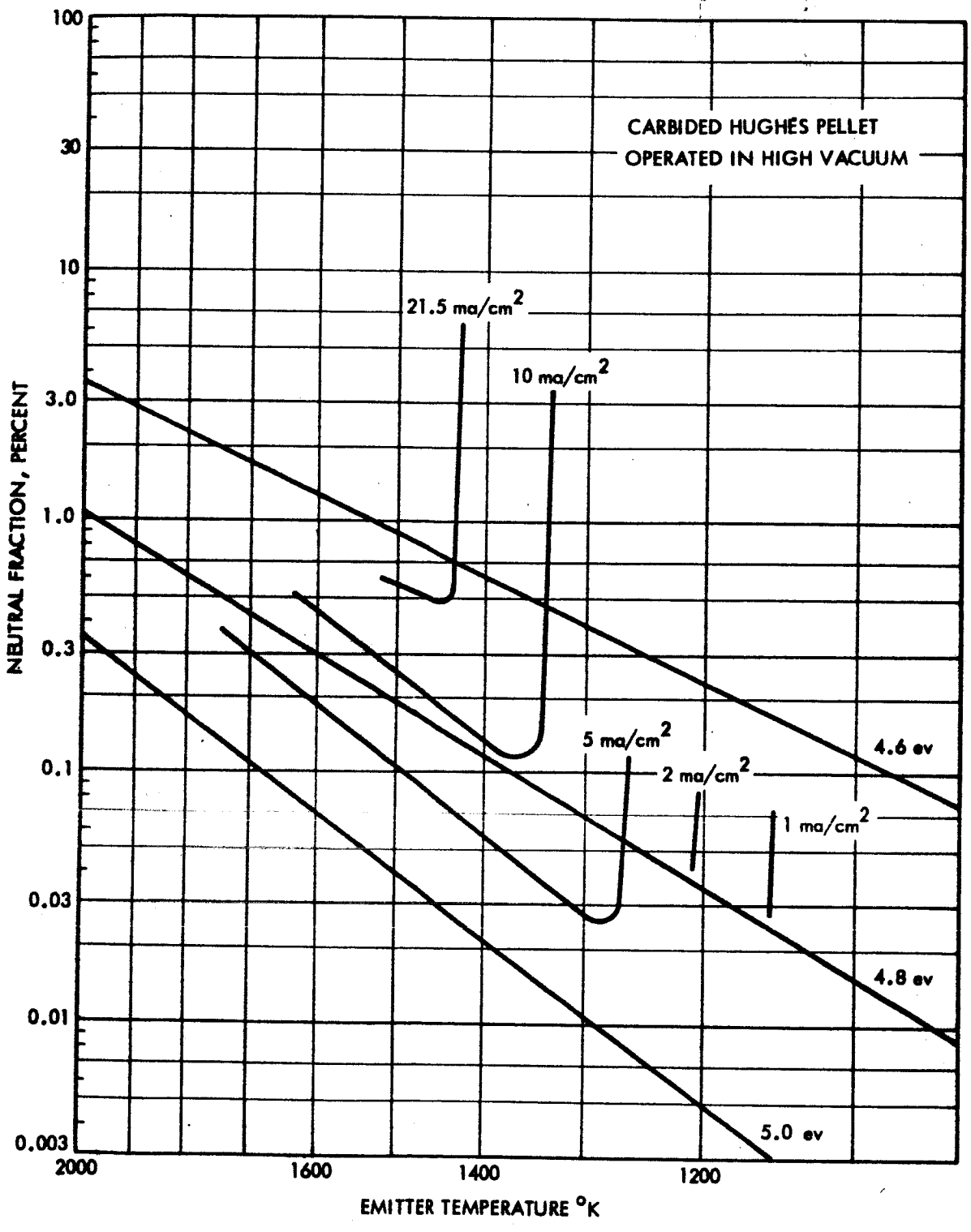


Cesium neutral fraction versus temperature of porous tungsten manufactured by Hughes Research Laboratory and whose surface was carbided. (G2A)

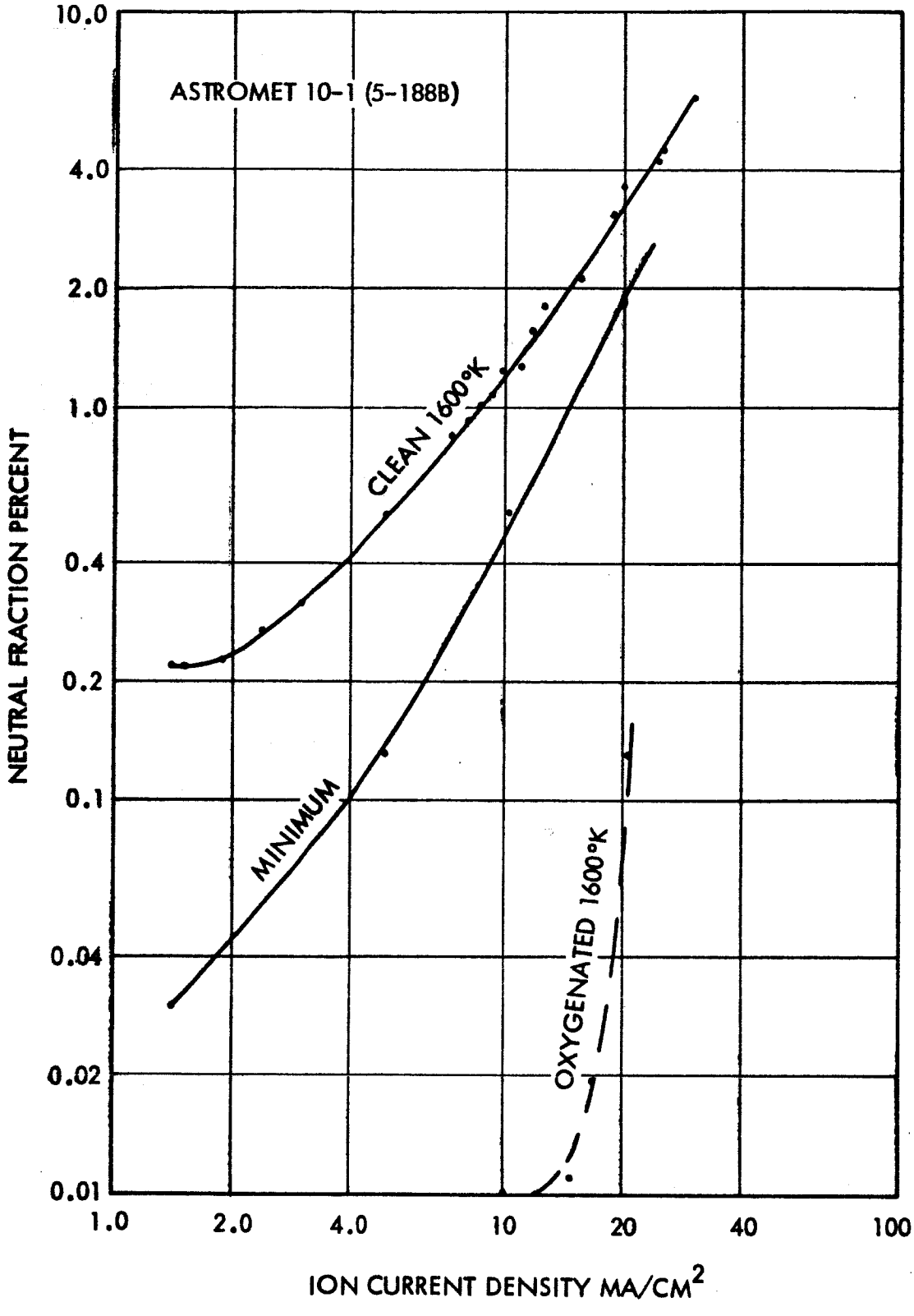


Cesium neutral fraction versus cesium ion current density from improved Astromet 10-1 (5-188B) porous tungsten.

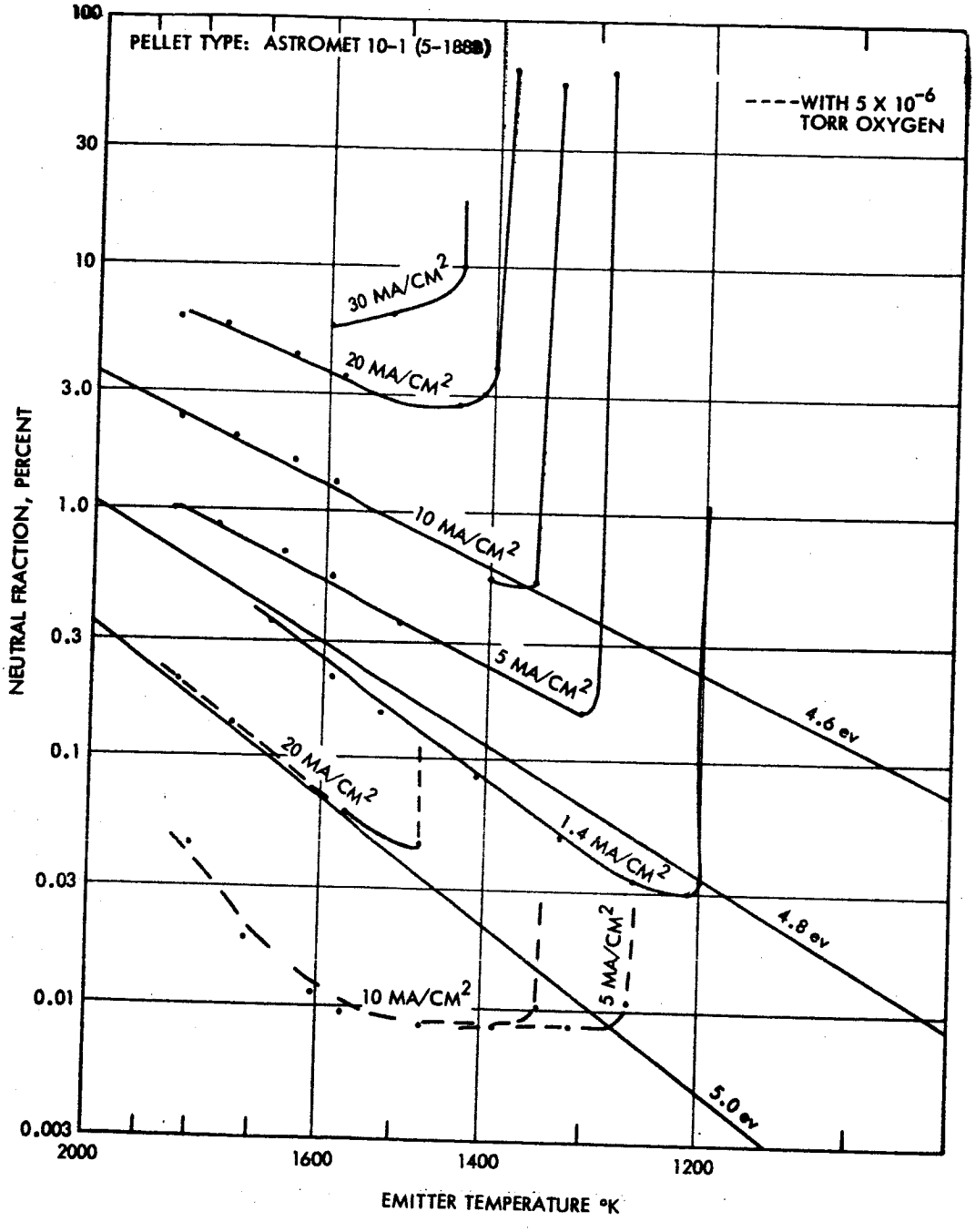


Cesium neutral fraction versus temperature of improved Astromet 10-1 (5-188B) porous tungsten.

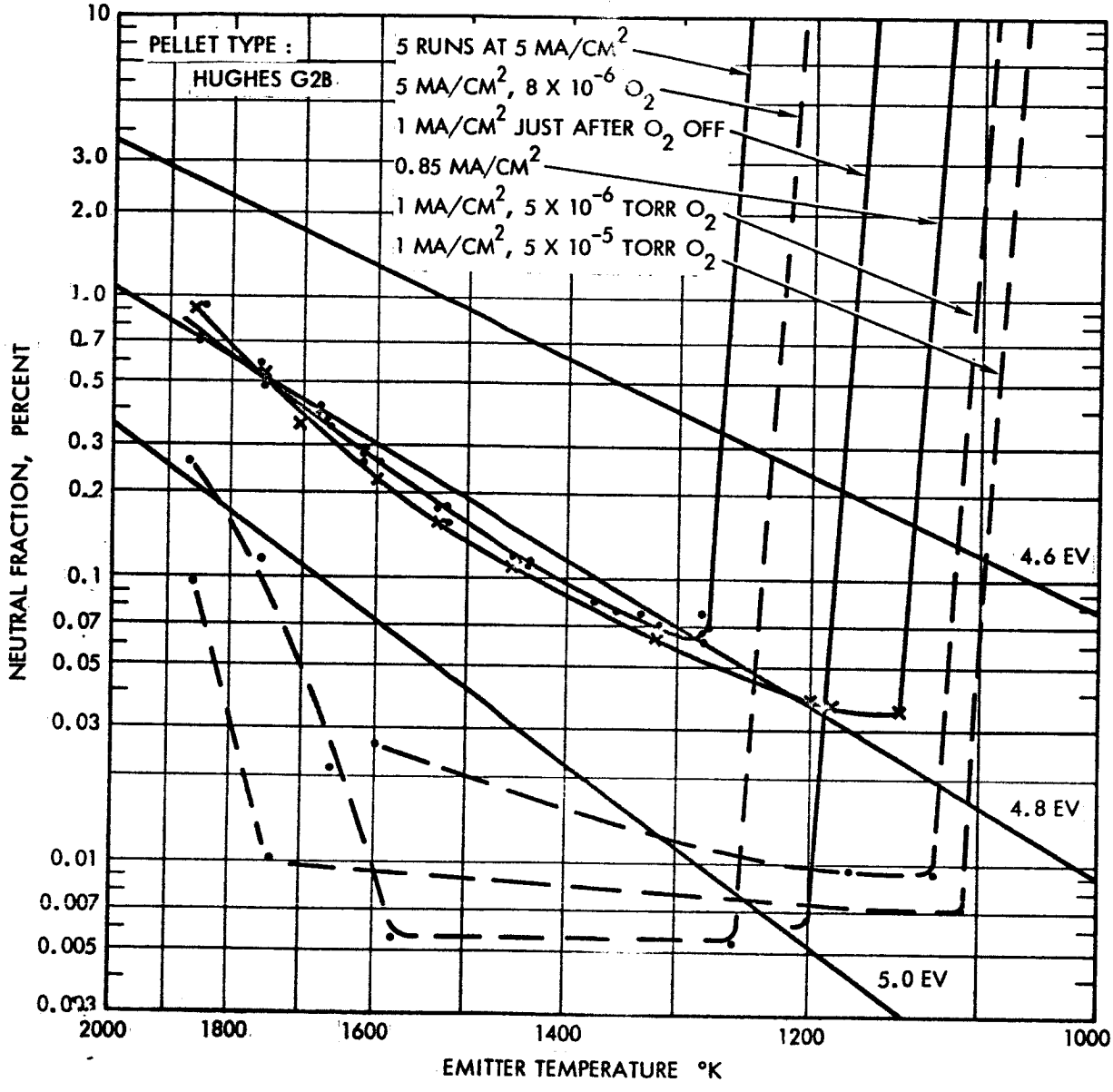


Cesium neutral fraction versus temperature of Hughes porous tungsten. (G2B)

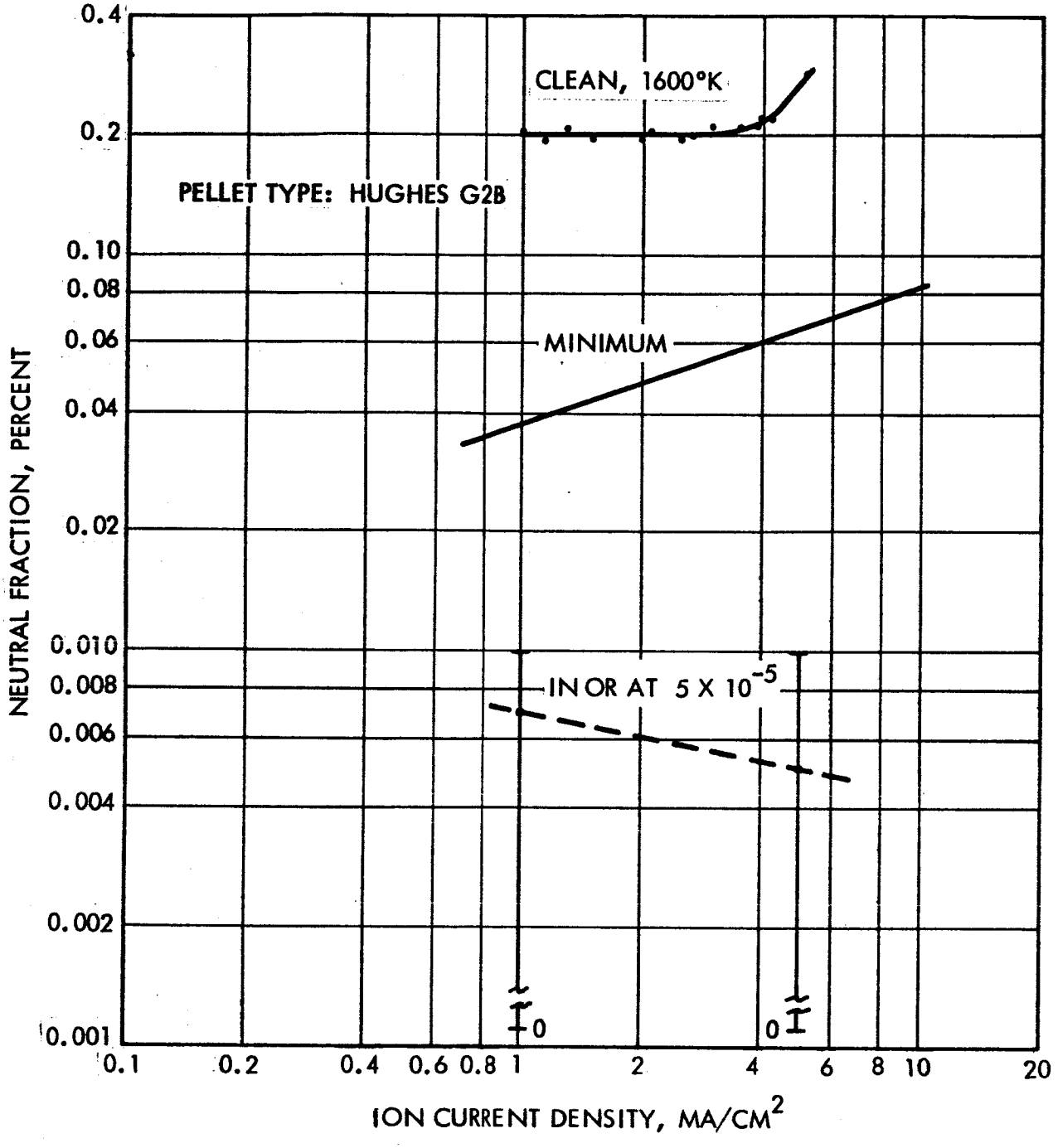


Cesium neutral fraction versus cesium ion current density from Hughes porous tungsten manufactured from fine spherical powder. (G2B)

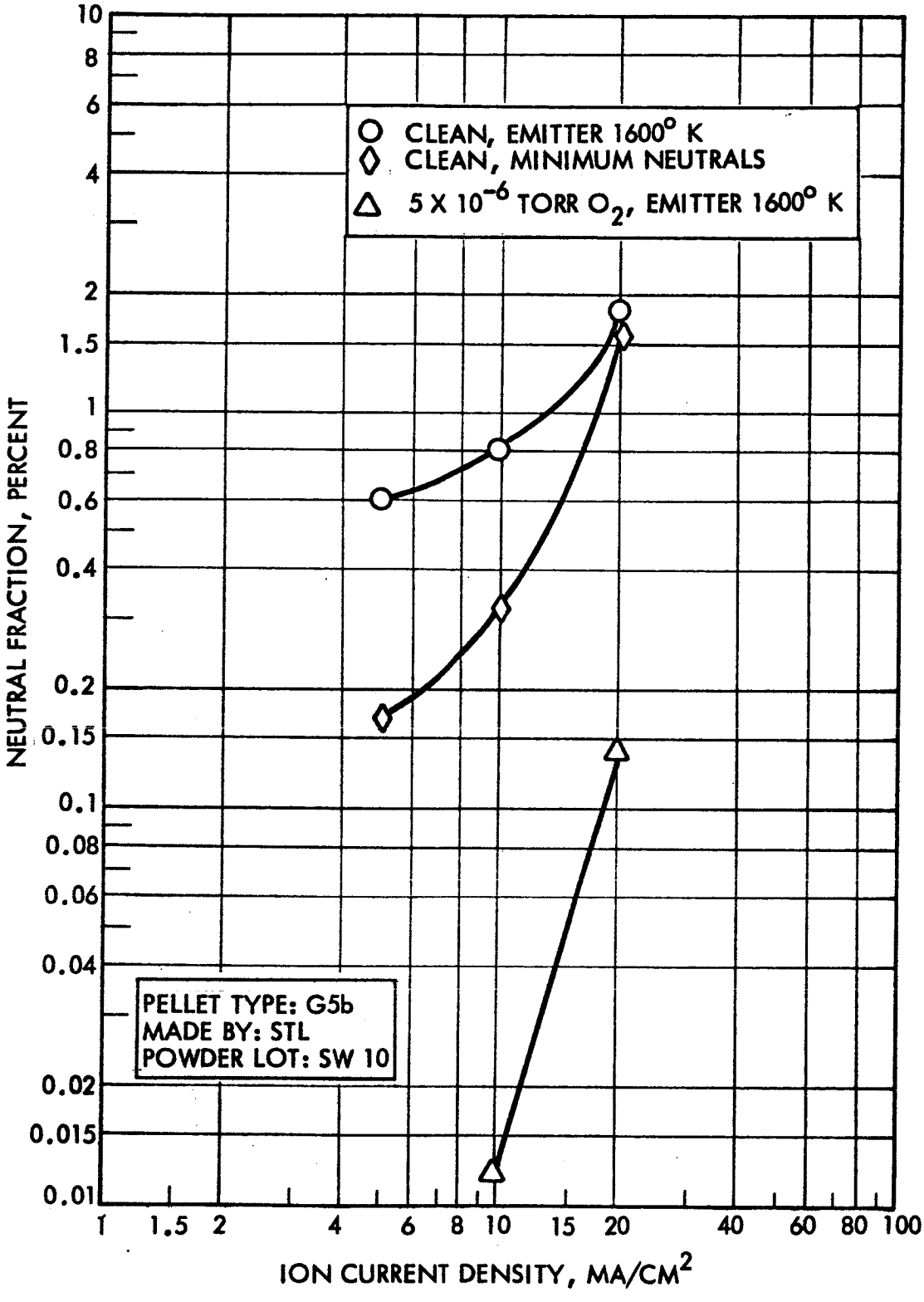


Cesium neutral fraction versus ion current density from porous tungsten manufactured by STL (SW10). (G5B)

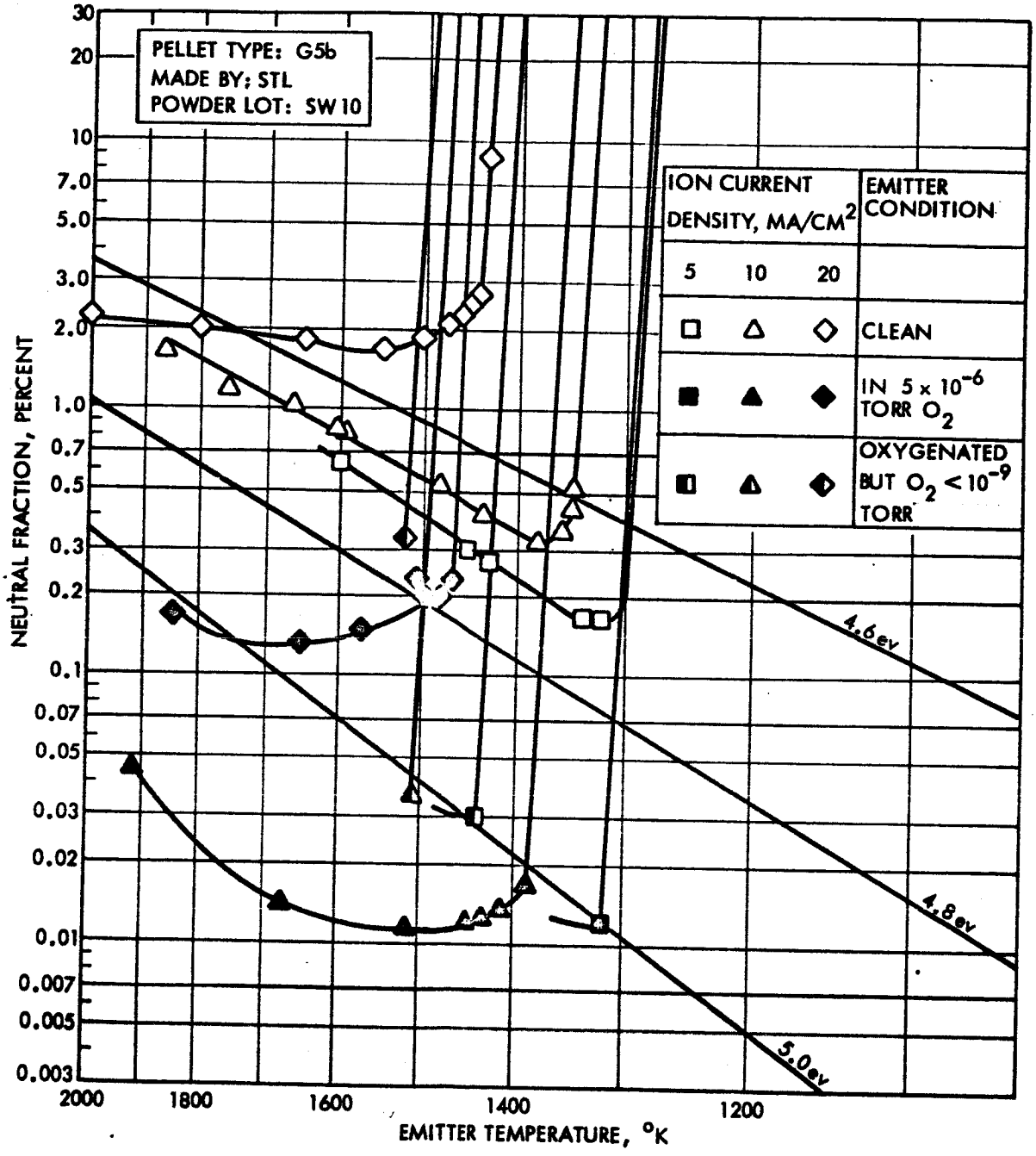


Cesium neutral fraction versus temperature of porous tungsten made by STL (SW10) (G5B).

# APPENDIX III

## ENGINEERING SHEETS
## ON
## TEST RESULTS

IONIZER PELLET EVALUATION REPORT

PELLET TYPE E 6

MADE BY EOS

AVERAGE PARTICLE SIZE

TEST NO. 1 DATE Feb 1964

PORES PER CM$^2$

AVERAGE PORE SIZE

PARTICLE SIZE DISTRIBUTION

| MICRON DIAMETER | PERCENT |
|---|---|
| >7.5 | |
| 7.5 - 5.0 | |
| 5.0 - 3.3 | |
| 3.3 - 2.25 | |
| 1.5 - 1.0 | |
| <1.0 | |

PORE SIZE DISTRIBUTION

| MICRON DIAMETER | PERCENT |
|---|---|
| >1.6 | |
| 1.2 - 1.6 | |
| 0.8 - 1.2 | |
| 0.4 - 0.8 | |
| <0.4 | |

PELLET DIAMETER (EFFECTIVE) 0.18

TRANSMISSION COEFFICIENT $1.34 \times 10^{-4}$ %

PRESSURE 10 (air) TORR

CALCULATED TRUE DENSITY

SURFACE TREATMENT None

SAMPLE INFORMATION * Increased 27 % during testing.

AVERAGE DISTANCE BETWEEN PORES μ

THICKNESS $5 \times 10^{-2}$ CM, DENSITY %

Δp/Δt TORR/SEC

WORK FUNCTION 4.81 *, ev

*SAHA-L. EQ. - % NEUTRALS AT 1 Ma/cm

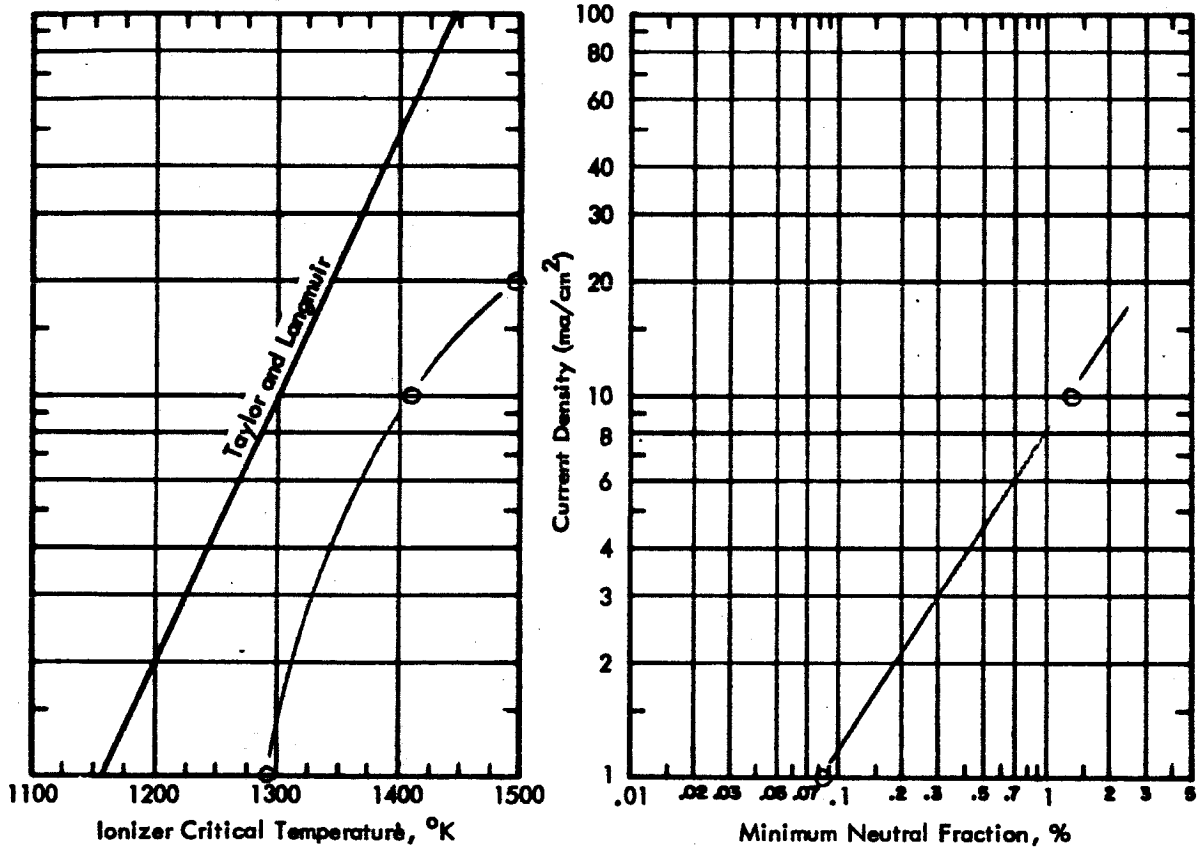


CONCLUSIONS: Neutral fraction low 1-5 ma/cm$^2$ - increases rapidly above. Critical temperature high - increases rapidly above 10 ma/cm$^2$. Would probably been better results if sputtering and etching were used.

TEST MADE BY: Shelton/Cho REPORT PREPARED BY: H. Shelton

IONIZER PELLET EVALUATION REPORT

PELLET TYPE E-7A

MADE BY EOS

AVERAGE PARTICLE SIZE 4-8 μ

PARTICLE SIZE DISTRIBUTION

| MICRON DIAMETER | PERCENT |
|---|---|
| >7.5 | ____ |
| 7.5 - 5.0 | ____ |
| 5.0 - 3.3 | ____ |
| 3.3 - 2.25 | ____ |
| 1.5 - 1.0 | ____ |
| <1.0 | ____ |

PELLET DIAMETER (EFFECTIVE) 0.18

TRANSMISSION COEFFICIENT _____ BY

PRESSURE 10 (air) TORR

CALCULATED TRUE DENSITY _____

SURFACE TREATMENT None.

SAMPLE INFORMATION Cracked before tests were completed

TEST NO. 2 DATE May 1964

PORES PER $CM^2$ _____

AVERAGE PORE SIZE _____

PORE SIZE DISTRIBUTION

| MICRON DIAMETER | PERCENT |
|---|---|
| >1.6 | ____ |
| 1.2 - 1.6 | ____ |
| 0.8 - 1.2 | ____ |
| 0.4 - 0.8 | ____ |
| <0.4 | ____ |

AVERAGE DISTANCE BETWEEN PORES _____ μ

THICKNESS $5 \times 10^{-2}$ CM, DENSITY _____ %

$\Delta p/\Delta t$ _____ TORR/SEC

WORK FUNCTION 4.8 *, ev

*SAHA-L. EQ. - % NEUTRALS AT 1 Ma/cm

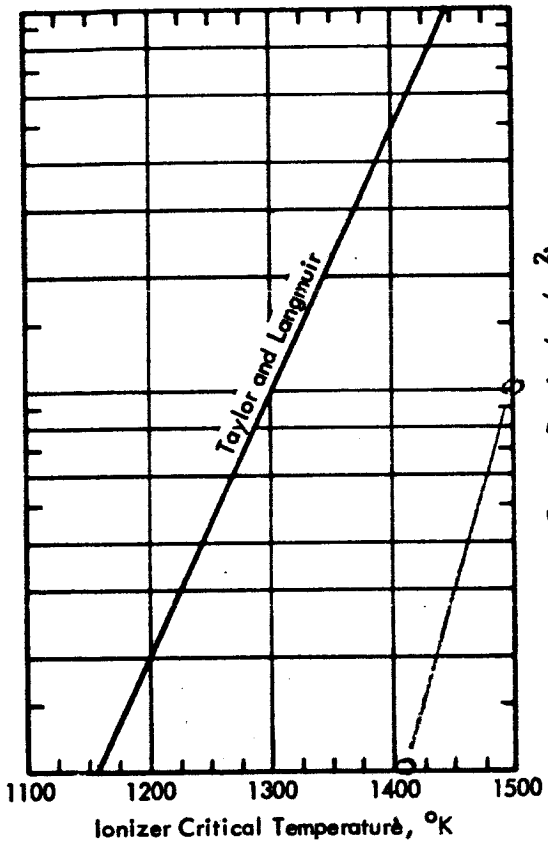


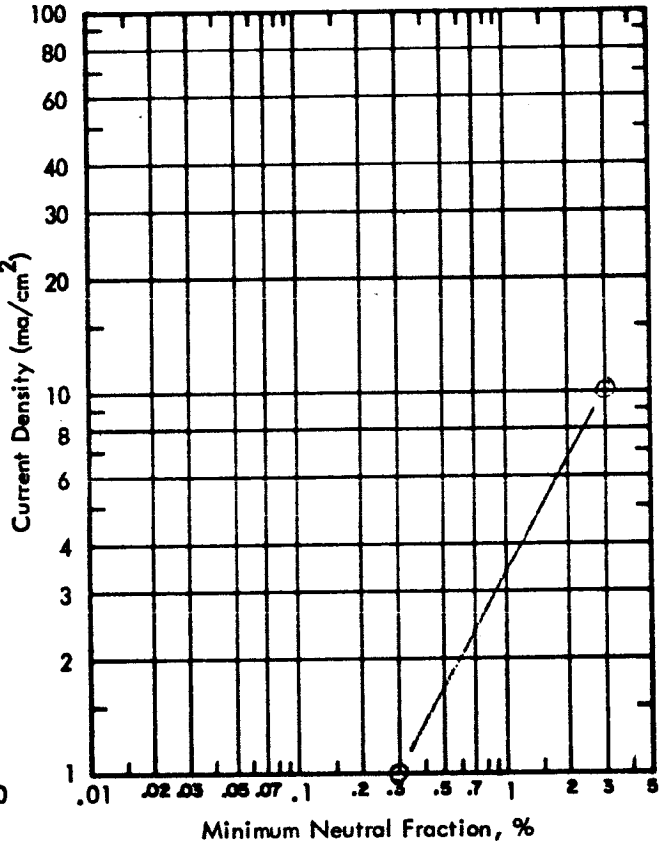


CONCLUSIONS: Neutral fraction high and increasing with current density. Critical temperature high. Would probably have benefited from sputtering and etching. Surface crack terminated test.

TEST MADE BY: Shelton/Cho REPORT PREPARED BY: H. Shelton

IONIZER PELLET EVALUATION REPORT

PELLET TYPE E-3

MADE BY EOS

AVERAGE PARTICLE SIZE _____

PARTICLE SIZE DISTRIBUTION

| MICRON DIAMETER | PERCENT |
|---|---|
| >7.5 | ____ |
| 7.5 - 5.0 | ____ |
| 5.0 - 3.3 | ____ |
| 3.3 - 2.25 | ____ |
| 1.5 - 1.0 | ____ |
| <1.0 | ____ |

PELLET DIAMETER (EFFECTIVE) 0.18

TRANSMISSION COEFFICIENT _____ BY

PRESSURE 10 (air) TORR

CALCULATED TRUE DENSITY _____

SURFACE TREATMENT Etch + Sputter

SAMPLE INFORMATION Brazed by EOS

TEST NO. 3 DATE May 1964

PORES PER CM$^2$ _____

AVERAGE PORE SIZE _____

PORE SIZE DISTRIBUTION

| MICRON DIAMETER | PERCENT |
|---|---|
| >1.6 | ____ |
| 1.2 - 1.6 | ____ |
| 0.8 - 1.2 | ____ |
| 0.4 - 0.8 | ____ |
| <0.4 | ____ |

AVERAGE DISTANCE BETWEEN PORES _____ μ

THICKNESS 5 x 10$^{-2}$ CM, DENSITY _____ %

Δp/Δt _____ TORR/SEC

WORK FUNCTION 4.55 *, ev

*SAHA-L. EQ. - % NEUTRALS AT 1 Ma/cm

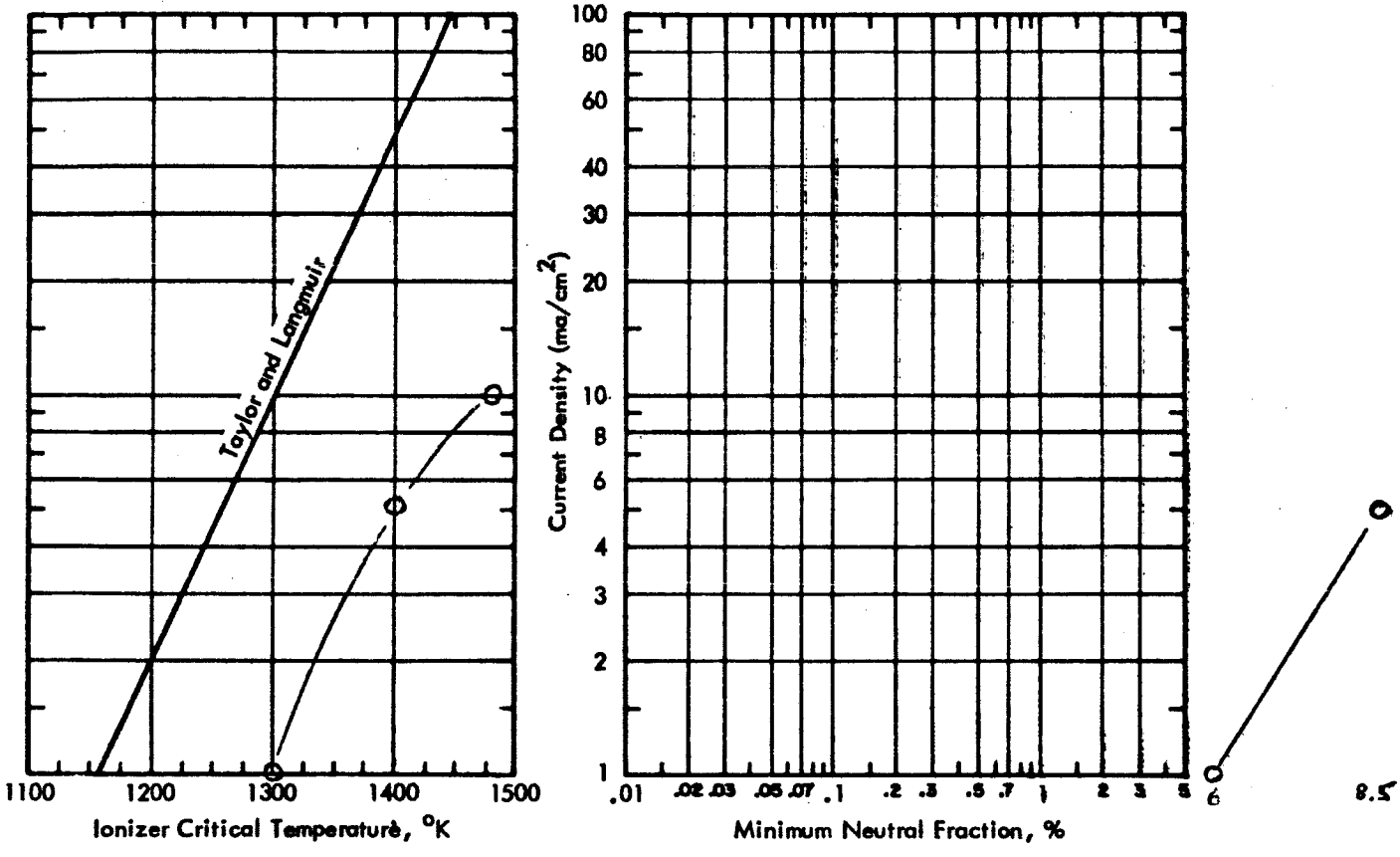


CONCLUSIONS: Brazed by E.O.S. - Neutrals high. Probable contaminant or surface closure.

TEST MADE BY: Shelton/Cho REPORT PREPARED BY: H. Shelton

IONIZER PELLET EVALUATION REPORT

PELLET TYPE E-4

MADE BY EOS

AVERAGE PARTICLE SIZE 2-5 μ

TEST NO. 4 DATE June 1964

PORES PER CM$^2$ _____

AVERAGE PORE SIZE _____

| PARTICLE SIZE DISTRIBUTION MICRON DIAMETER | PERCENT |
|---|---|
| >7.5 | ____ |
| 7.5 - 5.0 | ____ |
| 5.0 - 3.3 | ____ |
| 3.3 - 2.25 | ____ |
| 1.5 - 1.0 | ____ |
| <1.0 | ____ |

| PORE SIZE DISTRIBUTION MICRON DIAMETER | PERCENT |
|---|---|
| >1.6 | ____ |
| 1.2 - 1.6 | ____ |
| 0.8 - 1.2 | ____ |
| 0.4 - 0.8 | ____ |
| <0.4 | ____ |

PELLET DIAMETER (EFFECTIVE) 0.18

TRANSMISSION COEFFICIENT _____ BY

PRESSURE 10 (air) TORR

CALCULATED TRUE DENSITY _____

SURFACE TREATMENT Etch + Spatter

SAMPLE INFORMATION _____

AVERAGE DISTANCE BETWEEN PORES _____ μ

THICKNESS 5 x 10$^{-2}$ CM, DENSITY _____ %

Δp/Δt _____ TORR/SEC

WORK FUNCTION 4.82 *, ev

*SAHA-L. EQ. - % NEUTRALS AT 1 Ma/cm

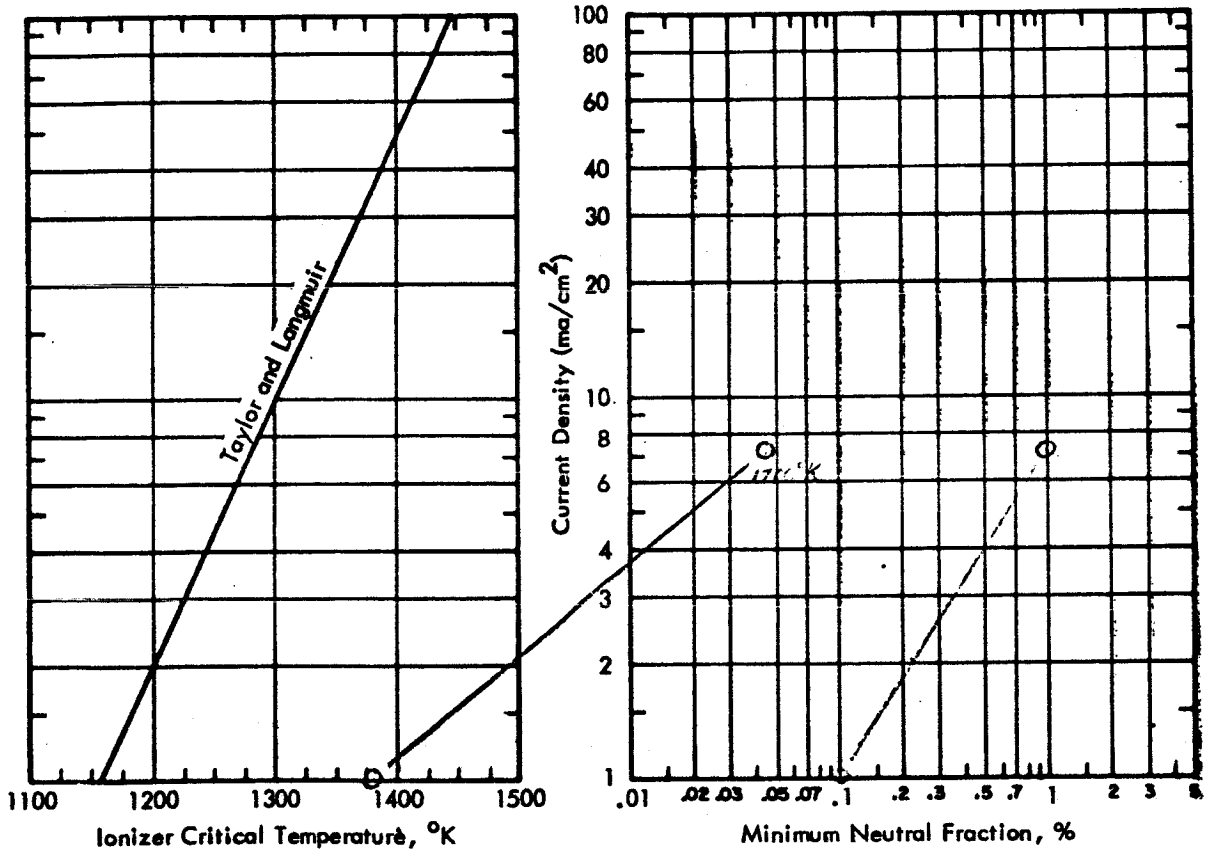


CONCLUSIONS: Poor results due to surface sintering

TEST MADE BY: Shelton/Cho REPORT PREPARED BY: H. Shelton

IONIZER PELLET EVALUATION REPORT

PELLET TYPE MOD E

MADE BY Philips

AVERAGE PARTICLE SIZE _____

PARTICLE SIZE DISTRIBUTION

| MICRON DIAMETER | PERCENT |
|---|---|
| >7.5 | ____ |
| 7.5 - 5.0 | ____ |
| 5.0 - 3.3 | ____ |
| 3.3 - 2.25 | ____ |
| 1.5 - 1.0 | ____ |
| <1.0 | ____ |

PELLET DIAMETER (EFFECTIVE) 0.18

TRANSMISSION COEFFICIENT ~ $6 \times 10^{-5}$ * BY

PRESSURE 10 (air) TORR

CALCULATED TRUE DENSITY _____

SURFACE TREATMENT Ekt. + Sputter

SAMPLE INFORMATION * Decreased ~40 % during test

TEST NO. 5 DATE June 1964

PORES PER $CM^2$ _____

AVERAGE PORE SIZE _____

PORE SIZE DISTRIBUTION

| MICRON DIAMETER | PERCENT |
|---|---|
| >1.6 | ____ |
| 1.2 - 1.6 | ____ |
| 0.8 - 1.2 | ____ |
| 0.4 - 0.8 | ____ |
| <0.4 | ____ |

AVERAGE DISTANCE BETWEEN PORES _____ μ

THICKNESS $5 \times 10^{-2}$ CM, DENSITY _____ %

$\Delta p/\Delta t$ _____ TORR/SEC

WORK FUNCTION 4.72 *, ev

*SAHA-L. EQ. - % NEUTRALS AT 1 Ma/cm

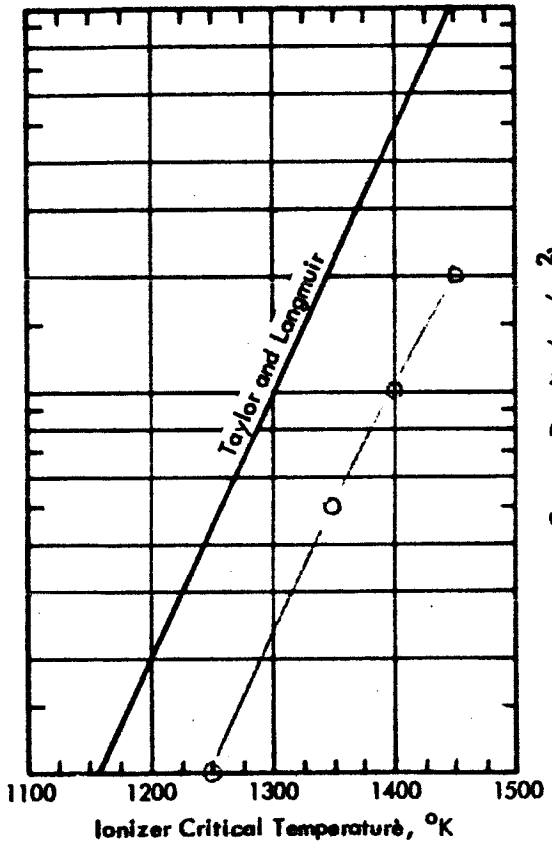


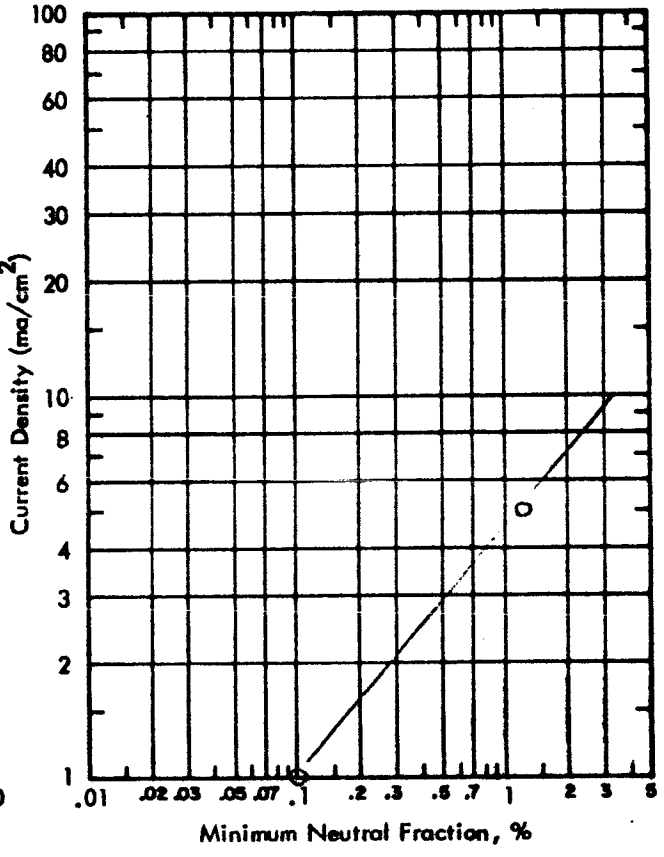


CONCLUSIONS: Valid test on clean tungsten (by sputtering) but high neutrals because of poor pore count.

TEST MADE BY: Shelton/Cho REPORT PREPARED BY: H. Shelton

IONIZER PELLET EVALUATION REPORT

PELLET TYPE E 3

MADE BY EOS

AVERAGE PARTICLE SIZE 1 - 4 μ

PARTICLE SIZE DISTRIBUTION

| MICRON DIAMETER | PERCENT |
|---|---|
| >7.5 | |
| 7.5 - 5.0 | |
| 5.0 - 3.3 | |
| 3.3 - 2.25 | |
| 1.5 - 1.0 | |
| <1.0 | |

PELLET DIAMETER (EFFECTIVE) 0.18

TRANSMISSION COEFFICIENT ~ $1 \times 10^{-5}$ *BY

PRESSURE 10 (air) TORR

CALCULATED TRUE DENSITY

SURFACE TREATMENT Etch + Sputter

SAMPLE INFORMATION * Decreased ~40% during test.

TEST NO. 6 DATE June 1964

PORES PER $CM^2$

AVERAGE PORE SIZE

PORE SIZE DISTRIBUTION

| MICRON DIAMETER | PERCENT |
|---|---|
| >1.6 | |
| 1.2 - 1.6 | |
| 0.8 - 1.2 | |
| 0.4 - 0.8 | |
| <0.4 | |

AVERAGE DISTANCE BETWEEN PORES μ

THICKNESS $5 \times 10^{-2}$ CM, DENSITY %

Δp/Δt TORR/SEC

WORK FUNCTION 4.72 *, ev

*SAHA-L. EQ. - % NEUTRALS AT 1 Ma/cm

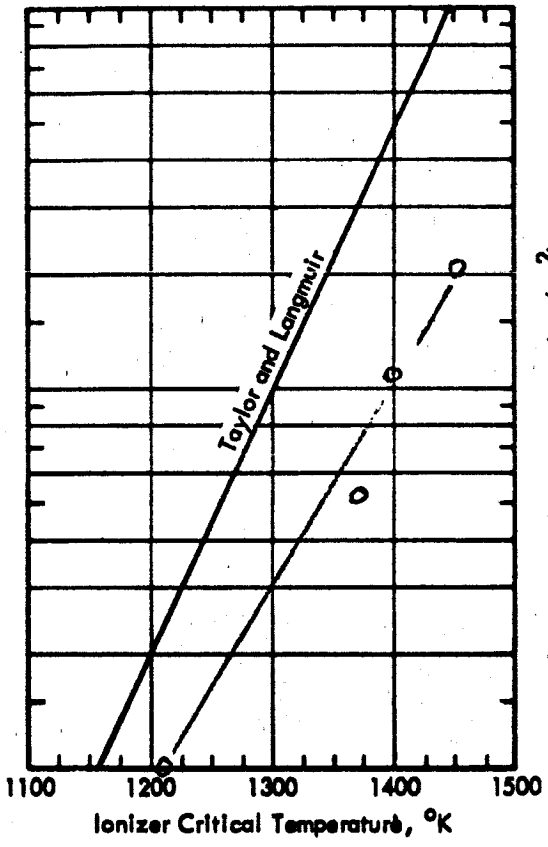


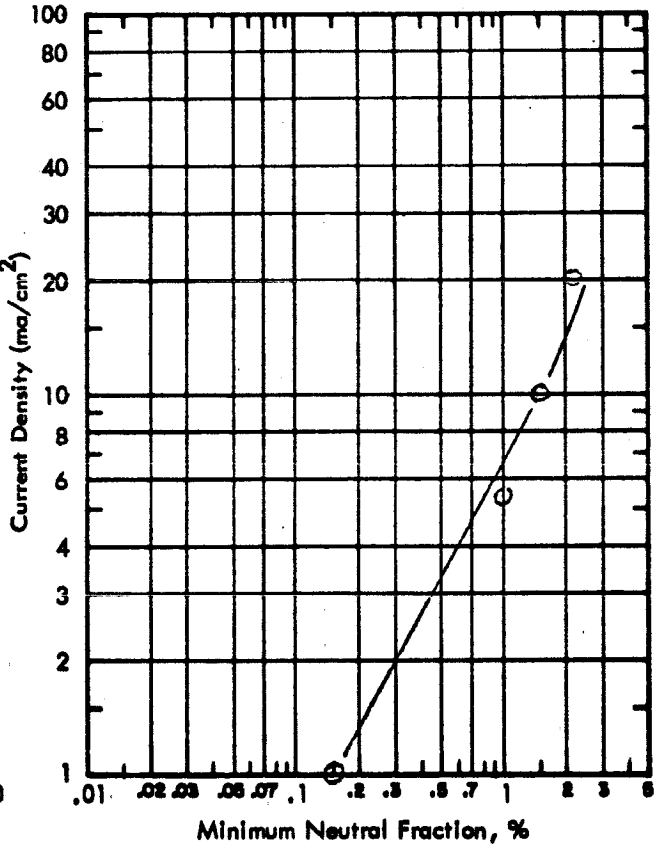


CONCLUSIONS: Repeat test with etching and sputtering. Excellent results.

TEST MADE BY: Shelton/Cho REPORT PREPARED BY: H. Shelton

IONIZER PELLET EVALUATION REPORT

PELLET TYPE E 4

MADE BY E.A.S

AVERAGE PARTICLE SIZE _____

PARTICLE SIZE DISTRIBUTION

| MICRON DIAMETER | PERCENT |
|---|---|
| >7.5 | ____ |
| 7.5 - 5.0 | ____ |
| 5.0 - 3.3 | ____ |
| 3.3 - 2.25 | ____ |
| 1.5 - 1.0 | ____ |
| <1.0 | ____ |

PELLET DIAMETER (EFFECTIVE) 0.18

TRANSMISSION COEFFICIENT ~ $2 \times 10^{-5}$ *BY

PRESSURE 10 (air) TORR

CALCULATED TRUE DENSITY _____

SURFACE TREATMENT Etch + Sputter

SAMPLE INFORMATION * Increased ~100% during test

TEST NO. 7 DATE June, 1964

PORES PER CM$^2$ _____

AVERAGE PORE SIZE _____

PORE SIZE DISTRIBUTION

| MICRON DIAMETER | PERCENT |
|---|---|
| >1.6 | ____ |
| 1.2 - 1.6 | ____ |
| 0.8 - 1.2 | ____ |
| 0.4 - 0.8 | ____ |
| <0.4 | ____ |

AVERAGE DISTANCE BETWEEN PORES _____ μ

THICKNESS $5 \times 10^{-2}$ CM, DENSITY _____ %

Δp/Δt _____ TORR/SEC

WORK FUNCTION 4.76 *, ev

*SAHA-L. EQ. - % NEUTRALS AT 1 Ma/cm

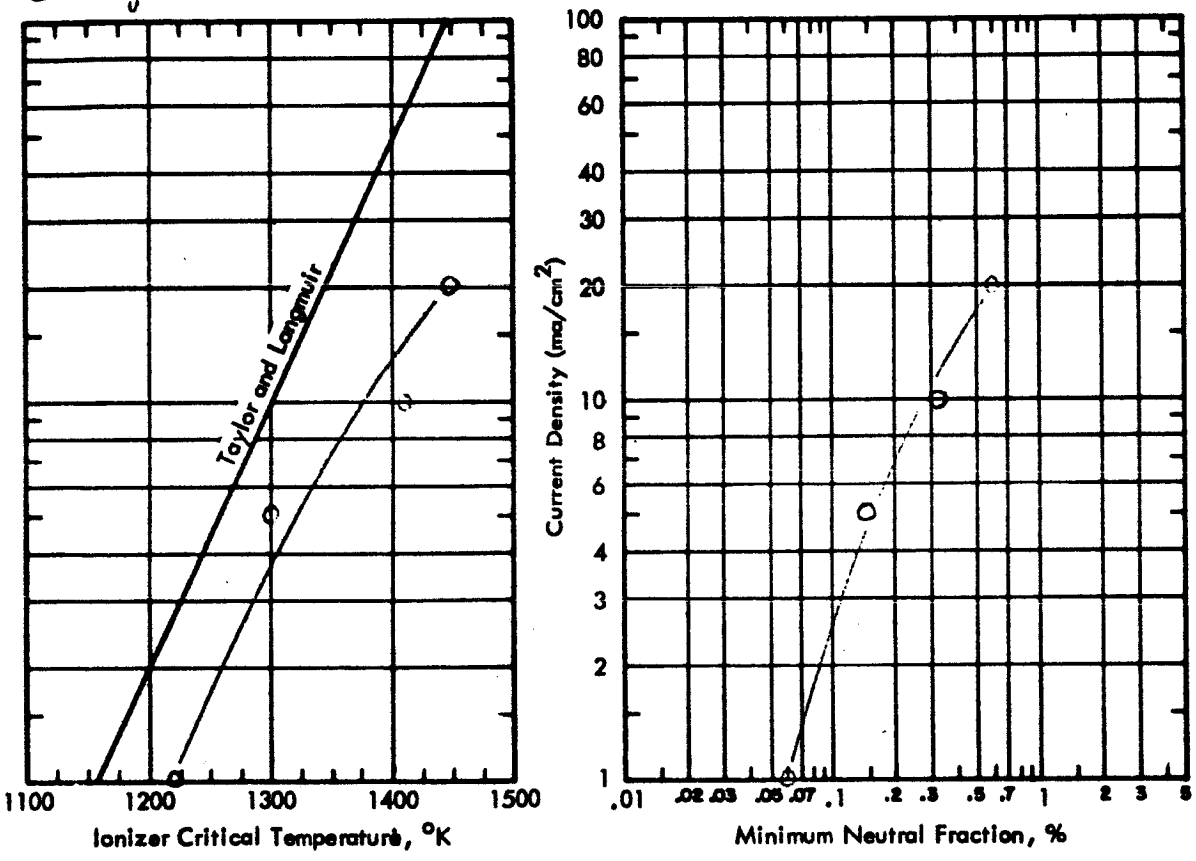


CONCLUSIONS: Superior high current density performance. About 1/2% neutrals at 1450°K for 20 ma/cm$^2$.

TEST MADE BY: Shelton/Cho REPORT PREPARED BY: H. Shelton

IONIZER PELLET EVALUATION REPORT

PELLET TYPE 10-1

MADE BY Astrosect

AVERAGE PARTICLE SIZE

TEST NO. 8 DATE Aug 1964

PORES PER $CM^2$

AVERAGE PORE SIZE

PARTICLE SIZE DISTRIBUTION

| MICRON DIAMETER | PERCENT |
|---|---|
| >7.5 | |
| 7.5 - 5.0 | |
| 5.0 - 3.3 | |
| 3.3 - 2.25 | |
| 1.5 - 1.0 | |
| <1.0 | |

PORE SIZE DISTRIBUTION

| MICRON DIAMETER | PERCENT |
|---|---|
| >1.6 | |
| 1.2 - 1.6 | |
| 0.8 - 1.2 | |
| 0.4 - 0.8 | |
| <0.4 | |

PELLET DIAMETER (EFFECTIVE) 0.18

TRANSMISSION COEFFICIENT $4.3 \times 10^{-5}$* BY

PRESSURE 10 (air) TORR

CALCULATED TRUE DENSITY

SURFACE TREATMENT Etching

SAMPLE INFORMATION * Alloy test. Supplied machined & rid of Cu.

AVERAGE DISTANCE BETWEEN PORES μ

THICKNESS $5 \times 10^{-2}$ CM, DENSITY %

$\Delta p/\Delta t$ TORR/SEC

WORK FUNCTION 4.65 *, ev

*SAHA-L. EQ. - % NEUTRALS AT 1 Ma/cm

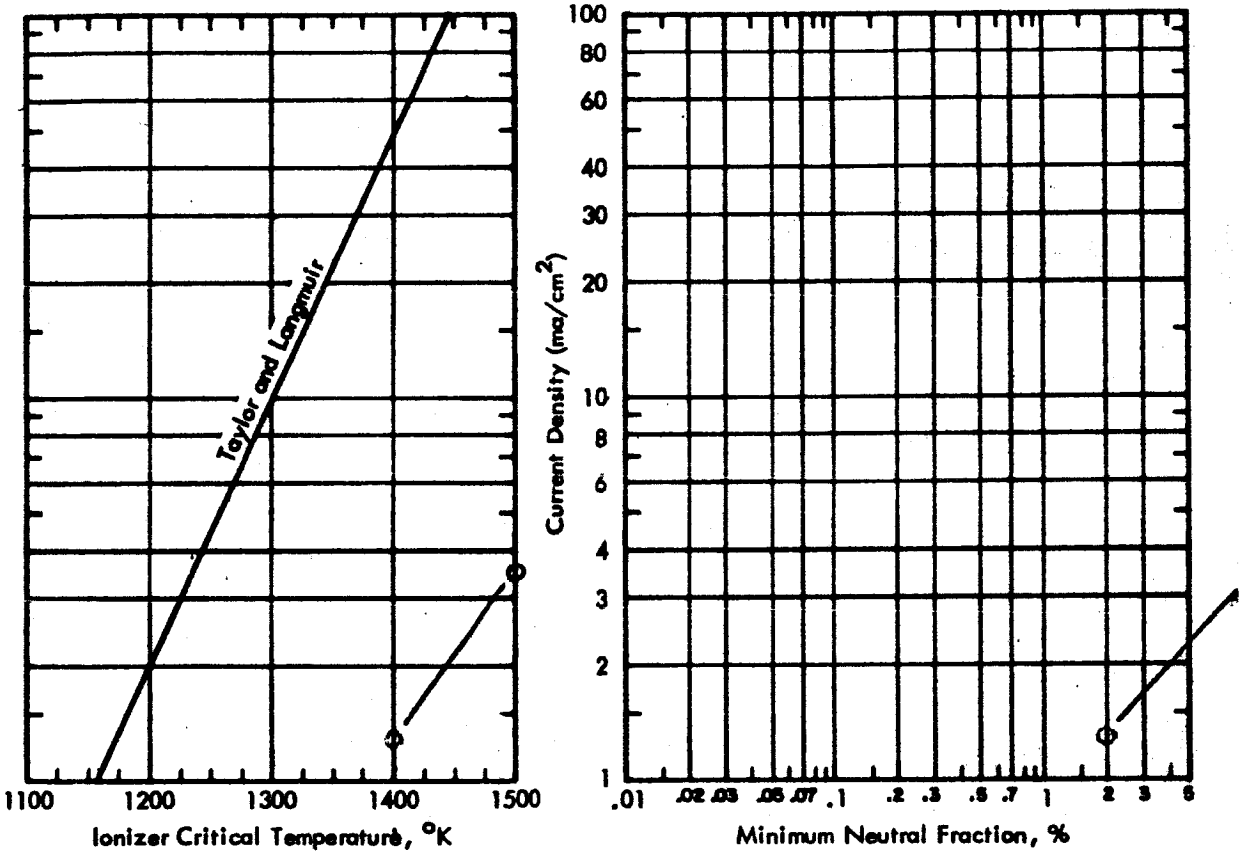


CONCLUSIONS: Performance improved after re-etching. However, results are very poor because of low, non-uniform pore count.

TEST MADE BY: Shelton/Cho REPORT PREPARED BY: H. Shelton

IONIZER PELLET EVALUATION REPORT

PELLET TYPE 1-10 (G1) TEST NO. 9 DATE July 1964

MADE BY EOS PORES PER CM$^2$ _____

AVERAGE PARTICLE SIZE 1-10 μ AVERAGE PORE SIZE _____

| PARTICLE SIZE DISTRIBUTION MICRON DIAMETER | PERCENT |
|---|---|
| >7.5 | ____ |
| 7.5 - 5.0 | ____ |
| 5.0 - 3.3 | ____ |
| 3.3 - 2.25 | ____ |
| 1.5 - 1.0 | ____ |
| <1.0 | ____ |

| PORE SIZE DISTRIBUTION MICRON DIAMETER | PERCENT |
|---|---|
| >1.6 | ____ |
| 1.2 - 1.6 | ____ |
| 0.8 - 1.2 | ____ |
| 0.4 - 0.8 | ____ |
| <0.4 | ____ |

PELLET DIAMETER (EFFECTIVE) 0.18 AVERAGE DISTANCE BETWEEN PORES _____ μ

TRANSMISSION COEFFICIENT $1.07 \times 10^{-4}$* BY THICKNESS $5 \times 10^{-2}$ CM, DENSITY _____ %

PRESSURE 10 (air) TORR Δp/Δt _____ TORR/SEC

CALCULATED TRUE DENSITY _____ WORK FUNCTION 4.85 *, ev

SURFACE TREATMENT Etch + Sputter *SAHA-L. EQ. - % NEUTRALS AT 1 Ma/cm

SAMPLE INFORMATION * Decreased 11% during testing

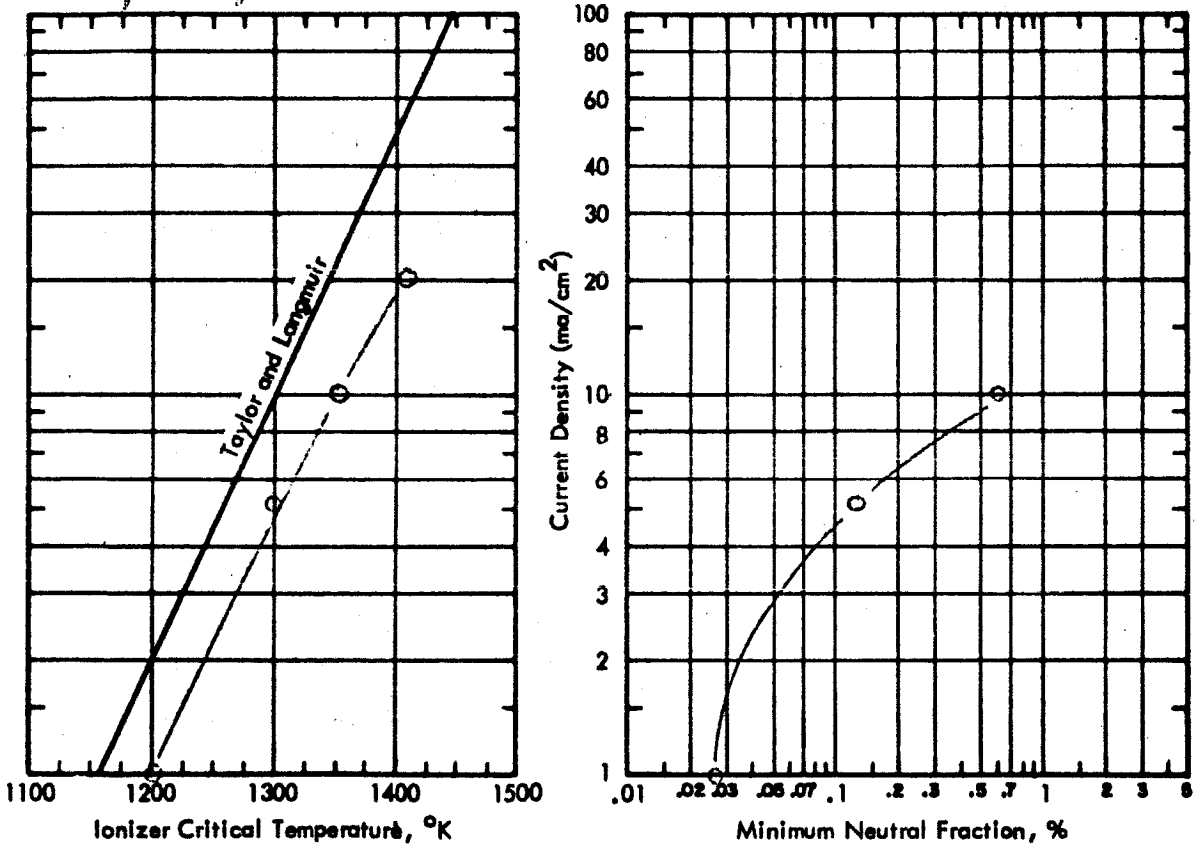


CONCLUSIONS: Show steady increase of neutrals with current density. Good critical temperature. 2% neutrals at 1430°K for 20 ma/cm$^2$.

TEST MADE BY: Shelton/Cho REPORT PREPARED BY: H. Shelton

IONIZER PELLET EVALUATION REPORT

PELLET TYPE 12-1 (Third Gen.) TEST NO. 10 DATE July 1964

MADE BY Astromet PORES PER CM$^2$ _____

AVERAGE PARTICLE SIZE _____ AVERAGE PORE SIZE _____

| PARTICLE SIZE DISTRIBUTION MICRON DIAMETER | PERCENT |
|---|---|
| >7.5 | ____ |
| 7.5 - 5.0 | ____ |
| 5.0 - 3.3 | ____ |
| 3.3 - 2.25 | ____ |
| 1.5 - 1.0 | ____ |
| <1.0 | ____ |

| PORE SIZE DISTRIBUTION MICRON DIAMETER | PERCENT |
|---|---|
| >1.6 | ____ |
| 1.2 - 1.6 | ____ |
| 0.8 - 1.2 | ____ |
| 0.4 - 0.8 | ____ |
| <0.4 | ____ |

PELLET DIAMETER (EFFECTIVE) 0.18 AVERAGE DISTANCE BETWEEN PORES _____ μ

TRANSMISSION COEFFICIENT Very low BY THICKNESS 5 x 10$^{-2}$ CM, DENSITY _____ %

PRESSURE 10 (air) TORR $\Delta p/\Delta t$ _____ TORR/SEC

CALCULATED TRUE DENSITY _____ WORK FUNCTION 4.69 *, ev

SURFACE TREATMENT Etch + Sputter

SAMPLE INFORMATION Supplied machined and rid of Cu.

*SAHA-L. EQ. - % NEUTRALS AT 1 Ma/cm

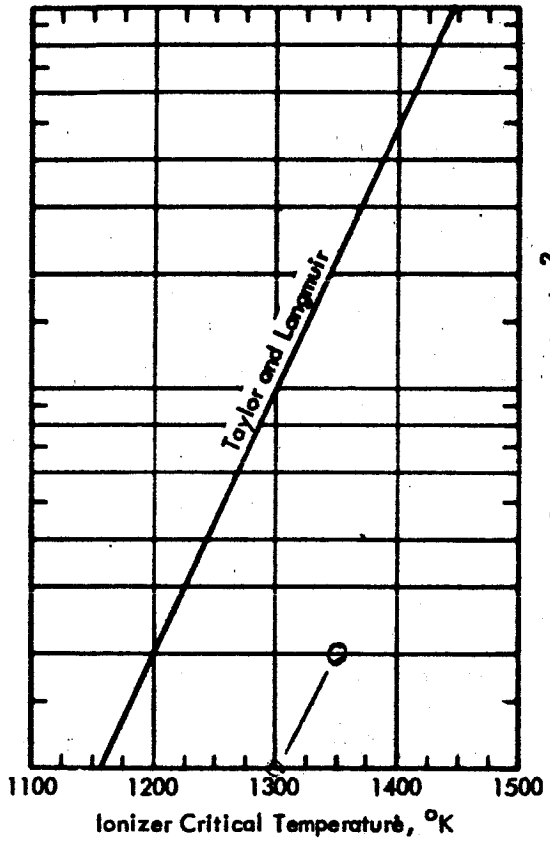


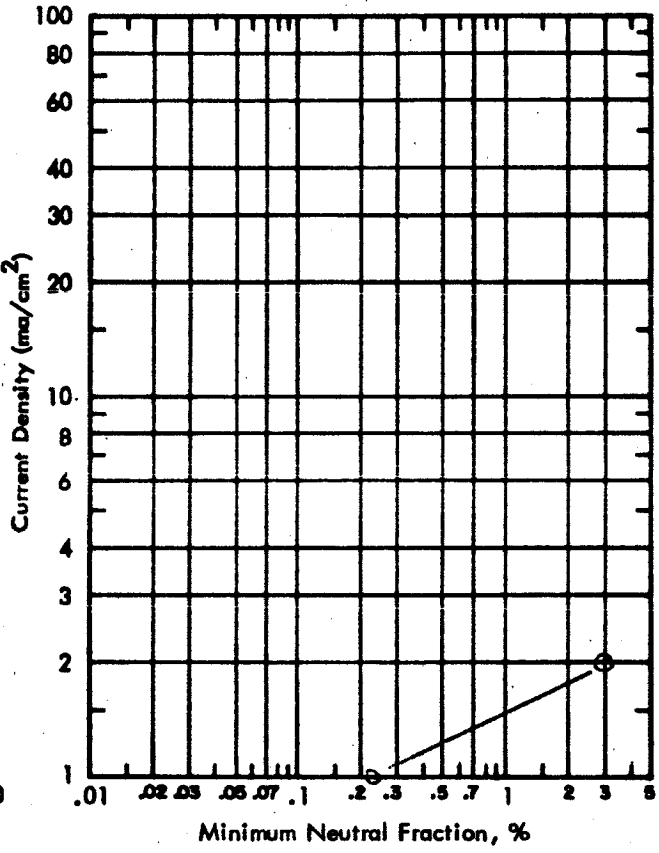


CONCLUSIONS: Low permeability because of braze penetration on reverse side. Test poor, but possibly invalid.

TEST MADE BY: Shelton/Cho REPORT PREPARED BY: H. Shelton

IONIZER PELLET EVALUATION REPORT

PELLET TYPE 1-10 (G1) After Elox

MADE BY EOS

AVERAGE PARTICLE SIZE 1-10 μ

PARTICLE SIZE DISTRIBUTION

| MICRON DIAMETER | PERCENT |
|---|---|
| >7.5 | |
| 7.5 - 5.0 | |
| 5.0 - 3.3 | |
| 3.3 - 2.25 | |
| 1.5 - 1.0 | |
| <1.0 | |

PELLET DIAMETER (EFFECTIVE) 0.18

TRANSMISSION COEFFICIENT $4.8 \times 10^{-5}$ BY

PRESSURE 10 (air) TORR

CALCULATED TRUE DENSITY

SURFACE TREATMENT Elox

SAMPLE INFORMATION

TEST NO. 11 DATE Aug 1964

PORES PER $CM^2$

AVERAGE PORE SIZE

PORE SIZE DISTRIBUTION

| MICRON DIAMETER | PERCENT |
|---|---|
| >1.6 | |
| 1.2 - 1.6 | |
| 0.8 - 1.2 | |
| 0.4 - 0.8 | |
| <0.4 | |

AVERAGE DISTANCE BETWEEN PORES μ

THICKNESS $5 \times 10^{-2}$ CM, DENSITY %

Δp/Δt TORR/SEC

WORK FUNCTION 4.83 *, ev

*SAHA-L. EQ. - % NEUTRALS AT 1 Ma/cm

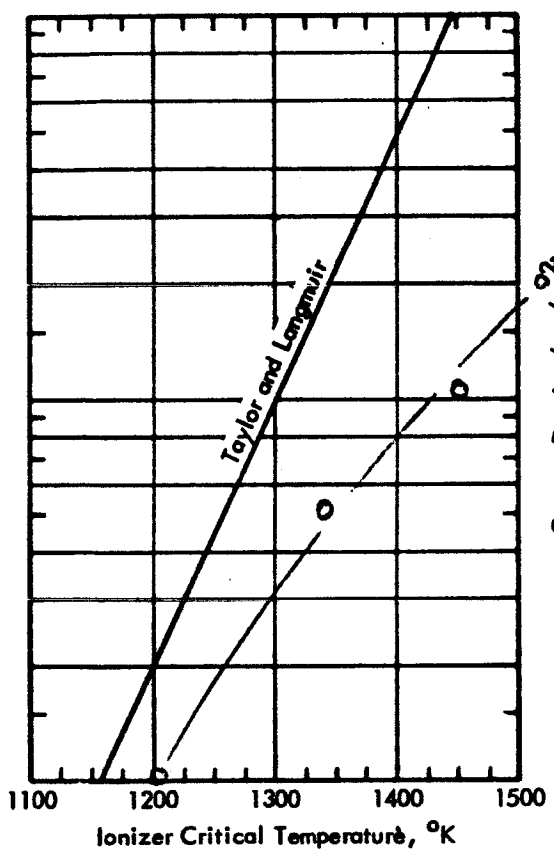


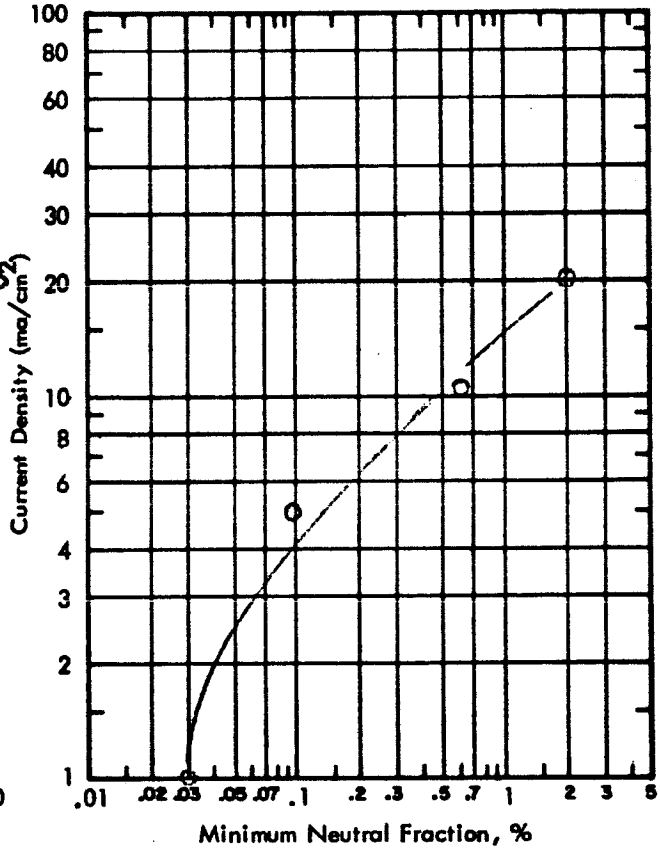


CONCLUSIONS: After elox machining. Critical temperatures at high current density higher and more sloppy after elox.

TEST MADE BY: Shelton/Cho REPORT PREPARED BY: H. Shelton

IONIZER PELLET EVALUATION REPORT

PELLET TYPE E4 - Ta (10%)

MADE BY EOS

AVERAGE PARTICLE SIZE 2 - 5 μ

PARTICLE SIZE DISTRIBUTION

| MICRON DIAMETER | PERCENT |
|---|---|
| >7.5 | |
| 7.5 - 5.0 | |
| 5.0 - 3.3 | |
| 3.3 - 2.25 | |
| 1.5 - 1.0 | |
| <1.0 | |

PELLET DIAMETER (EFFECTIVE) 0.18

TRANSMISSION COEFFICIENT $4.9 \times 10^{-5}$ BY

PRESSURE 10 (air) TORR

CALCULATED TRUE DENSITY

SURFACE TREATMENT E.B. + Sputter

SAMPLE INFORMATION

TEST NO. 12 DATE Sept 1964

PORES PER $CM^2$

AVERAGE PORE SIZE

PORE SIZE DISTRIBUTION

| MICRON DIAMETER | PERCENT |
|---|---|
| >1.6 | |
| 1.2 - 1.6 | |
| 0.8 - 1.2 | |
| 0.4 - 0.8 | |
| <0.4 | |

AVERAGE DISTANCE BETWEEN PORES μ

THICKNESS $5 \times 10^{-2}$ CM, DENSITY %

Δp/Δt TORR/SEC

WORK FUNCTION 4.83 *, ev

*SAHA-L. EQ. - % NEUTRALS AT 1 Ma/cm

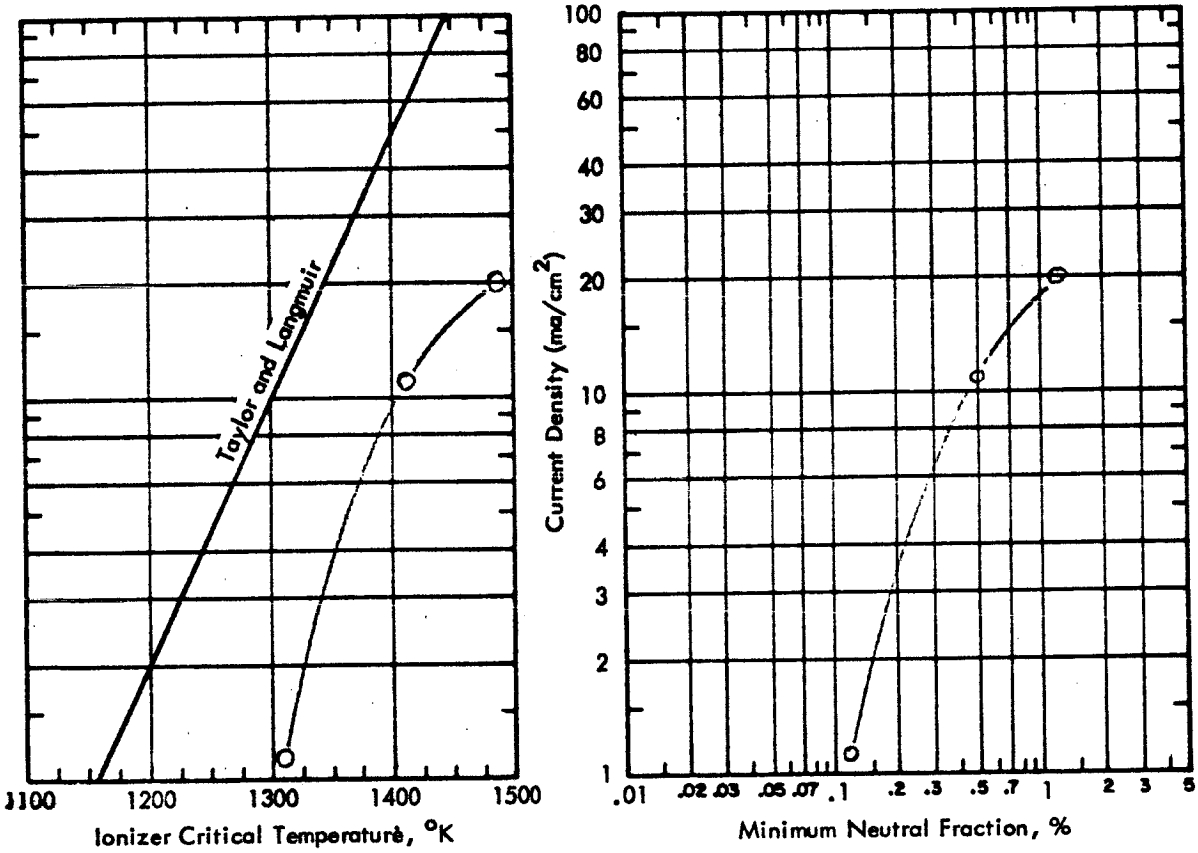


CONCLUSIONS: Knees rounded at low current density. Good high current density performance (~2 percent neutrals at 1420°K for 20 ma/$cm^2$)

TEST MADE BY: Shelton/Cho REPORT PREPARED BY: H. Shelton

IONIZER PELLET EVALUATION REPORT

PELLET TYPE G2a

MADE BY Hughes

AVERAGE PARTICLE SIZE 4.8

PARTICLE SIZE DISTRIBUTION

| MICRON DIAMETER | PERCENT |
|---|---|
| >7.5 | |
| 7.5 - 5.0 | |
| 5.0 - 3.3 | |
| 3.3 - 2.25 | |
| 1.5 - 1.0 | |
| <1.0 | |

PELLET DIAMETER (EFFECTIVE) 0.18

TRANSMISSION COEFFICIENT $5.0 \times 10^{-5}$ * BY

PRESSURE 10 (air) TORR

CALCULATED TRUE DENSITY

SURFACE TREATMENT Etch + Sputter

SAMPLE INFORMATION * Increased 3% during test

TEST NO. 13 DATE Sept 1964

PORES PER $CM^2$

AVERAGE PORE SIZE

PORE SIZE DISTRIBUTION

| MICRON DIAMETER | PERCENT |
|---|---|
| >1.6 | |
| 1.2 - 1.6 | |
| 0.8 - 1.2 | |
| 0.4 - 0.8 | |
| <0.4 | |

AVERAGE DISTANCE BETWEEN PORES ____ μ

THICKNESS $5 \times 10^{-2}$ CM, DENSITY ____ %

Δp/Δt ____ TORR/SEC

WORK FUNCTION 4.81 *, ev

*SAHA-L. EQ. - % NEUTRALS AT 1 Ma/cm

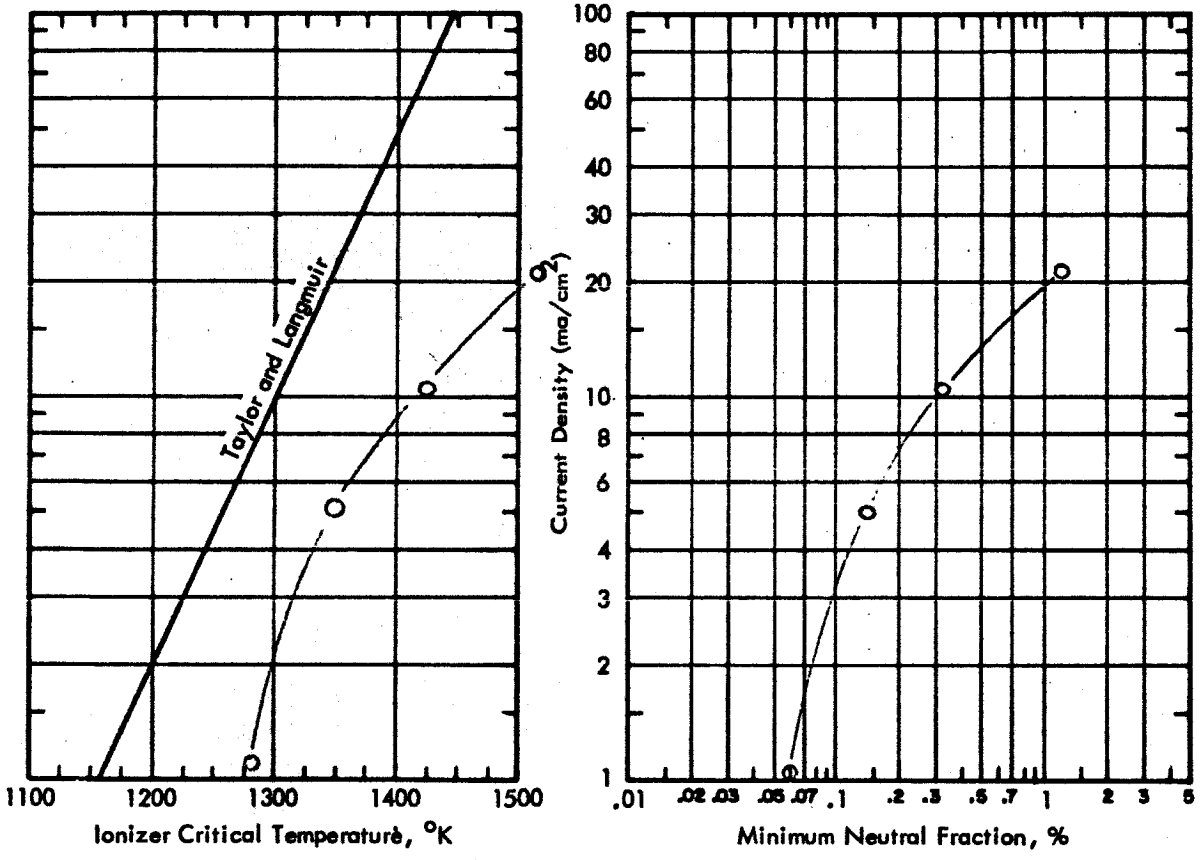


CONCLUSIONS: Neutrals low and indicate high pore count. Critical temperature unaccountably high.

TEST MADE BY: Shelton/Cho REPORT PREPARED BY: H. Shelton

IONIZER PELLET EVALUATION REPORT

PELLET TYPE EOS Block No. 5 (G3) TEST NO. 14 DATE Oct. 1964

MADE BY EOS

AVERAGE PARTICLE SIZE _____

PARTICLE SIZE DISTRIBUTION

| MICRON DIAMETER | PERCENT |
|---|---|
| >7.5 | ____ |
| 7.5 - 5.0 | ____ |
| 5.0 - 3.3 | ____ |
| 3.3 - 2.25 | ____ |
| 1.5 - 1.0 | ____ |
| <1.0 | ____ |

PELLET DIAMETER (EFFECTIVE) 0.18

TRANSMISSION COEFFICIENT $6.0 \times 10^{-5}$ BY

PRESSURE 10 (air) TORR

CALCULATED TRUE DENSITY _____

SURFACE TREATMENT Etch + Sputter

SAMPLE INFORMATION _____

PORES PER $CM^2$ _____

AVERAGE PORE SIZE _____

PORE SIZE DISTRIBUTION

| MICRON DIAMETER | PERCENT |
|---|---|
| >1.6 | ____ |
| 1.2 - 1.6 | ____ |
| 0.8 - 1.2 | ____ |
| 0.4 - 0.8 | ____ |
| <0.4 | ____ |

AVERAGE DISTANCE BETWEEN PORES _____ μ

THICKNESS $5 \times 10^{-2}$ CM, DENSITY _____ %

Δp/Δt _____ TORR/SEC

WORK FUNCTION 4.81 *, ev

*SAHA-L. EQ. - % NEUTRALS AT 1 Ma/cm

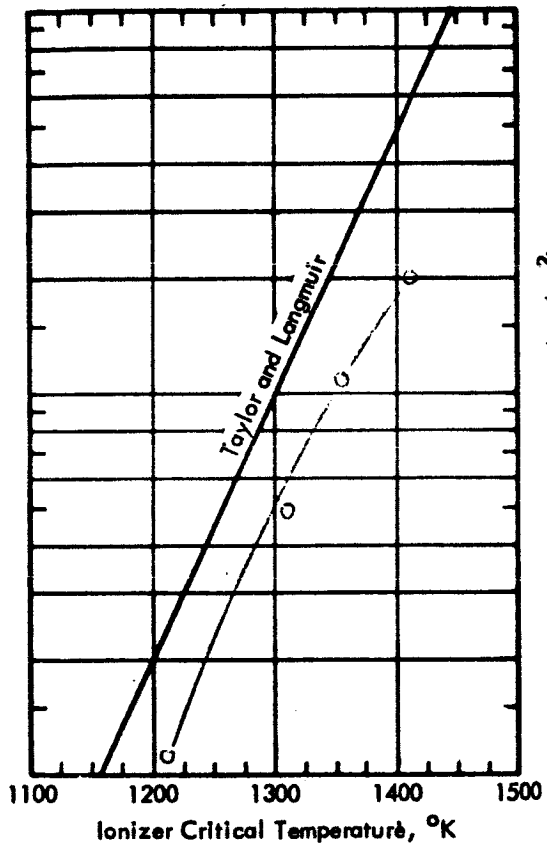


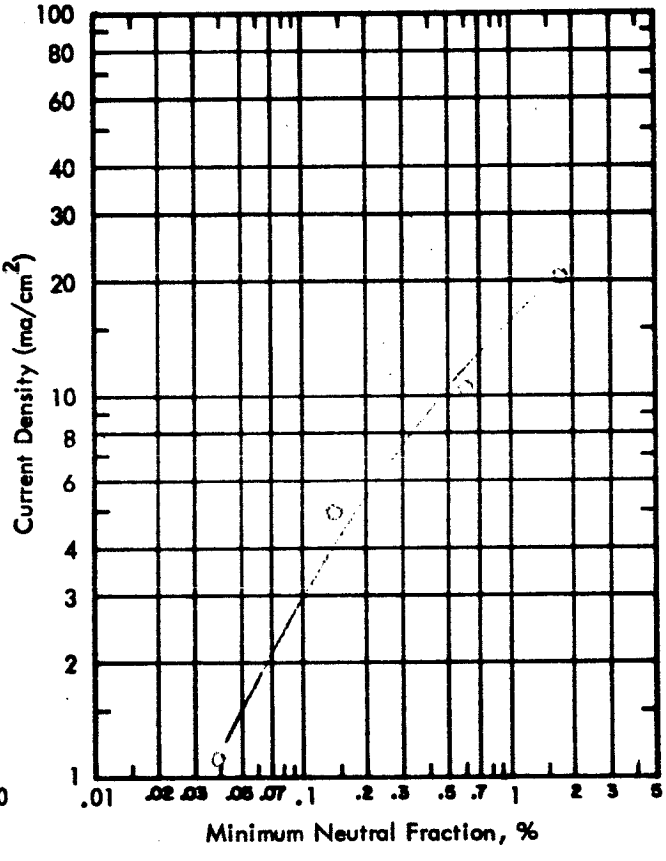


CONCLUSIONS: Neutrals and critical temperature continuously increase with current densities. Knees sharp and solid tungsten appearing. (About 2% neutrals at 1430°K for 20 $ma/cm^2$).

TEST MADE BY: Shelton/Cho REPORT PREPARED BY: H. Shelton

IONIZER PELLET EVALUATION REPORT

PELLET TYPE LB 2% Ta

MADE BY EOS

AVERAGE PARTICLE SIZE 1-3μ Ta, 1.7-5μ W

TEST NO. 15 DATE Nov 12, 1964

PORES PER CM$^2$ _____

AVERAGE PORE SIZE _____

| PARTICLE SIZE DISTRIBUTION MICRON DIAMETER | PERCENT |
|---|---|
| >7.5 | ____ |
| 7.5 - 5.0 | ____ |
| 5.0 - 3.3 | ____ |
| 3.3 - 2.25 | ____ |
| 1.5 - 1.0 | ____ |
| <1.0 | ____ |

| PORE SIZE DISTRIBUTION MICRON DIAMETER | PERCENT |
|---|---|
| >1.6 | ____ |
| 1.2 - 1.6 | ____ |
| 0.8 - 1.2 | ____ |
| 0.4 - 0.8 | ____ |
| <0.4 | ____ |

PELLET DIAMETER (EFFECTIVE) 0.18

TRANSMISSION COEFFICIENT $3.9 \times 10^{-5}$ BY

PRESSURE 10 (air) TORR

CALCULATED TRUE DENSITY _____

SURFACE TREATMENT Etch + Sputter

SAMPLE INFORMATION _____

AVERAGE DISTANCE BETWEEN PORES _____ μ

THICKNESS $5 \times 10^{-2}$ CM, DENSITY _____ %

Δp/Δt _____ TORR/SEC

WORK FUNCTION 4.9 *, ev

*SAHA-L. EQ. - % NEUTRALS AT 1 Ma/cm

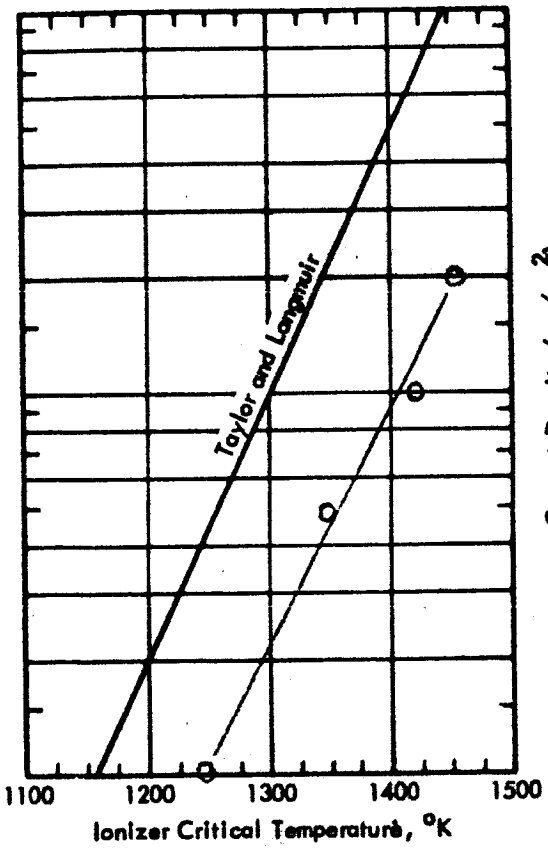


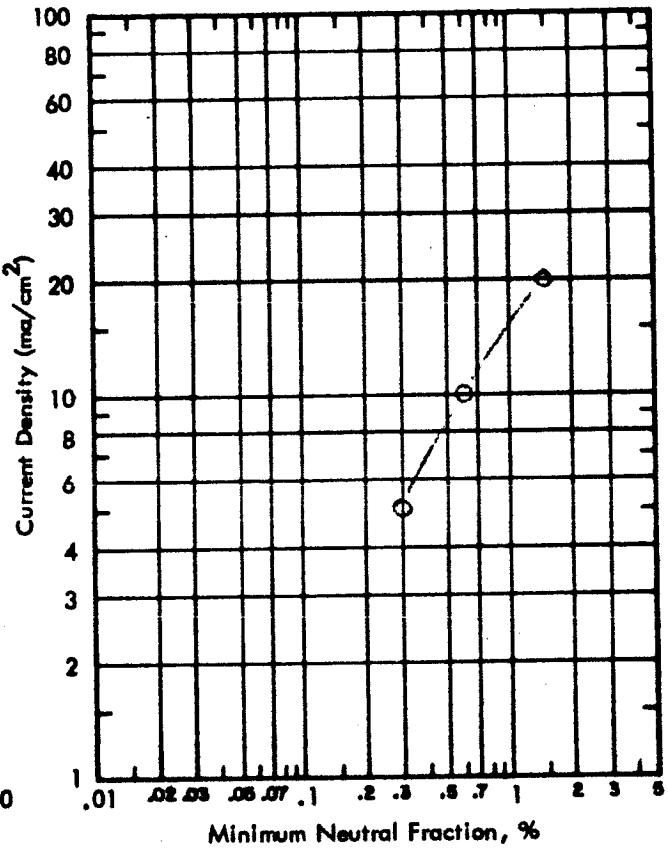


CONCLUSIONS: Critical temperature high - rounded knees. Work function high at low current density probably because of oxygen associated with tantalum. (2% at 1600°K at 20 ma/cm$^2$).

TEST MADE BY: Shelton/Cho REPORT PREPARED BY: H. Shelton

IONIZER PELLET EVALUATION REPORT

PELLET TYPE LB 5% Ta

MADE BY EOS

AVERAGE PARTICLE SIZE 1-3μ Ta, 1.7-5μ W

PARTICLE SIZE DISTRIBUTION

| MICRON DIAMETER | PERCENT |
|---|---|
| >7.5 | |
| 7.5 - 5.0 | |
| 5.0 - 3.3 | |
| 3.3 - 2.25 | |
| 1.5 - 1.0 | |
| <1.0 | |

PELLET DIAMETER (EFFECTIVE) 0.18

TRANSMISSION COEFFICIENT $5.3 \times 10^{-5}$ * BY

PRESSURE 10 (air) TORR

CALCULATED TRUE DENSITY

SURFACE TREATMENT Elec + Sputter

SAMPLE INFORMATION * Increased 3% during test.

TEST NO. 16 DATE Nov 20, 1964

PORES PER $CM^2$

AVERAGE PORE SIZE

PORE SIZE DISTRIBUTION

| MICRON DIAMETER | PERCENT |
|---|---|
| >1.6 | |
| 1.2 - 1.6 | |
| 0.8 - 1.2 | |
| 0.4 - 0.8 | |
| <0.4 | |

AVERAGE DISTANCE BETWEEN PORES μ

THICKNESS $5 \times 10^{-2}$ CM, DENSITY %

Δp/Δt TORR/SEC

WORK FUNCTION 4.8 *, ev

*SAHA-L. EQ. - % NEUTRALS AT 1 Ma/cm

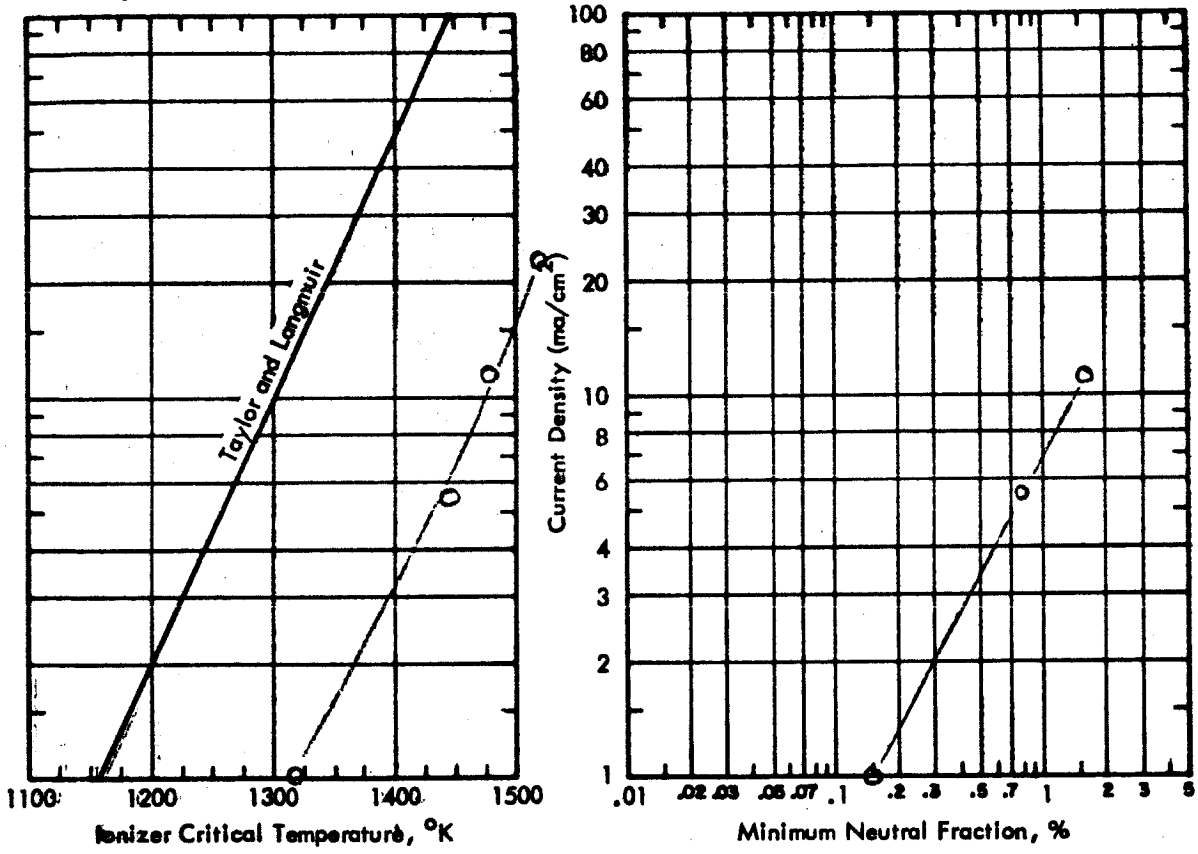


CONCLUSIONS: Critical temperatures and neutrals high. (7% neutrals at 1600°K at 20 $ma/cm^2$).

TEST MADE BY: Shelton/Cho REPORT PREPARED BY: H. Shelton

IONIZER PELLET EVALUATION REPORT

PELLET TYPE LB 10% Ta

MADE BY EOS

AVERAGE PARTICLE SIZE 1-3μ Ta, 1.7-5μ W

TEST NO. 17 DATE Nov 25, 1964

PORES PER CM$^2$ _____

AVERAGE PORE SIZE _____

PARTICLE SIZE DISTRIBUTION

| MICRON DIAMETER | PERCENT |
|---|---|
| >7.5 | ____ |
| 7.5 - 5.0 | ____ |
| 5.0 - 3.3 | ____ |
| 3.3 - 2.25 | ____ |
| 1.5 - 1.0 | ____ |
| <1.0 | ____ |

PORE SIZE DISTRIBUTION

| MICRON DIAMETER | PERCENT |
|---|---|
| >1.6 | ____ |
| 1.2 - 1.6 | ____ |
| 0.8 - 1.2 | ____ |
| 0.4 - 0.8 | ____ |
| <0.4 | ____ |

PELLET DIAMETER (EFFECTIVE) 0.18

TRANSMISSION COEFFICIENT $4.5 \times 10^{-5}$* BY

PRESSURE 10 (air) TORR

CALCULATED TRUE DENSITY _____

SURFACE TREATMENT _____

SAMPLE INFORMATION *Increased 10% during test.

AVERAGE DISTANCE BETWEEN PORES _____ μ

THICKNESS $5 \times 10^{-2}$ CM, DENSITY _____ %

Δp/Δt _____ TORR/SEC

WORK FUNCTION 4.95 *, ev

*SAHA-L. EQ. - % NEUTRALS AT 1 Ma/cm

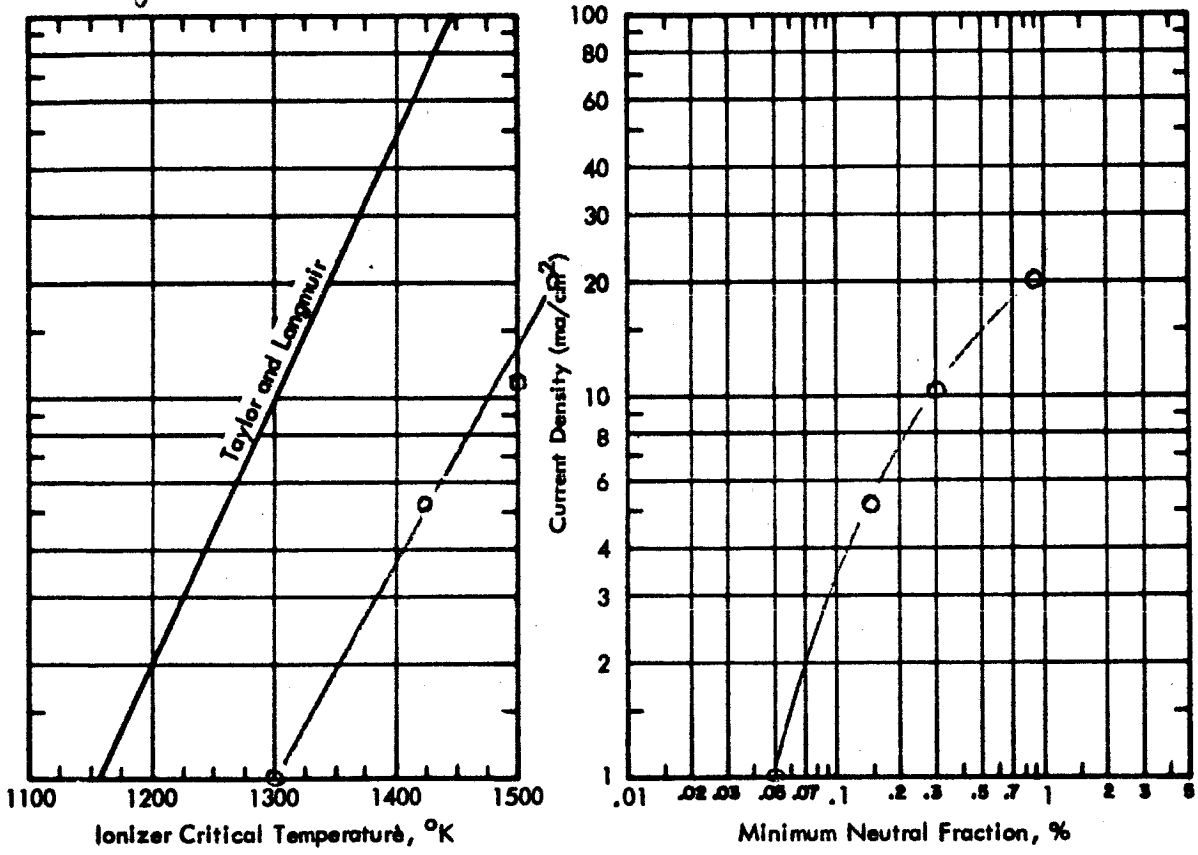


CONCLUSIONS: Same general characteristics of Ta series (15-17) - rounded drooping knees - oxygenated - high critical temperatures. (1 1/2% neutrals at 1600°K for 20 ma/cm$^2$).

TEST MADE BY: Shelton/Cho REPORT PREPARED BY: H. Shelton

IONIZER PELLET EVALUATION REPORT

PELLET TYPE G-4 (Bar No. 2)
MADE BY EOS
AVERAGE PARTICLE SIZE _____

PARTICLE SIZE DISTRIBUTION

| MICRON DIAMETER | PERCENT |
|---|---|
| >7.5 | ____ |
| 7.5 - 5.0 | ____ |
| 5.0 - 3.3 | ____ |
| 3.3 - 2.25 | ____ |
| 1.5 - 1.0 | ____ |
| <1.0 | ____ |

PELLET DIAMETER (EFFECTIVE) 0.18
TRANSMISSION COEFFICIENT $1.3 \times 10^{-4}$ BY
PRESSURE 10 (air) TORR
CALCULATED TRUE DENSITY _____
SURFACE TREATMENT Etch + Sputter
SAMPLE INFORMATION Befor elaxing

TEST NO. 18 DATE Dec 1964
PORES PER $CM^2$ _____
AVERAGE PORE SIZE _____

PORE SIZE DISTRIBUTION

| MICRON DIAMETER | PERCENT |
|---|---|
| >1.6 | ____ |
| 1.2 - 1.6 | ____ |
| 0.8 - 1.2 | ____ |
| 0.4 - 0.8 | ____ |
| <0.4 | ____ |

AVERAGE DISTANCE BETWEEN PORES _____ μ
THICKNESS $5 \times 10^{-2}$ CM, DENSITY _____ %
Δp/Δt _____ TORR/SEC
WORK FUNCTION 4.84 *, ev
*SAHA-L. EQ. - % NEUTRALS AT 1 Ma/cm

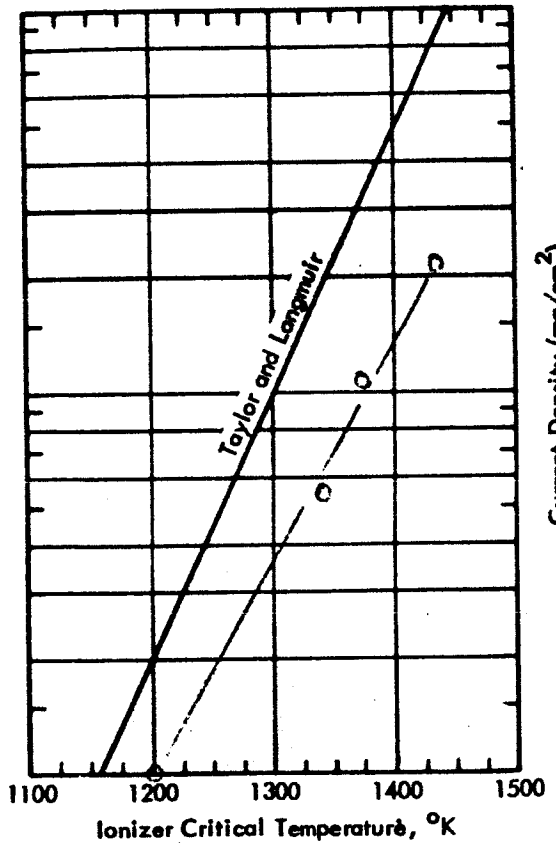


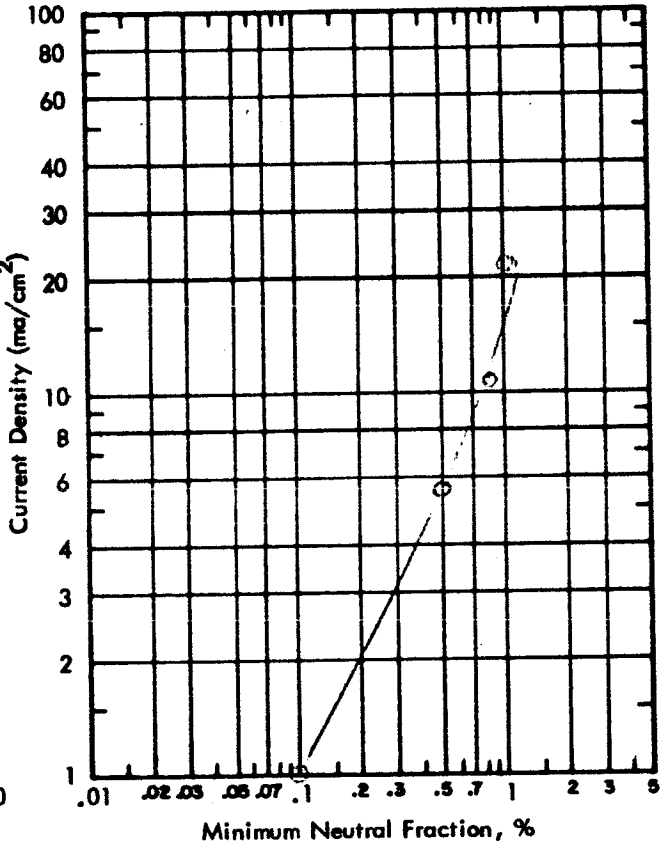


CONCLUSIONS: Good current density performance. (1% at 1430°K at 20 ma/$cm^2$).

TEST MADE BY: Shelton/Cho REPORT PREPARED BY: H. Shelton

IONIZER PELLET EVALUATION REPORT

PELLET TYPE G-4 (Bar 2)

MADE BY EOS

AVERAGE PARTICLE SIZE _____

PARTICLE SIZE DISTRIBUTION

| MICRON DIAMETER | PERCENT |
|---|---|
| >7.5 | ____ |
| 7.5 - 5.0 | ____ |
| 5.0 - 3.3 | ____ |
| 3.3 - 2.25 | ____ |
| 1.5 - 1.0 | ____ |
| <1.0 | ____ |

PELLET DIAMETER (EFFECTIVE) 0.18

TRANSMISSION COEFFICIENT _____ BY

PRESSURE 10 (air) TORR

CALCULATED TRUE DENSITY _____

SURFACE TREATMENT _____

SAMPLE INFORMATION _____

TEST NO. 19 DATE Jan 1965

PORES PER $CM^2$ _____

AVERAGE PORE SIZE _____

PORE SIZE DISTRIBUTION

| MICRON DIAMETER | PERCENT |
|---|---|
| >1.6 | ____ |
| 1.2 - 1.6 | ____ |
| 0.8 - 1.2 | ____ |
| 0.4 - 0.8 | ____ |
| <0.4 | ____ |

AVERAGE DISTANCE BETWEEN PORES _____ μ

THICKNESS $5 \times 10^{-2}$ CM, DENSITY _____ %

Δp/Δt _____ TORR/SEC

WORK FUNCTION 4.87 (both clean & carbided)*, ev

*SAHA-L. EQ. - % NEUTRALS AT 1 Ma/cm

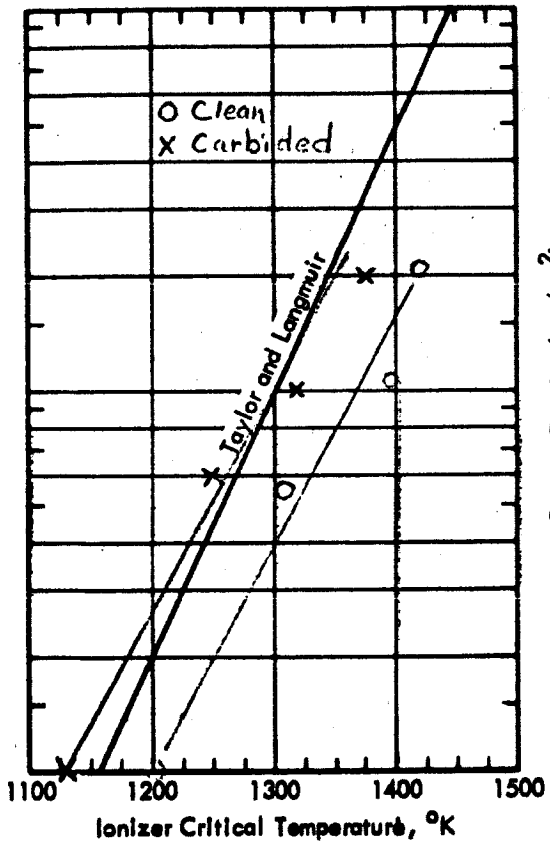


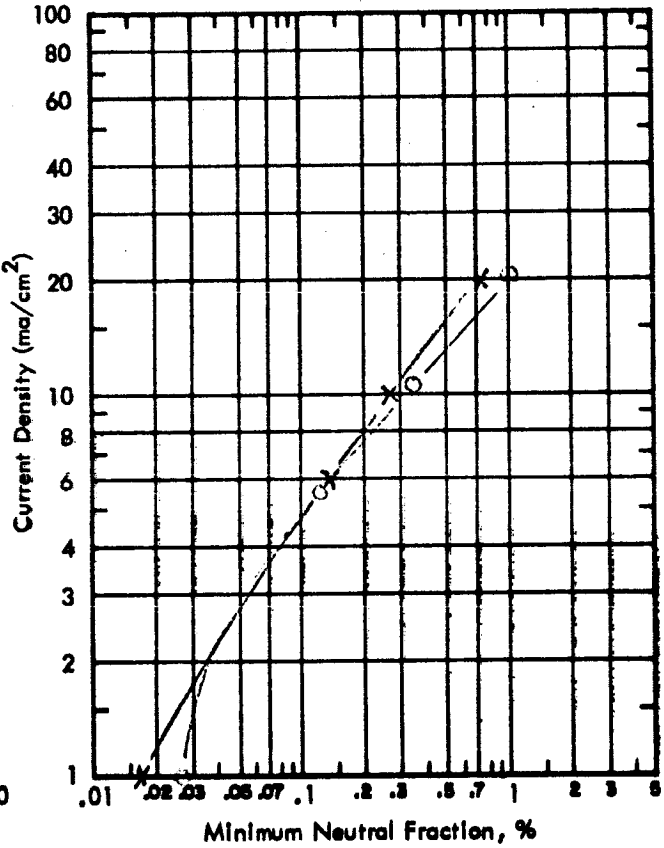


CONCLUSIONS: After elox machining, surface carbided upon initial operation. (Low criticals and low neutrals). After oxygen and sputtering results nearly identical with test number 18.

TEST MADE BY: Shelton/Cho REPORT PREPARED BY: H. Shelton

IONIZER PELLET EVALUATION REPORT

PELLET TYPE G-2a - Carbided

MADE BY Hucles

AVERAGE PARTICLE SIZE 4.8 μ

PARTICLE SIZE DISTRIBUTION

| MICRON DIAMETER | PERCENT |
|---|---|
| >7.5 | |
| 7.5 - 5.0 | |
| 5.0 - 3.3 | |
| 3.3 - 2.25 | |
| 1.5 - 1.0 | |
| <1.0 | |

PELLET DIAMETER (EFFECTIVE) 0.18

TRANSMISSION COEFFICIENT $5.1 \times 10^{-5}$ BY

PRESSURE 10 (air) TORR

CALCULATED TRUE DENSITY

SURFACE TREATMENT Sputter

SAMPLE INFORMATION

TEST NO. 20 DATE Jan 1965

PORES PER $CM^2$

AVERAGE PORE SIZE

PORE SIZE DISTRIBUTION

| MICRON DIAMETER | PERCENT |
|---|---|
| >1.6 | |
| 1.2 - 1.6 | |
| 0.8 - 1.2 | |
| 0.4 - 0.8 | |
| <0.4 | |

AVERAGE DISTANCE BETWEEN PORES μ

THICKNESS $5 \times 10^{-2}$ CM, DENSITY %

Δp/Δt TORR/SEC

WORK FUNCTION *, ev

*SAHA-L. EQ. - % NEUTRALS AT 1 Ma/cm

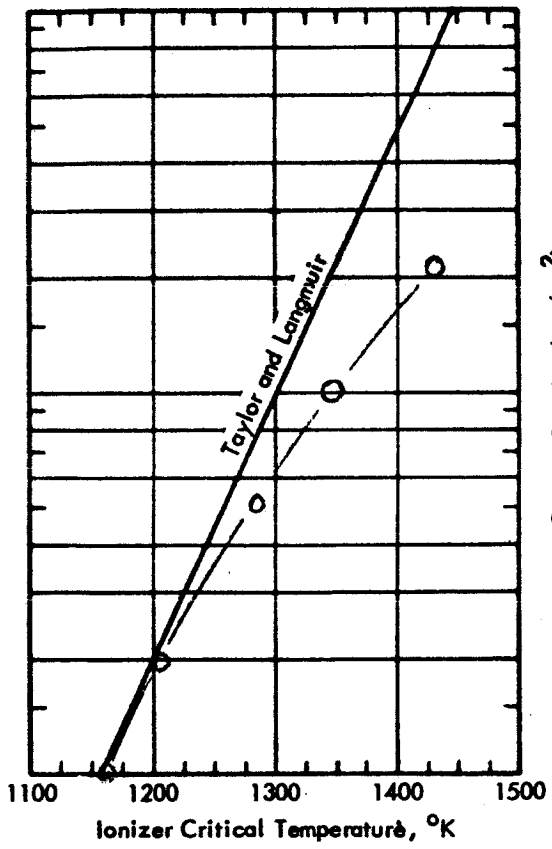


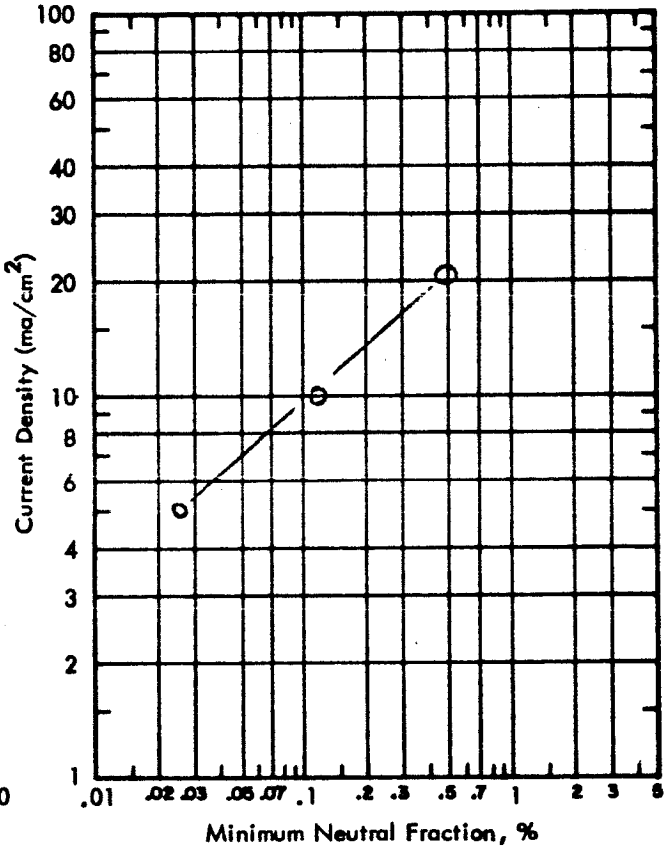


CONCLUSIONS: Generally lower critical temperature and neutrals (1/2% at 1430°K at 20 $ma/cm^2$).

TEST MADE BY: Shelton/Cho REPORT PREPARED BY: H. Shelton

IONIZER PELLET EVALUATION REPORT

PELLET TYPE 10-1 (5-188B)

MADE BY Astromet

AVERAGE PARTICLE SIZE _____

PARTICLE SIZE DISTRIBUTION

| MICRON DIAMETER | PERCENT |
|---|---|
| >7.5 | ____ |
| 7.5 - 5.0 | ____ |
| 5.0 - 3.3 | ____ |
| 3.3 - 2.25 | ____ |
| 1.5 - 1.0 | ____ |
| <1.0 | ____ |

PELLET DIAMETER (EFFECTIVE) 0.18

TRANSMISSION COEFFICIENT .3 X 10$^{-4}$% BY

PRESSURE 10 (air) TORR

CALCULATED TRUE DENSITY _____

SURFACE TREATMENT Etch + Sputter

SAMPLE INFORMATION ★ Increased 10% during test

TEST NO. 21 DATE Mar 1, 1965

PORES PER CM$^2$ _____

AVERAGE PORE SIZE _____

PORE SIZE DISTRIBUTION

| MICRON DIAMETER | PERCENT |
|---|---|
| >1.6 | ____ |
| 1.2 - 1.6 | ____ |
| 0.8 - 1.2 | ____ |
| 0.4 - 0.8 | ____ |
| <0.4 | ____ |

AVERAGE DISTANCE BETWEEN PORES _____ μ

THICKNESS 5 x 10$^{-2}$ CM, DENSITY _____ %

Δp/Δt _____ TORR/SEC

WORK FUNCTION 4.8 *, ev

*SAHA-L. EQ. - % NEUTRALS AT 1 Ma/cm

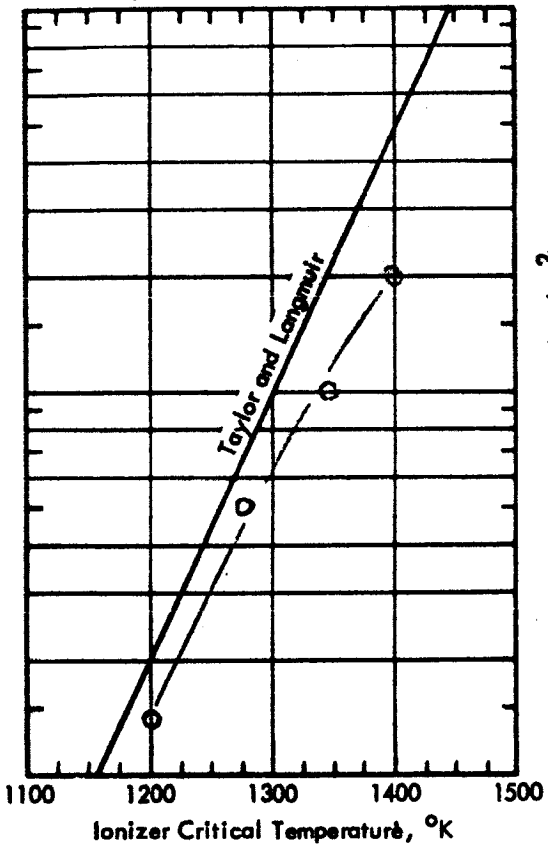


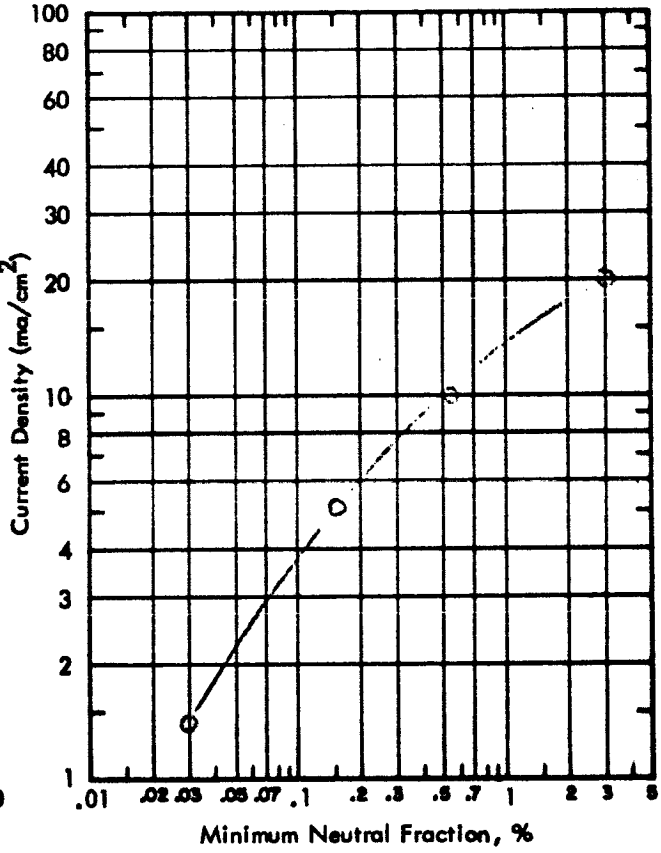


CONCLUSIONS: Excellent results below 10 ma/cm$^2$ (3% neutrals at 1420°K at 20 ma/cm$^2$).

TEST MADE BY: Shelton/Hall REPORT PREPARED BY: H. Shelton

IONIZER PELLET EVALUATION REPORT

PELLET TYPE G2B

MADE BY Hughes

AVERAGE PARTICLE SIZE _____

PARTICLE SIZE DISTRIBUTION

| MICRON DIAMETER | PERCENT |
|---|---|
| >7.5 | ____ |
| 7.5 - 5.0 | ____ |
| 5.0 - 3.3 | ____ |
| 3.3 - 2.25 | ____ |
| 1.5 - 1.0 | ____ |
| <1.0 | ____ |

PELLET DIAMETER (EFFECTIVE) 0.18

TRANSMISSION COEFFICIENT very low BY

PRESSURE 10 (air) TORR

CALCULATED TRUE DENSITY _____

SURFACE TREATMENT Etch + Sputter

SAMPLE INFORMATION _____

TEST NO. 22 DATE March 1965

PORES PER CM$^2$ _____

AVERAGE PORE SIZE _____

PORE SIZE DISTRIBUTION

| MICRON DIAMETER | PERCENT |
|---|---|
| >1.6 | ____ |
| 1.2 - 1.6 | ____ |
| 0.8 - 1.2 | ____ |
| 0.4 - 0.8 | ____ |
| <0.4 | ____ |

AVERAGE DISTANCE BETWEEN PORES _____ μ

THICKNESS 5 x 10$^{-2}$ CM, DENSITY _____ %

Δp/Δt _____ TORR/SEC

WORK FUNCTION 4.9 *, ev

*SAHA-L. EQ. - % NEUTRALS AT 1 Ma/cm

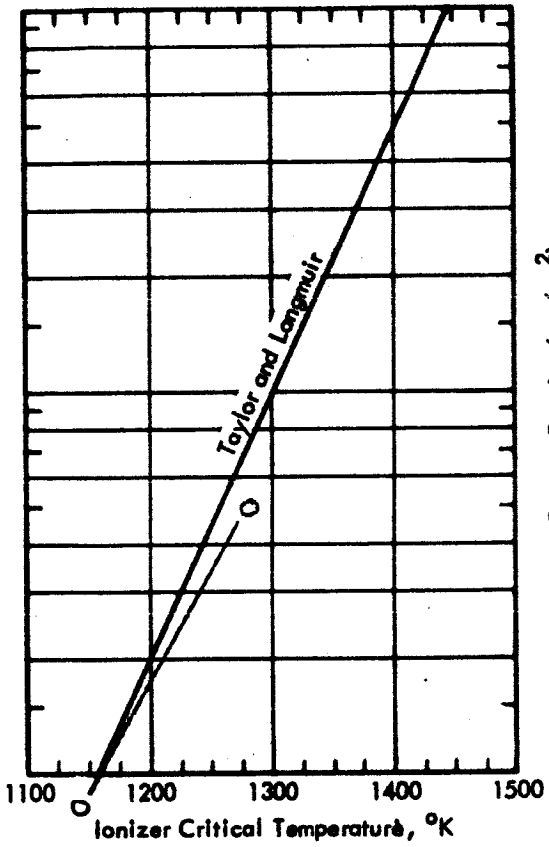


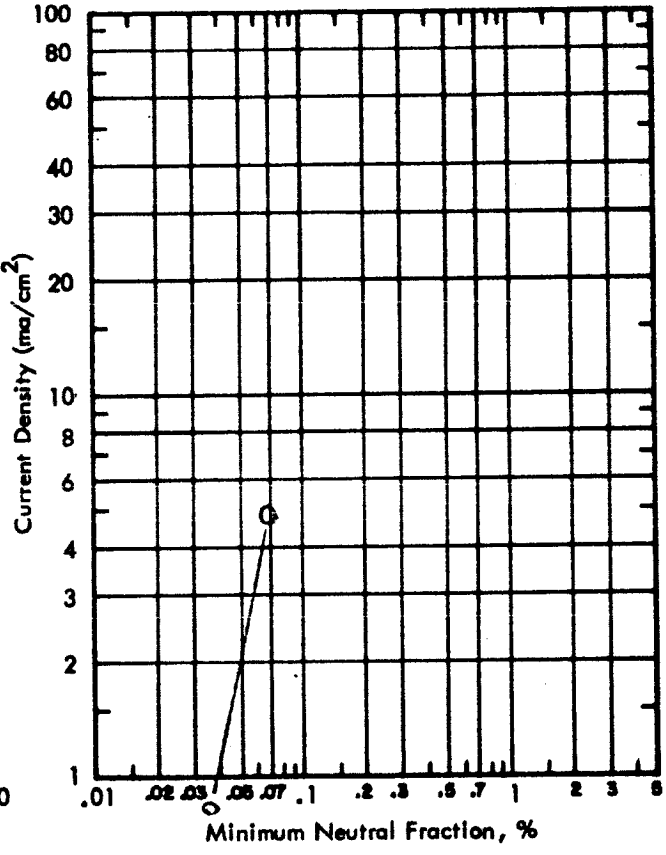


CONCLUSIONS: Results very good up to 5 ma/cm$^2$. Couldn't exceed because of very low permeability.

TEST MADE BY: Shelton/Hall REPORT PREPARED BY: H. Shelton

IONIZER PELLET EVALUATION REPORT

PELLET TYPE 65b

MADE BY STL

AVERAGE PARTICLE SIZE 10μ (Spherical)

TEST NO. 23 DATE 4/65

PORES PER CM$^2$ _____

AVERAGE PORE SIZE _____

| PARTICLE SIZE DISTRIBUTION MICRON DIAMETER | PERCENT |
|---|---|
| >7.5 | ____ |
| 7.5 - 5.0 | ____ |
| 5.0 - 3.3 | ____ |
| 3.3 - 2.25 | ____ |
| 1.5 - 1.0 | ____ |
| <1.0 | ____ |

| PORE SIZE DISTRIBUTION MICRON DIAMETER | PERCENT |
|---|---|
| >1.6 | ____ |
| 1.2 - 1.6 | ____ |
| 0.8 - 1.2 | ____ |
| 0.4 - 0.8 | ____ |
| <0.4 | ____ |

PELLET DIAMETER (EFFECTIVE) 0.18

TRANSMISSION COEFFICIENT 4.1 X10$^{-5}$ BY

PRESSURE 10 (air) TORR

CALCULATED TRUE DENSITY _____

SURFACE TREATMENT etched & sputtered

SAMPLE INFORMATION * at end of test; very low at beginning

AVERAGE DISTANCE BETWEEN PORES _____ μ

THICKNESS 5 x 10$^{-2}$ CM, DENSITY _____ %

Δp/Δt _____ TORR/SEC

WORK FUNCTION ~4.8 *, ev

*SAHA-L. EQ. - % NEUTRALS AT 1 Ma/cm

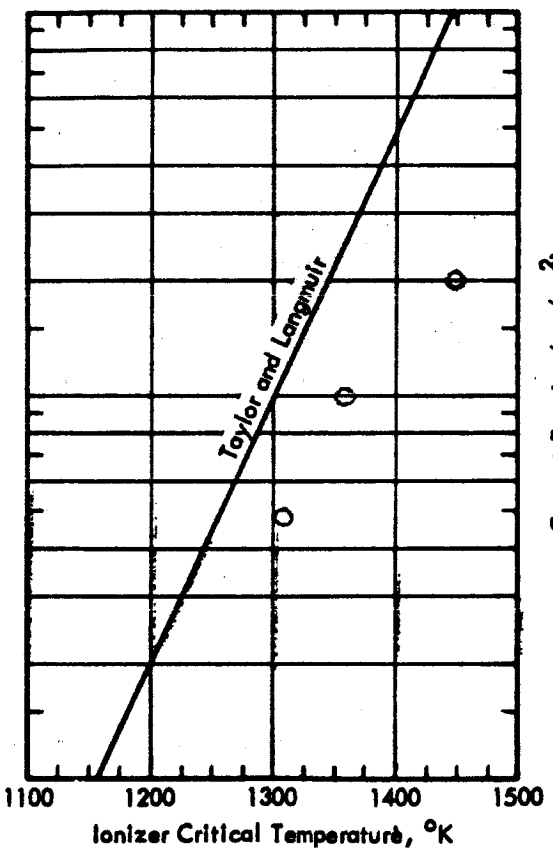


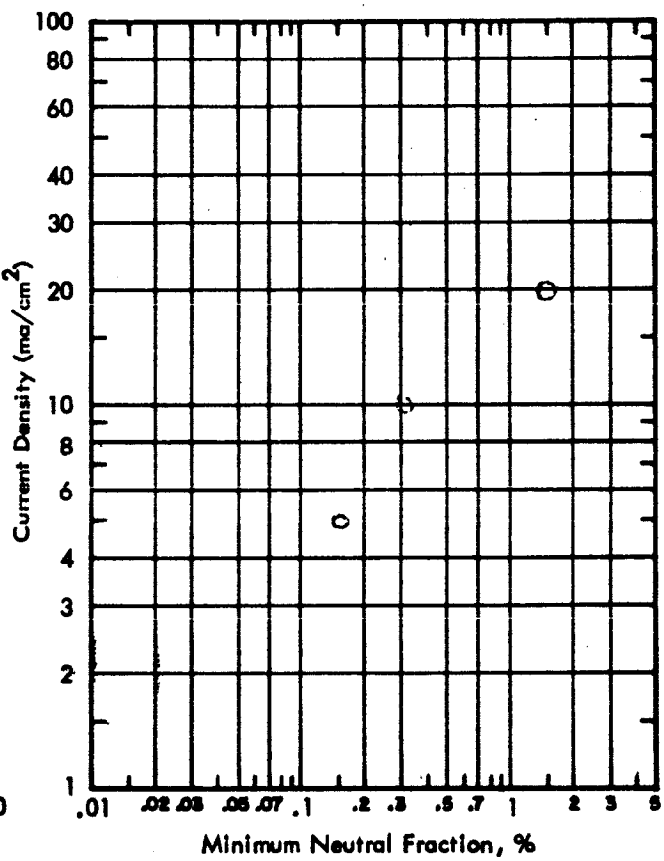


CONCLUSIONS: Results very good up to 10 ma/cm$^2$. Neutral fraction and critical temperature low. Effect of pore density abruptly seen at higher current densities.

TEST MADE BY: Shelton/Hall REPORT PREPARED BY: H. Shelton